REGULATION OF SYNAPSE AND NEURONAL FUNCTION BY LOSS OF *TSC1* IN THE STRIATUM

By

By Katelyn N Benthall

A dissertation submitted in partial satisfaction of the

requirements for the degree of

Doctor of Philosophy

in

Molecular and Cell Biology

in the

Graduate Division

of the

University of California, Berkeley

Committee in Charge:

Professor Helen Bateup, Chair
Professor Marla Feller
Professor Hillel Adesnik
Professor Linda Wilbrecht

Summer 2019

ABSTRACT

REGULATION OF SYNAPSE AND NEURONAL FUNCTION BY LOSS OF *TSC1* IN THE STRIATUM

By Katelyn Nicole Benthall

Doctor of Philosophy in Molecular and Cell Biology

University of California, Berkeley

Professor Helen Bateup, Chair

mTORC1 is a central signaling hub that integrates intra- and extracellular signals to regulate a variety of cellular metabolic processes. Mutations in regulators of mTORC1 lead to neurodevelopmental disorders associated with autism, which is characterized by repetitive, inflexible behaviors. These behaviors likely result from alterations in striatal circuits that control motor learning and habit formation. However, the consequences of mTORC1 dysregulation on striatal neuron physiology are largely unknown. To investigate this, I deleted the mTORC1 negative regulator *Tsc1* postnatally and prenatally from identified striatonigral and striatopallidal neurons and examined how cell autonomous upregulation of mTORC1 activity affects their morphology and physiology. I find that postnatal loss of *Tsc1* increases the excitability of striatonigral, but not striatopallidal, neurons and selectively enhances corticostriatal synaptic transmission. I find that prenatal deletion of *Tsc1* also enhances excitability of striatonigral, but not striatopallidal, neurons, and that this occurs through an increase in cortico-striatonigral synaptic transmission. I also observe that a loss of endocannabinoid-LTD drives enhanced cortical excitation of striatonigral neurons, and that this is associated with improved motor routine learning.

To investigate the molecular mechanism driving these synaptic changes, I performed translating ribosome affinity purification to determine gene expression changes in mice with loss of *Tsc1* from either striatonigral or striatopallidal neurons. I find that *Tsc1* deletion results in numerous translational differences in striatal neurons, and that many of these differences are specific to either striatonigral or striatopallidal neurons. Further, I extend my findings in the *Tsc1* model to the *Cntnap2-/-* ASD mouse model, and find that corticostriatal transmission and motor routine learning are also enhanced by deletion of *Cntnap2.* These findings highlight the critical role of corticostriatal transmission in ASD mouse models, with implications for striatonigral pathway dysfunction in neuropsychiatric disease.

Acknowledgements

I would like to thank my mentor Helen Bateup for her stellar leadership and guidance through the last six years. Her high scientific expectations and standards motivated me to put forward my best effort, and her gentle but enthusiastic mentorship deepened my appreciation and enjoyment of science. I am incredibly proud to have had the opportunity to work with her.

I would also like to thank my committee members, Marla Feller, Hillel Adesnik, and Linda Wilbrecht for their unwavering support and invaluable advice. They were amazing advocates for me, and knowing they had my back gave me the strength and confidence to take on all the challenges of graduate school.

I would like to say thank you to my close friend and lab partner Villy Karalis, who is both an incredible scientist and human being. Her sharp and sometimes dark sense of humor kept me sane in the most trying times, and being able to confide in her helped me overcome innumerable challenges.

Thank you to all my of lab mates, especially Polina Kosillo for her scientific advice and the delicious desserts, Dan Kramer for his positive attitude and the intriguing scientific discussions, and John Blair for keeping the lab running. And especially to Katie Cording, who has been an incredibly fun mentee. I couldn't ask for a better person to work with on this project, and am excited to see where she takes it.

And thank you to my dear friend and housemate Irene Grossrubatscher, who helped me see that there are many rewards to been found outside of the lab, too. Her open heart and adventurous spirit invited me to embrace joy in life and to be unapologetically myself.

I also want to thank Adam Hoagland for being a wonderful companion. His creative and fun-loving nature kept me feeling positive and energized, and his steadfast confidence in me kept me grounded in difficult times. Thank you for making so many incredible memories with me around the bay and beyond.

I also would like to say thank you to my friends Toby Turney and Victoria Chou, who motivated me to get moving though yoga, dance, and music, and who always put a smile on my face no matter what kind of day I was having.

And thank you to my parents, mom for always being only a phone call away, and Todd for his constant support. They have been my cheerleaders my whole life, and their unconditional love gave me the courage to move to California and take on this endeavor. I couldn't have done it without them. Also thank you to my sister Kelsey, who is a constant source of inspiration to me, and who motivates me to be the best version of myself.

Table of Contents

INTRODUCTION: COMMON THEMES OF SYNAPTIC DYSFUNCTION IN MOUSE MODELS OF AUTISM SPECTRUM DISORDER

Autism spectrum disorder (ASD) is a neurodevelopmental condition characterized by difficulties in social interaction, as well as restricted and repetitive motor behaviors [1]. People with ASD also often experience sensory issues, such that they experience hypo- or hypersensitivity, as well as trouble with emotional regulation. Though social and motor abnormalities lie at the core of ASD diagnosis, the signs and symptoms of ASD present differently across people, such that the spectrum includes a diverse patient population. For instance, social challenges in people with ASD can range from those who are completely nonverbal, to those who have difficulty with more nuanced aspects of communication, such as taking turns in conversation. Similarly diverse, motor challenges can include repetitive body movements, ritualistic or strongly habitual behaviors, narrowly restricted interests, and behavioral inflexibility [2].

The variability of traits across people on the autism spectrum reflects the numerous distinct genetic etiologies of the disorder, with over one thousand genes implicated but not yet confirmed [3]. About one-hundred of these genes have been linked to ASD with high-confidence, with many others suggested to be involved at lower confidence [3, 4]. Of these, a large proportion belong to one of two functional categories: (1) regulation of global gene expression, or (2) control of synaptic and neuronal excitability, both functions which modulate neural activity [5, 6]. Mutations that alter gene expression include those involved in chromatin remodeling, (*CHD8* and *MECP2*), as well as transcription factors (*FOXP* family). Other ASD-risk mutations affect gene expression downstream of transcription, such as the gene coding for RNA-binding protein FMRP. Further, mutations in mTORC1 pathway components associated with ASD, such as *TSC1/2* and *PTEN*, alter expression at the protein synthesis level. These genes are important for brain development early in life, including neurogenesis, differentiation, and migration, while also playing an important role in regulation of neuronal excitability throughout one's lifetime.

Gene mutations in proteins controlling synaptic and neuronal excitability, such as ion channels, neurotransmitter receptors, release machinery, and scaffolding proteins, would be predicted to directly alter the function of the synapse, such as to either enhance or diminish neuronal communication. For example, genes encoding for proteins associated with NMDA receptors (*SYNGAP1*, *GRIN2B*), cell adhesion molecules (*NLGN3*, *SHANK* family, *CNTNAP2*), and sodium channels (*SCN2A*) are all implicated in ASD [5-7]. Indeed, altered ability of glutamate or GABA to mediate synaptic transmission has been one of the original hypotheses to explain circuit dysfunction in ASD, stating that changes to the ratio of excitation to inhibition (E/I ratio) that a cell receives can push the cell out of its optimal firing range. Network-level activity imbalances are expected to result, such that brain regions become hyper-excitable and neural processing becomes noisy [8]. Conceptual evidence of this comes from the fact that individuals with ASD also often have epilepsy, resulting from enhanced excitation or diminished inhibition in cortex or hippocampus [9]. However, the complexity of findings in recent studies suggest that thinking of ASD etiology as simply a static change to E/I ratio may be an oversimplification, since primary changes to synapse function may cause compensatory cell- and circuit-level effects that are just as culpable [10, 11].

Forming a cohesive hypothesis to explain the etiology of ASD has proven challenging, which is no surprise given the diverse patient presentation and numerous genes implicated. Despite this, the field is currently driven to identify the common node of dysfunction in ASD, the biological level at which pathology is shared among ASD patients. To this end, researchers are using genetic mouse models to understand how mutations in ASD-risk genes affect gene and protein expression, neuronal excitability, circuit activity, and mouse behavior in different brain regions and neuronal subtypes. This chapter aims to explore the link between gene expression and synaptic transmission, and investigate why mutations in genes that regulate these functions are prevalent in ASD. Recent findings from mouse models will be reviewed, with the goal of understanding if altered activity-dependent gene expression could be a potential common node of dysfunction in ASD.

Altered long-term synaptic plasticity in ASD mouse models

Long-term synaptic plasticity, or the long-lasting modulation of synaptic strength in response to neural activity, is a key regulator of neural excitability. For many years synaptic plasticity has been observed in multiple neuronal types across many experimental systems. It is believed that these activity-dependent changes in synapse strength occur *in vivo* in the human brain, and underlie the processes of learning and memory [12]. It is also hypothesized that aberrant plasticity processes could be responsible for neuropsychiatric disorders such that connections between neuronal populations may become too strong or weak, which pushes brain circuits into abnormal and dysfunctional activity patterns [13]. This line of reasoning may also apply to ASD, in that some neuronal populations have altered synaptic plasticity which leads to either hyper- or hypoactivity, which in turn leads to dysfunction in networks responsible for social and motor behavior. Consistent with this is the fact that ASD-risk genes are common players in synaptic plasticity, as mutations in gene and protein expression machinery as well as synaptic and neuronal excitability would be predicted to disrupt activity-dependent transcription and translation.

Long-term synaptic plasticity can be divided into two main categories - those processes which enhance synaptic connectivity, termed long-term potentiation (LTP), and those which diminish it, termed long-term depression (LTD). LTP and LTD can be further broken down into subtypes based on the physiological and molecular mechanisms of how the plasticity is induced and how the effects are maintained. Different plasticity mechanisms prevail in different brain regions and depend on the specific synaptic connections involved, as well as the presence or absence of various molecular components at those particular synapses [14]. Synaptic plasticity subtypes are extremely diverse and not entirely defined, with induction protocols and postulated mechanisms varying across experimental paradigms. However, two mechanisms stand out as being most commonly described, both involving glutamate binding to receptors at the postsynapse: (1) NMDA receptor-dependent changes in intracellular calcium signaling that lead to changes in surface AMPA receptor density, as well as gene expression chagnes, and (2) metabotropic glutamate receptor (mGluR) dependent activation of G-protein coupled receptor (GPCR) signaling cascades that cause release of calcium from internal stores and ultimately affect protein synthesis and gene

expression [14]. In both cases there is a direct link between neural activity, transcription, and translation, which can render plasticity dysfunctional if broken at any stage.

The occurrence of synaptic plasticity and its effect on cellular excitability aren't determined simply by activation of NMDA receptors or mGluRs at the postsynaptic membrane, but also rely on other factors present at both the local synaptic and whole cell level. One determinant of a synapse's ability to undergo plasticity and the magnitude of that change is the phenomenon of metaplasticity, or the idea that a synapse's state can determine its current ability to undergo plasticity processes. Synaptic state takes into account (1) a synapse's prior activity history, defined as silent, recently silent, active, potentiated, or depressed, (2) the presence of neuromodulatory molecules, such as dopamine, serotonin, acetylcholine, and neuropeptides, and (3) the strength of neighboring synapses, for example depression of neighboring inhibitory synapses can prime an excitatory synapse to undergo potentiation [15]. Another way in which the effects of synaptic plasticity are modulated is through the phenomenon of homeostatic plasticity, which describes a process by which the cell regulates its overall activity in the face of potential whole cell activity imbalances caused by LTP and LTD [16, 17]. For instance, if many synapses onto a cell are weakened, as in the case of sensory deprivation, all synapses onto that cell will be strengthened, or scaled up, such that the weight of individual synapses remain proportionately the same but the overall activity of those synapses is increased to maintain the cell in its optimal firing range [16, 17]. In some cases it is hypothesized that the processes that govern plasticity and maintain overall cellular excitability that have gone awry in neuropsychiatric disorders, including ASD [10, 18].

In the next sections, I will consider the roles of individual ASD-risk genes in activity-dependent transcription and translation, and examine the consequences on neural activity characterized in mouse models.

Regulation of transcription and protein metabolism

MECP2

DNA methylation is a form of epigenetics, or a transcriptional regulatory mechanism that changes gene expression not by altering the DNA sequence itself but rather by another method. In this case, methyl groups can be added to the DNA to alter how it is recognized by transcription machinery. For example, when the promoter region of a gene is methylated transcription of that gene is repressed. DNA methylation is crucial for proper synaptic plasticity, as pharmacological inhibition of methylation impairs LTP [19]. The *MECP2* gene is important for DNA methylation in the brain and, when mutated, results in an X-linked disorder termed Rett syndrome that is classified as an ASD. Rett syndrome involves a loss of function of the Methyl CPG-binding protein 2 (MeCP2), important for regulating gene expression through modification of chromatin. The mechanism of gene regulation by MeCP2 is still not entirely understood – though it is classically thought of as a transcriptional repressor, studies indicate that transcription is increased in mice with loss of MeCP2, so it may actually act as an activator [20, 21]. MeCP2 is also hypothesized to be involved in messenger RNA (mRNA) splicing that determines which protein isoforms are translated. Evidence suggests that in its dephosphorylated form, MeCP2 binds the promoter of *BDNF* and other genes important

for brain function, preventing transcription. However, MeCP2 is phosphorylated in response to neural activity, which frees up the promoter to permit transcription [22].

Mice with loss of MeCP2 have been thoroughly characterized in electrophysiological experiments, and though various changes across brain regions have been documented with regards to baseline synaptic transmission, it is clear that plasticity, specifically LTP, is impaired [22-24]. Interestingly, mildly symptomatic mice showed smaller LTP deficits than mice with profound symptoms, suggesting that LTP deficits are directly correlated with behavioral symptoms in *MECP2*-null mice. Further, the same study examined the cause of this reduced LTP and found that it was a saturation effect, such that the synapses involved were already so potentiated that they were unable to undergo further LTP [22, 25]. This hyper-potentiation may reflect a failure of homeostatic plasticity, such that the cell's activity has not be scaled down appropriately, and the cell is kept at the ceiling of its potentiation range. Notably, LTP is also impaired by *MeCP2* duplications, though baseline synaptic transmission changes are opposite those seen with *MeCP2* deletion [26]. Interestingly LTP seems to be primarily affected, as studies have only identified minor changes to LTD in mice with *MECP2* deletion [27].

CHD8

Another method of epigenetics is chromatin remodeling, in which transcription is regulated by how DNA is packed around histones into a nucleosome [28]. To be transcribed, DNA must be unfolded, or unpacked from these structures. It is in this way that chromodomain helicase DNA-binding protein 8 (CHD8) regulates gene expression. The gene coding for this protein, *CHD8*, is one of the leading ASD-risk gene candidates that has recently been identified by genetic studies [29]. Characterization of synaptic and behavioral changes in mice with *CHD8* mutation have recently begun, and though synaptic plasticity has yet to be investigated directly, it is clear that loss of CHD8 alters processes that rely on plasticity such as motor learning [30]. Further, the fact that CHD8 regulates expression of other ASD-risk genes such as *PTEN* and *FOXP1* suggests that plasticity changes with *CHD8* deletion may reflect those observed in other ASD models [31].

TSC1/2 and *PTEN*

TSC1, TSC2 and *PTEN* are ASD-risk genes that converge on the mTOR signaling pathway, a central hub controlling cellular metabolic processes such as protein and lipid synthesis, cell growth, differentiation, proliferation, and autophagy [32]. Both the TSC1/2 protein complex and the PTEN protein repress mTOR complex 1 (mTORC1) signaling, and loss of function in any of these genes confers high risk of epilepsy and ASD. This risk is thought to originate from the changes to translation that come about with the dysregulation of mTOR complex 1 (mTORC1). However, given that PTEN is upstream of PI3K/Akt signaling, loss of *PTEN* also activates Akt signaling, while Akt phosphorylation is reduced in response to TSC1/2 disruption [33] . mTORC1 activation leads to phosphorylation of p70S6 kinase, which in turn phosphorylates ribosomal protein S6 to promote translation [34]. mTORC1 also phosphorylates the translation inhibitor 4E-BP1, which has the effect of increasing protein synthesis [33, 34]. Notably, dysregulation of eIF4E, the target of 4E-BP1, causes autism-related

behaviors and altered plasticity in mice, which result from increased translation [35, 36]. Thus in the case of hyperactive mTORC1 signaling, as occurs with *TSC1* or *PTEN* loss-of-function mutations, protein synthesis is abnormally high.

mTORC1-dependent protein synthesis has been shown to be critical to long-term synaptic plasticity, and inhibition or hyperactivation of mTORC1 dysregulates plasticity in multiple neuronal types and across various experimental paradigms [37]. The first pieces of evidence showing the dependence synaptic plasticity on mTORC1 activity comes from studies using mTORC1-inhibitor rapamycin, and show that rapamycin application blocks the late, protein synthesis-dependent component of LTP (L-LTP) while leaving the early protein synthesis-independent component (E-LTP) intact [38-40]. More recent studies take advantage of transgenic mouse models that investigate how loss of TSC1/2 or PTEN affect synaptic plasticity. Interestingly, genetic de-repression of mTORC1 has various consequences on excitatory and inhibitory signaling depending on experimental paradigm and neuronal sub-type, but the findings in these models are relatively consistent in regards to plasticity , [33, 41-48].

The first study to characterize synaptic plasticity in a TSC model was done in the Eker rat, which are rats with heterozygous loss of *TSC2*. In Eker rats, hippocampal LTP was diminished and LTD was either decreased or unaffected depending on the induction protocol used [49]. The LTP deficit was then replicated in hippocampal slices from a conditional *TSC1* mouse, with homozygous TSC1 loss restricted to GFAP-positive cells [50]. Interestingly, later studies showed that L-LTP can be induced by an E-LTP protocol in brain slices from animals with heterozygous loss of *TSC2*, indicating altered dynamics of E- and L-LTP in mTORC1 hyperactivity, such that a lower threshold is required to initiate the protein synthesis-dependent phase of LTP [47], which may explain the previously-described LTP deficit.

Deficits in mGluR-mediated synaptic plasticity are also found in mice with loss of *Tsc1* or *2*, namely in mGluR-LTD. A loss of mGluR-LTD was found in hippocampus of animals with homozygous conditional, postnatal loss of *Tsc1* [42], as well as in brain slices from mice expressing a dominant-negative form of *Tsc2* [48, 51, 52]. Loss of striatal mGluR-LTD has also been found in striatonigral neurons (Benthall, unpublished). Interestingly, NMDAR-LTD was not altered by *Tsc1* or *Tsc2* loss, suggesting that the LTD deficit observed in Eker rats may be due to an induction protocol that favored mGluR-LTD, and conversely, that the protocol in which LTD was altered, could have been preferentially evoking NMDAR-LTD.

Similar synaptic plasticity deficits have been found in mouse models of *PTEN* deficiency. Original studies show that in brain slices from mice with heterozygous loss of *PTEN*, hippocampal synapses are able to undergo LTP but that the magnitude of that LTP is smaller than in controls. LTD is completely abolished at these synapses [53]. Later studies specify that this is a deficit in NMDAR-LTD and not in mGluR-LTD [54]. These findings were repeated in mice with postnatal loss of *PTEN*, which showed that though cells didn't show morphological or baseline synaptic transmission changes that occur with prenatal deletion, they still show the same synaptic plasticity deficits [55]. Interestingly, these particular impairments in NMDAR-mediated plasticity may be cell-type dependent, as deficits in mGluR-LTD were observed in dentate gyrus cells of mice with *PTEN* deletion [56].

UBE3A and *15q11-13*

Mutations of *UBE3A* and the chromosomal region in which it is contained, *15p11-13*, are involved with both Angelman's syndrome (AS) and ASD [57]. The protein UBE3A is an E3 ubiquitin ligase that has important functions in tagging proteins for degradation via ubiquitination. Interestingly, *UBE3A* deletions are associated with AS, while duplications of the region and excess UBE3A protein have a higher association with ASD. Many studies have described altered synaptic transmission in mouse models of AS, showing loss of NMDAR-mediated LTP and LTD [58, 59]. Indeed, an intimate link has been shown between Ube3a and plasticity, as neuronal activity induces *Ube3a* transcription and that this regulates immediate-early gene *Arc* and excitatory synapse development [60]. Differently than in most models, mGluR-LTD is actually enhanced with deletion of *UBE3A* due to a difference in Homer isoforms expressed [61]. Interestingly, one study observed a loss of homeostatic plasticity as measured by a lack of synaptic scaling in primary cultures of UBE3A knock-out neurons [62]. A similar loss of synaptic scaling has been shown in the case of *UBE3A* overexpression, though LTP and LTD have yet to be characterized in the duplication model [63]. Notably, studies suggest that *UBE3A* is upstream of mTORC1 signaling, so the pathways involved in *UBE3A* mouse models may converge with those of *TSC1/2* and *PTEN* [64].

FMR1

Fragile X syndrome (FXS) is a disorder in which about half the patients meet clinical criteria for ASD. It is caused by mutations in the *FMR1* gene, which codes for FMRP, an RNA-binding protein that is thought to negatively regulate mRNA translation [65]. Studies show an age-dependent reduction of cortical NMDAR-LTP. However, mixed results are reported for hippocampal LTP, with some seeing no effect and some seeing a loss of LTP in *FMR1* knock-out mice [66-71]. The loss of LTP is not a complete abolishment but rather an increase in the induction threshold due to aberrant calcium signaling in dendrites and spines. LTP could be induced in the cortex of *FMR1* knock-out animals when experimental conditions improved calcium signaling, indicating that the machinery for LTP downstream of calcium signaling is functional in cells with no FMRP [72].

FMR1 deletion is a unique ASD-risk mutation when it comes to LTD. Though NMDAR-LTD has been reported to be impaired [71], *FMR1* models generally show an enhancement of mGluR-LTD similar to that seen in *UBE3A*, though this has been much more extensively characterized than in the case of *UBE3A.* Enhanced mGluR-LTD has been shown in hippocampus and cerebellum, and has been shown to not rely on protein synthesis as mGluR-LTD would normally [73-75]. The mGluR-LTD in *FMR1* has been proposed to share a common mechanism with mAChR-LTD, as both activate Gq-coupled intracellular signaling pathways, and to rely on NMDAR signaling [76, 77]. Changes in mGluR-LTD can have direct effects on LTP in *FMR1* animals, as mGluR-LTD primes synapses to undergo LTP [78]. Under normal circumstances this priming is protein synthesis-dependent, but in the case of exaggerated mGluR-LTD as in *FMR1* knock-out the priming occurs independently of protein synthesis [78]. FRMP has been proposed to be activated downstream of mTORC1 [79], and so might be involved in a similar signaling pathway as that of TSC1/2 and PTEN.

Direct regulators of synaptic and neuronal excitability

SCN2A

Mutations in *SCN2A* have been identified in both epilepsy and ASD, and lead to a change in function of Nav1.2, the voltage-gated sodium channel encoded by the gene [80]. Interestingly, mutations associated with epilepsy cause gain of function in Nav1.2, while those associated with ASD are more often loss-of-function mutations [81]. Intrinsic excitability changes result, which alter the ability of the cell to undergo synaptic plasticity. Namely, NMDAR-LTP could not be induced in the cortex because the loss of Nav1.2 function decreased dendritic back-propagation of action potentials, thereby eliminating the necessary dendritic calcium signaling necessary for LTP [82]. The same loss of LTP was found in hippocampus in XX model [83].

CNTNAP2

CNTNAP2, an ASD-risk gene that codes for CASPR2, is a member of the neurexin family that anchors potassium channels to the axon [84, 85]. Mutations in *CNTNAP2* are associated with ASD and epilepsy, and are found to impact synaptic plasticity mechanisms. Though LTP and LTD have yet to be thoroughly characterized, these is evidence that despite altered AMPA:NMDA ratios, LTP is intact in *CNTNAP2* mutant mice in hippocampal CA1 pyramidal neurons [86]. The primary effect on plasticity reported thus far, however, is on homeostatic plasticity. Loss of CASPR2 prevents homeostatic synaptic upscaling in primary cortical cultures [87]. Further, CASPR2 was found to be necessary for experience-dependent homeostatic plasticity in the cortex of visually-deprived mice [87].

NLGN1/3

Neuroligins are a family of proteins found on the postsynaptic membrane that are involved in the formation and maintenance of synapses, and have been implicated in ASD [88]. They are the ligand for neurexins that are on the presynaptic membrane, and the connection between these two proteins stabilizes the synapses structure [88]. Neuroligins also interact with other synaptic proteins to localize them to the postsynaptic density [88, 89]. Evidence from silencing *NLGN1* in the amygdala using shRNA shows that NMDAR-LTP is absent with loss of NLGN1 function [90]. Similarly, *NLGN3* knock-out reduces NMDAR-LTP in hippocampus [91-93]. Interestingly, this LTP deficit is timing and age-dependent, as acute loss of *NLGN1* but not *NLGN3* recapitulates this deficit in younger mice [94]. LTD is also compromised by NLGN loss, as striatal endocannabinoid-mediated LTD (eCB-LTD), a special case of mGluR-LTD, is lost in mice with a *NLGN3* mutation [95]. Heterozygous loss of *NLGN1* causes a deficit in NMDAR-LTD but an enhancement of mGluR-LTD in hippocampus [96].

SHANK3

SHANK proteins act as scaffolds at the postsynaptic density, anchoring synaptic proteins like ion channels and neurotransmitter receptors to the cytoskeleton and components of G-protein signaling pathways. They have been shown to play a role in NMDAR-dependent plasticity, as NMDAR-LTP is lost with hippocampal and striatal *SHANK3* deletion, while NMDAR-LTD is left intact [97-102]. Further, mGluR-LTD is also

found to be deficient in primary hippocampal cultures and striatal and hippocampal slices, though one report found hippocampal mGluR-LTD to be intact [98, 99, 101, 103].

GRIN2B

NMDA receptors are composed of four subunits, two of which must be NR1, encoded by the *GRIN1* gene, and two of which may be any of four NR2 subunits or two NR3 subunits. One of those subunits is NR2B, coded for by the ASD-risk gene *GRIN2B* [104]. *GRIN2A*, which codes for NR2A, is also implicated in ASD but the evidence is not as strong as that for *GRIN2B* [4]. Pharmacological studies in hippocampus have shown that NR2B, unlike NR2A and NR2D, is required for NMDAR-LTD, with a smaller role in LTP [105]. These results are supported by genetic *GRIN2B* knock-outs, which show slightly reduced LTP and drastically reduced LTD in the hippocampus and cortex [106]. In addition, NR2B is found to be especially important for AMPAR internalization during LTD in the amygdala, and tightly binds to CaMKII in its activated form to localize it to the postsynaptic density [107, 108]. Extrasynaptic NR2B receptors are involved in the modulation of LTP in response to prolonged synaptic stimulation, a proposed homeostatic metaplasticity mechanism [109].

SYNGAP1

The ASD-risk gene *SYNGAP1* codes for synaptic GTPase activating protein, or SYNGAP1, which is a postsynaptic protein important for repressing signaling pathways associated with NMDAR-LTP and AMPAR-insertion [110-113]. In mice with heterozygous loss of *SYNGAP1*, hippocampal LTP is reduced [114]. This loss of LTP is correlated with a rapid maturation and accelerated GluN2a insertion at excitatory synapses, suggesting a ceiling effect on excitation that occludes further LTP [115]. Interestingly, SYNGAP1 preferentially couples to NR2B over other NMDAR subunits, granting NR2B the ability to inhibit AMPAR insertion, as opposed to NR2A activation which increases surface AMPARs [111]. Further, SYNGAP1 sits at the interface of the NR2B and mTORC1 signaling pathways, mediating the mTORC1-dependent synthesis of AMPARs in response to NR2B-containing NMDAR activation [116]. This pathway is critical for proper homeostatic synaptic plasticity, as SYNGAP1 is required for proper scaling-up of excitatory synapses following activity blockade [116].

Conclusions

Gene mutations that confer high risk for ASD tend to either be in regions coding for regulators of gene expression and protein metabolism, or in regions that mediate neuronal excitability and communication. Proper function of this gene-synapse loop is critical for long-term synaptic plasticity and, as demonstrated in the mouse models outlined here, when broken at critical points causes abnormal plasticity. In the vast majority of cases, these abnormalities are deficits, in which LTP or LTD or both are abolished with the ASD-risk mutation. However, *FMR1* and *UBE3A* deletions are special cases in which mGluR-LTD is enhanced. As the field progresses and the mechanisms of altered synaptic plasticity are identified across different ASD mouse models, we may be able to understand why LTD or LTP are primarily affected with certain gene mutations, and why some cause enhanced instead of diminished plasticity.

One challenge to understanding the mechanism of synaptic dysfunction in ASD is the ability to discern primary changes from secondary, or compensatory changes that happen during development as the circuits attempt to normalize function. For example, the E/I ratio hypothesis of ASD suggests that too much excitation or too little inhibition could drive a circuit to dysfunction and so, assuming this is correct, it would follow that the gene mutations found in ASD patients all lead to a primary change to glutamatergic or GABAergic transmission. These primary changes to synaptic E/I balance could endow cells with an enhanced or diminished propensity for synaptic plasticity. For example, cells which receive too little inhibition could be primed to undergo spike-timing dependent LTP more readily than normal, and synaptic strength in circuits containing those cells could become potentiated to the point of saturation, such that the mechanisms for LTP have reached a ceiling level and can't induce or maintain further potentiation. Alternatively, is it possible that cells with a primary lack of synaptic inhibition have attempted to normalize cellular activity by homeostatic plasticity, and have engaged excitatory synapse down-scaling mechanisms to the point of overdrive. In this case the cell may be unable to undergo LTD because the mechanisms underlying induction or maintenance are diverted to maintain proper cell excitability and are unavailable to be used for synapse-specific LTD.

Another possibility is that the primary effect of ASD-risk gene mutations is to directly disrupt synaptic plasticity processes, perhaps by changing the signaling pathways by which NMDARs or mGluRs cause AMPAR synthesis or insertion following synaptic stimulation. This could lead to secondary changes in synaptic strength - for example, a cell's inability to undergo LTD could result of the cell's inability to appropriately remove unnecessary glutamatergic synapses, and lead to an overabundance of excitatory synapses. Indeed, this phenomenon has been shown to occur in the cortical excitatory neurons of a TSC mouse model [117]. Because of the interdependence of gene expression and synaptic activity, it has been difficult to distinguish which of these possibilities is occurring. Take the case of *GRIN2B* mutations, for example. It might seem obvious that dysfunction of the NMDAR would directly disrupt NMDAR-LTP and LTD, and that the primary change in that case would be the plasticity deficits. However, this hypothesis is complicated by the fact that NMDAR-mediated current plays a large role in excitatory transmission onto inhibitory interneurons [118, 119]. This means that loss of NMDAR function results in synaptic hypoexcitability of GABAergic cells, and a decrease of GABA release onto principal neurons. Thus, the *GRIN2B* mutation could be driving a primary change to synaptic strength in inhibitory neurons and directly increasing the network E/I ratio. Regardless of whether changes to synaptic plasticity are primary results of the gene deletions or secondary to changes in neuronal and synaptic excitability, they are commonly found across ASD mouse models and may serve as a common node of cell and circuit dysfunction.

Dissertation research question

Because it is yet unclear which specific brain region(s) are responsible in the pathogenesis of ASD, studies investigating the synaptic effects of ASD-risk gene deletions have focused on many different cell types across the brain. It is likely, however, that dysfunction of a subset of brain regions involved in generating social and

motor behavior is particularly important to the behavioral manifestations of ASD. One such brain region is the basal ganglia, a group of subcortical structures involved in motor learning, action selection, and habit formation [120, 121]. These motor behavioral are particularly dependent upon activity of spiny projection neurons (SPNs) in the striatum, which serves as the input nucleus of the basal ganglia, receiving excitatory inputs from cortex and thalamus and then sending inhibitory projections to downstream basal ganglia nuclei [121, 122]. These inhibitory outputs are the origin of the two basal ganglia pathways, the direct pathway and the indirect pathway, which are thought to select actions in a complementary fashion [123]. Specifically, activation of direct pathway SPNs (dSPNs) promotes motor behavior, and activation of indirect pathway SPNs (iSPNs) suppresses inappropriate actions, and it is thought that in this way that depending on the context, the striatum will choose an appropriate behavior to be performed while preventing undesirable actions [124]. In addition to action selection, another important function of the striatum is action chunking, or the subconscious linking of actions that are often performed in sequence and maybe underlie habit and routine formation [125]. Dysfunction of activity of SPNs could disrupt of action selection, habit learning, and routine formation and cause the motor aspects of ASD. Thus the focus of my dissertation is to elucidate the effects of loss of ASD-risk gene *Tsc1* on the activity of dSPNs and iSPNs, and to determine if these effects can lead to ASD-linked behaviors in mice. Further, I will explore molecular mechanisms behind changes to SPNs that occur with *Tsc1* deletion, and extend my findings to other ASD-risk gene mouse models.

References

1. American Psychological Association, *Diagnostic and statistical manual of mental disorders : DSM-5. 5th edn.* 2013.
2. Autism Speaks, *What is Autism?* 2019 [cited 2019 July 15]; Available from: https://www.autismspeaks.org/what-autism.
3. National Institutes of Health, *Autism Spectrum Disorder*. 2019 [cited 2019 July 15]; Available from: https://ghr.nlm.nih.gov/condition/autism-spectrum-disorder#.
4. SFARI. *SFARI Gene*. 2019 [cited 2019 July 15]; Available from: https://gene.sfari.org/.
5. Levitt, P. and D.B. Campbell, *The genetic and neurobiologic compass points toward common signaling dysfunctions in autism spectrum disorders.* J Clin Invest, 2009. **119**(4): p. 747-54.
6. De Rubeis, S., et al., *Synaptic, transcriptional and chromatin genes disrupted in autism.* Nature, 2014. **515**(7526): p. 209-15.
7. An, J.Y., et al., *Genome-wide de novo risk score implicates promoter variation in autism spectrum disorder.* Science, 2018. **362**(6420).
8. J. L. R. Rubenstein, M.M.M., *Model of autism: increased ratio of excitation/inhibition in key neural systems.* Genes, Brain and Behavior, 2003. **2**: p. 255–267.
9. Cellot, G. and E. Cherubini, *GABAergic signaling as therapeutic target for autism spectrum disorders.* Front Pediatr, 2014. **2**: p. 70.
10. Nelson, S.B. and V. Valakh, *Excitatory/Inhibitory Balance and Circuit Homeostasis in Autism Spectrum Disorders.* Neuron, 2015. **87**(4): p. 684-98.
11. Antoine, M.W., et al., *Increased Excitation-Inhibition Ratio Stabilizes Synapse and Circuit Excitability in Four Autism Mouse Models.* Neuron, 2019. **101**(4): p. 648-661 e4.
12. Abraham, W.C., O.D. Jones, and D.L. Glanzman, *Is plasticity of synapses the mechanism of long-term memory storage?* NPJ Sci Learn, 2019. **4**: p. 9.
13. Klein, M.E., H. Monday, and B.A. Jordan, *Proteostasis and RNA Binding Proteins in Synaptic Plasticity and in the Pathogenesis of Neuropsychiatric Disorders.* Neural Plast, 2016. **2016**: p. 3857934.
14. Malenka, R.C. and M.F. Bear, *LTP and LTD: an embarrassment of riches.* Neuron, 2004. **44**(1): p. 5-21.
15. Wickliffe C. A., B.M.F., *Metaplasticity: the plasticity of synaptic plasticity.* Trends Neurosci, 1996. **19**: p. 126-130.
16. Turrigiano, G.G. and S.B. Nelson, *Homeostatic plasticity in the developing nervous system.* Nat Rev Neurosci, 2004. **5**(2): p. 97-107.
17. Turrigiano, G.G., and Sacha B Nelson, *Hebb and homeostasis in neuronal plasticity.* Current Opinion in Neurobiology, 2000. **10**: p. 358-364.
18. Ramocki, M.B. and H.Y. Zoghbi, *Failure of neuronal homeostasis results in common neuropsychiatric phenotypes.* Nature, 2008. **455**(7215): p. 912-8.
19. Munoz, P., et al., *Inhibition of DNA Methylation Impairs Synaptic Plasticity during an Early Time Window in Rats.* Neural Plast, 2016. **2016**: p. 4783836.
20. Chahrour, M., Sung Yun Jung, Chad Shaw, Xiaobo Zhou, Stephen T. C. Wong, Jun Qin, Huda Y. Zoghbi, *MeCP2, a Key Contributor to Neurological Disease, Activates and Represses Transcription.* Science, 2008. **320**.

21. Horvath, P.M. and L.M. Monteggia, *MeCP2 as an Activator of Gene Expression.* Trends Neurosci, 2018. **41**(2): p. 72-74.
22. Li, H., et al., *Loss of activity-induced phosphorylation of MeCP2 enhances synaptogenesis, LTP and spatial memory.* Nat Neurosci, 2011. **14**(8): p. 1001-8.
23. Moretti, P., et al., *Learning and memory and synaptic plasticity are impaired in a mouse model of Rett syndrome.* J Neurosci, 2006. **26**(1): p. 319-27.
24. Dani, V.S. and S.B. Nelson, *Intact long-term potentiation but reduced connectivity between neocortical layer 5 pyramidal neurons in a mouse model of Rett syndrome.* J Neurosci, 2009. **29**(36): p. 11263-70.
25. Weng, S.M., et al., *Synaptic plasticity deficits in an experimental model of rett syndrome: long-term potentiation saturation and its pharmacological reversal.* Neuroscience, 2011. **180**: p. 314-21.
26. Na, E.S., et al., *The impact of MeCP2 loss- or gain-of-function on synaptic plasticity.* Neuropsychopharmacology, 2013. **38**(1): p. 212-9.
27. Lozovaya, N., et al., *Early alterations in a mouse model of Rett syndrome: the GABA developmental shift is abolished at birth.* Sci Rep, 2019. **9**(1): p. 9276.
28. Koberstein, J.N., Shane G. Poplawski, Mathieu E. Wimmer, Giulia Porcari, Charlly Kao,, D.R. Bruce Gomes, Hakon Hakonarson, Nancy R. Zhang, Robert T. Schultz,, and L.P. Ted Abel, *Learning-dependent chromatin remodeling highlights noncoding regulatory regions linked to autism.* Science Signaling, 2018. **11**.
29. O'Roak, B.J., et al., *Sporadic autism exomes reveal a highly interconnected protein network of de novo mutations.* Nature, 2012. **485**(7397): p. 246-50.
30. Platt, R.J., et al., *Chd8 Mutation Leads to Autistic-like Behaviors and Impaired Striatal Circuits.* Cell Rep, 2017. **19**(2): p. 335-350.
31. Cotney, J., et al., *The autism-associated chromatin modifier CHD8 regulates other autism risk genes during human neurodevelopment.* Nat Commun, 2015. **6**: p. 6404.
32. Saxton, R.A. and D.M. Sabatini, *mTOR Signaling in Growth, Metabolism, and Disease.* Cell, 2017. **168**(6): p. 960-976.
33. Weston, M.C., H. Chen, and J.W. Swann, *Loss of mTOR repressors Tsc1 or Pten has divergent effects on excitatory and inhibitory synaptic transmission in single hippocampal neuron cultures.* Front Mol Neurosci, 2014. **7**: p. 1.
34. Hoeffer, C.A. and E. Klann, *mTOR signaling: at the crossroads of plasticity, memory and disease.* Trends Neurosci, 2010. **33**(2): p. 67-75.
35. Santini, E., et al., *Exaggerated translation causes synaptic and behavioural aberrations associated with autism.* Nature, 2013. **493**(7432): p. 411-5.
36. Gkogkas, C.G., et al., *Autism-related deficits via dysregulated eIF4E-dependent translational control.* Nature, 2013. **493**(7432): p. 371-7.
37. Santini, E., T.N. Huynh, and E. Klann, *Mechanisms of translation control underlying long-lasting synaptic plasticity and the consolidation of long-term memory.* Prog Mol Biol Transl Sci, 2014. **122**: p. 131-67.
38. Stoica, L., et al., *Selective pharmacogenetic inhibition of mammalian target of Rapamycin complex I (mTORC1) blocks long-term synaptic plasticity and memory storage.* Proc Natl Acad Sci U S A, 2011. **108**(9): p. 3791-6.

39. Tang, S.J., et al., *A rapamycin-sensitive signaling pathway contributes to long-term synaptic plasticity in the hippocampus.* Proc Natl Acad Sci U S A, 2002. **99**(1): p. 467-72.
40. Hou, L. and E. Klann, *Activation of the phosphoinositide 3-kinase-Akt-mammalian target of rapamycin signaling pathway is required for metabotropic glutamate receptor-dependent long-term depression.* J Neurosci, 2004. **24**(28): p. 6352-61.
41. Bateup, H.S., et al., *Excitatory/inhibitory synaptic imbalance leads to hippocampal hyperexcitability in mouse models of tuberous sclerosis.* Neuron, 2013. **78**(3): p. 510-22.
42. Bateup, H.S., et al., *Loss of Tsc1 in vivo impairs hippocampal mGluR-LTD and increases excitatory synaptic function.* J Neurosci, 2011. **31**(24): p. 8862-9.
43. Tsai, P.T., et al., *Autistic-like behaviour and cerebellar dysfunction in Purkinje cell Tsc1 mutant mice.* Nature, 2012. **488**(7413): p. 647-51.
44. Normand, E.A., et al., *Temporal and mosaic Tsc1 deletion in the developing thalamus disrupts thalamocortical circuitry, neural function, and behavior.* Neuron, 2013. **78**(5): p. 895-909.
45. Zhao, J.P. and A. Yoshii, *Hyperexcitability of the local cortical circuit in mouse models of tuberous sclerosis complex.* Mol Brain, 2019. **12**(1): p. 6.
46. Benthall, K.N., S.L. Ong, and H.S. Bateup, *Corticostriatal Transmission Is Selectively Enhanced in Striatonigral Neurons with Postnatal Loss of Tsc1.* Cell Rep, 2018. **23**(11): p. 3197-3208.
47. Ehninger, D., et al., *Reversal of learning deficits in a Tsc2+/− mouse model of tuberous sclerosis.* Nature Medicine, 2008. **14**: p. 843.
48. Auerbach, B.D., E.K. Osterweil, and M.F. Bear, *Mutations causing syndromic autism define an axis of synaptic pathophysiology.* Nature, 2011. **480**(7375): p. 63-8.
49. von der Brelie, C., et al., *Impaired synaptic plasticity in a rat model of tuberous sclerosis.* Eur J Neurosci, 2006. **23**(3): p. 686-92.
50. Zeng, L.H., et al., *Abnormal glutamate homeostasis and impaired synaptic plasticity and learning in a mouse model of tuberous sclerosis complex.* Neurobiol Dis, 2007. **28**(2): p. 184-96.
51. Chevere-Torres, I., et al., *Metabotropic glutamate receptor-dependent long-term depression is impaired due to elevated ERK signaling in the DeltaRG mouse model of tuberous sclerosis complex.* Neurobiol Dis, 2012. **45**(3): p. 1101-10.
52. Potter, W.B., et al., *Reduced juvenile long-term depression in tuberous sclerosis complex is mitigated in adults by compensatory recruitment of mGluR5 and Erk signaling.* PLoS Biol, 2013. **11**(8): p. e1001627.
53. Wang, Y., A. Cheng, and M.P. Mattson, *The PTEN Phosphatase is Essential for Long-Term Depression of Hippocampal Synapses.* NeuroMolecular Medicine, 2006. **8**(3): p. 329-336.
54. Jurado, S., et al., *PTEN is recruited to the postsynaptic terminal for NMDA receptor-dependent long-term depression.* EMBO J, 2010. **29**(16): p. 2827-40.
55. Sperow, M., et al., *Phosphatase and tensin homologue (PTEN) regulates synaptic plasticity independently of its effect on neuronal morphology and migration.* J Physiol, 2012. **590**(4): p. 777-92.

56. Takeuchia K., M.J.G., Jing Zhoub, Luis F. Paradab, Michael V. L. Bennetta, R. Suzanne Zukina, *Dysregulation of synaptic plasticity precedes appearance of morphological defects in a Pten conditional knockout mouse model of autism.* PNAS, 2013. **110**(12): p. 4738–4743.
57. Vatsa, N. and N.R. Jana, *UBE3A and Its Link With Autism.* Front Mol Neurosci, 2018. **11**: p. 448.
58. Jiang, Y., et al., *Mutation of the Angelman Ubiquitin Ligase in Mice Causes Increased Cytoplasmic p53 and Deficits of Contextual Learning and Long-Term Potentiation.* Neuron, 1998. **21**: p. 799-811.
59. Cheron, G., et al., *Disruption of the LTD dialogue between the cerebellum and the cortex in Angelman syndrome model: a timing hypothesis.* Front Syst Neurosci, 2014. **8**: p. 221.
60. Greer, P.L., et al., *The Angelman Syndrome protein Ube3A regulates synapse development by ubiquitinating arc.* Cell, 2010. **140**(5): p. 704-16.
61. Pignatelli, M., et al., *Changes in mGlu5 receptor-dependent synaptic plasticity and coupling to homer proteins in the hippocampus of Ube3A hemizygous mice modeling angelman syndrome.* J Neurosci, 2014. **34**(13): p. 4558-66.
62. Pastuzyn, E.D. and J.D. Shepherd, *Activity-Dependent Arc Expression and Homeostatic Synaptic Plasticity Are Altered in Neurons from a Mouse Model of Angelman Syndrome.* Front Mol Neurosci, 2017. **10**: p. 234.
63. Xu, X., et al., *Excessive UBE3A dosage impairs retinoic acid signaling and synaptic plasticity in autism spectrum disorders.* Cell Res, 2018. **28**(1): p. 48-68.
64. Sun, J., et al., *UBE3A-mediated p18/LAMTOR1 ubiquitination and degradation regulate mTORC1 activity and synaptic plasticity.* Elife, 2018. **7**.
65. Bear, M.F., K.M. Huber, and S.T. Warren, *The mGluR theory of fragile X mental retardation.* Trends Neurosci, 2004. **27**(7): p. 370-7.
66. Li, J., et al., *Reduced cortical synaptic plasticity and GluR1 expression associated with fragile X mental retardation protein deficiency.* Mol Cell Neurosci, 2002. **19**(2): p. 138-51.
67. Zhao, M.G., et al., *Deficits in trace fear memory and long-term potentiation in a mouse model for fragile X syndrome.* J Neurosci, 2005. **25**(32): p. 7385-92.
68. Wilson, B.M. and C.L. Cox, *Absence of metabotropic glutamate receptor-mediated plasticity in the neocortex of fragile X mice.* Proc Natl Acad Sci U S A, 2007. **104**(7): p. 2454-9.
69. Martin, H.G.S., et al., *Age-Dependent Long-Term Potentiation Deficits in the Prefrontal Cortex of the Fmr1 Knockout Mouse Model of Fragile X Syndrome.* Cereb Cortex, 2016. **26**(5): p. 2084-2092.
70. Yau, S.Y., et al., *Impaired bidirectional NMDA receptor dependent synaptic plasticity in the dentate gyrus of adult female Fmr1 heterozygous knockout mice.* Neurobiol Dis, 2016. **96**: p. 261-270.
71. Tian, Y., et al., *Loss of FMRP Impaired Hippocampal Long-Term Plasticity and Spatial Learning in Rats.* Front Mol Neurosci, 2017. **10**: p. 269.
72. Meredith, R.M., et al., *Increased threshold for spike-timing-dependent plasticity is caused by unreliable calcium signaling in mice lacking fragile X gene FMR1.* Neuron, 2007. **54**(4): p. 627-38.

73. Huber, K.M., et al., *Altered synaptic plasticity in a mouse model of fragile X mental retardation.* Proc Natl Acad Sci U S A, 2002. **99**(11): p. 7746-50.
74. Koekkoek, S.K., et al., *Deletion of FMR1 in Purkinje cells enhances parallel fiber LTD, enlarges spines, and attenuates cerebellar eyelid conditioning in Fragile X syndrome.* Neuron, 2005. **47**(3): p. 339-52.
75. Nosyreva, E.D. and K.M. Huber, *Metabotropic receptor-dependent long-term depression persists in the absence of protein synthesis in the mouse model of fragile X syndrome.* J Neurophysiol, 2006. **95**(5): p. 3291-5.
76. Volk, L.J., Brad E. Pfeiffer, Jay R. Gibson, and Kimberly M. Huber, *Multiple Gq-Coupled Receptors Converge on a Common Protein Synthesis-Dependent Long-Term Depression That Is Affected in Fragile X Syndrome Mental Retardation.* The Journal of Neuroscience, 2007. **27**(43): p. 11624–11634.
77. Toft, A.K., C.J. Lundbye, and T.G. Banke, *Dysregulated NMDA-Receptor Signaling Inhibits Long-Term Depression in a Mouse Model of Fragile X Syndrome.* J Neurosci, 2016. **36**(38): p. 9817-27.
78. Auerbach, B.D. and M.F. Bear, *Loss of the fragile X mental retardation protein decouples metabotropic glutamate receptor dependent priming of long-term potentiation from protein synthesis.* J Neurophysiol, 2010. **104**(2): p. 1047-51.
79. Sharma, A., et al., *Dysregulation of mTOR signaling in fragile X syndrome.* J Neurosci, 2010. **30**(2): p. 694-702.
80. Weiss, L.A., et al., *Sodium channels SCN1A, SCN2A and SCN3A in familial autism.* Mol Psychiatry, 2003. **8**(2): p. 186-94.
81. Ben-Shalom, R., et al., *Opposing Effects on NaV1.2 Function Underlie Differences Between SCN2A Variants Observed in Individuals With Autism Spectrum Disorder or Infantile Seizures.* Biol Psychiatry, 2017. **82**(3): p. 224-232.
82. Spratt, P.W.E., et al., *The Autism-Associated Gene Scn2a Contributes to Dendritic Excitability and Synaptic Function in the Prefrontal Cortex.* Neuron, 2019.
83. Shin, W., et al., *Scn2a Haploinsufficiency in Mice Suppresses Hippocampal Neuronal Excitability, Excitatory Synaptic Drive, and Long-Term Potentiation, and Spatial Learning and Memory.* Front Mol Neurosci, 2019. **12**: p. 145.
84. Alarcon, M., et al., *Linkage, association, and gene-expression analyses identify CNTNAP2 as an autism-susceptibility gene.* Am J Hum Genet, 2008. **82**(1): p. 150-9.
85. Poot, M., *Connecting the CNTNAP2 Networks with Neurodevelopmental Disorders.* Mol Syndromol, 2015. **6**(1): p. 7-22.
86. Jurgensen, S. and P.E. Castillo, *Selective Dysregulation of Hippocampal Inhibition in the Mouse Lacking Autism Candidate Gene CNTNAP2.* J Neurosci, 2015. **35**(43): p. 14681-7.
87. Fernandes, D., et al., *Disrupted AMPA Receptor Function upon Genetic- or Antibody-Mediated Loss of Autism-Associated CASPR2.* Cereb Cortex, 2019.
88. Sudhof, T.C., *Neuroligins and neurexins link synaptic function to cognitive disease.* Nature, 2008. **455**(7215): p. 903-11.
89. Levinson, J.N. and A. El-Husseini, *Building excitatory and inhibitory synapses: balancing neuroligin partnerships.* Neuron, 2005. **48**(2): p. 171-4.

90. Kim, J., et al., *Neuroligin-1 is required for normal expression of LTP and associative fear memory in the amygdala of adult animals.* Proc Natl Acad Sci U S A, 2008. **105**(26): p. 9087-92.
91. Jedlicka, P., J. Muellerleile, and S.W. Schwarzacher, *Synaptic Plasticity and Excitation-Inhibition Balance in the Dentate Gyrus: Insights from In Vivo Recordings in Neuroligin-1, Neuroligin-2, and Collybistin Knockouts.* Neural Plast, 2018. **2018**: p. 6015753.
92. Jedlicka, P., et al., *Neuroligin-1 regulates excitatory synaptic transmission, LTP and EPSP-spike coupling in the dentate gyrus in vivo.* Brain Struct Funct, 2015. **220**: p. 47-58.
93. Wu, X., et al., *Neuroligin-1 Signaling Controls LTP and NMDA Receptors by Distinct Molecular Pathways.* Neuron, 2019. **102**(3): p. 621-635 e3.
94. Jiang, M., et al., *Conditional ablation of neuroligin-1 in CA1 pyramidal neurons blocks LTP by a cell-autonomous NMDA receptor-independent mechanism.* Mol Psychiatry, 2017. **22**(3): p. 375-383.
95. Martella, G., et al., *The neurobiological bases of autism spectrum disorders: the R451C-neuroligin 3 mutation hampers the expression of long-term synaptic depression in the dorsal striatum.* Eur J Neurosci, 2018. **47**(6): p. 701-708.
96. Dang, R., et al., *Regulation of hippocampal long term depression by Neuroligin 1.* Neuropharmacology, 2018. **143**: p. 205-216.
97. Bozdagi, O., et al., *Haploinsufficiency of the autism-associated Shank3 gene leads to deficits in synaptic function, social interaction, and social communication.* Mol Autism, 2010. **1**(1): p. 15.
98. Kouser, M., et al., *Loss of predominant Shank3 isoforms results in hippocampus-dependent impairments in behavior and synaptic transmission.* J Neurosci, 2013. **33**(47): p. 18448-68.
99. Speed, H.E., et al., *Autism-Associated Insertion Mutation (InsG) of Shank3 Exon 21 Causes Impaired Synaptic Transmission and Behavioral Deficits.* J Neurosci, 2015. **35**(26): p. 9648-65.
100. Fourie, C., et al., *Dietary Zinc Supplementation Prevents Autism Related Behaviors and Striatal Synaptic Dysfunction in Shank3 Exon 13-16 Mutant Mice.* Front Cell Neurosci, 2018. **12**: p. 374.
101. Lee, K., et al., *Autism-associated Shank3 mutations alter mGluR expression and mGluR-dependent but not NMDA receptor-dependent long-term depression.* Synapse, 2019. **73**(8): p. e22097.
102. Jaramillo, T.C., et al., *Altered Striatal Synaptic Function and Abnormal Behaviour in Shank3 Exon4-9 Deletion Mouse Model of Autism.* Autism Res, 2016. **9**(3): p. 350-75.
103. Wang, X., et al., *Altered mGluR5-Homer scaffolds and corticostriatal connectivity in a Shank3 complete knockout model of autism.* Nat Commun, 2016. **7**: p. 11459.
104. O'Roak, B.J., et al., *Exome sequencing in sporadic autism spectrum disorders identifies severe de novo mutations.* Nat Genet, 2011. **43**(6): p. 585-9.
105. France, G., et al., *Multiple roles of GluN2B-containing NMDA receptors in synaptic plasticity in juvenile hippocampus.* Neuropharmacology, 2017. **112**(Pt A): p. 76-83.

106. Brigman, J.L., et al., *Loss of GluN2B-containing NMDA receptors in CA1 hippocampus and cortex impairs long-term depression, reduces dendritic spine density, and disrupts learning.* J Neurosci, 2010. **30**(13): p. 4590-600.
107. Bayer K. U., D.K.P., Leonard AS, Hell JW, Schulman H., *Interaction with the NMDA receptor locks CaMKII in an active conformation.* Nature, 2001. **411**(6839): p. 801-805.
108. Yu, S.Y., D.C. Wu, and R.Z. Zhan, *GluN2B subunits of the NMDA receptor contribute to the AMPA receptor internalization during long-term depression in the lateral amygdala of juvenile rats.* Neuroscience, 2010. **171**(4): p. 1102-8.
109. Delgado, J.Y., et al., *Rapid homeostatic downregulation of LTP by extrasynaptic GluN2B receptors.* J Neurophysiol, 2018. **120**(5): p. 2351-2357.
110. Krapivinsky, G., et al., *SynGAP-MUPP1-CaMKII synaptic complexes regulate p38 MAP kinase activity and NMDA receptor-dependent synaptic AMPA receptor potentiation.* Neuron, 2004. **43**(4): p. 563-74.
111. Kim, M.J., et al., *Differential roles of NR2A- and NR2B-containing NMDA receptors in Ras-ERK signaling and AMPA receptor trafficking.* Neuron, 2005. **46**(5): p. 745-60.
112. Araki, Y., et al., *Rapid dispersion of SynGAP from synaptic spines triggers AMPA receptor insertion and spine enlargement during LTP.* Neuron, 2015. **85**(1): p. 173-189.
113. Vazquez, L.E., et al., *SynGAP regulates spine formation.* J Neurosci, 2004. **24**(40): p. 8862-72.
114. Kopanitsa, M.V., et al., *Chronic treatment with a MEK inhibitor reverses enhanced excitatory field potentials in Syngap1(+/-) mice.* Pharmacol Rep, 2018. **70**(4): p. 777-783.
115. Clement, J.P., et al., *SYNGAP1 links the maturation rate of excitatory synapses to the duration of critical-period synaptic plasticity.* J Neurosci, 2013. **33**(25): p. 10447-52.
116. Wang, C.C., R.G. Held, and B.J. Hall, *SynGAP regulates protein synthesis and homeostatic synaptic plasticity in developing cortical networks.* PLoS One, 2013. **8**(12): p. e83941.
117. Tang, G., et al., *Loss of mTOR-dependent macroautophagy causes autistic-like synaptic pruning deficits.* Neuron, 2014. **83**(5): p. 1131-43.
118. Hanson, J.E., et al., *GluN2B antagonism affects interneurons and leads to immediate and persistent changes in synaptic plasticity, oscillations, and behavior.* Neuropsychopharmacology, 2013. **38**(7): p. 1221-33.
119. Lei, S., Chris J. McBain, *Distinct NMDA Receptors Provide Differential Modes of Transmission at Mossy Fiber-Interneuron Synapses.* Neuron, 2002. **33**: p. 921–933.
120. Graybiel, A.M., *The basal ganglia: learning new tricks and loving it.* Curr Opin Neurobiol, 2005. **15**(6): p. 638-44.
121. Smith, Y., et al., *Microcircuitry of the direct and indirect pathways of the basal ganglia.* Neuroscience, 1998. **86**(2): p. 353–387.
122. Kreitzer, A.C., *Physiology and pharmacology of striatal neurons.* Annu Rev Neurosci, 2009. **32**: p. 127-47.

123. Kreitzer, A.C. and R.C. Malenka, *Striatal plasticity and basal ganglia circuit function.* Neuron, 2008. **60**(4): p. 543-54.
124. Kravitz, A.V., et al., *Regulation of parkinsonian motor behaviours by optogenetic control of basal ganglia circuitry.* Nature, 2010. **466**(7306): p. 622-6.
125. Graybiel, A.M. and S.T. Grafton, *The striatum: where skills and habits meet.* Cold Spring Harb Perspect Biol, 2015. **7**(8): p. a021691.

CHAPTER 1: CORTICOSTRIATAL TRANSMISSION IS SELECTIVELY ENHANCED IN STRIATONIGRAL NEURONS WITH ACUTE LOSS OF *TSC1*

Katelyn Nicole Benthall

Department of Molecular and Cell Biology
University of California, Berkeley

Introduction

The mechanistic target of rapamycin (mTOR) signaling pathway is a central coordinator of cell metabolism. Activation of mTOR complex 1 (mTORC1) signals cell growth processes via stimulation of protein synthesis, organelle biogenesis, and suppression of autophagy [1]. In the nervous system, mTORC1 controls neuronal output by regulating intrinsic excitability, synaptic transmission, and long-term synaptic plasticity in a cell type-specific manner [2-8]. Tight regulation of mTOR signaling is essential, as its dysregulation is associated with a variety of neurological and psychiatric disorders [9, 10]. In particular, several neurodevelopmental disorders are caused by mutations in regulators of mTORC1. One of these, tuberous sclerosis complex (TSC), is caused by mutations in the *TSC1* or *2* genes, which encode components of a protein complex that negatively regulates mTORC1 signaling [11]. Loss of the TSC1/2 complex causes deregulated and constitutively active mTORC1, leading to a syndrome characterized by high rates of epilepsy, intellectual disability, and autism spectrum disorder (ASD) [12, 13]. How dysregulated mTORC1 signaling causes these diverse phenotypes is not well understood, but current hypotheses suggest that mTOR-dependent alterations in neuronal excitability and synaptic balance cause aberrant circuit development and function.

The specific physiological phenotypes associated with mTORC1 deregulation are cell type-dependent, suggesting that the cellular context plays an important role in determining the outcome of mTOR-pathway mutations. For example, in the hippocampus, loss of Tsc1 impairs long-term synaptic plasticity and inhibitory synapse function leading to network hyperactivity [2, 3, 5, 14]. Mosaic deletion of *Tsc1* from thalamic neurons alters their passive membrane properties and action potential kinetics in an age-dependent manner [7]. Loss of Tsc1 in the hypothalamus causes intrinsic hypoexcitability of Pomc- but not Agrp-expressing neurons [8]. In the cerebellum, deletion of *Tsc1* from Purkinje cells causes hypoexcitability and cell death with no major effects on synaptic transmission [6]. This diversity of responses to mTORC1 activation highlights the need to examine the consequences of mTOR signaling alterations in a cell type- and circuit-specific manner.

Emerging evidence suggests that changes in the activity of striatal neurons may underlie the repetitive, inflexible behaviors associated with ASD [15]. The striatum is the main input structure of the basal ganglia, a group of subcortical nuclei that control action selection, motor learning, and habit formation [16, 17]. The principal cells of the striatum are GABAergic spiny projection neurons (SPNs) that can be divided into two subtypes: striatonigral neurons of the direct pathway (dSPNs) that express type 1 dopamine receptors (D1) and striatopallidal neurons of the indirect pathway (iSPNs), which express type 2 dopamine receptors (D2) [18]. Striatal SPNs are driven by glutamatergic inputs from cortex and thalamus and project to distinct basal ganglia nuclei based on their subtype [19, 20]. Coordinated activity among ensembles of dSPNs and iSPNs determines basal ganglia output such that appropriate actions are selected while competing actions are suppressed [21, 22]. Disruptions in the balance of activity between dSPNs and iSPNs result in altered motor behaviors in a variety of neurological and psychiatric disorders [23-25], including mouse models of ASD [15]. Despite the known involvement of mTOR signaling in ASD, both in TSC and in other forms of autism [26-29], the consequences of mTORC1 dysregulation on striatal activity are largely unknown.

To elucidate the impact of TSC-mTOR signaling on striatal neuron function, we conditionally deleted *Tsc1* from striatonigral and striatopallidal neurons and examined their morphological and physiological properties. We find that acute, postnatal deletion of *Tsc1* results in a cell type-specific increase in dSPN excitability, mediated by changes in passive membrane properties, potassium channels, and dendritic morphology. In addition, loss of Tsc1 causes a selective enhancement of corticostriatal synaptic transmission in dSPNs with no major changes to thalamic or inhibitory inputs. These results indicate that increased excitability of dSPNs is a primary effect of deregulated TSC-mTOR signaling, which may lead to striatal circuit dysfunction by altering the balance of activity between dSPNs and iSPNs.

Results

Upregulation of mTORC1 and somatic hypertrophy in SPNs with Tsc1 deletion

To define the consequences of mTORC1 activation on striatal neuron function, we used a viral strategy to delete *Tsc1* from a subset of neurons in the dorsolateral striatum. We injected dilute AAV5-Cre-mCherry or AAV5-Cre-GFP into the striatum of juvenile *Tsc1$^{fl/fl}$;D2-GFP* or *Tsc1$^{fl/fl}$;D1-tdTomato* mice, respectively, and performed experiments 11-15 days later. This paradigm enables fluorescence-based identification and subsequent comparison of control (WT) and Tsc1 knock-out (KO) dSPNs and iSPNs in the same striatal slice (Figure 1A-F and Figure S1A-F). With this approach, we can isolate the cell autonomous effects of mTORC1 deregulation, independent of developmental or compensatory alterations, as only 25% of cells in the injection area express Cre recombinase and the injection site is restricted to the dorsal striatum (Figure S1G,H). In striatal sections, immunostaining with a phospho-antibody against the downstream mTORC1 pathway target S6 (p-S6, Ser240/244) revealed an increase in mTORC1 activity in all Tsc1 KO dSPNs and iSPNs compared to neighboring uninfected neurons (Figure. 1B-G and Figure S1B-F). This confirms that Tsc1/2 complex function is impaired and mTORC1 is cell-autonomously upregulated in Cre-expressing neurons.

A common phenotype associated with upregulation of mTORC1 signaling is somatic hypertrophy, which likely results from overactivation of mTORC1-regulated growth processes [3, 4, 6, 7, 30]. To investigate if striatal neurons display this phenotype, we reconstructed somas in three dimensions from histology sections and measured soma volume using the NeuN signal. Tsc1 KO dSPNs and iSPNs had significantly increased soma volume compared to controls (Figure 1H), consistent with previous findings. A significant difference in soma volume was also detected between dSPN and iSPN control cells, with dSPNs having slightly larger cell bodies (Figure 1H). We confirmed these results in a separate analysis of iSPNs in *Tsc1$^{fl/fl}$;D2-GFP* mice using the GFP signal to measure soma volume (iSPNs WT mean = 255.5 ± 2.4μm^3, iSPN KO mean = 291.8 ± 2.7μm^3, p<0.0001 K-S test).

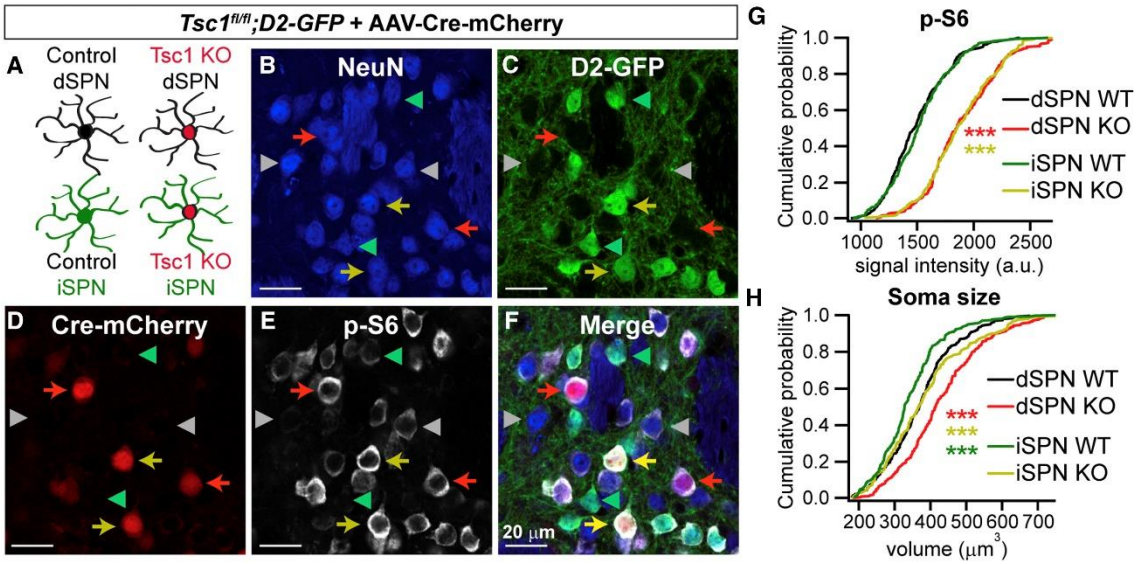

Figure 1. Mosaic loss of *Tsc1* from striatal neurons induces mTORC1 activation and somatic hypertrophy.

(A) Schematic showing the four cell types present in each striatal slice of a *Tsc1$^{fl/fl}$;D2-GFP* mouse injected with AAV5-Cre-mCherry. iSPNs are identified by GFP fluorescence and Tsc1 KO neurons are identified by nuclear mCherry expression.
(B-F) Confocal images of striatal sections immunostained with antibodies against the neuronal marker NeuN, GFP, and phosphorylated S6 (p-S6, Ser240/244), showing increased p-S6 in Cre-expressing dSPNs (red arrows) and iSPNs (yellow arrows). Grey (dSPNs) and green arrowheads (iSPNs) indicate Cre-negative control neurons.
(G-H) Cumulative distribution of p-S6 levels (G) and soma volume (H) for neurons of each genotype. n=300 neurons per genotype from 3 mice, 100 neurons per mouse. ***,p<0.0001, Kolmogorov-Smirnov test; red stars indicate significance for dSPN KO versus dSPN WT, yellow stars denote significance for iSPN KO versus iSPN WT, green stars indicate significance for dSPN WT versus iSPN WT. See also Figure S1.

Intrinsic excitability is selectively enhanced in Tsc1 KO dSPNs

To understand how loss of Tsc1 affects striatal neuron function, we first investigated how intrinsic excitability is affected by *Tsc1* deletion. We performed whole-cell current clamp recordings of identified WT and Tsc1 KO dSPNs and iSPNs in striatal slices from *Tsc1$^{fl/fl}$;D2-GFP* mice injected with AAV5-Cre-mCherry. Recordings for this and all subsequent experiments were performed from cells in the dorsolateral striatum. We injected a depolarizing current step (75pA to 400pA; 500ms) and measured firing frequency as a function of current step amplitude. We observed the previously-reported difference in frequency-current relationship between dSPN and iSPN control cells [31], with iSPNs having significantly increased intrinsic excitability (Figure 2A,B and Table S1). Interestingly, we found a significant difference between dSPN WT and Tsc1 KO neurons, with dSPN KO cells firing at a higher rate in response to current injection (Figure 2A,B and Table S1). Notably, no significant difference in frequency-current relationship was found between iSPN WT and KO neurons (Figure. 2A,B).

As another measure of excitability, we determined the rheobase, the minimum current required to elicit a single action potential, by applying a series of depolarizing current steps in 10pA increments (75pA to 300pA; 500ms). Rheobase was significantly decreased in dSPN Tsc1 KO cells compared to controls, with no changes in Tsc1 KO iSPNs (Figure 2C). Lower rheobase current in Tsc1 KO dSPNs is consistent with increased excitability as it indicates that less depolarization is required to evoke action potential firing. Consistent with the enhanced excitability of Tsc1 KO dSPNs, membrane resistance was significantly increased and capacitance was significantly decreased compared to controls (Figure S1I,J). We found no differences in the passive properties of iSPN WT and Tsc1 KO cells (Figure S1I-K). Together these findings show that postnatal loss of Tsc1 selectively enhances the intrinsic excitability of dSPNs.

In addition to passive membrane properties, inwardly-rectifying potassium channels (Kirs) are important for setting the membrane excitability of SPNs [20, 31, 32]. Previous work has shown that the excitability difference between SPN subtypes is associated with greater Kir current in dSPNs compared to iSPNs [31]. We therefore tested whether loss of Tsc1 affects Kir currents in striatal neurons. To activate potassium conductances, we applied a series of voltage steps (-150mV to -60mV; 500ms) in 10mV increments in whole-cell voltage clamp recordings. The predominant current in SPNs at hyperpolarized membrane potentials is through Kir channels; however, there is some contribution of leak conductances. To isolate Kir current, we blocked Kir channels with 1mM CsCl and repeated the voltage step protocol. Kir currents were isolated from the Cs-insensitive leak conductances using digital subtraction (Figure 2D) [33]. As previously

reported, Kir current was significantly larger in dSPN than iSPN control cells (Figure 2D,E and Table S1). Consistent with the enhanced intrinsic excitability of dSPN Tsc1 KO neurons, there was a significant decrease in Kir current in dSPN Tsc1 KO cells compared to controls (Figure 2D,E and Table S1). Interestingly, we also observed a small enhancement of Kir current in Tsc1 KO iSPNs compared to WT iSPNs (Figure 2D,E).

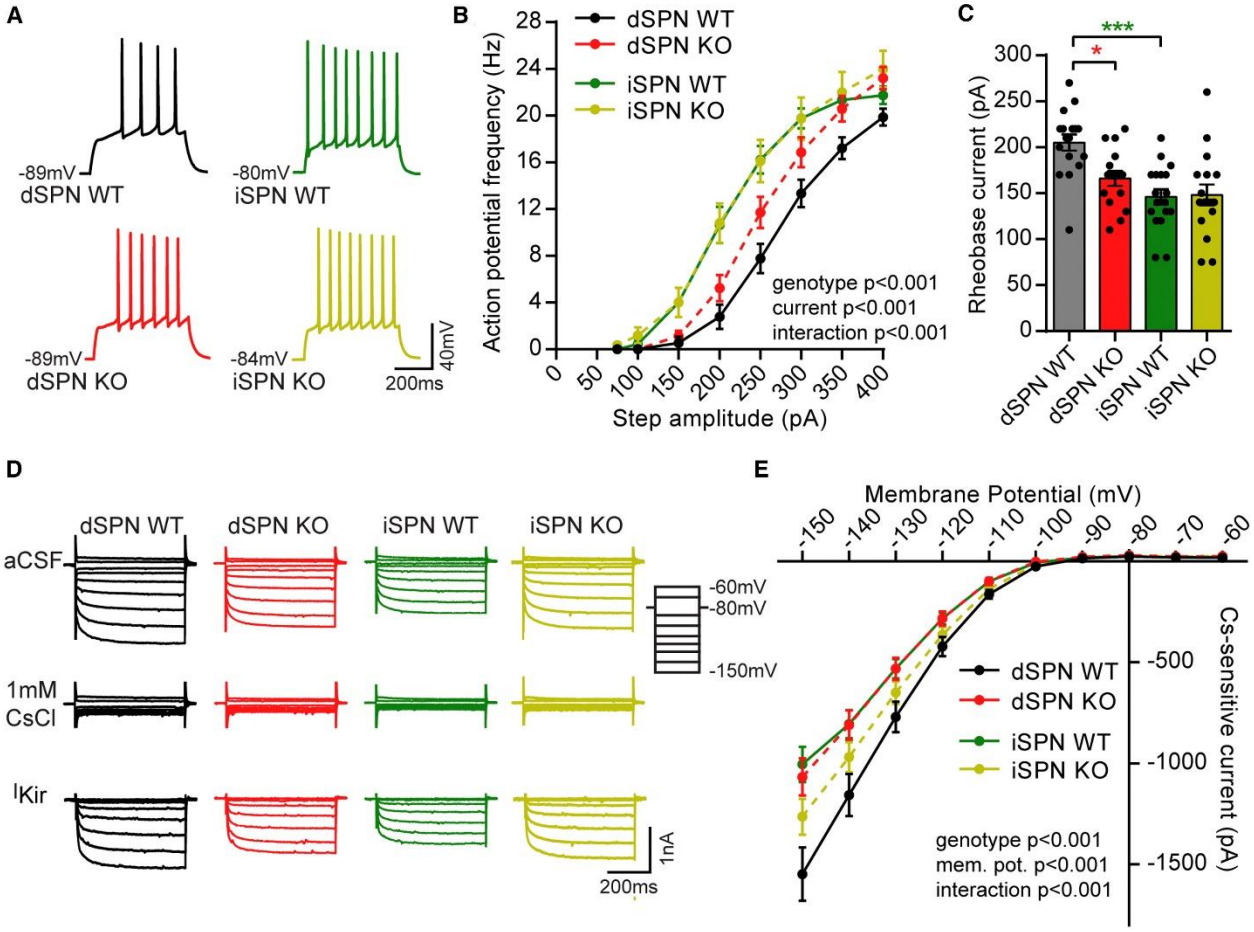

Figure 2. Postnatal loss of *Tsc1* increases the intrinsic excitability of dSPNs.
(A) Example traces showing action potentials evoked by a 250pA current step for each cell type. The resting membrane potential is indicated to the left of each trace.
(B) Frequency-current relationship for control (WT) and Tsc1 KO dSPNs and iSPNs, displayed as mean +/- SEM. Two-way ANOVA P values are shown. P values for the Sidak's post-hoc tests are in Table S1. dSPN WT n=18 neurons from 15 mice, dSPN KO n=21 neurons from 14 mice, iSPN WT n=18 neurons from 16 mice, iSPN KO n=17 neurons from 13 mice.
(C) Bar graph shows the mean +/- SEM rheobase for each condition. Dots indicate the values for individual neurons. *,p<0.05; ***,p<0.001, one-way ANOVA with Sidak post-hoc tests (see Table S2 for all P values); dSPN WT n=17 neurons from 15 mice, dSPN KO n=16 neurons from 13 mice, iSPN WT n=18 neurons from 16 mice, iSPN KO n=17 neurons from 13 mice.
(D) Example traces of inward-rectifying potassium channel currents in dSPNs and iSPNs. Kir channel currents were obtained by applying negative voltage steps to the membrane (-150mV to -60mV in 10mV increments) in the presence and absence of 1mM CsCl. The cesium-sensitive component (I_{Kir}) was revealed using digital subtraction.
(E) Quantification of I_{Kir} at different membrane potentials across genotypes. Data are represented as mean +/- SEM. Two-way ANOVA P values are shown. P values for the Sidak's post-hoc tests are in Table S2.

dSPN WT n=10 neurons from 10 mice, dSPN KO n=10 neurons from 8 mice, iSPN WT n=10 neurons from 10 mice, iSPN KO n=9 neurons from 9 mice. See also Figure S1.

Dendritic complexity is reduced in Tsc1 KO dSPNs

The degree of dendritic arborization strongly influences the membrane excitability of SPNs [31]. We therefore examined how dendrite morphology is affected by loss of Tsc1 as this could contribute to changes in excitability. Neurobiotin was dialyzed into cells during whole-cell recordings and visualized in fixed tissue sections using fluorophore-conjugated avidin. Dendritic arbors were reconstructed in three dimensions (Figure 3A) and arborization was quantified by Sholl analysis. We found that the dendritic complexity of dSPN Tsc1 KO cells was significantly decreased compared to that of controls, while iSPN Tsc1 KO and control cells had a similar Sholl profile (Figure 3A-C and Table S1). Consistent with these findings, total dendritic length was significantly decreased in dSPN Tsc1 KO cells, resulting from decreased dendrite branching (Figure 3D-F and Tables S2 and S3). Similar to prior reports [31], we found that dSPN control cells had significantly greater dendritic complexity, total dendritic length, number of primary dendrites, and branch points compared to iSPNs (Figure 3D-F and Tables S2 and S3). Taken together, these results demonstrate that acute loss of Tsc1 and cell-autonomous activation of mTORC1 signaling affects the intrinsic properties of dSPNs in multiple ways, with the net effect of enhancing their excitability.

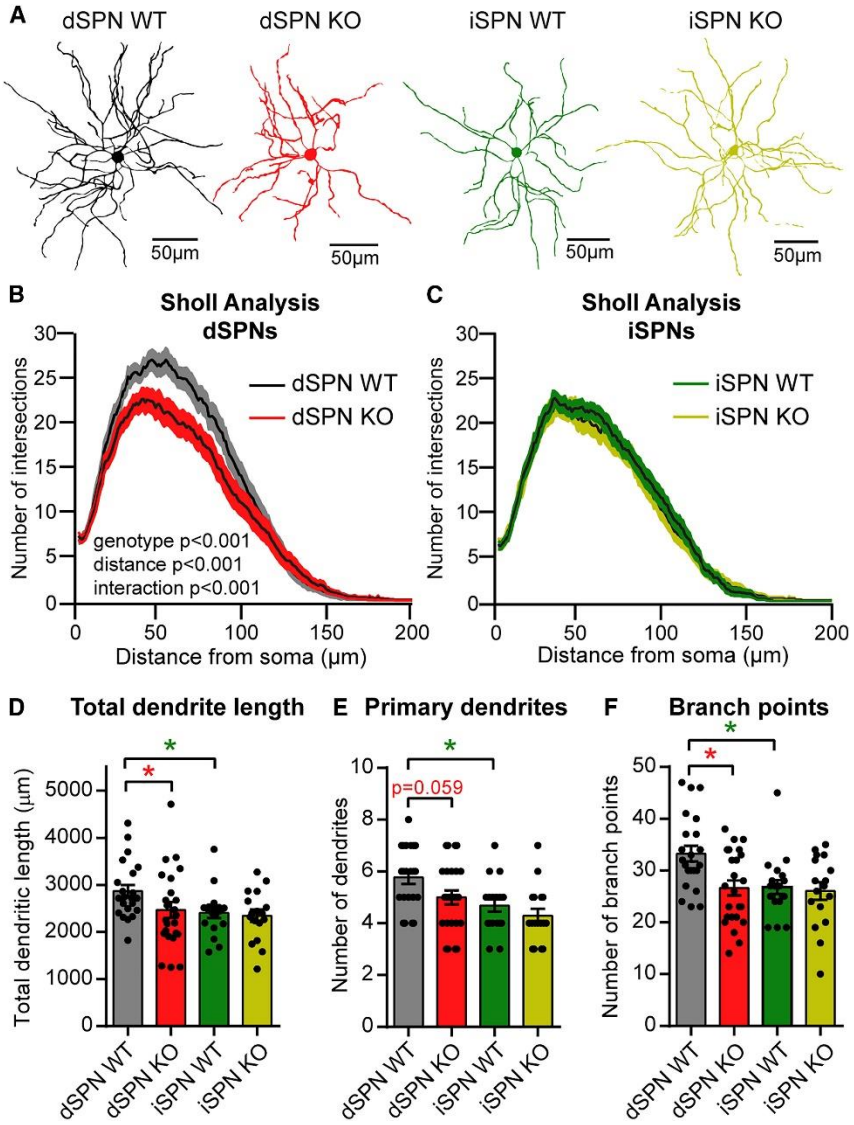

Figure 3. Tsc1 KO dSPNs have reduced dendritic arborization.
(A) Example 3-dimensional (3D) reconstructions of neurobiotin-filled SPNs of each condition.
(B,C) 3D Sholl analysis of dSPN and iSPN dendritic arbors. Circles of increasing radii were drawn at 1μm intervals from the center of the soma and the number of dendrite crossings was quantified for each condition. Black lines indicate the mean and shaded regions show the SEM. Two-way ANOVA P values are shown (see also Table S1).
(D-F) Mean +/- SEM of the total dendrite length (D), number of primary dendrites (E), and number of dendrite branch points (F) per neuron quantified by 3D Sholl analysis for each condition. Dots indicate the values for individual neurons. *,p<0.05, Kruskal-Wallis with Dunn's post-hoc test (total dendritic length and number of branch points, see Table S3 for P values) and one-way ANOVA with Sidak post-hoc test (number of primary dendrites, see Table S2 for P values). For all graphs, dSPN WT n=22 neurons from 21 mice, dSPN KO n=24 neurons from 19 mice, iSPN WT n=19 neurons from 19 mice, iSPN KO n=17 neurons from 16 mice.

Loss of Tsc1 does not affect synaptic inhibition in SPNs

mTORC1 is an important regulator of synaptic properties in several neuron types and changes in synaptic function are thought to underlie mTOR-related disorders [34]. For example, in hippocampal neurons, loss of Tsc1 and activation of mTORC1 increases

the excitatory/inhibitory synaptic ratio due to a strong decrease in inhibitory synapse function [2]. To determine how loss of Tsc1 affects the synaptic properties of striatal neurons, we examined baseline inhibitory transmission by recording miniature inhibitory postsynaptic currents (mIPSCs) in *Tsc1$^{fl/fl}$;D2-GFP* mice injected with AAV5-Cre-mCherry (Figure 4A). No differences in average mIPSC amplitude or frequency were observed with *Tsc1* deletion in either SPN type (Figure 4B-E). To determine whether loss of Tsc1 affects evoked inhibitory synaptic transmission, we recorded electrically-evoked IPSCs in simultaneously recorded pairs of WT and Tsc1 KO dSPNs or iSPNs. We found no difference in IPSC amplitude between Tsc1 KO SPNs and controls (Figure 4F-H). Because SPNs receive many sources of inhibition [35] that could be differentially affected by *Tsc1* deletion and may be masked by measurements of bulk inhibition, we assayed inhibition in an input-specific manner. Fast-spiking parvalbumin-expressing interneurons (PV cells) control the spiking of SPNs via feed-forward inhibition [36] and their dysfunction has been implicated in striatal-based disorders [37]. To selectively activate inputs from PV cells, we bred the *Tsc1$^{fl/fl}$;D1-tdTomato* mice to mice expressing FlpO recombinase under the *parvalbumin* promoter (*Pvalb-2A-FlpO-D*, [38]). Juvenile mice were injected with AAV5-fDIO-ChR2-EYFP [39] and AAV5-Cre-GFP to selectively express Flp in PV cells and delete *Tsc1* from a subset of striatal neurons, respectively. We performed simultaneous paired recordings of Tsc1 KO and control dSPNs and activated PV cell inputs using full field optical stimulation (Figure 4I-J). We found no difference in the amplitude of optically-evoked IPSCs (oIPSCs) between Tsc1 KO and control dSPNs (Figure 4K). Together these results show that acute, postnatal loss of Tsc1 does not strongly affect inhibitory synaptic function in SPNs.

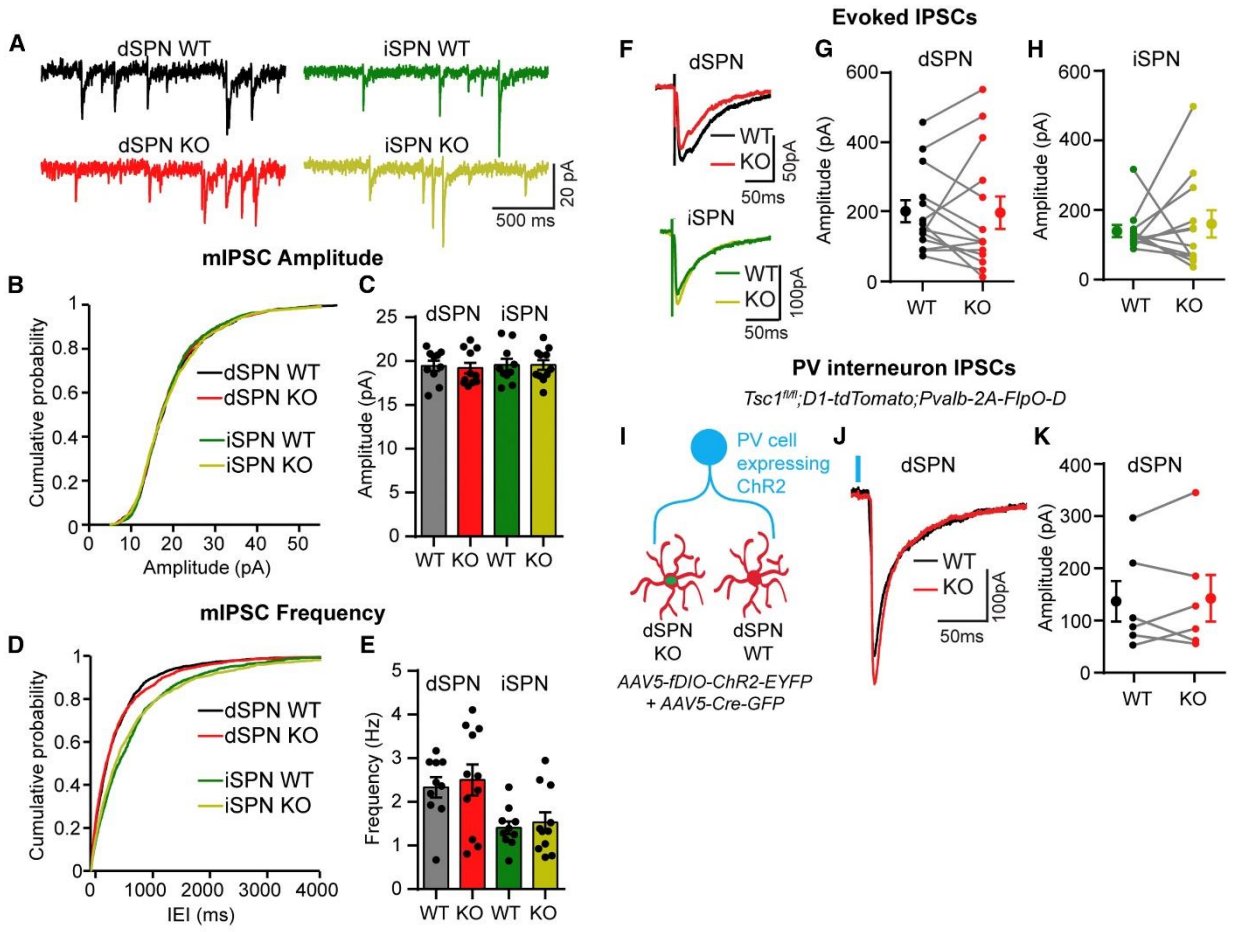

Figure 4. Inhibitory synaptic transmission is not affected by loss of Tsc1.

(A) Example traces of miniature inhibitory post-synaptic currents (mIPSCs) recorded from each cell type.

(B) Cumulative distribution of mIPSC amplitudes from neurons of each genotype.

(C) Mean +/- SEM mIPSC amplitude per neuron for each genotype.

(D) Cumulative distribution of mIPSC inter-event intervals (IEI) from neurons of each genotype.

(E) Mean +/- SEM mIPSC frequency per neuron. For B-E, n=200 mIPSCs per neuron, dSPN WT n=10 neurons from 7 mice, dSPN KO n=11 neurons from 8 mice, iSPN WT n=10 neurons from 9 mice, iSPN KO n=11 neurons from 9 mice.

(F) Examples of simultaneously recorded IPSCs from pairs of Tsc1 WT and KO dSPNs and iSPNs, evoked by intra-striatal electrical stimulation.

(G,H) Graphs displaying the IPSC amplitude recorded from pairs of Tsc1 WT and KO dSPNs (G, n=14 pairs from 10 mice) or iSPNs (H, n=12 pairs from 10 mice).

(I) An AAV5 expressing Flp-dependent ChR2 was injected into the striatum of *Tsc1$^{fl/fl}$;D1-tdTomato;Pvalb-2A-FlpO-D* mice, followed by injection of AAV5-Cre-GFP. Paired recordings were made between Tsc1 WT and KO dSPNs and PV-neuron inputs were activated by blue light stimulation.

(J) Examples of simultaneously recorded PV-IPSCs from a pair of Tsc1 WT and KO dSPNs, evoked by optogenetic stimulation. Blue line indicates light onset.

(K) Graph displaying the PV-IPSC amplitude recorded in pairs of Tsc1 WT and KO dSPNs, n=6 pairs from 6 mice.

For all panels, dots indicate the values of individual neurons. For panels G, H, & K the filled circles with error bars indicate the group mean +/- SEM. See Tables S2 and S4 for P values for statistical comparisons.

Synaptic excitation is selectively increased in Tsc1 KO dSPNs

SPNs exhibit low baseline firing activity but are strongly driven by glutamatergic inputs [40]. In other neuron types, loss of Tsc1 affects excitatory synaptic properties [3, 4]. To test whether loss of Tsc1 affects excitatory synaptic transmission in SPNs, we recorded miniature excitatory postsynaptic currents (mEPSCs) in *Tsc1$^{fl/fl}$;D2-GFP* mice injected with AAV5-Cre-mCherry (Figure 5A). No difference in the average mEPSC amplitude was found between conditions; however, the frequency of mEPSCs was selectively increased in dSPN Tsc1 KO cells compared to controls (Figure 5B-E). We verified that these results were not specific to the *D2-GFP* transgenic mouse line by repeating this experiment in *Tsc1$^{fl/fl}$;D1-tdTomato* mice. Again, we found a selective increase in mEPSC frequency in Tsc1 KO dSPNs but not iSPNs (Figure S2A-C). Enhanced mEPSC frequency can result from either an increase in the number of excitatory synapses or an increase in presynaptic release probability. To test whether synapse number was affected by Tsc1 loss, we measured the density of dendritic spines, the sites of excitatory synapses onto SPNs, and found no difference between control and Tsc1 KO dSPNs (Figure S2D,E).

To determine whether loss of Tsc1 affects evoked excitatory synaptic transmission, we recorded electrically-evoked EPSCs in simultaneously recorded pairs of WT and Tsc1 KO dSPNs or iSPNs (Figure 5F). Consistent with the mEPSC experiments, dSPN Tsc1 KO cells had significantly larger EPSCs than controls (Figure 5G). No difference in EPSC amplitude was observed between iSPN WT and Tsc1 KO cells (Figure 5H). To test whether increased EPSC amplitude and mEPSC frequency in Tsc1 KO dSPNs were due to changes in presynaptic release probability, we performed paired-pulse experiments and found a decrease in the paired-pulse ratio in dSPN Tsc1 KO cells compared to controls, indicating enhanced presynaptic release probability (Figure 5I-K). No differences in the paired-pulse ratio were observed between iSPN WT and Tsc1 KO cells (Figure 5I-K). These results demonstrate that loss of Tsc1 selectively alters excitatory/inhibitory synaptic balance in dSPNs via a strengthening of glutamatergic inputs without a concurrent change to GABAergic transmission.

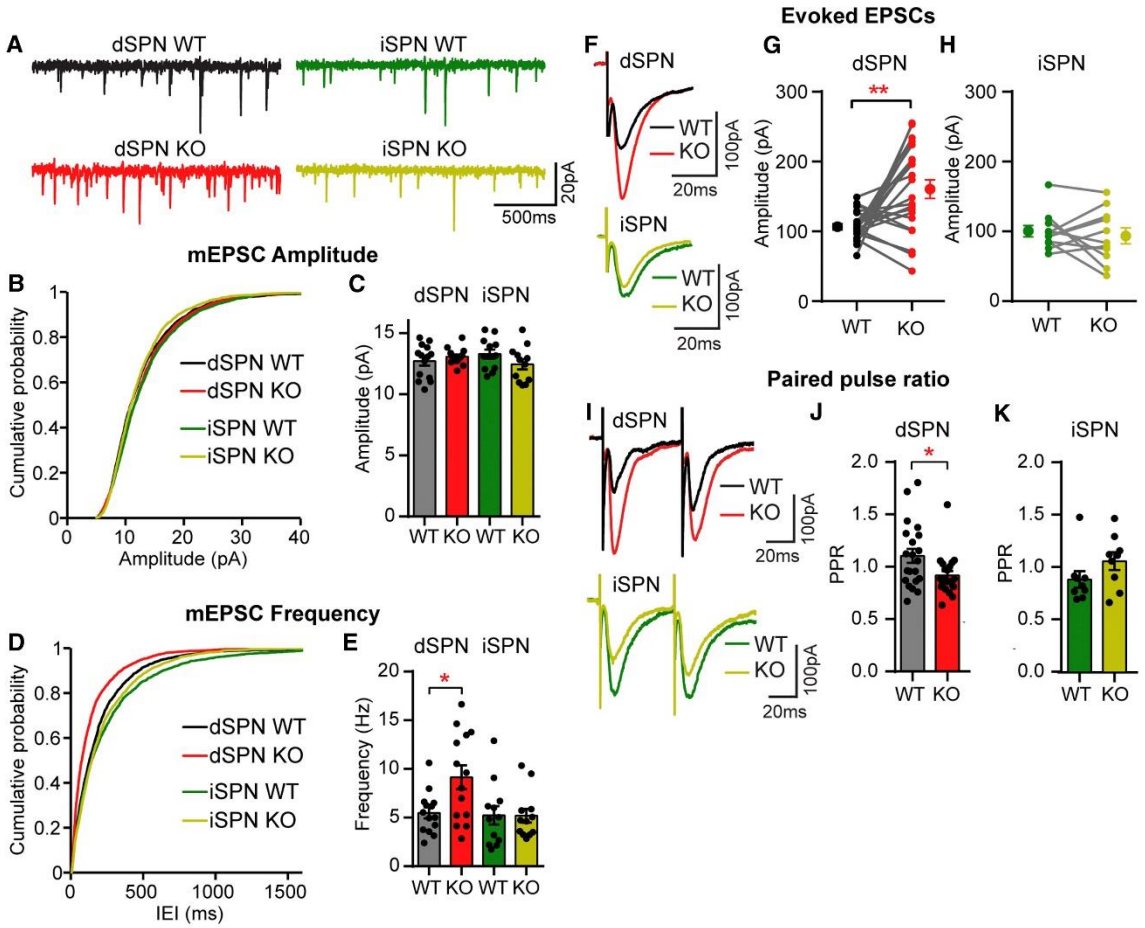

Figure 5. Excitatory synaptic transmission is increased in Tsc1 KO dSPNs.
(A) Example traces of miniature excitatory post-synaptic currents (mEPSCs) recorded from each cell type.
(B) Cumulative distribution of mEPSC amplitudes from neurons of each genotype.
(C) Mean +/- SEM mEPSC amplitude per neuron for each genotype.
(D) Cumulative distribution of mEPSC inter-event intervals (IEI) from neurons of each genotype.
(E) Mean +/- SEM mEPSC frequency per neuron. *,p<0.05, one-way ANOVA with Sidak post-hoc test. For B-E, n=200 mEPSCs per neuron, dSPN WT n=14 neurons from 10 mice, dSPN KO n=14 neurons from 10 mice, iSPN WT n=12 neurons from 8 mice, iSPN KO n=12 neurons from 8 mice.
(F) Examples of simultaneously recorded EPSCs from Tsc1 WT and KO pairs of dSPN and iSPNs evoked by intra-striatal electrical stimulation.
(G,H) Graphs displaying the EPSC amplitude recorded from pairs of Tsc1 WT and KO dSPNs (G, n=22 pairs from 19 mice) or iSPNs (H, n=11 pairs from 6 mice). **,p<0.01, paired t-test. Dots indicate the values of individual neurons, filled circles with error bars indicate the group mean +/- SEM.
(I) Example recordings of electrically-evoked EPSCs from two stimuli delivered 50ms apart.
(J,K) Mean +/- SEM paired pulse ratio (PPR, defined as the amplitude of the second EPSC peak divided by the first) in Tsc1 WT and KO dSPNs (J, n=21 cells from 19 mice) and iSPNs (K, n=9 cells from 6 mice). *,p<0.05, unpaired t-test.
For all panels, dots indicate the values of individual neurons. See Tables S2 and S4 for P values for statistical comparisons. See also Figure S2.

Selective enhancement of corticostriatal transmission onto Tsc1 KO dSPNs

The major excitatory inputs to the striatum arise from the cortex and thalamus [41], either or both of which could mediate the increased excitatory drive observed in dSPN Tsc1 KO cells. Determining the source of the enhanced excitation is important for

understanding its functional consequences, as thalamostriatal terminals are involved in attention and switching between tasks, whereas corticostriatal synapses are implicated in motor learning and habit formation [16, 17, 42]. To activate specific glutamatergic inputs, we expressed channelrhodopsin (AAV5-ChR2-mCherry) in either the thalamus or cortex of *Tsc1$^{fl/fl}$;D1-tdTomato* mice injected with AAV5-Cre-GFP (Figure 6A,D) and measured input-specific synaptic responses in simultaneously recorded pairs of WT and Tsc1 KO dSPNs. In response to optical stimulation of thalamostriatal terminals, we found no difference in the amplitude of subthreshold excitatory postsynaptic potentials (oEPSPs) between control and Tsc1 KO dSPNs (Figure 6B,C). However, stimulation of cortical terminals resulted in significantly greater oEPSP amplitude in dSPN Tsc1 KO cells compared to WT, indicating that corticostriatal drive is selectively enhanced in Tsc1 KO dSPNs (Figure 6E,F).

To understand how stronger corticostriatal input could affect dSPN activity, we measured cortically-driven action potentials (oAPs) in simultaneously recorded pairs of dSPN WT and Tsc1 KO cells in the absence of synaptic blockers. To achieve robust cortical ChR2 expression sufficient to drive SPN firing, we bred *Tsc1$^{fl/fl}$;D1-tdTomato* mice to mice expressing ChR2-YFP under the *Thy1* promoter (*Thy1-ChR2-YFP*), which is expressed in cortical neurons [43] (Figure 6G). Optical stimulation of corticostriatal terminals resulted in a significantly shorter latency to fire in dSPN Tsc1 KO cells compared to simultaneously recorded controls (Figure 6H,I). We also observed a trend toward decreased jitter in Tsc1 KO dSPNs (Figure 6J). These results demonstrate that loss of Tsc1 from dSPNs enhances corticostriatal transmission and alters dSPN firing properties in response to cortical stimulation.

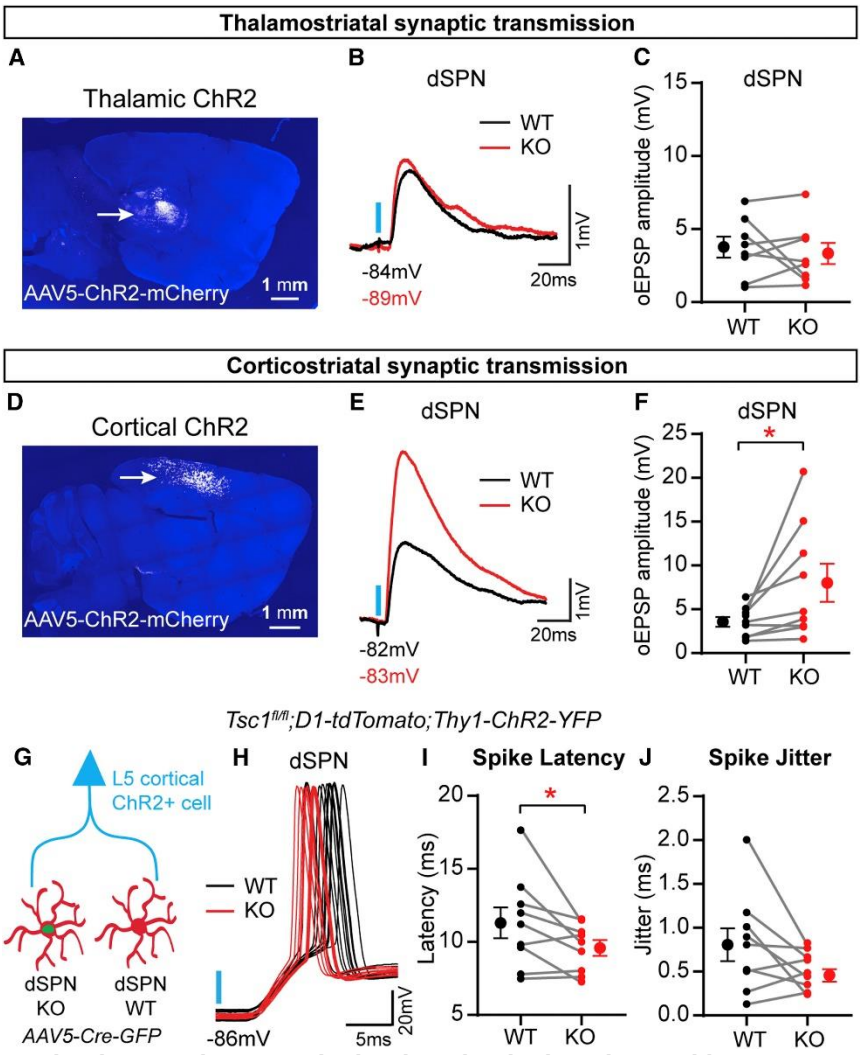

Figure 6. Corticostriatal synaptic transmission is selectively enhanced in Tsc1 KO dSPNs.

(A) AAV5-ChR2-mCherry was injected into the thalamus of neonate *Tsc1$^{fl/fl}$;D1-tdTomato* mice, followed by injection of AAV5-Cre-GFP into the dorsal striatum at P14-16. Confocal image of a sagittal section showing ChR2-mCherry expression in the thalamus (arrow).

(B) Examples of simultaneously recorded excitatory post-synaptic potentials (EPSPs) from a pair of Tsc1 WT and KO dSPNs, evoked by blue light stimulation of thalamostriatal terminals (blue line).

(C) Graph displaying thalamostriatal optogenetically-evoked EPSP ("oEPSP") amplitude recorded in pairs of Tsc1 WT and KO dSPNs, n=8 pairs of neurons from 5 mice.

(D) AAV5-ChR2-mCherry was injected into the cortex of neonate *Tsc1$^{fl/fl}$;D1-tdTomato* mice, followed by injection of AAV5-Cre-GFP into the dorsal striatum at P14-16. Confocal image of a sagittal section showing ChR2-mCherry expression in the cortex (arrow).

(E) Examples of simultaneously recorded EPSPs from a pair of Tsc1 WT and KO dSPNs, evoked by blue light stimulation of corticostriatal terminals (blue line).

(F) Graph displaying corticostriatal oEPSP amplitude recorded in pairs of Tsc1 WT and KO dSPNs. *,p<0.05; paired t-test; n=9 pairs of neurons from 8 mice.

(G) *Tsc1$^{fl/fl}$;D1-tdTomato;Thy1-ChR2-YFP* mice were injected with AAV5-Cre-GFP, and recordings of light-evoked corticostriatal action potentials (oAPs) were made from simultaneous pairs of dSPN WT and KO cells.

(H) Examples of corticostriatal oAPs recorded over 6 trials from a pair of Tsc1 WT and KO dSPNs. Blue line indicates light onset.

(I) Graph displaying the average spike latency per neuron for pairs of simultaneously recorded Tsc1 WT and KO dSPNs. Spike latency was defined as the time in milliseconds from the onset of blue light stimulation to the action potential threshold. *,$p<0.05$; paired t-test.
(J) Graph displaying the spike jitter per neuron for pairs of simultaneously recorded Tsc1 WT and KO dSPNs. Jitter was defined as the standard deviation of latency to action potential threshold for 4-11 stimulation trials per neuron. For I & J, n=9 pairs of neurons from 9 mice.
For panels C,F,I & J, dots indicate the values of individual neurons, filled circles with error bars indicate the group mean +/- SEM for paired recordings. See Table S4 for P values for statistical comparisons.

Discussion

In this study, we determined how activation of mTORC1 signaling affects striatal physiology by deleting the mTORC1 negative regulator *Tsc1* from a subset of neurons in the dorsal striatum. With this approach, we gained a detailed understanding of how TSC-mTORC1 signaling affects SPN morphology and function in a cell-autonomous manner, independent of major network or developmental alterations. We found that the primary effect of Tsc1 loss was an increase in dSPN excitability with minimal effects on iSPNs. Both intrinsic and corticostriatal synaptic excitability were enhanced by *Tsc1* deletion in dSPNs without concurrent changes to synaptic inhibition or thalamostriatal excitation. The net effect of these changes was decreased latency of Tsc1 KO dSPNs to fire in response to cortical stimulation. These findings demonstrate that loss of Tsc1 and constitutive activation of mTORC1 signaling strongly affects the properties of direct pathway neurons such that cortical excitation is facilitated, with relatively little impact on neurons comprising the indirect pathway.

An interesting aspect of our study is that we observed increased dSPN, but not iSPN, intrinsic excitability due to acute loss of Tsc1, which was associated with increased membrane resistance and reduced capacitance. The increased excitability of Tsc1 KO dSPNs contrasts with the reduced excitability that has been observed in other cell types with Tsc1 loss including hippocampal CA1 neurons, thalamic neurons, and Purkinje cells [2, 6, 7]. Compared to these cell types, we observed a relatively modest increase in soma size in Tsc1 KO SPNs (~14% increase in SPNs versus a 41% increase in CA1 neurons with Tsc1 loss [3]). We also found that dendritic arborization was reduced in Tsc1 KO dSPNs. This decreased dendritic complexity likely has a stronger impact on the cell's passive membrane properties relative to the small increase in soma size leading to a net decrease in membrane capacitance and increase in resistance. These changes in passive membrane properties, together with the reduced Kir currents we observed, likely drive increased excitability in Tsc1 KO dSPNs. The fact that Tsc1 KO iSPNs showed a similar small increase in soma size as dSPNs but did not have major changes in dendritic morphology or Kir currents further indicates that these factors were responsible for the excitability changes in Tsc1 KO dSPNs. Notably, loss of Tsc1 has been shown to have cell type-specific effects on the excitability of hypothalamic neurons, whereby Pomc-expressing Tsc1 KO neurons exhibit hypoexcitability but Agrp-expressing Tsc1 KO neurons show no change in excitability, similar to iSPNs [8].

Cell type-specific changes in intrinsic excitability and dendritic morphology have been observed in SPNs in response to a variety of disease-related insults. For example, intrinsic excitability is increased and dendritic arborization is decreased in dSPNs but not iSPNs in L-DOPA induced dyskinesia, in which mTOR signaling has been implicated as hyperactive [44-46]. Huntington's disease mouse models are associated with low mTOR signaling and display altered potassium currents as well as iSPN-specific degeneration [47-49]. The fact that phenotypes specific to either dSPNs or iSPNs are seen across mTOR-associated diseases is likely due to molecular differences between the two SPN subtypes. Although dSPNs and iSPNs are similar in many respects, they express distinct profiles of receptors and signaling molecules [50], which will define their response to disease-related perturbations. Since the mTOR pathway integrates a variety of intra- and extracellular signals, and shows extensive cross-talk with other signaling pathways, the outcomes of its activation are highly sensitive to the cellular context. Here we find no

differences in the basal phosphorylation state of the mTORC1-pathway target S6 between dSPNs and iSPNs. In addition, Tsc1 loss elevated p-S6 levels to a similar extent in dSPNs and iSPNs. Together these observations suggest that the core components of mTORC1 signaling are not different between dSPNs and iSPNs but that the consequences of mTORC1 activation on downstream pathways are cell type-dependent.

Changes in synaptic transmission are often, but not always [6], observed in response to loss of Tsc1 [2-4, 14]. In particular, we have previously shown that deletion of *Tsc1* from hippocampal CA1 neurons causes a loss of inhibitory synaptic transmission resulting in increased excitatory/inhibitory synaptic ratio [2]. Changes in E/I balance are hypothesized to contribute to ASD pathophysiology [51] and a recent study showed cell type-specific alterations in E/I ratio in dSPNs resulting from mutations in the ASD-risk gene *Nlgn3* [52]. Here we found that synaptic E/I balance was also selectively altered in dSPNs following *Tsc1* deletion; however, this was driven by an increase in excitatory synaptic drive without a change in inhibition. The downstream consequences of increased E/I ratio in dSPNs remain to be explored, however, such a change is likely to increase the efficacy of the direct pathway to suppress basal ganglia output nuclei, thereby relieving their inhibition of downstream motor centers [24, 53]. Notably, corticostriatal synaptic transmission was selectively increased in Tsc1 KO dSPNs while thalamostriatal transmission was unaltered. Similar pathway-specific increases in corticostriatal transmission have been observed in the *Shank3B*$^{-/-}$ mouse model of autism and in the *Sapap3*$^{-/-}$ mouse model of obsessive-compulsive disorder [54, 55], suggesting that enhanced corticostriatal activity in the dorsal striatum may be involved in the pathophysiology of multiple psychiatric disorders.

We found that the enhanced corticostriatal transmission in Tsc1 KO dSPNs was mediated by an increase in presynaptic release probability. This is supported by our observation of decreased paired-pulse ratio with no changes in mEPSC amplitude or dendritic spine density, which would indicate alterations in postsynaptic strength or synapse number, respectively. Since Cre expression was limited to striatal neurons in our model and the cortical inputs were wild-type for *Tsc1*, this suggests a change in retrograde signaling from SPN dendrites to excitatory presynaptic terminals. Corticostriatal synapses are known to undergo endocannabinoid-dependent long-term depression (eCB-LTD), which is mediated by changes in presynaptic release probability [56]. It is possible that deregulated mTORC1 signaling interferes with the production or release of endocannabinoids or other retrograde signaling molecules from dSPNs, a direction that could be explored in future studies. Such a mechanism may also explain the input-specificity of the phenotype, as thalamostriatal synapses do not undergo substantial eCB-LTD [57].

The relative timing of activation of the direct and indirect pathways is important for habit formation [58]. For example, shorter latency of dSPNs to fire relative to iSPNs in response to cortical stimulation is correlated with preference to use more habitual strategies when learning an operant task [58]. Interestingly, we found that *Tsc1* deletion caused dSPNs to fire with reduced latency in response to optogenetic cortical stimulation. Further, there was a trend toward decreased action potential jitter in Tsc1 KO dSPNs across multiple stimulation trials, which could have implications for spike-timing dependent plasticity [59]. These results suggest that loss of Tsc1 and upregulation of mTORC1 in SPNs enhances cortical activation of the direct pathway, which may have

consequences on striatal function in the context of mTOR-related disorders. Future studies will determine if the cellular changes described here result in altered striatal-associated behaviors, with the goal of understanding how striatal dysfunction contributes to psychiatric disorders such as ASD.

Experimental Procedures

Mice

Animal experiments were performed in accordance with protocols approved by UC Berkeley's Animal Care and Use Committee. Male and female mice were used for all experiments. The ages used are indicated below for each experiment. All *D2-GFP* and *D1-tdTomato* mice used for experiments were hemizygous for the BAC transgene to avoid potential physiological or behavioral alterations [60, 61, 62].

Mouse line	**Source**	**Reference**
Tsc1$^{fl/fl}$	JAX strain #005680	[63]
Drd2-EGFP (referred to as D2-GFP)	GENSAT (MMRRC #000230-UNC)	[64]
Drd1a-tdTomato (referred to as D1-tdTomato)	JAX strain #016204	[65]
Pvalb-2A-FlpO-D	JAX strain #022730	[66]
Thy1-ChR2-YFP	JAX strain #007612	[67]

Stereotaxic surgery

Mice were anesthetized with isoflurane and mounted on a stereotaxic frame equipped with ear cups. 800nl of an AAV serotype 5 chicken β-Actin promoter-driven Cre-mCherry or Cre-EGFP virus (Penn Vector Core) was unilaterally injected into the dorsolateral striatum of postnatal day (P) 14-16 *Tsc1$^{fl/fl}$;D2-GFP* or *Tsc1$^{fl/fl}$;D1-tdTomato* mice, respectively. Injections were made at A/P +0.7 mm, M/L +1.65 mm, D/V -2.4 mm relative to Bregma at a rate of 100 nl/min. Cre virus was diluted 20-30 times in sterile saline to achieve sparse transduction. Mice were used for experiments 11-15 days after Cre virus injection at P25-31.

For the oIPSC experiments, Flp-dependent Ef1a promoter-driven AAV-fDIO-ChR2-EYFP virus [39] was injected unilaterally into the dorsolateral striatum of P15-17 *Tsc1;D1-tdTomato;Pvalb-2A-FlpO-D* mice, followed by injection of AAV-Cre-GFP at P34-37. For oAP experiments, *Tsc1$^{fl/fl}$;D1-tdTomato;Thy1-ChR2-YFP* mice were injected with AAV5-Cre-EGFP into the dorsolateral striatum at P20-27. For oEPSP experiments, CAG promoter-driven AAV-ChR2-mCherry was injected into either the cortex or thalamus of cryo-anesthetized neonatal mice. At P14-16, AAV5-Cre-EGFP virus was injected into the dorsolateral striatum as described above. For oEPSP experiments, neonatal mice (P0-3) were briefly cryo-anesthetized and placed in a head mold. 200 nL of AAV serotype 5, CAG promoter-driven ChR2-mCherry virus (Penn Vector Core, diluted 1:2) was injected at 200 nL/min unilaterally at three different cortical or thalamic sites. To target the cortex, injections were made halfway between bregma and lambda with three injections made between 0 and 1.5 mm from the sagittal suture, 0.5 mm down from the surface of the head. To target the thalamus, the injections were made approximately 1 mm anterior to lambda with the injection sites -1 to 1mm from the sagittal suture, 3 mm down from the surface of the head. At P14-16, AAV5-Cre-GFP virus was injected into the dorsolateral striatum as described above. Injection sites were verified post-hoc by fluorophore expression.

Immunohistochemistry

P25-31 mice were perfused transcardially with 1× PBS and 4% paraformaldehyde. Brains were post-fixed in 4% paraformaldehyde overnight and sectioned at 30 µm. Sections were blocked for 1h at room temperature (RT) in BlockAid (Thermo Fisher Scientific) and incubated overnight at 4°C with antibodies against phosphorylated (Ser240/244) S6 ribosomal protein (1:800, Cell Signaling Technology, catalog # 5364S), GFP (1:5000, Abcam #ab13970) and NeuN (1:800, Millipore #MAB377). The following day, sections were washed and incubated for 1h at RT with Alexa Fluor 633-, 488-, and 405-conjugated secondary antibodies (1:500, Invitrogen #A-21070, A11039, and A-31553). Sections were mounted onto slides using ProLong Gold antifade reagent (Invitrogen).

Imaging and analysis

Z-stack images were taken on a confocal microscope (Olympus Fluoview FV1000) with a 20x objective using the same exposure and acquisition settings for each section. To quantify p-S6 levels and soma volume, regions of interest (ROIs) were automatically generated in Imaris software based on the NeuN signal. The mean fluorescence intensity per ROI and average soma volume were calculated using Imaris. iSPNs were identified based on the expression of D2-GFP.

Dendrite morphology reconstruction

For anatomical reconstruction, 4mg/mL neurobiotin was included in the internal solution during whole-cell recordings. Slices were recovered and fixed in 4% paraformaldehyde for 24-48 h. After washes in PBS, slices were reacted with 1:750 streptavidin-AlexaFluor 633 (Invitrogen) in 2.5% Triton-X prepared in PBS for 1h. Sections were then washed and coverslipped using ProLong Gold antifade reagent. Dendrite arborization were quantified using 3D Sholl analysis in Imaris software. For dendritic spine analysis, proximal (50µm from soma) and distal (100µm from soma) dendrites were imaged on a Zeiss LSM 880 NLO AxioExaminer with Airyscan. Dendrites and spines were reconstructed in three dimensions and analyzed in Imaris.

Slice preparation for electrophysiology

Most slice physiology experiments were performed using P25-31 mice. Exceptions were the oIPSC experiments, in which mice were P46-51, and the oAP experiments, in which mice were P33-40 to allow for sufficient ChR2 expression. For all experiments, mice were perfused transcardially with ice-cold ACSF (pH=7.4) containing (in mM): 127 NaCl, 25 $NaHCO_3$, 1.25 NaH_2PO_4, 2.5 KCl, 1$MgCl_2$, 2$CaCl_2$, and 25 glucose, bubbled continuously with carbogen (95% O_2 and 5% CO_2). Brains were rapidly removed and coronal slices (275 µm) were cut on a VT1000S vibrotome (Leica) in oxygenated ice-cold choline-based external solution (pH=7.8) containing (in mM): 110 choline chloride, 25 $NaHCO_3$, 1.25 $NaHPO_4$, 2.5 KCl, 7 $MgCl_2$, 0.5 $CaCl_2$, 25 glucose, 11.6 sodium ascorbate, and 3.1 sodium pyruvate. Slices were recovered in ACSF at 34°C for 15 minutes and then kept at RT before recording.

Whole-cell patch-clamp recording

Recordings were made with a MultiClamp 700B amplifier (Molecular Devices) at RT using 3-5 MOhm glass patch electrodes. Current clamp recordings were made using a

potassium-based internal solution (pH=7.4) containing (in mM): 135 $KMeSO_4$, 5 KCl, 5 HEPES, 4 Mg-ATP, 0.3 Na-GTP, 10 phosphocreatine, and 1 ETGA. For intrinsic excitability and Kir experiments, NBQX (10 μM), CPP (10 μM) and picrotoxin (50 μM) were added to the external solution to block synaptic transmission. No holding current was applied to the membrane.

Voltage-clamp recordings were made using a cesium-based internal solution (pH=7.4) containing (in mM): 120 $CsMeSO_4$, 15 CsCl, 10 TEA-Cl, 8 NaCl, 10 HEPES, 0.2-5 EGTA, 5 QX-314, 4 Mg-ATP, and 0.3 Na-GTP. For eIPSC experiments, recordings were made using a high chloride cesium-based internal solution to maximize IPSC amplitude (pH=7.2) containing (in mM): 125 CsCl, 10 TEA-Cl, 10 HEPES, 4 Mg-ATP, 0.3 Na-GTP, 8 Na_2CrePO_4, 0.1 EGTA, and 3.3 QX-314. For experiments measuring synaptic currents, cells were held at -80 mV and recordings were acquired with the amplifier Bessel filter set at 3 kHz. Excitatory synaptic transmission experiments were performed in the presence of picrotoxin (50 μM) and CPP (10 μM) to isolate AMPAR-mediated currents, and inhibitory synaptic transmission experiments were performed in the presence of NBQX (10 μM) and CPP (10 μM) to isolate GABAergic events.

Miniature synaptic transmission was assessed in the presence of TTX (1 μM) to prevent action potential-mediated release. Picrotoxin (50 μM) and CPP (10 μM) were included for mEPSC experiments and NBQX (10 μM) and CPP (10 μM) were included for mIPSC experiments. Traces were analyzed in Igor Pro, and miniature events were identified and measured using custom software. To electrically evoke EPSCs and IPSCs, a concentric bipolar stimulating electrode (FHC) was placed in the striatum 200 μm ventral to the recording site and a 0.2 ms stimulus was applied. For paired-pulse experiments, the interstimulus-interval was 50 ms. Optogenetic stimulation consisted of a full-field pulse of blue light (10 mW/mm^2, 470 nm, 0.2-0.5 ms) using a 63x objective. Recordings with a series resistance >25 MOhms or holding current above -200 pA were rejected.

Statistical analyses

Two-tailed paired or unpaired t-tests were used for comparisons between two groups. A one-way ANOVA with Sidak's post-doc test was used to compare the means of three or more groups. A two-way ANOVA with Sidak's post-hoc test was used to compare mean differences between groups for experiments with two independent variables. P-values were corrected for multiple comparisons. For data that did not pass the D'Agostino and Pearson normality test, the Kruskal-Wallis with Dunn's post-hoc test was used. Cumulative distributions were analyzed using the Kolmogorov-Smirnov test. Values for all statistical comparisons are provided in Tables S1-4.

References

1. Saxton, R.A. and D.M. Sabatini, *mTOR Signaling in Growth, Metabolism, and Disease.* Cell, 2017. **168**(6): p. 960-976.
2. Bateup, H.S., et al., *Excitatory/inhibitory synaptic imbalance leads to hippocampal hyperexcitability in mouse models of tuberous sclerosis.* Neuron, 2013. **78**(3): p. 510-22.
3. Bateup, H.S., et al., *Loss of Tsc1 in vivo impairs hippocampal mGluR-LTD and increases excitatory synaptic function.* J Neurosci, 2011. **31**(24): p. 8862-9.
4. Tavazoie, S.F., et al., *Regulation of neuronal morphology and function by the tumor suppressors Tsc1 and Tsc2.* Nat Neurosci, 2005. **8**(12): p. 1727-34.
5. Ehninger, D., et al., *Reversal of learning deficits in a Tsc2(+/-) mouse model of tuberous sclerosis.* Nat Med, 2008. **14**(8): p. 843-8.
6. Tsai, P.T., et al., *Autistic-like behaviour and cerebellar dysfunction in Purkinje cell Tsc1 mutant mice.* Nature, 2012. **488**(7413): p. 647-51.
7. Normand, E.A., et al., *Temporal and mosaic Tsc1 deletion in the developing thalamus disrupts thalamocortical circuitry, neural function, and behavior.* Neuron, 2013. **78**(5): p. 895-909.
8. Yang, S.B., et al., *Rapamycin ameliorates age-dependent obesity associated with increased mTOR signaling in hypothalamic POMC neurons.* Neuron, 2012. **75**(3): p. 425-36.
9. Costa-Mattioli, M. and L.M. Monteggia, *mTOR complexes in neurodevelopmental and neuropsychiatric disorders.* Nature Neuroscience, 2013. **16**: p. 1537.
10. Lipton, J.O. and M. Sahin, *The neurology of mTOR.* Neuron, 2014. **84**(2): p. 275-91.
11. Crino, P.B., K.L. Nathanson, and E.P. Henske, *The tuberous sclerosis complex.* N Engl J Med, 2006. **355**(13): p. 1345-56.
12. Crino, P.B., *Evolving neurobiology of tuberous sclerosis complex.* Acta Neuropathol, 2013. **125**(3): p. 317-32.
13. Curatolo, P., R. Moavero, and P.J. de Vries, *Neurological and neuropsychiatric aspects of tuberous sclerosis complex.* Lancet Neurol, 2015. **14**(7): p. 733-45.
14. Weston, M.C., H. Chen, and J.W. Swann, *Loss of mTOR repressors Tsc1 or Pten has divergent effects on excitatory and inhibitory synaptic transmission in single hippocampal neuron cultures.* Front Mol Neurosci, 2014. **7**: p. 1.
15. Fuccillo, M.V., *Striatal Circuits as a Common Node for Autism Pathophysiology.* Front Neurosci, 2016. **10**: p. 27.
16. Graybiel, A.M., *The basal ganglia: learning new tricks and loving it.* Curr Opin Neurobiol, 2005. **15**(6): p. 638-44.
17. Graybiel, A.M. and S.T. Grafton, *The striatum: where skills and habits meet.* Cold Spring Harb Perspect Biol, 2015. **7**(8): p. a021691.
18. Gerfen, C.R. and D.J. Surmeier, *Modulation of striatal projection systems by dopamine.* Annu Rev Neurosci, 2011. **34**: p. 441-66.
19. Smith, Y., et al., *Microcircuitry of the direct and indirect pathways of the basal ganglia.* Neuroscience, 1998. **86**(2): p. 353–387.
20. Kreitzer, A.C., *Physiology and pharmacology of striatal neurons.* Annu Rev Neurosci, 2009. **32**: p. 127-47.

21. Mink, J.W., *The Basal Ganglia and Involuntary Movements.* Neurological Review, 2003. **60**: p. 12-15.
22. Klaus, A., et al., *The Spatiotemporal Organization of the Striatum Encodes Action Space.* Neuron, 2017. **95**(5): p. 1171-1180 e7.
23. Gunaydin, L.A. and A.C. Kreitzer, *Cortico-Basal Ganglia Circuit Function in Psychiatric Disease.* Annu Rev Physiol, 2016. **78**: p. 327-50.
24. Kravitz, A.V., et al., *Regulation of parkinsonian motor behaviours by optogenetic control of basal ganglia circuitry.* Nature, 2010. **466**(7306): p. 622-6.
25. Bateup, H.S., et al., *Distinct subclasses of medium spiny neurons differentially regulate striatal motor behaviors.* Proc Natl Acad Sci U S A, 2010. **107**(33): p. 14845-50.
26. Curatolo, P., V. Napolioni, and R. Moavero, *Autism spectrum disorders in tuberous sclerosis: pathogenetic pathways and implications for treatment.* J Child Neurol, 2010. **25**(7): p. 873-80.
27. Davis, P.E., et al., *Tuberous Sclerosis: A New Frontier in Targeted Treatment of Autism.* Neurotherapeutics, 2015. **12**(3): p. 572-83.
28. Huber, K.M., et al., *Dysregulation of Mammalian Target of Rapamycin Signaling in Mouse Models of Autism.* J Neurosci, 2015. **35**(41): p. 13836-42.
29. Subramanian, M., et al., *Characterizing autism spectrum disorders by key biochemical pathways.* Front Neurosci, 2015. **9**: p. 313.
30. Meikle, L., et al., *A mouse model of tuberous sclerosis: neuronal loss of Tsc1 causes dysplastic and ectopic neurons, reduced myelination, seizure activity, and limited survival.* J Neurosci, 2007. **27**(21): p. 5546-58.
31. Gertler, T.S., C.S. Chan, and D.J. Surmeier, *Dichotomous anatomical properties of adult striatal medium spiny neurons.* J Neurosci, 2008. **28**(43): p. 10814-24.
32. Shen, W., et al., *Cholinergic modulation of Kir2 channels selectively elevates dendritic excitability in striatopallidal neurons.* Nature Neuroscience, 2007. **10**: p. 1458.
33. Cazorla, M., et al., *Striatal D2 receptors regulate dendritic morphology of medium spiny neurons via Kir2 channels.* J Neurosci, 2012. **32**(7): p. 2398-409.
34. Hoeffer, C.A. and E. Klann, *mTOR signaling: at the crossroads of plasticity, memory and disease.* Trends Neurosci, 2010. **33**(2): p. 67-75.
35. Tepper, J.M., et al., *Heterogeneity and diversity of striatal GABAergic interneurons.* Front Neuroanat, 2010. **4**: p. 150.
36. Koós, T. and J.M. Tepper, *Inhibitory control of neostriatal projection neurons by GABAergic interneurons.* Nature neuroscience, 1999. **2**: p. 467-472.
37. Gittis, A.H. and A.C. Kreitzer, *Striatal microcircuitry and movement disorders.* Trends Neurosci, 2012. **35**(9): p. 557-64.
38. Madisen, L., et al., *A robust and high-throughput Cre reporting and characterization system for the whole mouse brain.* Nat Neurosci, 2010. **13**(1): p. 133-40.
39. Fenno, L.E., et al., *Targeting cells with single vectors using multiple-feature Boolean logic.* Nat Methods, 2014. **11**(7): p. 763-72.
40. Wilson, C. and Y. Kawaguchi, *The Origins of Two-State Spontaneous Membrane Potential Fluctuations of Neostriatal Spiny Neurons* J Neurosci, 1996. **16**(7): p. 2397-2410.

41. Kreitzer, A.C. and R.C. Malenka, *Striatal plasticity and basal ganglia circuit function.* Neuron, 2008. **60**(4): p. 543-54.
42. Smith, Y., et al., *Thalamic contributions to Basal Ganglia-related behavioral switching and reinforcement.* J Neurosci, 2011. **31**(45): p. 16102-6.
43. Arenkiel, B.R., et al., *In vivo light-induced activation of neural circuitry in transgenic mice expressing channelrhodopsin-2.* Neuron, 2007. **54**(2): p. 205-18.
44. Fieblinger, T., et al., *Cell type-specific plasticity of striatal projection neurons in parkinsonism and L-DOPA-induced dyskinesia.* Nat Commun, 2014. **5**: p. 5316.
45. Santini, E., et al., *Inhibition of mTOR Signaling in Parkinson ' s Disease Prevents L -DOPA – Induced Dyskinesia.* Neuroscience, 2009. **2**(80): p. 1-11.
46. Santini, E., et al., *Dopamine- and cAMP-regulated phosphoprotein of 32-kDa (DARPP-32)-dependent activation of extracellular signal-regulated kinase (ERK) and mammalian target of rapamycin complex 1 (mTORC1) signaling in experimental parkinsonism.* J Biol Chem, 2012. **287**(33): p. 27806-12.
47. Lee, J.H., et al., *Reinstating aberrant mTORC1 activity in Huntington's disease mice improves disease phenotypes.* Neuron, 2015. **85**(2): p. 303-15.
48. Mitchell, I.J., A.J. Cooper, and M.R. Griffiths, *The selective vulnerability of stratopallidal neurons.* Progress in Neurobiology, 1999. **59**: p. 691-719.
49. Tong, X., et al., *Astrocyte Kir4.1 ion channel deficits contribute to neuronal dysfunction in Huntington's disease model mice.* Nature Neuroscience, 2014. **17**: p. 694.
50. Heiman, M., et al., *A translational profiling approach for the molecular characterization of CNS cell types.* Cell, 2008. **135**(4): p. 738-48.
51. Rubenstein, J.L. and M.M. Merzenich, *Model of autism: increased ratio of excitation/inhibition in key neural systems.* Genes Brain Behav, 2003. **2**(5): p. 255-67.
52. Rothwell, P.E., et al., *Autism-associated neuroligin-3 mutations commonly impair striatal circuits to boost repetitive behaviors.* Cell, 2014. **158**(1): p. 198-212.
53. Roseberry, T.K., et al., *Cell-Type-Specific Control of Brainstem Locomotor Circuits by Basal Ganglia.* Cell, 2016. **164**(3): p. 526-37.
54. Peixoto, R.T., et al., *Early hyperactivity and precocious maturation of corticostriatal circuits in Shank3B(-/-) mice.* Nat Neurosci, 2016. **19**(5): p. 716-24.
55. Wan, Y., et al., *Circuit-selective striatal synaptic dysfunction in the Sapap3 knockout mouse model of obsessive-compulsive disorder.* Biol Psychiatry, 2014. **75**(8): p. 623-30.
56. Surmeier, D.J., J. Plotkin, and W. Shen, *Dopamine and synaptic plasticity in dorsal striatal circuits controlling action selection.* Curr Opin Neurobiol, 2009. **19**(6): p. 621-8.
57. Wu, Y.W., et al., *Input- and cell-type-specific endocannabinoid-dependent LTD in the striatum.* Cell Rep, 2015. **10**(1): p. 75-87.
58. O'Hare, J.K., et al., *Pathway-Specific Striatal Substrates for Habitual Behavior.* Neuron, 2016. **89**(3): p. 472-9.
59. Shen, W., et al., *Dichotomous dopaminergic control of striatal synaptic plasticity.* Science, 2008. **321**(5890): p. 848-851.

60. Kramer, P. F., Christensen, C. H., Hazelwood, L. A., Dobi, A., Bock, R., Sibley, D. R., Mateo, Y. & Alvarez, V. A. 2011. Dopamine D2 receptor overexpression alters behavior and physiology in Drd2-EGFP mice. *J Neurosci,* 31**,** 126-32.
61. Chan, C. S., Peterson, J. D., Gertler, T. S., Glajch, K. E., Quintana, R. E., Cui, Q., Sebel, L. E., Plotkin, J. L., Shen, W., Heiman, M., Heintz, N., Greengard, P. & Surmeier, D. J. 2012. Strain-specific regulation of striatal phenotype in Drd2-eGFP BAC transgenic mice. *J Neurosci,* 32**,** 9124-32.
62. Nelson, A. B., Hang, G. B., Grueter, B. A., Pascoli, V., Luscher, C., Malenka, R. C. & Kreitzer, A. C. 2012. A comparison of striatal-dependent behaviors in wild-type and hemizygous Drd1a and Drd2 BAC transgenic mice. *J Neurosci,* 32**,** 9119-23.
63. Kwiatkowski, D. J. 2002. A mouse model of TSC1 reveals sex-dependent lethality from liver hemangiomas, and up-regulation of p70S6 kinase activity in Tsc1 null cells. *Human Molecular Genetics,* 11**,** 525-534.
64. Gong, S., Zheng, C., Doughty, M. L., Losos, K., Didkovsky, N., Schambra, U. B., Nowak, N. J., Joyner, A., Leblanc, G., Hatten, M. E. & Heintz, N. 2003. A gene expression atlas of the central nervous system based on bacterial artificial chromosomes. *Nature,* 425**,** 917-25.
65. Ade, K. K., Wan, Y., Chen, M., Gloss, B. & Calakos, N. 2011. An Improved BAC Transgenic Fluorescent Reporter Line for Sensitive and Specific Identification of Striatonigral Medium Spiny Neurons. *Front Syst Neurosci,* 5**,** 32.
66. Madisen, L., Zwingman, T. A., Sunkin, S. M., Oh, S. W., Zariwala, H. A., Gu, H., Ng, L. L., Palmiter, R. D., Hawrylycz, M. J., Jones, A. R., Lein, E. S. & Zeng, H. 2010. A robust and high-throughput Cre reporting and characterization system for the whole mouse brain. *Nat Neurosci,* 13**,** 133-40.
67. Arenkiel, B. R., Peca, J., Davison, I. G., Feliciano, C., Deisseroth, K., Augustine, G. J., Ehlers, M. D. & Feng, G. 2007. In vivo light-induced activation of neural circuitry in transgenic mice expressing channelrhodopsin-2. *Neuron,* 54**,** 205-18.

Supplemental Figures and Tables

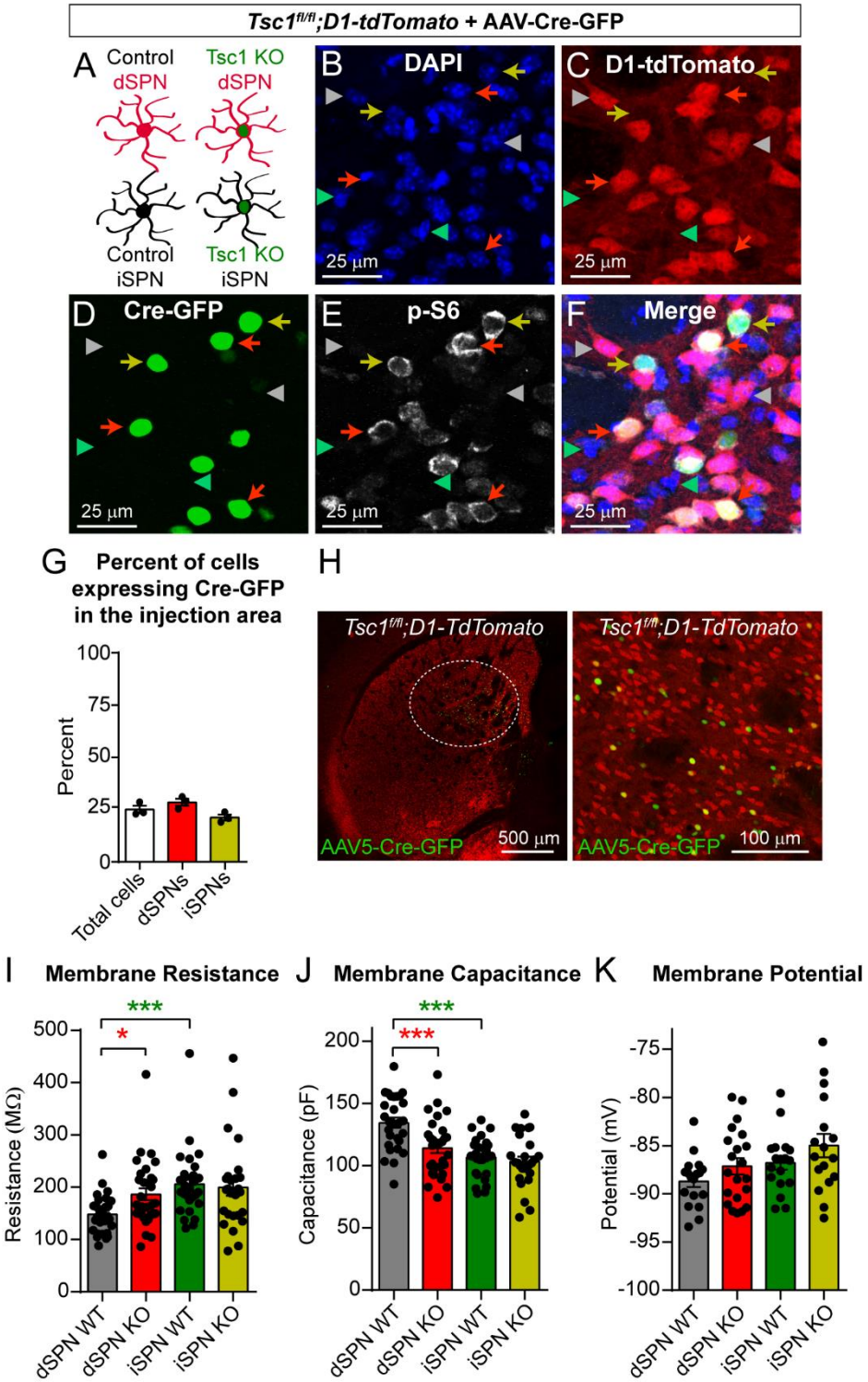

Supplemental Figure 1. Cre-expression in the dorsal striatum and passive membrane properties of Tsc1 KO SPNs, related to Figures 1 and 2.

(A) Schematic showing the four cell types present in each striatal slice of a *Tsc1$^{fl/fl}$;D1-tdTomato* mouse injected with AAV5-Cre-GFP. dSPNs are identified by tdTomato fluorescence and Tsc1 KO neurons are identified by nuclear GFP expression.
(B-F) Confocal images of striatal sections immunostained with antibodies against GFP and phosphorylated S6 (p-S6, Ser240/244), showing increased p-S6 in Cre-expressing dSPNs (red arrows) and iSPNs (yellow arrows). Grey (dSPNs) and green arrowheads (iSPNs) indicate Cre-negative control neurons.
(G) Percentage of Cre-GFP-expressing cells in the injection area in the dorsal striatum of *Tsc1$^{fl/fl}$;D1-tdTomato* mice (n=3 mice, 1137-1482 cells counted per mouse). “Total cells” is the percentage of Cre positive cells out of total DAPI-labeled cells, “dSPNs” is the percentage of all tdTomato-positive cells that are Cre-positive, “iSPNs” is the percentage of all tdTomato-negative cells that are Cre-positive. Bars represent mean +/- SEM, dots represent values from individual mice.
(H) Confocal images showing a subsaturating AAV5-Cre-GFP injection in the dorsal striatum of a *Tsc1$^{fl/fl}$;D1-tdTomato* mouse. White circle shows the injection area. Right panel shows zoom-in of the injection site.
(I-K) Mean +/- SEM membrane resistance (I), capacitance (J), and resting membrane potential (K) for cells of each condition. Membrane resistance and capacitance were measured from a -5 mV hyperpolarizing pulse applied to the membrane in voltage clamp. *,$p<0.05$; ***,$p<0.001$, Kruskal-Wallis with Dunn’s post-hoc test (membrane resistance, see Table S3 for P values) and one-way ANOVA with Sidak post-hoc test (membrane capacitance and resting membrane potential, see Table S2 for P values); dSPN WT n=28 neurons from 26 mice, dSPN KO n=31 neurons from 22 mice, iSPN WT n=28 neurons from 26 mice, iSPN KO n=36 neurons from 22 mice. Dots represent the values from individual neurons.

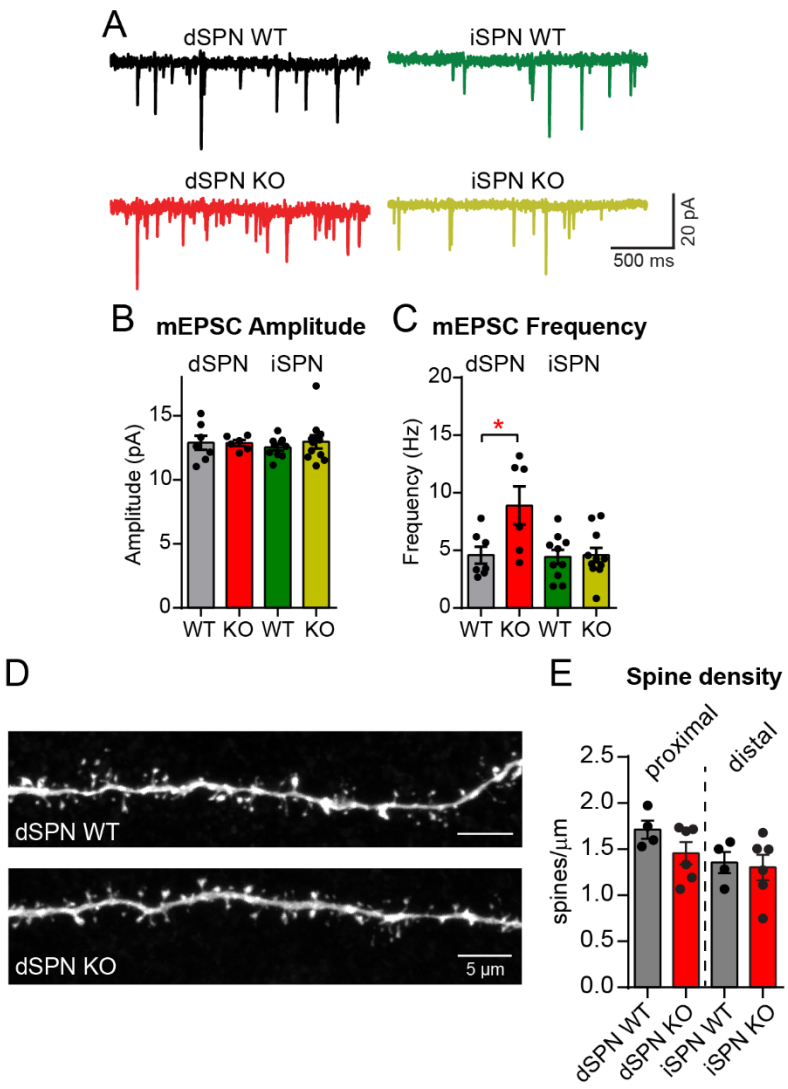

Supplemental Figure 2. *Tsc1* deletion increases mEPSC frequency in dSPNs but does not alter dendritic spine density, related to Figure 5.

(A) Example traces of miniature excitatory postsynaptic currents (mEPSCs) recorded from each cell type in a *Tsc1*$^{fl/fl}$*;D1-tdTomato* mouse injected with AAV5-Cre-GFP.

(B,C) Mean +/- SEM mEPSC amplitude (B) and frequency (C) per neuron for each genotype. *p<0.05, one-way ANOVA with Sidak post-hoc test (see Table S2 for P values). n=200 mEPSCs per neuron, dSPN WT n=7 neurons from 7 mice, dSPN KO n=6 neurons from 6 mice, iSPN WT n=10 neurons from 8 mice, iSPN KO n=11 neurons from 7 mice.

(D) Example images of dendritic spines from Tsc1 WT and KO dSPNs, which were filled with neurobiotin through a patch pipet. Striatal sections were fixed, stained with fluorescently-conjugated streptavidin, and imaged on a Zeiss LSM 880 NLO AxioExaminer with Airyscan.

(E) Quantification of proximal (50 □m from the soma) and distal (100 □m from the soma) dendritic spine density in Tsc1 WT and KO dSPNs. Data are represented as mean +/- SEM; dots display the average spine density for individual neurons. dSPN WT proximal n=8 dendrites from 4 neurons from 4 mice, dSPN KO proximal n=12 dendrites from 6 neurons from 4 mice, dSPN WT distal n=8 dendrites from 4 neurons from 4 mice, dSPN KO distal n=12 dendrites from 6 neurons from 4 mice. See Table S4 for P values.

Table S1. Two-way ANOVA values, related to Figures 2 and 3.

Figure panel	Test	Source of variation	F value	Comparison	DF	P value
2B	ANOVA	Interaction	2.345		21	0.0007
		Current step (pA)	289.9		7	<0.0001
		Genotype	30.85		3	<0.0001
	Sidak post-hoc			75pA, dMSN WT v iMSN WT	560	> 0.9999
				75pA, dMSN WT v dMSN KO	560	> 0.9999
				75pA, iMSN WT v iMSN KO	560	> 0.9999
				100pA, dMSN WT v iMSN WT	560	0.9999
				100pA, dMSN WT v dMSN KO	560	> 0.9999
				100pA, iMSN WT v iMSN KO	560	0.9976
				150pA, dMSN WT v iMSN WT	560	0.1337
				150pA, dMSN WT v dMSN KO	560	0.9991
				150pA, iMSN WT v iMSN KO	560	> 0.9999
				200pA, dMSN WT v iMSN WT	560	< 0.0001
				200pA, dMSN WT v dMSN KO	560	0.4437
				200pA, iMSN WT v iMSN KO	560	> 0.9999
				250pA, dMSN WT v iMSN WT	560	< 0.0001
				250pA, dMSN WT v dMSN KO	560	0.0432
				250pA, iMSN WT v iMSN KO	560	> 0.9999
				300pA, dMSN WT v iMSN WT	560	0.0002
				300pA, dMSN WT v dMSN KO	560	0.0940
				300pA, iMSN WT v iMSN KO	560	> 0.9999
				350pA, dMSN WT v iMSN WT	560	0.0411
				350pA, dMSN WT v dMSN KO	560	0.1211
				350pA, iMSN WT v iMSN KO	560	0.9986
				400pA, dMSN WT v iMSN WT	560	0.7760
				400pA, dMSN WT v dMSN KO	560	0.1355
				400pA, iMSN WT v iMSN KO	560	0.6082
2E	ANOVA	Interaction	3.269		27	< 0.0001
		Voltage step (mV)	368.5		9	< 0.0001
		Genotype	18.46		3	< 0.0001
	Sidak post-hoc			-150pA, dMSN WT v iMSN WT	350	< 0.0001
				-150pA, dMSN WT v dMSN KO	350	< 0.0001
				-150pA, iMSN WT v iMSN KO	350	0.0011
				-140pA, dMSN WT v iMSN WT	350	< 0.0001
				-140pA, dMSN WT v dMSN KO	350	< 0.0001
				-140pA, iMSN WT v iMSN KO	350	0.0981
				-130pA, dMSN WT v iMSN WT	350	0.0022
				-130pA, dMSN WT v dMSN KO	350	0.0023
				-130pA, iMSN WT v iMSN KO	350	0.4017
				-120pA, dMSN WT v iMSN WT	350	0.2054
				-120pA, dMSN WT v dMSN KO	350	0.2088
				-120pA, iMSN WT v iMSN KO	350	0.8118
				-110pA, dMSN WT v iMSN WT	350	0.9222
				-110pA, dMSN WT v dMSN KO	350	0.9115
				-110pA, iMSN WT v iMSN KO	350	0.9960
				-100pA, dMSN WT v iMSN WT	350	0.9999
				-100pA, dMSN WT v dMSN KO	350	0.9997
				-100pA, iMSN WT v iMSN KO	350	> 0.9999

				-90pA, dMSN WT v iMSN WT	350	> 0.9999
				-90pA, dMSN WT v dMSN KO	350	> 0.9999
				-90pA, iMSN WT v iMSN KO	350	> 0.9999
				-80pA, dMSN WT v iMSN WT	350	> 0.9999
				-80pA, dMSN WT v dMSN KO	350	> 0.9999
				-80pA, iMSN WT v iMSN KO	350	> 0.9999
				-70pA, dMSN WT v iMSN WT	350	> 0.9999
				-70pA, dMSN WT v dMSN KO	350	> 0.9999
				-70pA, iMSN WT v iMSN KO	350	> 0.9999
				-60pA, dMSN WT v iMSN WT	350	> 0.9999
				-60pA, dMSN WT v dMSN KO	350	> 0.9999
				-60pA, iMSN WT v iMSN KO	350	> 0.9999
3B,C	ANOVA	Interaction	1.409		660	<0.0001
		Radius	366.7		220	<0.0001
		Genotype	231.5		3	<0.0001

Table S2. One-way ANOVA values, related to Figures 2, 3, 4, 5, S1 and S2.

Figure panel	F value	DF	P value	Post-hoc test	Comparison	P value
2C	9.078	67	p<0.0001	Sidak	dMSN WT v iMSN WT	<0.0001
					dMSN WT v dMSN KO	0.0124
					iMSN WT v iMSN KO	0.9977
					dMSN WT v dMSN KO	0.0006
					iMSN WT v iMSN KO	0.9133
3E	5.578	81	p=0.0016	Sidak	dMSN WT v iMSN WT	0.0131
					dMSN WT v dMSN KO	0.0592
					iMSN WT v iMSN KO	0.3271
4C	0.08534	41	p=0.9676	Sidak	dMSN WT v iMSN WT	0.9992
					dMSN WT v dMSN KO	0.9852
					iMSN WT v iMSN KO	>0.9999
4E	4.664	41	p=0.0072	Sidak	dMSN WT v iMSN WT	0.0516
					dMSN WT v dMSN KO	0.9534
					iMSN WT v iMSN KO	0.9811
5C	1.130	51	p=0.3463	Sidak	dMSN WT v iMSN WT	0.5513
					dMSN WT v dMSN KO	0.8195
					iMSN WT v iMSN KO	0.2775
5E	4.735	51	p=0.0057	Sidak	dMSN WT v iMSN WT	0.9959
					dMSN WT v dMSN KO	0.0139
					iMSN WT v iMSN KO	>0.9999
S1J	12.96	112	p<0.0001	Sidak	dMSN WT v iMSN WT	<0.0001
					dMSN WT v dMSN KO	0.0006
					iMSN WT v iMSN KO	0.9133
S1K	2.910	73	p=0.0405	Sidak	dMSN WT v iMSN WT	0.3404
					dMSN WT v dMSN KO	0.4866
					iMSN WT v iMSN KO	0.4037
S2B	0.2274	33	p=0.8766	Sidak	dMSN WT v iMSN WT	0.9246
					dMSN WT v dMSN KO	>0.9999
					iMSN WT v iMSN KO	0.8254
S2C	5.179	33	p=0.0053	Sidak	dMSN WT v iMSN WT	0.9990

					dMSN WT v dMSN KO	0.0112
					iMSN WT v iMSN KO	0.9987
S2E	1.828	19	p=0.1826	Sidak	dMSN WT proximal v dMSN KO proximal	0.3301
					dMSN WT distal v dMSN KO distal	0.9475

Table S3. Kruskal-Wallis test values, related to Figures 3 and S1.

Figure panel	Kruskal-Wallis statistic	Post-hoc test	Comparison	P value
3D	9.178	Dunn's	dMSN WT v iMSN WT	0.0463
			dMSN WT v dMSN KO	0.0494
			iMSN WT v iMSN KO	>0.9999
3F	11.66	Dunn's	dMSN WT v iMSN WT	0.0119
			dMSN WT v dMSN KO	0.0183
			iMSN WT v iMSN KO	>0.9999
S1I	17.01	Dunn's	dMSN WT v iMSN WT	0.0003
			dMSN WT v dMSN KO	0.0216
			iMSN WT v iMSN KO	>0.9999

Table S4. Student's t-test values, related to Figures 4, 5, and 6.

Figure panel	Test	t and p values
4G	Two-tailed Student's paired t-test	t_{13}=0.1369, p=0.8932
4H	Two-tailed Student's paired t-test	t_{11}=0.4825, p=0.6389
4K	Two-tailed Student's paired t-test	t_{5}=0.3667, p=0.7289
5G	Two-tailed Student's paired t-test	t_{21}=3.537, p=0.0020
5H	Two-tailed Student's paired t-test	t_{10}=0.6201, p=0.5491
5J	Two-tailed Student's t-test	t_{40}=2.363, p=0.0231
5K	Two-tailed Student's t-test	t_{16}=1.514, p=0.1495
6C	Two-tailed Student's paired t-test	t_{7}=0.6406, p=0.5422
6F	Two-tailed Student's paired t-test	t_{8}=2.399, p=0.0432
6I	Two-tailed Student's paired t-test	t_{8}=2.366, p=0.0455
6J	Two-tailed Student's paired t-test	t_{8}=1.873, p=0.0979

CHAPTER 2: LOSS OF ENDOCANNABINOID-LTD AND ENHANCED CORTICOSTRIATAL TRANSMISSION IN STRIATONIGRAL NEURONS ARE ASSOCIATED WITH IMPROVED MOTOR ROUTINE LEARNING IN A MOUSE MODEL OF AUTISM

Katelyn Nicole Benthall

Department of Molecular and Cell Biology,
University of California, Berkeley

Introduction

Autism spectrum disorder (ASD) is a neurodevelopmental disorder characterized by social and communication deficits, as well as the presence of restricted and repetitive behaviors (RRBs) [1]. Though the neural basis of ASD is not yet identified, a growing body of evidence suggests a strong genetic component to ASD. A number of genes have been associated with ASD, and among these are single gene mutations that cause a syndrome in which ASD occurs along with a collection of other neurological and medical conditions [2]. One such syndrome is tuberous sclerosis complex (TSC), a disorder caused by mutations in either *TSC1* or *TSC2*, in which about half of patients meet the clinical criteria for ASD diagnosis and most have epilepsy [3]. Under normal circumstances, the TSC1 and TSC2 proteins form a heterodimer that negatively regulates the mTORC1 signaling pathway, a central hub controlling cellular metabolic processes such as protein and lipid synthesis, cell growth, differentiation, and autophagy [4]. In the case of loss of function of the TSC1/2 complex, the mTORC1 pathway is upregulated, leading to excessive protein synthesis. Dysregulation of mTORC1 signaling is not limited to TSC but may be a common consequence of ASD-risk gene mutations, with up to 15% of ASD cases attributable to altered mTORC1 signaling [5].

While epilepsy in TSC has been shown to arise from altered excitability in excitatory forebrain circuits, the brain regions and cell types important for ASD in TSC patients are less well understood. [6, 7]. We hypothesized that dysfunction of the striatum, a subcortical nucleus that mediates motor learning, action selection, and habit formation, might also contribute to the RRBs observed in TSC patients with ASD [8]. Indeed, striatal dysfunction has been implicated in non-syndromic forms of ASD by structural and functional MRI studies [9-11]. Further, metabolism was found to be different in TSC children with ASD compared to TSC children without ASD [12]. Compellingly, this altered striatal activity was correlated with the presence of RRBs in the TSC children with ASD [12].

Mouse studies support these findings, showing that ASD-risk gene mutations endow the striatum with an enhanced ability to acquire motor routines, a proposed explanation for the generation RRBs [13]. Changes to striatal synapses are associated with enhancement of motor learning in ASD mouse models, suggesting striatal dysfunction in ASD occurs at the level of synaptic transmission [8, 14-17]. Our group has previously shown input- and cell type-specific changes in synaptic transmission in striatal neurons with postnatal loss of Tsc1. Therefore, the goal of this study was to determine whether these synaptic changes are sufficient to cause RRBs in the context of TSC.

Striatal function is dependent on the coordinated activity of two subpopulations of GABAergic principal cells: direct pathway spiny projection neurons (dSPNs) and indirect pathway spiny projection neurons (iSPNs) [18]. These two subpopulations are anatomically intermingled in the striatum, but are biochemically and morphologically distinct [19, 20]. For example, dSPNs express D1 dopamine receptors and M4 muscarinic acetylcholine receptors, while iSPNs express D2 dopamine receptors and A2a adenosine receptors. dSPNs and iSPNs are also distinct in their projection targets, diverging as they leave the striatum to innervate the globus pallidus internal segment (GPi) as well as substantia nigra pars reticulata (SNr), or the globus pallidus external

segment (GPe), respectively [21]. Functionally, at the most simple level, activation of dSPNs increases motor behavior while activation of iSPNs inhibits motor behavior, and it is in this way that the striatum selects appropriate actions to be performed for any given context, while inappropriate actions are suppressed [22-24]. Cortical and thalamic inputs make the primary glutamatergic synapses onto dSPN and iSPNs, and modification of the strength of this excitatory drive by long-term synaptic plasticity mediates motor learning and habit formation [25].

Previous experiments show that corticostriatal transmission is selectively affected by postnatal loss of *Tsc1* in the striatum, but the behavioral consequences of and mechanism driving this change were previously unknown [26]. Further, it is unclear if the synaptic changes that occur with postnatal *Tsc1* deletion are directly relevant for studying disease phenotypes, as TSC patients have loss of *Tsc1/2* throughout their lifetime. To address these open questions, we conditionally deleted *Tsc1* prenatally in either dSPNs or iSPNs, and investigated the impact on striatal-dependent motor learning. We find that motor routine learning is enhanced in mice with *Tsc1* deletion restricted to dorsal striatal dSPNs, but not iSPNs. Further, we find that loss of Tsc1 causes a non-cell autonomous enhancement in corticostriatal drive of dSPNs but not iSPNs. Mechanistically, we observe that this is associated with a loss of retrograde endocannabinoid-mediated long-term depression (eCB-LTD) at corticostriatal synapses onto dSPNs. Together these findings implicate striatal TSC-mTORC1 signaling in corticostriatal synaptic dysfunction and the generation of RRBs in ASD.

Results

Upregulation of mTORC1 and somatic hypertrophy in SPNs with Tsc1 deletion

In order to test whether alterations in striatal circuits are sufficient to drive RRBs in TSC, we generated mice with dSPN- or iSPN-restricted deletion of *Tsc1* (Fig 1A,B). We bred conditional *Tsc1* mice (*Tsc1*^{cKO}) with the striatal-restricted *D1-Cre* or *A2a-Cre* lines to achieve dSPN- or iSPN-specific loss of Tsc1 [27, 28]. In addition, we bred in a tdTomato fluorescent Cre reporter (*Ai9* transgene) to visualize Cre-expressing cells [29]. We used the EY217 *D1-Cre* founder line from GENSAT as it has more restricted striatal expression than the commonly used EY262 line. In preliminary studies we found that *Tsc1*^{cKO}*;D1-Cre*(EY262) mice died prematurely, around post-natal day 15, which was not the case for Cre-positive *Tsc1*^{WT} or *Tsc1*^{cHet} animals, who had a normal lifespan. The premature mortality was likely driven by seizures due to cortical Cre expression and *Tsc1* deletion in this line. *Tsc1*^{cKO}*;D1-Cre*(EY217) did not exhibit premature mortality, which is likely due to the more striatal-restricted Cre expression in this line, which is primarily limited to the dorsal striatum.

To confirm that *Tsc1* deletion upregulated the mTORC1 signaling pathway in dSPNs and iSPNs, brain sections from *Tsc1*^{cKO}*;D1-Cre;Ai9* and *Tsc1*^{cKO}*;A2a-Cre;Ai9* mice were stained with a phospho-antibody against the mTORC1 pathway target S6 (pS6 240/244) (Fig. 1C,F). Both dSPNs and iSPNs with homozygous *Tsc1* deletion (dSPN-Tsc1 KO) showed increased p-S6 signal compared to wild-type (WT), indicating a loss of Tsc1 function and mTORC1 pathway hyperactivity (Fig. 1D,G). We also measured soma volume, as increased soma size is a common cellular phenotype across TSC models. Moderate somatic hypertrophy was present in dSPNs and iSPNs with homozygous *Tsc1* loss, as soma volume measurements were significantly increased over WT levels (Fig. 1E,H).

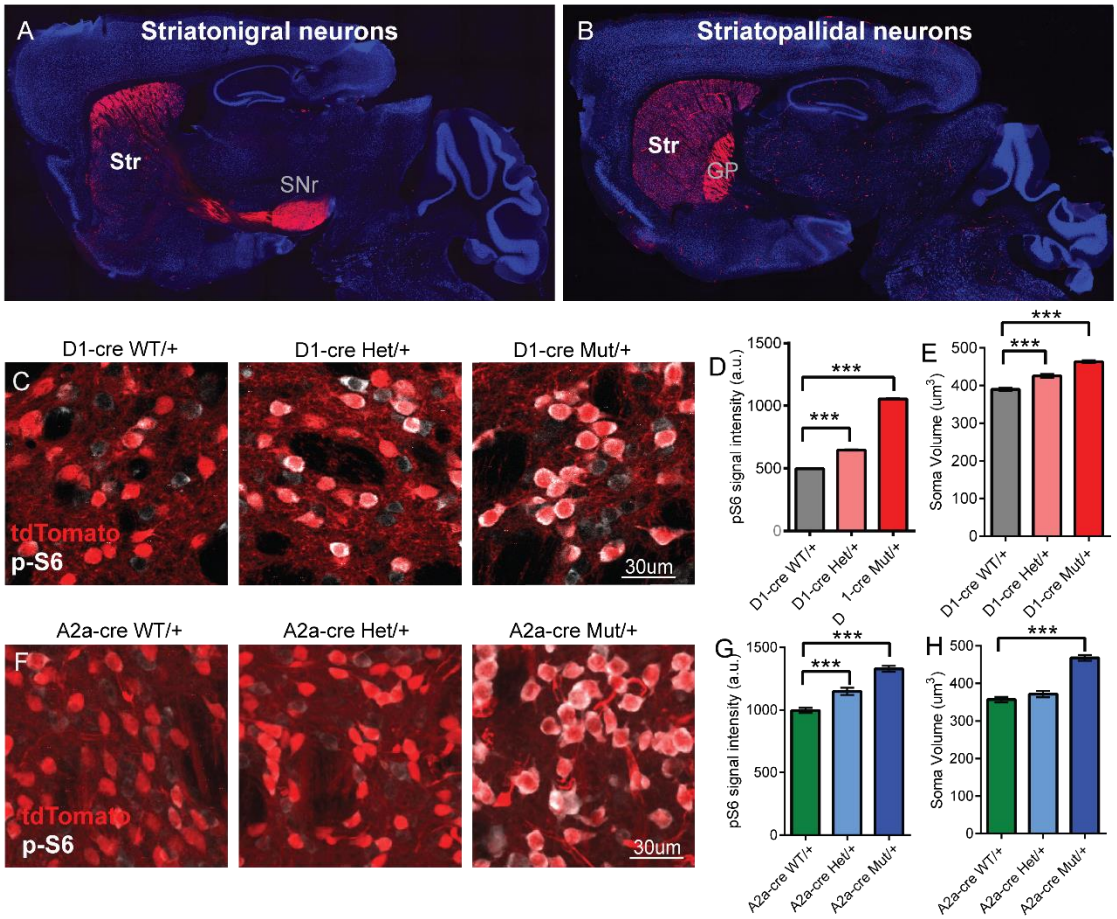

Figure 1. Developmental loss of *Tsc1* from striatal neurons induces mTORC1 activation and somatic hypertrophy.
(A-B) Sagittal brain section images showing the expression pattern of a *Tsc1^{cKO};D1-cre;Ai9* mouse (A) and a *Tsc1^{cKO};A2a-cre;Ai9* mouse (B). Note striatal restriction of the EY217 D1-cre line.
(C,F) Confocal images of striatal sections from a *Tsc1^{cKO};D1-cre;Ai9* mouse (C) and a *Tsc1^{cKO};A2a-cre;Ai9* mouse (F) immunostained with antibodies against phosphorylated S6 (p-S6, Ser240/244).
(D-E) Average of dSPN pS6 fluorescence intensity (left) and soma volume (right). pS6 signal is significantly increased in Tsc1-Het and Tsc1-KO dSPNs compared to controls. Soma volume is significantly increased in Tsc1-Het and Tsc1-KO dSPNs compared to controls.
(G-H) Average of iSPN pS6 fluorescence intensity (left) and soma volume (right). pS6 signal is significantly increased in Tsc1-Het and Tsc1-KO dSPNs compared to controls. Soma volume is significantly increased in Tsc1-KO dSPNs compared to controls.

Enhanced motor routine acquisition in mice with Tsc1 loss from dSPNs but not iSPNs

A variety of behavior assays have been used in mouse models of ASD to investigate the circuit basis of motor behavioral abnormalities and RRBs. We first investigated general locomotor activity and self-grooming behavior in the open field and found no significant difference in dSPN- or iSPN-Tsc1 KO mice compared to controls (Fig. 2A-C). We also did not find significant changes in the marble burying task (Fig. 2D), which has been used as a measure of RRBs in ASD mouse models. These results suggest that loss of Tsc1 from a single type of striatal projection neuron is not sufficient to alter gross motor behavior or induce spontaneous stereotypies.

The accelerating rotarod task is a striatal-dependent motor learning assay that has been shown to be altered in multiple mouse models of ASD [13, 15, 30-32]. In this test, mice learn to run on a rod revolving at increasing speed. It requires four days of training with three trials performed each day, over the course of which mice develop a stereotyped motor routine to stay on the apparatus. Control mice improve at the task over training, with an average learning rate of 2.7 +/- 0.39 rpm/day. We found that despite similar initial rotarod performance on trial 1, motor learning was significantly enhanced in mice with homozygous loss of *Tsc1* in dSPNs compared to littermate controls (Fig. 2E,F). Interestingly, mice with heterozygous deletion of *Tsc1* in dSPNs displayed an intermediate motor learning phenotype (Fig. 2E,F). Strikingly, we found no change in either initial motor performance or motor learning ability in mice with *Tsc1* deletion restricted to iSPNs (Fig. 2G,H), indicating that the motor learning phenotype is dSPN-specific.

Patients with TSC have a germline heterozygous mutation in either *TSC1* or *TSC2*; however, “second-hit” somatic mutations causing loss of heterozygosity may also contribute to neuropsychiatric phenotypes [33]. To examine motor learning in a model that reflects the genotype of TSC patients, the majority of which have mutations in *TSC2*, we tested germline *Tsc2* heterozygous mice in the accelerating rotarod. *Tsc2* heterozygotes had normal initial motor performance but exhibited a small but significant increase in motor learning compared to WT littermates that became apparent in the more challenging trials of the test (Fig. S1). Together with the data shown in Fig. 1E,F these results suggest that 1) haploinsufficiency of *Tsc1* or *Tsc2* is sufficient to alter striatal-dependent motor learning and 2) the increased motor learning in dSPN-Tsc1 KO mice is not likely to be an aberrant phenotype due to the manipulation of *Tsc1* in a single cell population, an artificial situation that probably does not occur in TSC patients but is nonetheless useful in mouse studies.

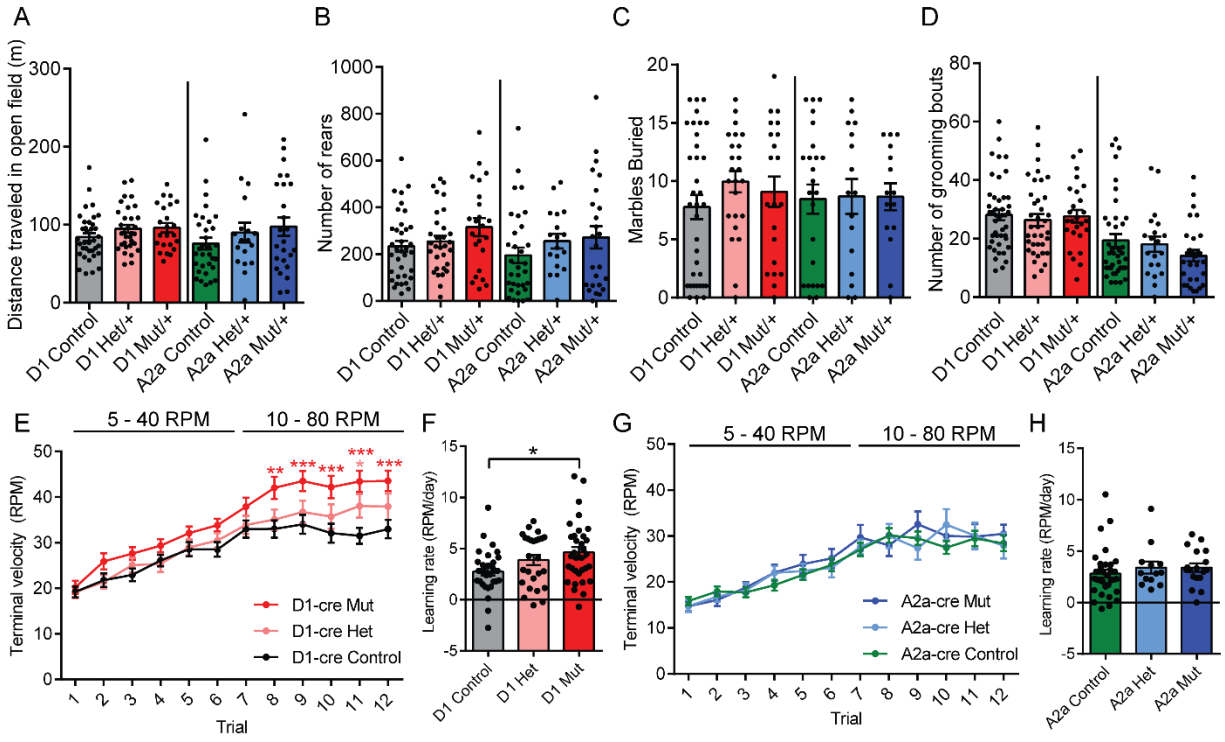

Figure 2. Mice with developmental loss of *Tsc1* in dSPNs but not iSPNs have enhanced motor routine learning.

(A-B) Average distance traveled and number of rears in the open field. No significant differences were found between Tsc1-Het or Tsc1-KO mice compared to controls.

(C) Average marbles buried by *Tsc1^{cKO};D1-cre;Ai9* and *Tsc1^{cKO};A2a-cre;Ai9* mice.

(D) Quantification of grooming bouts observed in *Tsc1^{cKO};D1-cre;Ai9* and *Tsc1^{cKO};A2a-cre;Ai9* mice.

(E,F) Accelerating rotarod learning curve (E) and learning rate (F) of *Tsc1^{cKO};D1-cre;Ai9* mice. Tsc1-Het mice had significantly improved performances on the final day of training, and Tsc1-KO mice were significantly improved on the final two training days compared to controls. Tsc1-KO mice had greater learning rates than littermate controls.

(G-H) Accelerating rotarod learning curve (G) and learning rate (H) of *Tsc1^{cKO};A2a-cre;Ai9* mice.

Loss of Tsc1 increases cortical drive of direct pathway striatal neurons

Motor learning relies on corticostriatal transmission, so it is possible that changes in SPN response to cortical activity could account for enhanced motor routine acquisition in mice with loss of function of the Tsc1/2 complex. Indeed, previous work identified increased cortico-dSPN but not thalamo-dSPN excitability in mice with postnatal *Tsc1* deletion. However, whether this is also the case for mice with prenatal heterozygous or homozygous *Tsc1* deletion was unexplored [26]. To test this, we crossed the *Tsc1^{cKO};D1-Cre;Ai9* and *Tsc1^{cKO};A2a-Cre;Ai9* mice to the *Thy1-ChR2-YFP* line, which expresses channelrhodopsin (ChR2-YFP) in a subset of cortical layer V pyramidal cells (Fig. 3A) [34]. This allowed for selective stimulation of cortical terminals with light, during which postsynaptic SPN responses could be measured. Ten blue light pulses at 40Hz were delivered over the recording site to stimulate glutamate release from cortical terminals, and SPN postsynaptic potentials were recorded in current-clamp mode. By varying the intensity of cortical stimulation, either subthreshold depolarizations or action potentials (APs) could be elicited in SPNs with a given probability. We quantified the number of APs evoked by this stimulation paradigm as a

percent of total stimulation events. The 10 pulse stimulation paradigm was repeated at different light intensities to generate an input-output curve of cortico-striatal transmission. Cortical terminal stimulation caused a significantly higher number of APs across all light intensities in dSPNs with homozygous loss of *Tsc1* compared to WT. Notably, loss of one copy of *Tsc1* was sufficient to increase cortico-striatal drive as dSPN-Tsc1 Het neurons showed an intermediate phenotype between dSPN-Tsc1 KO and WT (Fig. 3B,C).

We performed the 10 pulse cortical stimulation experiment in iSPNs and found that WT iSPNs were more readily driven to spike than dSPNs, consistent with their increased intrinsic excitability [19, 26]. Interestingly, loss of either one or two copies of *Tsc1* had no effect on cortico-striatal excitation of the indirect pathway (Fig. 3D,E) as the number of APs elicited from iSPNs during cortical stimulation was not different between genotypes at any light intensity (Fig. 3D,E). These physiology results are highly consistent with the behavioral findings in the rotarod test, whereby deletion of *Tsc1* has a selective impact on dSPNs, while iSPNs are remarkably unaffected.

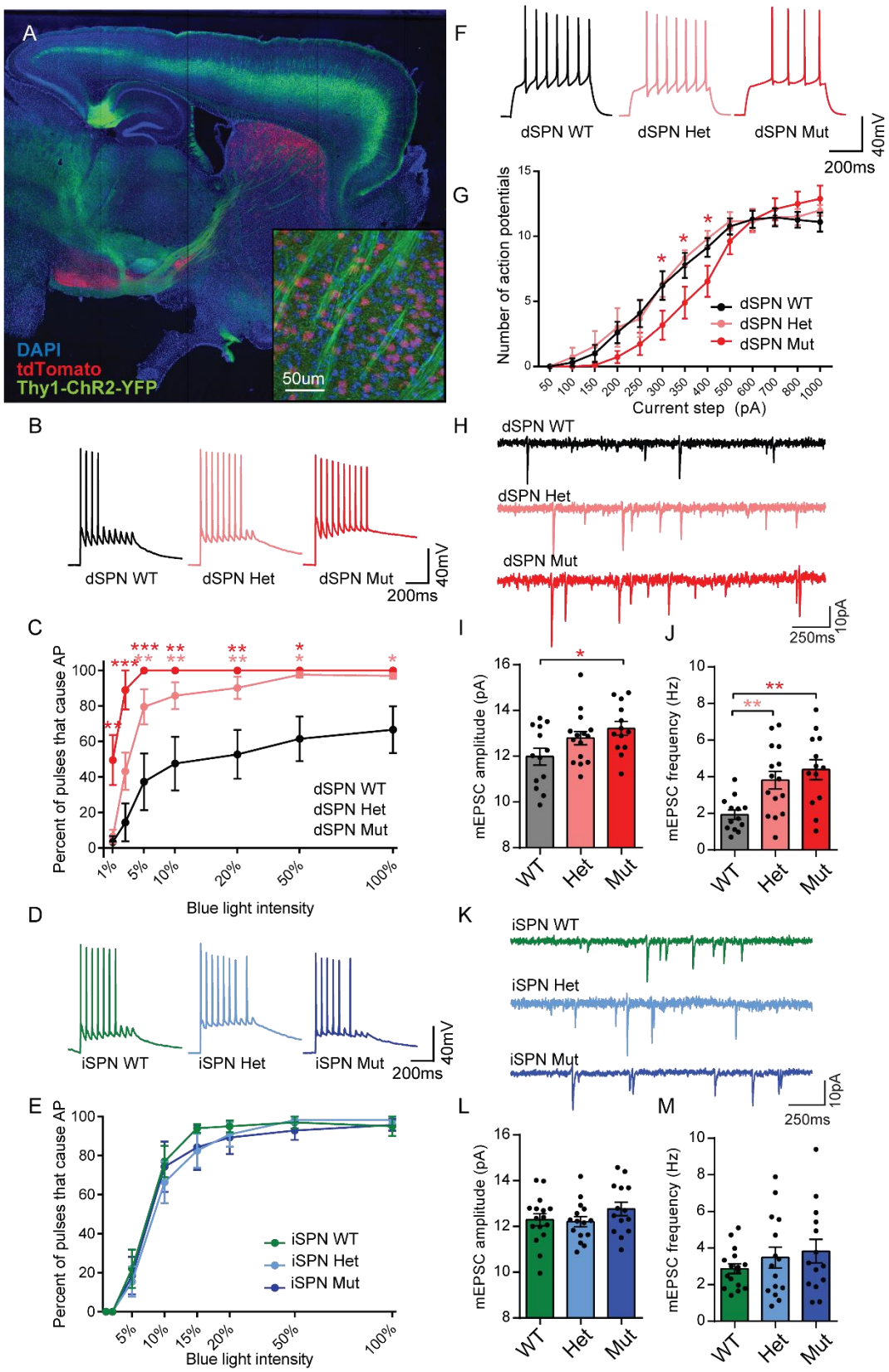

Figure 3. Synaptic cortico-dSPN excitability is increased with developmental *Tsc1* loss.

(A) Image of sagittal brain section from a *Tsc1^{cKO};D1-cre;Ai9;Thy1-ChR2-EYFP* mouse. Note cortical terminals labeled with ChR2-EYFP in striatum (inset).
(B-C) Example traces (B) and quantification as an input-output curve (C) of oAPs evoked in dSPNs by cortical terminal stimulation. Tsc1-Het and Tsc1-KO dSPNs had significantly higher probability to fire an oAP compared to controls.
(D-E) Example traces (D) and quantification as an input-output curve (E) of oAPs evoked in iSPNs by cortical terminal stimulation. No significant differences were found in oAP firing probability across light intensities.
(F-G) Current clamp example traces (F) and quantified current-frequency relationship (G). Tsc1-KO dSPNs had significantly reduced firing at 300-400pA current steps compared to controls.
(H-J) mEPSC example traces (H) and quantification of amplitude (I) and frequency (J) in dSPNs. Tsc1-KO dSPNs had significantly increased mEPSC amplitude and frequency compared to controls. mEPSC frequency was significantly increased in Tsc1-Het dSPNs.
(K-M) mEPSC example traces (K) and quantification of amplitude (L) and frequency (M) in iSPNs. There were no significant difference to excitatory transmission by genotype.

Increased cortico-dSPN excitability results from enhanced synaptic excitation

Enhanced dSPN-Tsc1 Het/KO responses to cortical terminal stimulation could result from increased intrinsic membrane excitability, increased synaptic excitation, or both. Indeed, *Tsc1* deletion has diverse effects on intrinsic and synaptic excitability depending on the cell type studied. To test if changes to intrinsic excitability occur in dSPN-Tsc1 KO neurons, we injected positive current and measured the number of APs fired as a function of current step amplitude. The input-output curve for dSPNs with homozygous loss of *Tsc1* was shifted slightly to the right relative to dSPN-Tsc1 WT and Het neurons, indicating a small intrinsic membrane hypoexcitability (Fig. 3F,G).

Intrinsic membrane hypoexcitability has been observed in other TSC mouse models, and it is possible that this could be due to the somatic hypertrophy observed in *Tsc1* deleted dSPNs [6, 35, 36]. However, it does not explain the enhanced corticostriatal excitability observed in dSPNs. We then assayed global excitatory synaptic function by recording mEPSCs in dSPNs, and found an increase in the amplitude and frequency of miniature excitatory events onto dSPNs with homozygous loss of *Tsc1* compared to controls (Fig. 3H-J). An increase in mEPSC frequency but not amplitude was also observed in dSPNs with heterozygous *Tsc1* deletion (Fig. 3H-J). Thus, the cortico-dSPN hyperexcitability is likely driven by enhanced corticostriatal synaptic connectivity rather than by intrinsic excitability. Consistent with a lack of cortico-iSPN excitability change, no significant changes in mEPSC amplitude or frequency were observed in iSPNs with loss of Tsc1 (Fig. 3K-M).

Considering the increase in cortico-dSPN excitability and the fact that thalamic inputs are not altered by postnatal *Tsc1* deletion [26], it is likely that the increased mEPSCs onto *Tsc1* deleted dSPNs are mediated completely or at least in part by enhanced corticostriatal transmission. To test this directly we recorded AMPAR-mediated excitatory currents evoked by optical stimulation of cortical terminals (oEPSCs) in *Tsc1^{cKO};D1-Cre;Ai9;Thy1-ChR2-YFP* mice. Indeed, stimulation of cortical terminals resulted in significantly larger AMPAR-mediated oEPSCs in dSPNs with homozygous loss of *Tsc1* compared to WT across light intensities. dSPNs with heterozygous loss of *Tsc1* trended toward increased oEPSC amplitude than controls but this was not statistically significant. (Fig. 4A,B). AMPAR:NMDAR ratios were unchanged across genotypes (Fig. 4C,D,S2).

Endocannabinoid-mediated long-term depression is impaired at cortico-dSPN synapses in Tsc1 KO neurons

One mechanism that could explain enhanced corticostriatal transmission in dSPN-Tsc1 KO neurons is a loss of long-term synaptic depression (LTD) at those synapses, which would render cells unable to depress excitatory inputs. Corticostriatal terminals express CB1 receptors that mediate endocannabinoid-LTD (eCB-LTD), the predominant form of striatal synaptic depression. Upon coincident activation of metabotropic glutamate receptors (mGluR1/5) and L-type calcium channels, SPNs release the endocanabinoids AEA or 2-AG, which act as retrograde signals that activate presynaptic CB1Rs to decrease corticostriatal transmission [37]. Historically it has been thought that eCB-LTD occurs in iSPNs and is absent in dSPNs, but recent studies using more selective stimulation of corticostriatal terminals have revealed eCB-LTD in both SPN subtypes [38]. Notably, since loss of another form of mGluR-dependent LTD expressed in the hippocampus has been reported in multiple TSC mouse models, and disruption of 2-AG release from dSPNs causes enhanced excitation and repetitive behaviors, we reasoned that loss of eCB-LTD could occur in dSPNs with *Tsc1* deletion [6, 7, 39-42].

To test this, we induced eCB-LTD in dSPNs with wash-on of the group 1 mGluR agonist DHPG and monitored the amplitude of AMPAR-mediated events in response to optogenetic cortical terminal stimulation. Cells were held at -50mV to facilitate the opening of L-type calcium channels. While dSPN-Tsc1 WT neurons showed a long-lasting synaptic depression to 79% of baseline levels (measured 40 minutes after DHPG wash-on), eCB-LTD did not occur in dSPNs with *Tsc1* deletion, which exhibited only a small reduction in oEPSC amplitude during DHPG application that was not maintained (Fig. 4E). To ensure that the protocol was indeed inducing eCB-LTD, we performed the DHPG wash-on in the presence of AM-251, a CB1R antagonist, and saw that LTD was blocked in control dSPNs (Fig. S3). Further, these changes cannot be explained by a presynaptic difference in CB1R expression or activity, as application of the CB1R agonist WIN-2 depressed oEPSCs to the same extent in *Tsc1* deleted and control dSPNs (Fig. 4F).

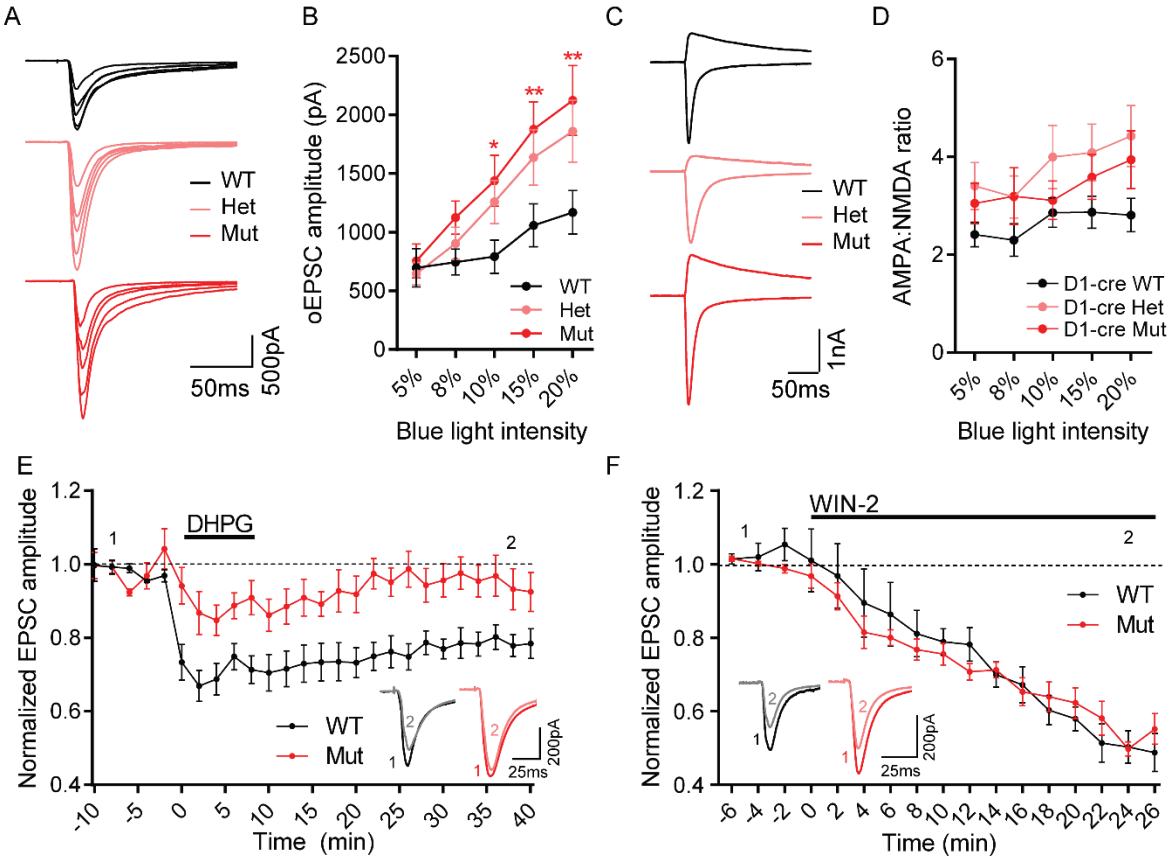

Figure 4. Enhanced cortico-dSPN synaptic transmission is driven by a loss of mGluR-LTD.
(A-B) Example cortically-mediated AMPAR-mediated oEPSC traces (A) and amplitude quantification (B) across light intensities. Tsc1-Het and KO dSPNs have significantly larger AMPAR currents that controls.
(C-D) AMPA:NMDA example traces (C) and quantification (D) across light intensities.
(E) DHPG-induced eCB-LTD of cortically-mediated oEPSCs is significantly impaired in Tsc1-KO dSPNs compared to controls. Example traces in inset show amplitudes at baseline and last five minutes of recording.
(F) Application of CB1R-agonist WIN-2 causes decrement in oEPSC amplitude in both Tsc1-WT and Tsc1-KO dSPNs.

Discussion

Here we use conditional gene deletion to investigate whether loss of *Tsc1* from striatal neurons was sufficient to induce repetitive motor behaviors related to ASD. We find that prenatal loss of *Tsc1*, similarly to postnatal deletion in SPNs as well as in other cell types, upregulates the mTORC1 signaling pathway and increases soma size [7, 26, 35, 36, 43, 44]. We show that prenatal *Tsc1* loss from dSPNs but not iSPNs enhances motor routine learning without inducing spontaneous RRBs including grooming and marble burying, and that this effect is not driven by locomotor hyperactivity. Further, we find that increased motor learning in mice with *Tsc1* deletion is associated with increased cortico-dSPN synaptic excitability and a loss of eCB-LTD. Notably, loss of only one copy of *Tsc1* is sufficient to increase cortical drive of dSPNs and increase motor learning. These findings extend our previous characterization of postnatal *Tsc1* loss to a more disease-relevant model by illustrating the importance of striatal circuits in generating repetitive behaviors in TSC and identifying a potential synaptic mechanism driving this behavior.

Our main goal was to investigate how cell-type specific loss of *Tsc1* affects behaviors linked to ASD and identify a synaptic mechanism driving these behaviors. It has been shown that loss of *Tsc1* function in the cerebellum and thalamus are sufficient to drive social behavior deficits and spontaneous RRBs including repetitive self-grooming in TSC mouse models, and we hypothesized that dysfunction of the striatum might also contribute to RRBs observed in TSC patients with ASD [35, 36]. We tested grooming and marble burying in mice with dSPN or iSPN *Tsc1* loss. The lack of an effect on the performance of these repetitive behaviors in our striatal model suggests that disruption of SPN activity alone is not sufficient to drive these specific repetitive behaviors, and that other brain regions may be more important for executing these behaviors. Indeed, the striatum has been shown to be important for the proper sequencing of grooming action patterns but not the initiation of grooming bouts [45], so our SPN-specific manipulation would not necessarily be expected to show differences in total time spent grooming.

Intriguingly, we found an enhancement in performance on the accelerating rotarod, a motor learning task that has been shown to rely on SPN activity and corticostriatal transmission [30], in mice with loss of Tsc1 in dSPNs in the dorsal striatum. Previous work has shown that striatal mTORC1 signaling is critical for motor learning on the accelerating rotarod assay, as inhibition of mTORC1 in SPNs by intrastriatal injection of rapamycin or mTOR-siRNA impairs learning [46]. Our results are congruent with these findings and show that the mTORC1-dependence of motor skill learning is bidirectional, as increasing the signaling pathway enhances performance. Importantly, the accelerating rotarod task has recently been recognized as a commonly-altered ASD-linked behavior, as deletion of at least 4 other of ASD-risk genes causes enhanced rotarod performance [13, 15, 31, 32]. In most cases, these are global gene deletions in which brain regions and circuits outside of the striatum could contribute to the phenotype. However one study showed that deletion of the ASD-risk gene *Nlgn3* in dSPNs, but not iSPNs, is sufficient to drive increased rotarod learning by enhancing the mouse's ability to perform a stereotyped stepping pattern, and that this is associated with dSPN disinhibition [13]. It is possible that an enhancement of the striatum's ability

or propensity to link motor sequences and form routines underlies the RRBs observed in people with ASD.

Our observation that loss of *Tsc1* increases cortico-dSPN synaptic excitability is consistent with the synaptic phenotype of decreased inhibitory synaptic transmission onto *Nlgn3* deleted dSPNs, as both models display net increases in dSPN excitatory/inhibitory synaptic balance and increased rotarod learning. Interestingly, however, no changes to eCB-LTD were detected in SPNs with *Nlgn3* loss, suggesting that increased dSPN synaptic excitability is sufficient to enhance rotarod learning without requiring alterations to plasticity processes [13]. This brings up the question of how exactly changes to cortico-dSPN synaptic excitability and eCB-LTD are driving enhanced motor learning in our model. For example, is the increase in cortico-dSPN synaptic excitation secondary to a loss of eCB-LTD, or is the enhanced synaptic excitation a primary change that results in disrupted plasticity? And which synaptic mechanism is essential for driving increased rotarod learning? One thing we know is that it is unlikely that striatal *Tsc1* deletion drives a non-specific primary increase in synaptic excitation, as thalamostriatal transmission is unaffected by postnatal *Tsc1* loss [26]. Further, there is a presynaptic release probability change associated with the increased corticostriatal transmission in dSPNs with postnatal *Tsc1* deletion, and considering the gene deletion is restricted to the postsynaptic dSPNs, a retrograde signaling mechanism must be primarily accountable [26].

A reasonable possibility then is that a primary loss of eCB-LTD causes deficits in excitatory synapse weakening that lead to enhanced synaptic excitability. This is supported by the fact that direct disruption of endocannabinoid synthesis and release from dSPNs increases the excitatory synaptic transmission they receive [39]. Further, mGluR5 KO mice show increased density of dendritic spines in cortex, which is the site cortical synapses onto dSPNs [47]. The enhancement of excitatory transmission could even be a developmental phenotype, such that early-life corticostriatal synaptic pruning that relies on the same mechanisms as mGluR-LTD doesn't properly occur and results in corticostriatal hyperconnectivity [48]. This is supported by the observation that the maturational increase in synaptic excitation onto dSPNs emerges between three and four weeks of age, a developmental stage at which pruning of corticostriatal inputs occurs (Fig. S4) [49]. However, whether enhanced rotarod learning is driven primarily by altered plasticity or by increased corticostriatal connectivity is unclear. Though enhanced excitation/inhibition ratio of dSPNs is found to be the primary cause of increased motor learning in the *Nlgn3* model, others have found that eCB-mediated plasticity is indeed altered in this model [50]. Further, deficits in rotarod learning occur in mice lacking NMDAR1 in the striatum, and this is associated with disrupted striatal plasticity but normal AMPAR-mediated transmission [51]. Thus, it is possible that altered plasticity could be driving altered rotarod learning independently of changes to baseline synaptic transmission.

Another possible mechanism involves the circuit-level changes in striatal activity during motor learning. It has previously been shown that the dynamics of striatal activity differ between the early and late phases of rotarod learning, such that activity in the dorsomedial striatum (DMS) is more important for the initial training, whereas the dorsolateral striatum (DLS) is activated later in training as the motor pattern becomes routine [30]. Plasticity processes, including eCB-LTD, have been found to be important

for the transition of activity from the DMS to DLS during striatal-dependent learning [52]. Presynaptic plasticity in particular has been proposed to underlie the changes to corticostriatal coupling during rotarod learning, as the activity relationships between cortical somas and terminals are altered over the course of training [53]. Because our manipulation is targeted to the entire dorsal striatum, we are unable to disentangle the influence of DMS versus DLS activity on the enhanced rotarod performance in *Tsc1* deleted mice. However, it is possible that the loss of eCB-LTD that results from *Tsc1* deletion changes the way that this transition happens with the end result of enhanced motor learning. Thus, it is plausible that loss of eCB-LTD directly disrupts the transfer of SPN activity from the DMS to the DLS and this leads to enhanced motor learning, while enhanced cortico-dSPN excitability occurs in parallel but is not directly driving the motor learning phenotype.

Future studies will aim to elucidate the molecular mechanism of enhanced motor learning in mice with loss of *Tsc1* from dSPNs, and determine whether altered plasticity or excitatory transmission is responsible. Rescue studies involving administration of a CB1R agonist, such as WIN, could be used to disentangle synaptic mechanisms. In addition, biochemical studies will be used to determine the molecular mechanism of disrupted mGluR-LTD in *Tsc1* deleted dSPNs, and to investigate why dSPNs show stronger cellular phenotypes than iSPNs with *Tsc1* loss. Lastly, additional striatal-dependent behaviors will be assayed, such as those investigating the use of goal-directed or habitual learning strategies, to further characterize the contribution of striatal dysfunction in RRBs in a cell-type specific manner.

Experimental Procedures

Mouse lines

Animal experiments were performed in accordance with protocols approved by UC Berkeley's Animal Care and Use Committee. Male and female mice were used for all experiments. The ages used were p40-50 unless otherwise noted. All mice used for experiments were hemizygous for the *Ai9*, *D1-Cre*, *A2a-Cre*, or *Thy1-ChR2-YFP* transgene to avoid potential physiological or behavioral alterations.

The following mouse lines were used:

Mouse line	**Source**	**Reference**
Tsc1$^{fl/fl}$	JAX strain #005680	[27]
Drd1a-Cre (EY217)	GENSAT (MMRRC #030778-UCD)	[28]
Adora2a-Cre (KG139)	GENSAT (MMRRC #031168-UCD)	[28]
Ai9 (tdTomato)	JAX strain #007909	[29]
Thy1-ChR2-YFP	JAX strain #007612	[34]
Tsc2$^{+/-}$	JAX strain #004686	[54]

Immunohistochemistry

Mice were perfused transcardially with PBS and 4% paraformaldehyde. Brains were post-fixed in 4% paraformaldehyde overnight and sectioned at 30 μm. Sections were blocked for 1hr at room temperature in BlockAid (Thermo Fisher Scientific) and incubated for 36 hr at 4°C with antibodies against phosphorylated (Ser240/244) S6 ribosomal protein (1:800, Cell Signaling Technology, catalog # 5364S) and NeuN (1:800, Millipore, catalog # MAB377). Sections were washed and incubated for 1h at RT with Alexa Fluor 633- and 488-conjugated secondary antibodies (1:500, Invitrogen, catalog #'s A-21070 and A-31553). Sections were mounted onto slides using Vectashield reagent with DAPI (Vector Labs).

Imaging and analysis

Z-stack images were taken on a confocal microscope (Zeiss LSM 780 AxioExaminer) with a 20x objective using the same exposure and acquisition settings for each section. To quantify p-S6 levels and soma volume, regions of interest (ROIs) were automatically created based on the tdTomato signal in Imaris software. The mean fluorescence intensity per ROI and average soma volume were calculated using Imaris.

Behavior

Behavior studies were carried out in the dark phase of the light cycle under red lights (open field) or white lights (rotarod and marble burying). Mice were habituated to the behavior room for at least 30 min prior to testing and covered by a black-out curtain. Mice were given at least one day in between different tests. All behavior equipment was cleaned between each trial/mouse with 70% ethanol, and additionally rinsed in diluted soap followed by water at the end of the day. If male and female mice were to be tested on the same day, male mice were run in behavior first, returned to the husbandry room, after which all equipment was thoroughly cleaned, and female mice were brought in for habituation. All animals to be tested from a given cage were run in each behavior test in the same day. Behavioral tests were performed with adult male and females (6-10

weeks old). The experimenter was blind to genotype throughout the testing and scoring procedures.

Open field
Exploratory behavior in a novel environment and general locomotor activity were assessed by a 60 min session in an open field chamber (40 cm L x 40 cm W x 34 cm H) made of transparent plexiglass. Horizontal photobeams to measure rearing were positioned at 9 cm of height. The mouse was placed in the bottom right hand corner of the arena and behavior was recorded using an overhead camera and analyzed using the ANY-maze (Stoelting Co.) behavior tracking software. An observer manually scored grooming behavior during the first 20 minutes of the test.

Marble burying
Cages were filled 5 cm deep with corn-cob bedding, and 20 marbles were evenly spaced on top of the bedding in a 4x5 grid. Mice were placed in the test cage (1 mouse per cage) for 20 min, with white noise playing. After the test, mice were removed and returned to the home cage, and the number of unburied marbles was counted. A marble was considered unburied if half or more of it was left uncovered by bedding. A photo of the cage was taken pre-test and post-test as a record.

Rotarod
The accelerating rotarod test was used to examine motor learning. Mice were tested on a rotarod apparatus (Ugo Basile: 47650) for 4 consecutive days. Three trials were completed per day with a 5min break between trials. The rotarod was accelerated from 5-40 revolutions per minute (rpm) over 300s for trials 1-6 (days 1 and 2), and from 10-80 rpm over 300 s for trials 7-12 (days 3 and 4). On the first testing day, mice were acclimated to the apparatus by being placed on the rotarod rotating at a constant 5rpm for 60 s and returned to their home cage for 5 minutes prior to starting trial 1. Latency to fall, or to rotate off the top of the rotarod barrel, was measured by the rotarod stop-trigger timer.

<u>Slice preparation for electrophysiology</u>
Mice were perfused transcardially with ice-cold ACSF (pH=7.4) containing (in mM): 127 NaCl, 25 $NaHCO_3$, 1.25 NaH_2PO_4, 2.5 KCl, 1$MgCl_2$, 2 $CaCl_2$, and 25 glucose, bubbled continuously with carbogen (95% O_2 and 5% CO_2). Brains were rapidly removed and coronal slices (275 µm) were cut on a VT1000S vibrotome (Leica) in oxygenated ice-cold choline-based external solution (pH=7.8) containing (in mM): 110 choline chloride, 25 $NaHCO_3$, 1.25 $NaHPO_4$, 2.5 KCl, 7 $MgCl_2$, 0.5 $CaCl_2$, 25 glucose, 11.6 sodium ascorbate, and 3.1 sodium pyruvate. Slices were recovered in ACSF at 34°C for 15 minutes and then kept at RT before recording.

<u>Whole-cell patch-clamp recording</u>
Recordings were made with a MultiClamp 700B amplifier (Molecular Devices) at RT using 3-5 MOhm glass patch electrodes. Current clamp recordings were made using a potassium-based internal solution (pH=7.4) containing (in mM): 135 $KMeSO_4$, 5 KCl, 5 HEPES, 4 Mg-ATP, 0.3 Na-GTP, 10 phosphocreatine, and 1 ETGA. Traces were

analyzed in Igor Pro, and miniature events were identified and measured using custom software. Recordings with a series resistance >25 MOhms or holding current above -200 pA were rejected.

Current-clamp
For oAP experiments, optogenetic stimulation consisted of a full-field pulse of blue light (470 nm, 0.15-0.5 ms) through a 63x objective. For intrinsic excitability experiments (Fig. 3F,G only), NBQX (10 μM), CPP (10 μM) and picrotoxin (50 μM) were added to the external solution to block synaptic transmission. For the oAP experiments, inhibition was not blocked (Fig. 3B-E). No holding current was applied to the membrane.

Voltage-clamp
Voltage-clamp recordings were made using a cesium-based internal solution (pH=7.4) containing (in mM): 120 $CsMeSO_4$, 15 CsCl, 10 TEA-Cl, 8 NaCl, 10 HEPES, 1 EGTA, 5 QX-314, 4 Mg-ATP, and 0.3 Na-GTP. Recordings were acquired with the amplifier Bessel filter set at 3 kHz. Miniature synaptic transmission was assessed in the presence of TTX (1 μM) to prevent action potential-mediated release. Picrotoxin (50 μM) and CPP (10 μM) were included for mEPSC experiments to isolate AMPAR-mediated events. oEPSC experiments were performed in picrotoxin (50 μM) and CPP (10 μM), and optogenetic stimulation consisted of a full-field pulse of blue light (470 nm, 0.15 ms) through a 63x objective (Fig. 3B-E, 4A-F, S2-3). To measure AMPA/NMDA ratio, experiments were performed in 50 μM picrotoxin and the membrane was held at different potentials to isolate primarily AMPAR (-80 mV) or compound AMPAR and NMDAR (+40 mV) currents. The current at +40 mV was measured 50 ms after stimulation, by which time the AMPAR-mediated current has fully decayed.

Plasticity
eCB-LTD was induced by bath application of 100 μM DHPG for 10 min, following a 10 min baseline measurement of oEPSC amplitude. DHPG was subsequently washed off and oEPSC amplitude was monitored every 30 sec for an additional 40 min. Picrotoxin (50uM) was added to the bath during eCB-LTD experiments to isolate excitatory events, and perfusion flow rate was set to 5 mL/min. Cells were held at -50 mV to facilitate opening of L-type calcium channels. CB1R antagonist AM251 (10 μM) was added to the bath during a subset of eCB-LTD experiments n dSPN-Tsc1 WT cells verify that the LTD observed during these experiments was dependent upon CB1R activation. For CB1R agonism experiments, WIN2 (2 μM) was applied to the bath throughout the recording.

Statistical analyses
Two-tailed unpaired t-tests were used for comparisons between two groups, and F-test was used to confirm that variances were not significantly different. For data that did not pass D'Agostino & Pearson normality test, Mann Whitney test was used. A one-way ANOVA with Sidak's post-doc test was used to compare the means of three or more groups. A two-way ANOVA with Sidak's post-hoc tests was used to compare mean differences between groups for experiments with two independent variables. P-values were corrected for multiple comparisons. Cumulative distributions were analyzed using

the Kolmogorov-Smirnov test. For data that did not pass the D'Agostino and Pearson normality test, the Kruskal-Wallis with Dunn's post-hoc test was used. Values for all statistical comparisons are provided in Supplemental Tables S1-S4.

References

1. American Psychological Association, *Diagnostic and statistical manual of mental disorders : DSM-5. 5th edn.* 2013.
2. SFARI. *SFARI Gene*. 2019 [cited 2019 July 15]; Available from: https://gene.sfari.org/.
3. Curatolo, P., R. Moavero, and P.J. de Vries, *Neurological and neuropsychiatric aspects of tuberous sclerosis complex.* The Lancet Neurology, 2015. **14**(7): p. 733-745.
4. Saxton, R.A. and D.M. Sabatini, *mTOR Signaling in Growth, Metabolism, and Disease.* Cell, 2017. **168**(6): p. 960-976.
5. de Vries, P.J., *Targeted Treatments for Cognitive and Neurodevelopmental Disorders in Tuberous Sclerosis Complex.* Neurotherapeutics, 2010. **7**: p. 275-282.
6. Bateup, H.S., et al., *Excitatory/inhibitory synaptic imbalance leads to hippocampal hyperexcitability in mouse models of tuberous sclerosis.* Neuron, 2013. **78**(3): p. 510-22.
7. Bateup, H.S., et al., *Loss of Tsc1 in vivo impairs hippocampal mGluR-LTD and increases excitatory synaptic function.* J Neurosci, 2011. **31**(24): p. 8862-9.
8. Fuccillo, M.V., *Striatal Circuits as a Common Node for Autism Pathophysiology.* Front Neurosci, 2016. **10**: p. 27.
9. Turner, K.C., et al., *Atypically diffuse functional connectivity between caudate nuclei and cerebral cortex in autism.* Behav Brain Funct, 2006. **2**: p. 34.
10. Qiu, A., et al., *Basal ganglia shapes predict social, communication, and motor dysfunctions in boys with autism spectrum disorder.* J Am Acad Child Adolesc Psychiatry, 2010. **49**(6): p. 539-51, 551 e1-4.
11. Di Martino, A., et al., *Aberrant striatal functional connectivity in children with autism.* Biol Psychiatry, 2011. **69**(9): p. 847-56.
12. Asano, E., D.C. Chugani, O. Muzik, M. Behen, J. Janisse, R. Rothermel, T.J. Mangner, P.K. Chakraborty, H.T. Chugani, *Autism in tuberous sclerosis complex is related to both cortical and subcortical dysfunction.* Neurology, 2001. **57**: p. 1269-1277.
13. Rothwell, P.E., et al., *Autism-associated neuroligin-3 mutations commonly impair striatal circuits to boost repetitive behaviors.* Cell, 2014. **158**(1): p. 198-212.
14. Peixoto, R.T., et al., *Early hyperactivity and precocious maturation of corticostriatal circuits in Shank3B(-/-) mice.* Nat Neurosci, 2016. **19**(5): p. 716-24.
15. Platt, R.J., et al., *Chd8 Mutation Leads to Autistic-like Behaviors and Impaired Striatal Circuits.* Cell Rep, 2017. **19**(2): p. 335-350.
16. Jaramillo, T.C., et al., *Altered Striatal Synaptic Function and Abnormal Behaviour in Shank3 Exon4-9 Deletion Mouse Model of Autism.* Autism Res, 2016. **9**(3): p. 350-75.
17. Wang, X., et al., *Altered mGluR5-Homer scaffolds and corticostriatal connectivity in a Shank3 complete knockout model of autism.* Nat Commun, 2016. **7**: p. 11459.
18. Graybiel, A.M., *The basal ganglia: learning new tricks and loving it.* Curr Opin Neurobiol, 2005. **15**(6): p. 638-44.

19. Gertler, T.S., C.S. Chan, and D.J. Surmeier, *Dichotomous anatomical properties of adult striatal medium spiny neurons.* J Neurosci, 2008. **28**(43): p. 10814-24.
20. Heiman, M., et al., *A translational profiling approach for the molecular characterization of CNS cell types.* Cell, 2008. **135**(4): p. 738-48.
21. Gerfen, C.R. and D.J. Surmeier, *Modulation of striatal projection systems by dopamine.* Annu Rev Neurosci, 2011. **34**: p. 441-66.
22. Kreitzer, A.C., *Physiology and pharmacology of striatal neurons.* Annu Rev Neurosci, 2009. **32**: p. 127-47.
23. Bateup, H.S., et al., *Distinct subclasses of medium spiny neurons differentially regulate striatal motor behaviors.* Proc Natl Acad Sci U S A, 2010. **107**(33): p. 14845-50.
24. Kravitz, A.V., et al., *Regulation of parkinsonian motor behaviours by optogenetic control of basal ganglia circuitry.* Nature, 2010. **466**(7306): p. 622-6.
25. Graybiel, A.M. and S.T. Grafton, *The striatum: where skills and habits meet.* Cold Spring Harb Perspect Biol, 2015. **7**(8): p. a021691.
26. Benthall, K.N., S.L. Ong, and H.S. Bateup, *Corticostriatal Transmission Is Selectively Enhanced in Striatonigral Neurons with Postnatal Loss of Tsc1.* Cell Rep, 2018. **23**(11): p. 3197-3208.
27. Kwiatkowski, D.J., *A mouse model of TSC1 reveals sex-dependent lethality from liver hemangiomas, and up-regulation of p70S6 kinase activity in Tsc1 null cells.* Human Molecular Genetics, 2002. **11**(5): p. 525-534.
28. Gong, S., et al., *Targeting Cre recombinase to specific neuron populations with bacterial artificial chromosome constructs.* J Neurosci, 2007. **27**(37): p. 9817-23.
29. Madisen, L., et al., *A robust and high-throughput Cre reporting and characterization system for the whole mouse brain.* Nat Neurosci, 2010. **13**(1): p. 133-40.
30. Yin, H.H., et al., *Dynamic reorganization of striatal circuits during the acquisition and consolidation of a skill.* Nat Neurosci, 2009. **12**(3): p. 333-41.
31. Nakatani, J., et al., *Abnormal behavior in a chromosome-engineered mouse model for human 15q11-13 duplication seen in autism.* Cell, 2009. **137**(7): p. 1235-46.
32. Penagarikano, O., et al., *Absence of CNTNAP2 leads to epilepsy, neuronal migration abnormalities, and core autism-related deficits.* Cell, 2011. **147**(1): p. 235-46.
33. Crino, P.B., *Evolving neurobiology of tuberous sclerosis complex.* Acta Neuropathol, 2013. **125**(3): p. 317-32.
34. Arenkiel, B.R., et al., *In vivo light-induced activation of neural circuitry in transgenic mice expressing channelrhodopsin-2.* Neuron, 2007. **54**(2): p. 205-18.
35. Tsai, P.T., et al., *Autistic-like behaviour and cerebellar dysfunction in Purkinje cell Tsc1 mutant mice.* Nature, 2012. **488**(7413): p. 647-51.
36. Normand, E.A., et al., *Temporal and mosaic Tsc1 deletion in the developing thalamus disrupts thalamocortical circuitry, neural function, and behavior.* Neuron, 2013. **78**(5): p. 895-909.
37. Kreitzer, A.C. and R.C. Malenka, *Striatal plasticity and basal ganglia circuit function.* Neuron, 2008. **60**(4): p. 543-54.

38. Wu, Y.W., et al., *Input- and cell-type-specific endocannabinoid-dependent LTD in the striatum.* Cell Rep, 2015. **10**(1): p. 75-87.
39. Shonesy, B.C., et al., *Role of Striatal Direct Pathway 2-Arachidonoylglycerol Signaling in Sociability and Repetitive Behavior.* Biol Psychiatry, 2018. **84**(4): p. 304-315.
40. Chevere-Torres, I., et al., *Metabotropic glutamate receptor-dependent long-term depression is impaired due to elevated ERK signaling in the DeltaRG mouse model of tuberous sclerosis complex.* Neurobiol Dis, 2012. **45**(3): p. 1101-10.
41. Auerbach, B.D., E.K. Osterweil, and M.F. Bear, *Mutations causing syndromic autism define an axis of synaptic pathophysiology.* Nature, 2011. **480**(7375): p. 63-8.
42. Potter, W.B., et al., *Reduced juvenile long-term depression in tuberous sclerosis complex is mitigated in adults by compensatory recruitment of mGluR5 and Erk signaling.* PLoS Biol, 2013. **11**(8): p. e1001627.
43. Weston, M.C., H. Chen, and J.W. Swann, *Loss of mTOR repressors Tsc1 or Pten has divergent effects on excitatory and inhibitory synaptic transmission in single hippocampal neuron cultures.* Front Mol Neurosci, 2014. **7**: p. 1.
44. Tavazoie, S.F., et al., *Regulation of neuronal morphology and function by the tumor suppressors Tsc1 and Tsc2.* Nat Neurosci, 2005. **8**(12): p. 1727-34.
45. Kalueff, A.V., et al., *Neurobiology of rodent self-grooming and its value for translational neuroscience.* Nat Rev Neurosci, 2016. **17**(1): p. 45-59.
46. Bergeron, Y., et al., *mTOR signaling contributes to motor skill learning in mice.* Front Mol Neurosci, 2014. **7**: p. 26.
47. Chen, C.C., H.C. Lu, and J.C. Brumberg, *mGluR5 knockout mice display increased dendritic spine densities.* Neurosci Lett, 2012. **524**(1): p. 65-8.
48. Piochon, C., M. Kano, and C. Hansel, *LTD-like molecular pathways in developmental synaptic pruning.* Nat Neurosci, 2016. **19**(10): p. 1299-310.
49. Kuo, H.Y. and F.C. Liu, *Synaptic Wiring of Corticostriatal Circuits in Basal Ganglia: Insights into the Pathogenesis of Neuropsychiatric Disorders.* eNeuro, 2019. **6**(3).
50. Martella, G., et al., *The neurobiological bases of autism spectrum disorders: the R451C-neuroligin 3 mutation hampers the expression of long-term synaptic depression in the dorsal striatum.* Eur J Neurosci, 2018. **47**(6): p. 701-708.
51. Dang, M.T., et al., *Disrupted motor learning and long-term synaptic plasticity in mice lacking NMDAR1 in the striatum.* Proc Natl Acad Sci U S A, 2006. **103**(41): p. 15254-9.
52. Gremel, C.M., et al., *Endocannabinoid Modulation of Orbitostriatal Circuits Gates Habit Formation.* Neuron, 2016. **90**(6): p. 1312-1324.
53. Kupferschmidt, D.A., et al., *Parallel, but Dissociable, Processing in Discrete Corticostriatal Inputs Encodes Skill Learning.* Neuron, 2017. **96**(2): p. 476-489 e5.
54. Onda, H., Andreas Lueck, Peter W. Marks, Henry B. Warren, David J. Kwiatkowski, *Tsc2+/- mice develop tumors in multiple sites that express gelsolin and are influenced by genetic background.* The Journal of Clinical Investigation, 1999. **104**(6).

Supplementary Figures and Tables

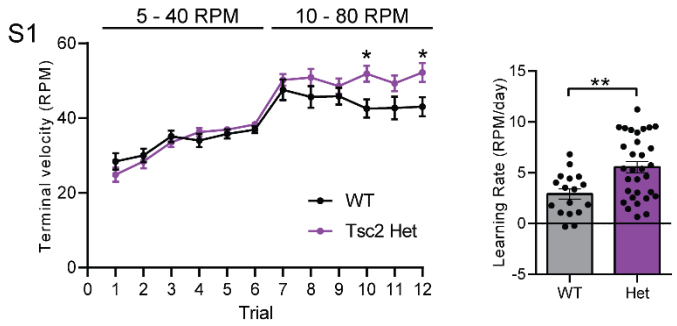

Figure S1. Rotarod learning is enhanced in global *Tsc2*+/- mice.
Performance on the accelerating rotarod is significantly increased in *Tsc2*+/- mice on the final training day compared to controls. Learning rate across the four days is significantly greater in *Tsc2*+/- mice.

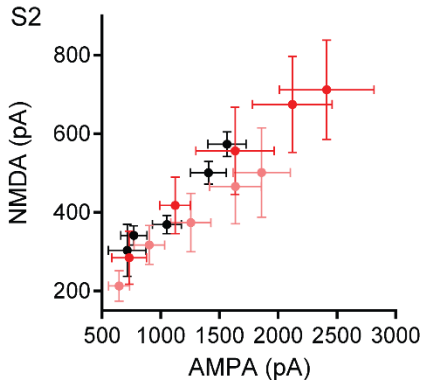

Figure S2. AMPA and NMDA currents are increased to a similar extent in mice with loss of Tsc1 from dSPNs.
Quantification of AMPA (x-axis) and NMDA (y-axis) current amplitudes across light intensities.

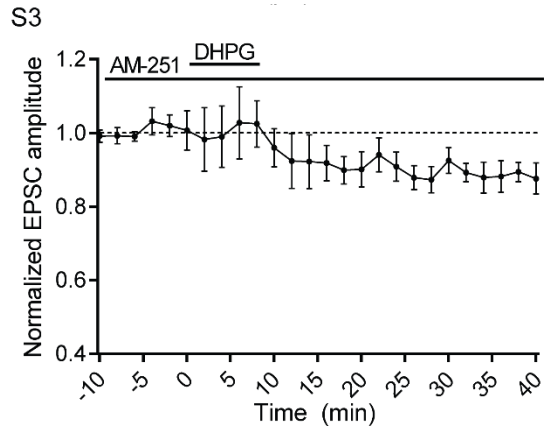

Figure S3. DHPG-mediated LTD in dSPNs is dependent upon eCB signaling.
DHPG-LTD cannot be induced in the presence of CB1R antagonist AM-251.

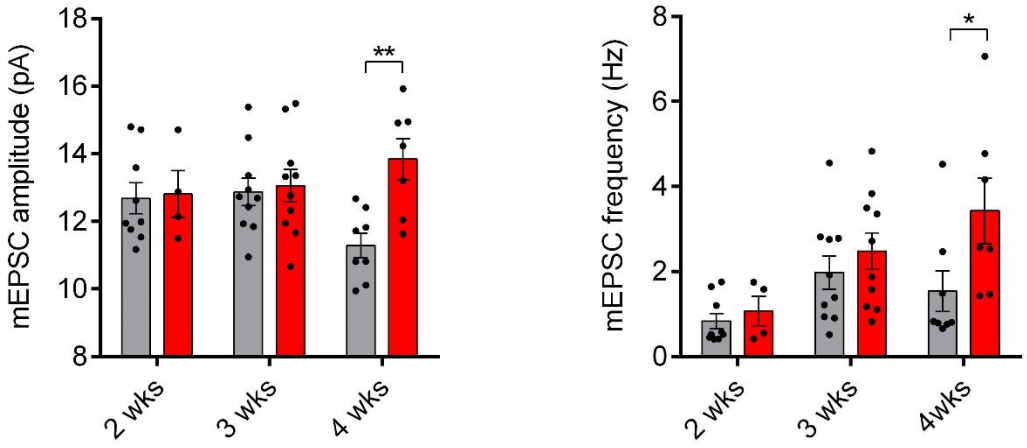

Figure S4. Developmental time-course of mEPSCs in Tsc1-WT and Tsc1-KO dSPNs.
Different mEPSC amplitude and frequency developmental time-course in dSPNs with *Tsc1* loss, consistent with changes in corticostriatal synaptic pruning deficits. Tsc1-WT columns are grey and Tsc1-KO columns are red.

Table S1. Two-way ANOVA values, related to figures 2-4, S1, S4.

Figure panel	Test	Source of variation	F value	Comparison	DF	P value
2E	ANOVA	Interaction	0.9925		22	0.4709
		Trial	34.71		11	< 0.0001
		Genotype	38.85		2	< 0.0001
	Sidak post-hoc			Trial 1, dSPN WT v dSPN Het	1037	0.9995
				Trial 1, dSPN WT v dSPN KO		0.9096
				Trial 2, dSPN WT v dSPN Het		0.9899
				Trial 2, dSPN WT v dSPN KO		0.2220
				Trial 3, dSPN WT v dSPN Het		0.6958
				Trial 3, dSPN WT v dSPN KO		0.1468
				Trial 4, dSPN WT v dSPN Het		0.9600
				Trial 4, dSPN WT v dSPN KO		0.3809
				Trial 5, dSPN WT v dSPN Het		0.9869
				Trial 5, dSPN WT v dSPN KO		0.3207
				Trial 6, dSPN WT v dSPN Het		0.7308
				Trial 6, dSPN WT v dSPN KO		0.0820
				Trial 7, dSPN WT v dSPN Het		0.9351
				Trial 7, dSPN WT v dSPN KO		0.1160
				Trial 8, dSPN WT v dSPN Het		0.7030
				Trial 8, dSPN WT v dSPN KO		0.0011
				Trial 9, dSPN WT v dSPN Het		0.5447
				Trial 9, dSPN WT v dSPN KO		0.0006
				Trial 10, dSPN WT v dSPN Het		0.3460
				Trial 10, dSPN WT v dSPN KO		0.0002
				Trial 11, dSPN WT v dSPN Het		0.0356
				Trial 11, dSPN WT v dSPN KO		< 0.0001
				Trial 12, dSPN WT v dSPN Het		0.1461

				Trial 12, dSPN WT v dSPN KO		0.0001
2G	ANOVA	Interaction	0.5481		22	0.9548
		Trial	25.85		11	< 0.0001
		Genotype	1.215		2	0.2972
	Sidak post-hoc			Trial 1, iSPN WT v iSPN Het	744	0.8859
				Trial 1, iSPN WT v iSPN KO		0.8563
				Trial 2, iSPN WT v iSPN Het		0.8709
				Trial 2, iSPN WT v iSPN KO		0.6465
				Trial 3, iSPN WT v iSPN Het		0.9788
				Trial 3, iSPN WT v iSPN KO		0.8760
				Trial 4, iSPN WT v iSPN Het		0.5066
				Trial 4, iSPN WT v iSPN KO		0.4173
				Trial 5, iSPN WT v iSPN Het		0.9304
				Trial 5, iSPN WT v iSPN KO		0.5181
				Trial 6, iSPN WT v iSPN Het		0.9609
				Trial 6, iSPN WT v iSPN KO		0.7748
				Trial 7, iSPN WT v iSPN Het		0.9697
				Trial 7, iSPN WT v iSPN KO		0.4453
				Trial 8, iSPN WT v iSPN Het		0.9979
				Trial 8, iSPN WT v iSPN KO		0.5569
				Trial 9, iSPN WT v iSPN Het		0.6250
				Trial 9, iSPN WT v iSPN KO		0.3420
				Trial 10, iSPN WT v iSPN Het		0.1121
				Trial 10, iSPN WT v iSPN KO		0.4636
				Trial 11, iSPN WT v iSPN Het		0.9635
				Trial 11, iSPN WT v iSPN KO		0.9819
				Trial 12, iSPN WT v iSPN Het		0.9730
				Trial 12, iSPN WT v iSPN KO		0.5970
3C	ANOVA	Interaction	1.223		12	0.2805
		Light intensity	19.85		6	< 0.0001

		Genotype	40.62		2	< 0.0001
	Sidak post-hoc			1%, dSPN WT v dSPN Het	88	0.9586
				1%, dSPN WT v dSPN KO		0.0025
				2%, dSPN WT v dSPN Het		0.0513
				2%, dSPN WT v dSPN KO		< 0.0001
				5%, dSPN WT v dSPN Het		0.0029
				5%, dSPN WT v dSPN KO		0.0004
				10%, dSPN WT v dSPN Het		0.0074
				10%, dSPN WT v dSPN KO		0.0030
				20%, dSPN WT v dSPN Het		0.0087
				20%, dSPN WT v dSPN KO		0.0080
				50%, dSPN WT v dSPN Het		0.0118
				50%, dSPN WT v dSPN KO		0.0347
				100%, dSPN WT v dSPN Het		0.0387
				100%, dSPN WT v dSPN KO		0.0742
3E	ANOVA	Interaction	0.2747		14	0.9959
		Light intensity	145.8		7	< 0.0001
		Genotype	0.8414		2	0.4326
	Sidak post-hoc			1%, iSPN WT v iSPN Het	199	>0.9999
				1%, iSPN WT v iSPN KO		>0.9999
				2%, iSPN WT v iSPN Het		>0.9999
				2%, iSPN WT v iSPN KO		>0.9999
				5%, iSPN WT v iSPN Het		0.6399
				5%, iSPN WT v iSPN KO		0.9050
				10%, iSPN WT v iSPN Het		0.3279
				10%, iSPN WT v iSPN KO		0.9392
				15%, iSPN WT v iSPN Het		0.2913
				15%, iSPN WT v iSPN KO		0.4713
				20%, iSPN WT v iSPN Het		0.8359
				20%, iSPN WT v iSPN KO		0.7617
				50%, iSPN WT v iSPN Het		0.9849

				50%, iSPN WT v iSPN KO		0.8650
				100%, iSPN WT v iSPN Het		0.8965
				100%, iSPN WT v iSPN KO		0.9957
3G	ANOVA	Interaction	1.229		24	0.2130
		Current Step	87.05		12	< 0.0001
		Genotype	6.373		2	0.0019
	Sidak post-hoc			50pA, dSPN WT v dSPN Het	345	>0.9999
				50pA, dSPN WT v dSPN KO		>0.9999
				100pA, dSPN WT v dSPN Het		0.9338
				100pA, dSPN WT v dSPN KO		0.9499
				150pA, dSPN WT v dSPN Het		0.8736
				150pA, dSPN WT v dSPN KO		0.6412
				200pA, dSPN WT v dSPN Het		0.9405
				200pA, dSPN WT v dSPN KO		0.1566
				250pA, dSPN WT v dSPN Het		0.9390
				250pA, dSPN WT v dSPN KO		0.0599
				300pA, dSPN WT v dSPN Het		0.9961
				300pA, dSPN WT v dSPN KO		0.0101
				350pA, dSPN WT v dSPN Het		0.8879
				350pA, dSPN WT v dSPN KO		0.0170
				400pA, dSPN WT v dSPN Het		0.8418
				400pA, dSPN WT v dSPN KO		0.0324
				500pA, dSPN WT v dSPN Het		0.9426
				500pA, dSPN WT v dSPN KO		0.5036
				600pA, dSPN WT v dSPN Het		0.9926
				600pA, dSPN WT v dSPN KO		0.9993

				700pA, dSPN WT v dSPN Het		0.9994
				700pA, dSPN WT v dSPN KO		0.8071
				800pA, dSPN WT v dSPN Het		0.9819
				800pA, dSPN WT v dSPN KO		0.4929
				1000pA, dSPN WT v dSPN Het		0.8105
				1000pA, dSPN WT v dSPN KO		0.2622
4B	ANOVA	Interaction	0.7969		8	0.6059
		Light intensity	0.8060		4	< 0.0001
		Genotype	8.364		2	0.0003
	Sidak post-hoc			5%, dSPN WT v dSPN Het	202	0.9900
				5%, dSPN WT v dSPN KO		0.9753
				8%, dSPN WT v dSPN Het		0.8962
				8%, dSPN WT v dSPN KO		0.6151
				10%, dSPN WT v dSPN Het		0.4108
				10%, dSPN WT v dSPN KO		0.0349
				15%, dSPN WT v dSPN Het		0.2562
				15%, dSPN WT v dSPN KO		0.0054
				20%, dSPN WT v dSPN Het		0.1482
				20%, dSPN WT v dSPN KO		0.0014
4D	ANOVA	Interaction				
		Light intensity				
		Genotype				
	Sidak post-hoc			5%, dSPN WT v dSPN Het		0.2533
				5%, dSPN WT v dSPN KO		0.3765
				8%, dSPN WT v dSPN Het		0.3178
				8%, dSPN WT v dSPN KO		0.3863
				10%, dSPN WT v dSPN Het		0.2277
				10%, dSPN WT v dSPN KO		0.8928
				15%, dSPN WT v dSPN Het		0.1855

				15%, dSPN WT v dSPN KO		0.4225
				20%, dSPN WT v dSPN Het		0.0596
				20%, dSPN WT v dSPN KO		0.1363
4E	ANOVA	Interaction	1.666		25	0.0272
		Time	5.195		25	< 0.0001
		Genotype	155.3		1	< 0.0001
4F	ANOVA	Interaction	0.4394		16	0.9685
		Time	24.64		16	< 0.0001
		Genotype	0.8739		1	0.3518
S1	ANOVA	Interaction	1.975		11	0.0287
		Trial	30.10		11	< 0.0001
		Genotype	10.97		1	0.0010
	Sidak post-hoc			Trial 1	552	0.9547
				Trial 2		>0.9999
				Trial 3		>0.9999
				Trial 4		0.9991
				Trial 5		>0.9999
				Trial 6		>0.9999
				Trial 7		0.9955
				Trial 8		0.6207
				Trial 9		0.9950
				Trial 10		0.0192
				Trial 11		0.2653
				Trial 12		0.0223
S4 (left)	ANOVA	Interaction	3.805		2	0.0303
		Trial	0.3626		2	0.6980
		Genotype	5.228		1	0.0273
	Sidak post-hoc			2 weeks	42	0.9982
				3 weeks		0.9871
				4 weeks		0.0026
S4 (right)	ANOVA	Interaction	1.641		2	0.2059
		Trial	4.846		2	0.0128
		Genotype	4.833		1	0.0335
	Sidak post-hoc			2 weeks	42	0.9866
				3 weeks		0.7844
				4 weeks		0.0241

Table S2. One-way ANOVA values, related to figures 2, 3.

Figure panel	F value	DF	P value	Post-hoc test	Comparison	P value
2B	2.128	90	0.1252	Sidak	dSPN WT v dSPN Het	0.8109
					dSPN WT v dSPN KO	0.0873
2D	0.2097	106	0.8112	Sidak	dSPN WT v dSPN Het	0.7768
					dSPN WT v dSPN KO	0.9876
3I	3.712	40	0.0337	Sidak	dSPN WT v dSPN Het	0.1353
					dSPN WT v dSPN KO	0.0205
3J	7.822	40	0.0014	Sidak	dSPN WT v dSPN Het	0.0099
					dSPN WT v dSPN KO	0.0011
3L	1.260	44	0.2942	Sidak	iSPN WT v iSPN Het	0.9591
					iSPN WT v iSPN KO	0.3502
3M	0.9151	44	0.4083	Sidak	iSPN WT v iSPN Het	0.6019
					iSPN WT v iSPN KO	0.3189

Table S3. Kruskal-Wallis test values, related to figures 1, 2.

Figure panel	Kruskal-Wallis statistic	Post-hoc test	Comparison	P value
1D	3090	Dunn's	dSPN WT v dSPN Het	<0.0001
			dSPN WT v dSPN KO	<0.0001
1E	465.2	Dunn's	dSPN WT v dSPN Het	0.001
			dSPN WT v dSPN KO	<0.0001
1G	92.20	Dunn's	iSPN WT v iSPN Het	0.0005
			iSPN WT v iSPN KO	<0.0001
1H	120.8	Dunn's	iSPN WT v iSPN Het	0.2932
			iSPN WT v iSPN KO	<0.0001
2A	3.213	Dunn's	dSPN WT v dSPN Het	0.2659
			dSPN WT v dSPN KO	0.2537
2A	1.819	Dunn's	iSPN WT v iSPN Het	0.6710
			iSPN WT v iSPN KO	0.4233
2B	2.882	Dunn's	iSPN WT v iSPN Het	0.2267
			iSPN WT v iSPN KO	0.4671
2C	1.634	Dunn's	dSPN WT v dSPN Het	0.4507
			dSPN WT v dSPN KO	0.7941
2C	0.03447	Dunn's	iSPN WT v iSPN Het	>0.9999
			iSPN WT v iSPN KO	>0.9999
2D	2.775	Dunn's	iSPN WT v iSPN Het	>0.9999
			iSPN WT v iSPN KO	0.2532
2F	6.746	Dunn's	dSPN WT v dSPN Het	0.2199
			dSPN WT v dSPN KO	0.0206
2H	2.574	Dunn's	iSPN WT v iSPN Het	0.8669
			iSPN WT v iSPN KO	0.2311

Table S4. Mann Whitney test, related to Figure S1.

Figure panel	Mann-Whitney U	p-value
S1	137	p=0.0057

CHAPTER 3: MOLECULAR MECHANISMS AND EXTENSION TO OTHER ASD MODELS

Katelyn Nicole Benthall

Department of Molecular and Cell Biology,
University of California, Berkeley

Introduction

Various cellular and synaptic phenotypes occur in SPNs with *Tsc1* loss, including somatic hypertrophy, and in dSPNs, altered dendritic arborization, increased glutamatergic transmission, and deficits in eCB-LTD [1]. However, the molecular mediators downstream of Tsc1/2-mTORC1 signaling responsible for these phenotypes is not yet known. The complexity of the mTORC1 signaling pathway makes identifying a molecular mechanism behind these changes a challenge – since mTORC1 controls a vast number of cellular processes through separate downstream effectors, it is possible that each cellular and synaptic phenotype results from disruption of discrete arms of the signaling pathway [2]. Further adding to this complexity is the fact that the timing of *Tsc1* disruption and the cell type in which the mutation occurs have profound effects on the cellular and synaptic phenotypes observed [1, 3-8]. Despite these considerations, efforts toward a mechanistic link between mTORC1 signaling and synaptic function are crucial to fully understand ASD in TSC, and may pave the way to new therapies.

One approach to identifying the molecular changes that occur with loss of *Tsc1* in SPNs is to assay the translational landscape of these cells and compare this to the profile of control SPNs. The translating ribosome affinity purification (TRAP) assay has been established for this purpose, in which ribosome-bound RNA can be isolated and sequenced in a cell-type specific manner [9]. Assaying actively translated RNA is particularly relevant to the TSC model, as a predominant effect of mTORC1 hyperactivity is exaggerated translation [2]. I therefore performed TRAP to determine genes whose translation is either up- or down-regulated in dSPNs and iSPNs with *Tsc1* deletion. This experiment serves as a jumping-off point in the search for a molecular mechanism, as candidates identified in this manner will be subsequently validated at the level of RNA expression using qPCR, or at the protein level using western blot or IHC. Rescue experiments can then be performed to determine if manipulation of a single candidate or combination of candidates is sufficient to reverse or prevent individual cell- and synapse-level phenotypes, with the ultimate goal of rescuing behavioral changes.

Discoveries regarding the molecular mechanism of synaptic dysfunction in TSC may even extend to treatments in other forms of ASD, since dysregulated Tsc1/2-mTORC1 signaling contributes to up to 15% of ASD cases in patients. These findings are reflected in mouse models of many ASD-risk genes, including the *Cntnap2*$^{-/-}$ model, in which loss of function of cell adhesion molecule contactin associated protein-like 2 gene (Cntnap2) is associated with increased mTORC1 pathway signaling [10]. To determine if there are convergent striatal phenotypes across multiple ASD models, I characterized the striatal physiology and repetitive behavior phenotypes in the *Cntnap2* model and compared these results to our findings in *Tsc1*. Interestingly, consistent with a common mechanism between *Tsc1* and *Cntnap2* deletion, a similar phenotype of enhanced corticostriatal transmission was observed in mice with *Cntnap2* deletion. Further, similarly to our Tsc1 model, enhanced motor learning occurred with Cntnap2 loss. Interestingly, *Cntnap2-/-* mice also displayed increased self-grooming and marble burying behaviors, in the absence of locomotor hyperactivity.

Results

Translational profiling identifies changes to mRNA expression in dSPNs and iSPNs with Tsc1 loss

In order to measure the translational profile of SPNs with *Tsc1* deletion, we generated conditional *Tsc1* mice that had dSPN- or iSPN-restricted expression of a GFP-tagged ribosomal subunit. We bred conditional *Tsc1* mice (*Tsc1*^{cKO}) with the striatal-restricted *D1-Cre* or *A2a-Are* lines to achieve dSPN- or iSPN-specific loss of Tsc1, and bred those to *DIO-L10a-GFP* mice that express GFP-tagged ribosomal subunit L10a in a Cre-dependent manner (*Tsc1*^{cKO}*;D1-Cre;L10a-GFP* and *Tsc1*^{cKO}*;A2a-Cre;L10a-GFP*) mice. This approach allows selective immuno-precipitation (IP) of ribosome-bound mRNA from genetically defined cell types *in vivo* using the GFP protein as an affinity tag.

To visually confirm that the expression of L10a-GFP was restricted to Cre-expressing cells, we also included the *Ai9* transgene (Fig. 1A). However, the *Ai9* transgene was not included in mice used for TRAP experiments to avoid confounds that may come about from tdTomato expression. I performed TRAP followed by cDNA library prep and next-generation Illumina sequencing to identify ribosome-bound mRNAs, which likely reflect mRNAs that are undergoing active translation [9]. We found that compared to the unbound samples, which reflect total RNA purified from all striatal cells, the dSPN TRAP samples were enriched for dSPN-specific genes (*Drd1*, *Tac1*, and *Pdyn*) and had comparably low expression of iSPN-specific genes (*Drd2*, *Penk*) (Fig. 1B). Likewise, the iSPN TRAP pulldowns were enriched for iSPN-specific genes and showed low expression of dSPN-specific genes compared to the unbound sample (Fig. 2A). This verifies that the TRAP protocol allows us to isolate mRNA in an SPN-subtype specific manner. Further, expression of only one gene was significantly different between the dSPN WT and KO unbound samples. This is expected since the manipulation of Tsc1 is restricted to dSPNs only, and indicates that the translational changes captured in this dataset are largely cell-autonomous (Fig. 1C). Similarly, relatively few genes were found to be significantly different between iSPN WT and KO samples (Fig. 2B).

Over 600 genes were found to be significantly changed ($p<0.05$) in the dSPN Tsc1-KO cells compared to Tsc1-WT dSPNs, while only a few genes were translated at significantly different levels in dSPN Tsc1-Het cells compared to WT (Fig. 1D,E). Gene ontology analysis of the top 300 most significantly changed genes revealed nine major categories of alterations at the level of biological processes, including changes to synaptic transmission, phosphorylation and intracellular signaling, and metabolic processes (Fig. 1F). A closer look at genes related to intracellular signaling indicates the MAPK-ERK and the PI3K-AKT-mTOR pathways are both altered, which may have consequences on intracellular effectors of neurotransmission. Notably, the translation of other ASD-associated genes were dysregulated by *Tsc1* loss in dSPNs, including *Cntnap2*, *Ntng2*, and *Nrep*. There is no obvious trend within these categories of genes being either consistently up- or down-regulated, perhaps due to the fact that primary expression changes caused by *Tsc1* deletion can cause compensatory changes, as it is impossible to disentangle primary from compensatory expression differences in our system (Fig. 1G, Tables S1,S2). Similarly, over 1600 genes were found to be

significantly different between Tsc1-WT and Tsc1-KO iSPNs, while relatively few genes were different between Tsc1-WT and Tsc1-Het iSPNs (Fig. 2C,D, Tables S3,S4).

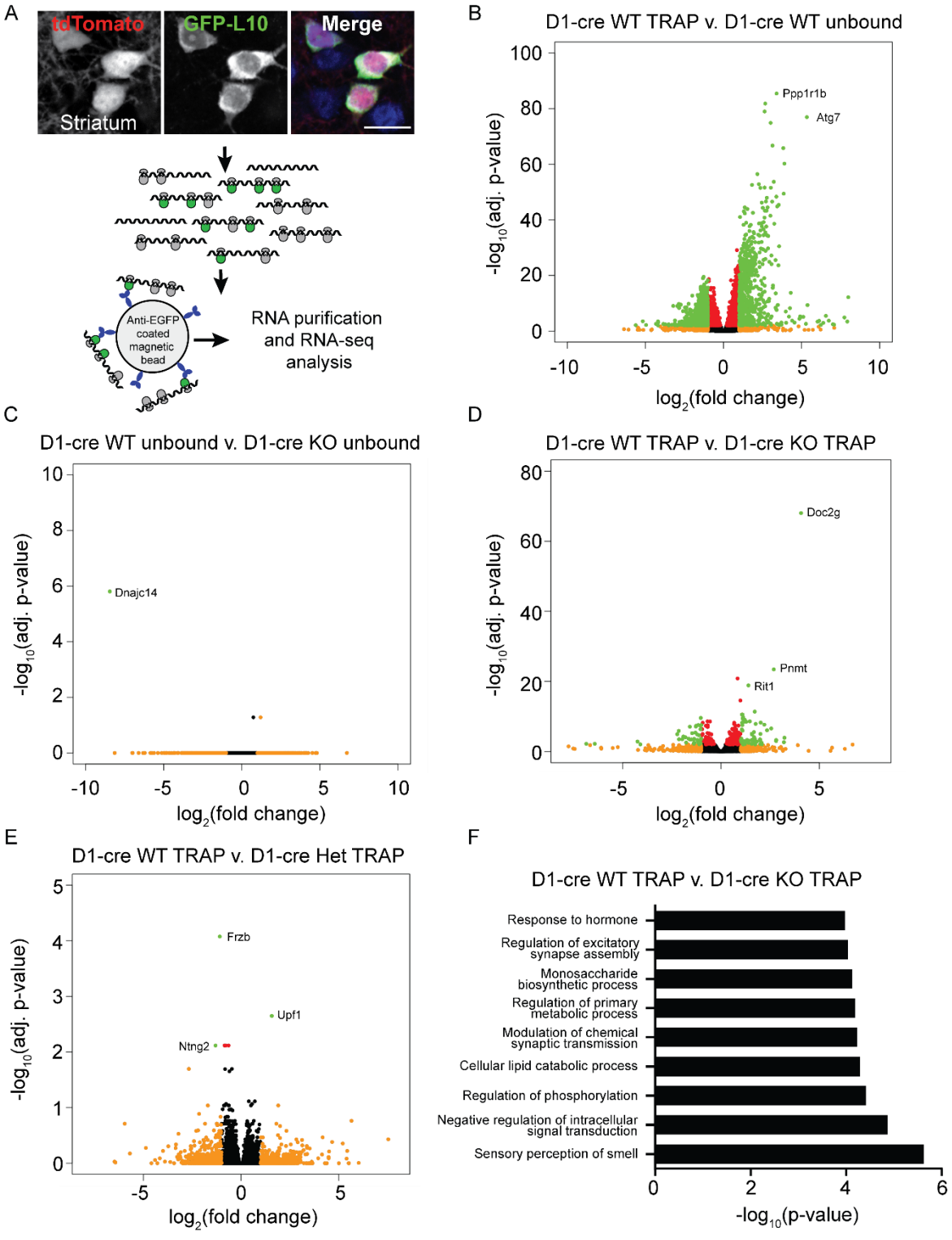

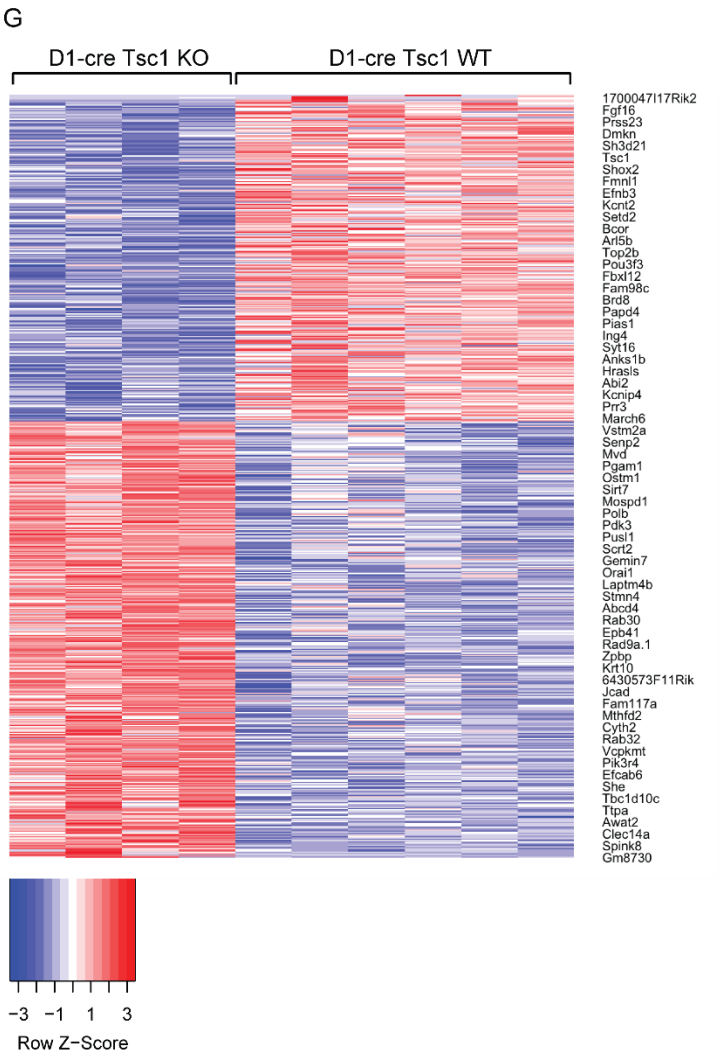

Figure 1. Translational profiling reveals differential gene expression in dSPNs with loss of *Tsc1*.
(A) Schematic of TRAP protocol. Striatal neurons expressing Cre and Cre-dependent L10a-EGFP are dissected from the brain and ribosomes are pulled down by antibody-bound magnetic beads. Ribosome-bound RNA is then purified and sequenced.
(B-E) Volcano plots of Tsc1-WT TRAP v unbound RNA (B), Tsc1-WT v Tsc1-KO unbound RNA (C), Tsc1-WT v Tsc1-KO TRAP RNA (D), and Tsc1-WT v Tsc1-Het RNA. Genes with particularly high expression and statistical significance are indicated.
(F) GO (gene ontology) analysis of the top 300 statistically significant genes.
(G) Heat map of top 100 statistically significant genes in Tsc1-WT and Tsc1-KO dSPNs. Red indicates enrichment and blue indicates depletion.

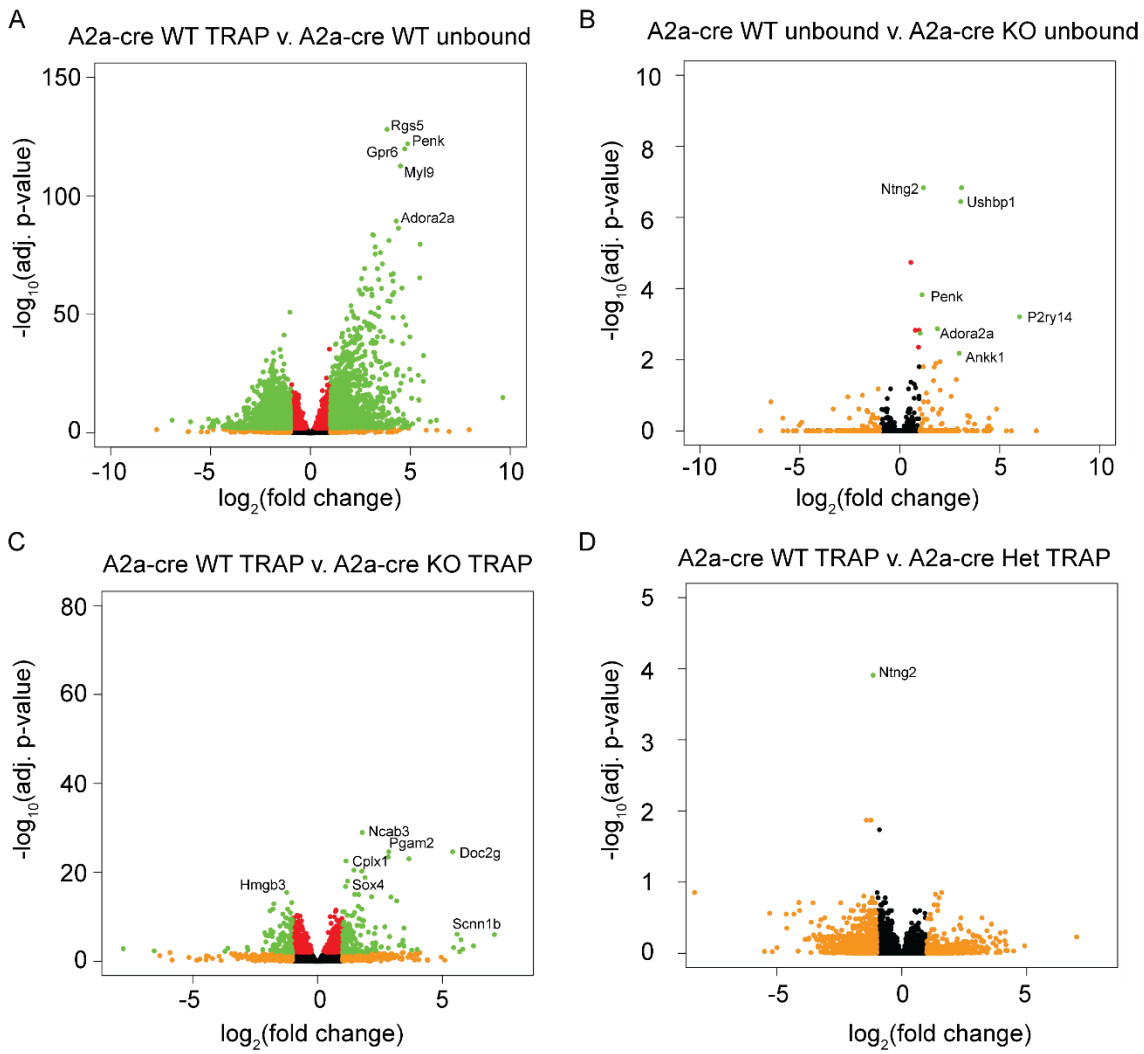

Figure 2. Translational profiling reveals differential gene expression in iSPNs with loss of *Tsc1*. (A-D) Volcano plots of Tsc1-WT TRAP v unbound RNA (B), Tsc1-WT v Tsc1-KO unbound RNA (C), Tsc1-WT v Tsc1-KO TRAP RNA (D), and Tsc1-WT v Tsc1-Het RNA. Genes with particularly high expression and statistical significance are indicated.

Deletion of ASD-risk gene Cntnap2 causes corticostriatal transmission and motor learning phenotypes similar to those in dSPN Tsc1-KO mice

Because of the link between *Cntnap2* and Tsc1/2-mTORC1 signaling found in the dSPN TRAP experiments and identified in previous studies [10], it is possible that a similar synaptic and behavioral phenotype occurs in the *Cntnap2*$^{-/-}$ model as I identified in the *Tsc1* model (see Chapter 1 and 2). To test this, I crossed the *Cntnap2*$^{+/-}$ mice to the *D1-tdTomato* line to distinguish dSPNs and iSPNs, and the *Thy1-ChR2-YFP* line, to express ChR2-YFP sparsely in cortical layer V pyramidal cells [11, 12]. This allowed for selective stimulation of cortical terminals with light, during which postsynaptic SPN responses could be measured. Ten blue light pulses were delivered over the recording site to stimulate glutamate release from cortical terminals, and SPN postsynaptic potential was recorded in current-clamp mode. Cortical stimulation sometimes elicited action potentials (APs) in postsynaptic dSPNs, and other times elicited a subthreshold

depolarization. The number of APs evoked by this stimulation paradigm was quantified, as a percent of total stimulation events. The 40 Hz stimulation was repeated at different light intensities to generate an input-output curve of APs as a relationship of cortical ChR2 stimulation intensity. Cortical stimulation caused a significantly higher number of APs across all light intensities in dSPNs and iSPNs with homozygous loss of *Cntnap2* as compared to wild-type controls, with the effect magnitude being larger in dSPNs (Fig. 3A-C).

The accelerating rotarod task is a striatal-dependent motor learning assay in which mice must learn to run on a rod revolving at increasing speed. Previously we had identified motor learning enhancements in mice with homozygous loss of *Tsc1* in dSPNs, and wanted to investigate if a similar phenotype occurs with *Cntnap2* loss. Indeed, mice with homozygous deletion of *Cntnap2* had increased rotarod learning on the final two training days, also reflected by an increased learning rate (Fig. 3D,E). This affect was not due to general hyperactivity, as indicated by a lack of change in locomotion and rearing in the open field (Fig. 3F,G). Because the *Cntnap2* model is a global gene deletion, we reasoned that behaviors dependent upon circuits outside the striatum could also be affected, therefore we used assayed grooming and marble burying as additional tests of RRBs. Interestingly, global deletion of *Cntnap2* resulted in increased grooming and marble burying, indicating that in addition to enhanced motor learning, other domains of repetitive behaviors are affected (Fig. 3H,I). Notably, the grooming effect was mainly specific to females and absent in males, while the other behaviors were not sex-specific.

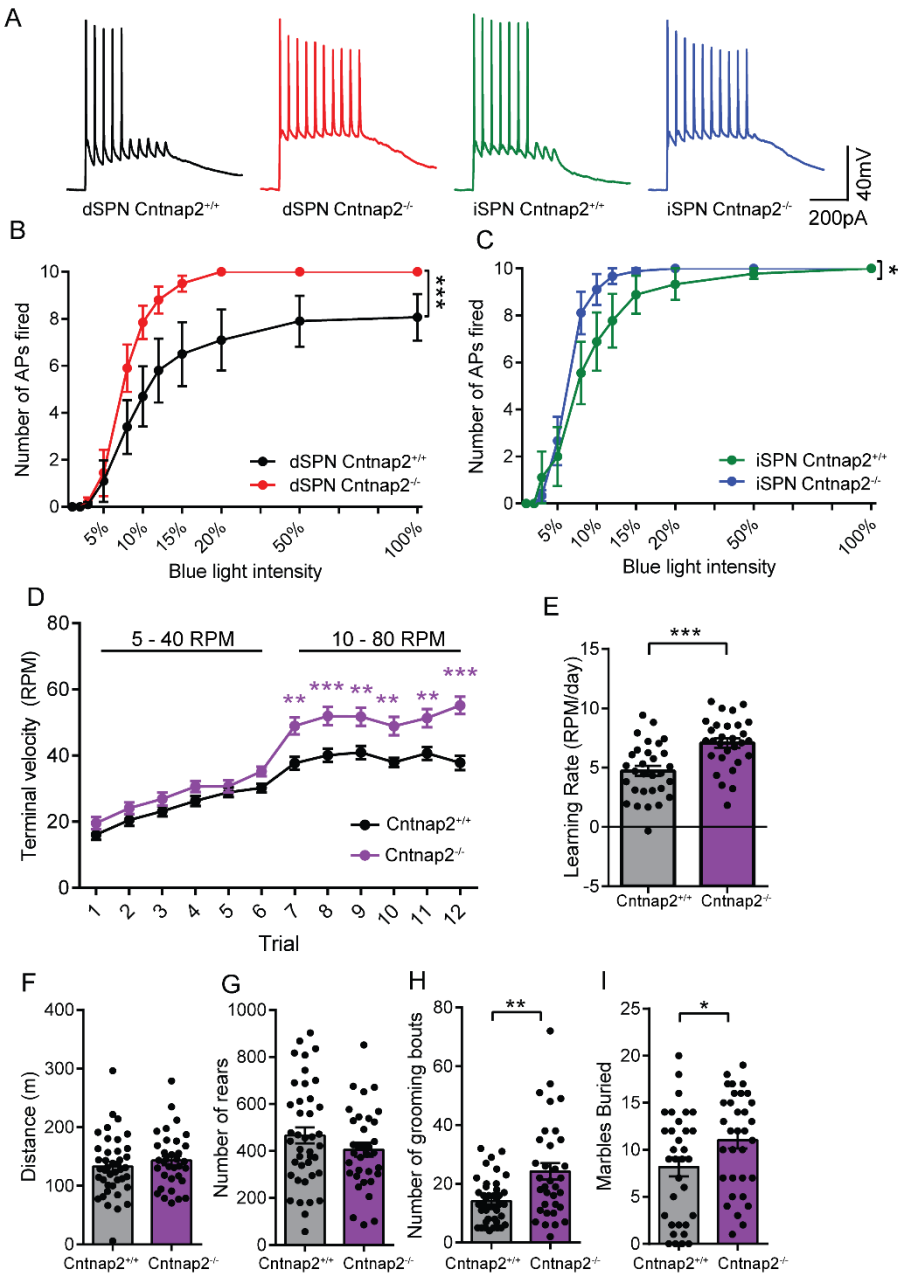

Figure 3. Enhanced corticostriatal excitability, motor learning, and repetitive behaviors in *Cntnap2-/-* mouse model of ASD.

(A) Example traces of oAPs elicited by cortical terminal stimulation in *Cntnap2*+/+ and *Cntnap2-/-* dSPNs and iSPNs.

(B-C) Quantification of oAP input-output curve by stimulation intensity. dSPNs (B) and iSPNs (C) from *Cntnap2-/-* mice fired significantly more oAPs in response to cortical stimulation than controls.

(D-E) Rotarod learning curve (D) is significantly increased in mice with *Cntnap2* deletion compared to controls on the final two days of training. Learning rate (E) is significantly higher in *Cntnap2-/-* mice.

(F-G) Quantification of average distance traveled (F) and number of rears (G) in the open field by genotype.

(H) Average number of grooming bouts is significantly increased in *Cntnap2-/-* mice compared to littermate controls.

(I) Marble burying behavior is increased in *Cntnap2-/-* mice compared to controls.

Discussion

Here we performed a translational profiling experiment in mice with loss of *Tsc1* from dSPNs or iSPNs, and identified novel candidates to consider as mechanistically involved in the cellular and synaptic changes identified with SPN-subtype specific deletion of *Tsc1* (see results presented in Chapters 1 and 2). Future studies will aim to pinpoint specific molecular mechanisms for the physiological and behavioral consequences of striatal *Tsc1* deletion, with the ultimate goal of rescuing ASD-relevant phenotypes through modulation of the molecular pathways responsible. One option would be to perform rescue studies using pharmacological or gene engineering technology to normalize expression or activity of proteins responsible for the phenotypes. These treatments could potentially also be applied to other mouse models in which mTORC1-signaling is dysregulated.

We have also expanded our findings of enhanced corticostriatal excitation and increased motor learning and repetitive behaviors resulting from striatal *Tsc1* deletion to the *Cntnap2*$^{-/-}$ ASD mouse model. This, along with other studies, suggests that altered corticostriatal transmission is a common phenotype associated with ASD-risk mutations [13, 14]. It also builds upon the existing literature on behavioral and synaptic changes in this model, which also show increased repetitive behavior in grooming and digging assay [15, 16]. However, another study on marble burying did not find an effect in the *Cntnap2-/-* model [17]. Interestingly, other groups find social behavioral abnormalities in the *Cntnap2-/-* model, but our lab did not observe affects in the three-chamber social approach test [15, 17, 18].

The exact synaptic and molecular mechanisms driving enhanced corticostriatal excitation in the *Cntnap2-/-* model remain to be investigated. The fact that this is a global deletion is important to consider, because changes to corticostriatal transmission may be the result of complex phenotypes occurring at both the presynaptic and postsynaptic site, as changes to excitatory neuron excitability and circuitry have been identified in *Cntnap2*$^{-/-}$ mice [16, 18-21]. Additionally, studies have reported altered numbers of inhibitory neurons in the cortex and a deficit in inhibitory synaptic transmission in the hippocampus [21, 22]. Regardless of the specific mechanism, which may be unique in each genetic ASD model, it appears that enhanced corticostriatal transmission is a commonality across mouse models of ASD, which provides an important foundation and research direction for future studies.

Experimental Procedures

Mouse lines

Animal experiments were performed in accordance with protocols approved by UC Berkeley's Animal Care and Use Committee. Male and female mice were used for all experiments. Mice were 7-10 weeks old unless otherwise noted. All mice used for experiments were hemizygous for transgenes to avoid potential physiological or behavioral alterations.

The following mouse lines were used:

Mouse line	**Source**	**Reference**
Tsc1$^{fl/fl}$	JAX strain #005680	[23]
Drd1a-Cre (EY217)	GENSAT (MMRRC #030778-UCD)	[24]
Adora2a-Cre (KG139)	GENSAT (MMRRC #031168-UCD)	[24]
EGFP-L10a	JAX strain #024750	[25]
Ai9 (tdTomato)	JAX strain #007909	[26]
Cntnap2$^{+/-}$	JAX strain #017482	[27]
Thy1-ChR2-YFP	JAX strain #007612	[12]
Drd1a-tdTomato	JAX strain #016204	[11]

Translating ribosome affinity purification (TRAP)

Anti-GFP magnetic bead preparation

Each TRAP experiment was performed on 3 samples in parallel, with a Tsc1-WT, Tsc1-Het, and Tsc1-KO mouse processed together. All steps were performed on ice unless otherwise noted. 150µL of Dynabeads® MyOne™ Streptavidin T1 (Lifetech 65601) were washed using a magnetic tube rack in RNase-free PBS and then incubated in Protein L solution (850µL PBS + 150µg Protein L) for 35 min at room temperature (RT). Beads were washed 5x with 3% IgG Protease-free BSA to block, then incubated with 150 µg of two different anti-GFP antibodies (19C8 and 19F7, Memorial Sloan Kettering Antibody and Bioresource Core), diluted in 900 µL PBS, for 1 hr at RT. Beads were then washed 3x in 0.15M KCl buffer without cyclohexamide (-CHX), then resuspended in 630 µL of 0.15M KCl (+CHX).

Brain lysate preparation and immunoprecipitation

Mice were anesthetized, and brains were dissected and blocked to contain mainly striatum. Bilateral striata from each animal were placed into separate glass homogenization tubes on ice, and pestles were inserted. Homogenization took place at 4°C (3 strokes at 300 RPM, 12 strokes at 900 RPM, Yamato Lab Stirrer LT400), care was taken to avoid generating bubbles. Lysates were poured into pre-chilled Eppendorf tubes and centrifuged for 10 min at 2,000 x g at 4 °C to precipitate large organelles. Samples were then transferred to a new pre-chilled tube and volumes were measured. 10% NP-40 (1/9 sample volume, ~70-80 µL) was added, then DHPC (1/9 new sample volume) was added, and samples were incubated on ice for 5 mins. DHPC stock is 200 mg dissolved in 1.38 mL ddH2O, and can be kept at 4°C protected from light for 2 weeks. Samples were then centrifuged for 10 min at 16,000 x g at 4 °C to precipitate mitochondria. Antibody-bound beads were resuspended by inversion, and 200 µL of

beads was added to three separate tubes. Supernatants from samples were then transferred into tubes with beads and incubated on rotators at 4 °C overnight.

Isolation and purification of RNA

Samples were spun down briefly and placed on magnets pre-chilled on ice. Supernatants were collected and transferred to pre-chilled “unbound” tubes. Beads were washed 4x with 0.35M KCl buffer, with samples sitting on ice for 1 min between washes to reduce background binding. Beads were resuspended in 350 µL RLT-beta-ME. 100 µL of unbound samples were added separately to 350 µL RLT-beta-ME. Samples (bound and unbound) were then rotated for 10 min at RT. Samples were placed on magnet and supernatants were removed and added into fresh tubes containing 350 µL of 80% EtOH, mixed, and then all 700 µL of sample + EtOH was added to RNeasy column (pre-chilled). 350 µL of unbound sample was also mixed with 350 µL of EtOH and added to RNeasy column. At this point there were 6 columns, one bound and one unbound sample for each mouse. Samples were centrifuged for 30 sec at 8000 x g at RT. Flow-through was passed through column twice more to repeat binding. Flow-through was then discarded and 500 µL of RPE buffer was added to each column and spun for 30 sec at 8000 x g. Flow-through was discarded and 500 µL of 80% EtOH was added to the column, spun for 2 min at 8000 x g at RT. Flow-through was discarded, and columns were dried by spinning for 5 mins at full speed with cap open. Dried columns were placed into new collection tubes (not pre-chilled) and 28 µL RNase-free water was added directly to the column membrane. Columns were incubated for 5 min at RT with caps closed, then spun for 1 min at max speed at RT. RNA concentration and quality was determined by Nanodrop and Bioanalyzer before submitting the samples for library prep and sequencing by the UC Berkeley Functional Genomics Laboratory and Genomics Sequencing Laboratory core facilities.

RNA sequencing and analysis

cDNA libraries were pooled and sequenced on an Illumina HiSeq4000 as 100 base pair paired-end reads. Reads were subsequently analyzed for quality using Fastqc (v0.11.7). Even though ribosomal RNA was selected against during library preparation, any remaining reads aligning to ribosomal RNA were removed from each sample through alignment using bowtie2 (v2.3.4.1). Each sample was then aligned to the mouse genome (mm10) using Kallisto (v0.44.0) and bootstrapped 100 times [28, 29]. Differential gene expression was then determined using the DESeq2 package in R (v3.6). Samples that were determined to be outliers based on PCA-based clustering strongly away from all other samples or TRAP samples clustering with the total RNA samples were removed from analysis.

<u>Slice preparation for electrophysiology</u>

Mice were perfused transcardially with ice-cold ACSF (pH=7.4) containing (in mM): 127 NaCl, 25 $NaHCO_3$, 1.25 NaH_2PO_4, 2.5 KCl, 1 $MgCl_2$, 2 $CaCl_2$, and 25 glucose, bubbled continuously with carbogen (95% O_2 and 5% CO_2). Brains were rapidly removed and coronal slices (275 □m) were cut on a VT1000S vibrotome (Leica) in oxygenated ice-cold choline-based external solution (pH=7.8) containing (in mM): 110 choline chloride, 25 $NaHCO_3$, 1.25 $NaHPO_4$, 2.5 KCl, 7 $MgCl_2$, 0.5 $CaCl_2$, 25 glucose, 11.6 sodium

ascorbate, and 3.1 sodium pyruvate. Slices were recovered in ACSF at 34°C for 15 minutes and then kept at RT before recording.

Whole-cell patch-clamp recording

Recordings were made with a MultiClamp 700B amplifier (Molecular Devices) at RT using 3-5 MOhm glass patch electrodes. Current clamp recordings were made using a potassium-based internal solution (pH=7.4) containing (in mM): 135 $KMeSO_4$, 5 KCl, 5 HEPES, 4 Mg-ATP, 0.3 Na-GTP, 10 phosphocreatine, and 1 ETGA. Traces were analyzed in Igor Pro, and miniature events were identified and measured using custom software. Recordings with a series resistance >25 MOhms or holding current above -200pA were rejected. For oAP experiments, optogenetic stimulation consisted of a full-field pulse of blue light (470nm, 0.05ms) using a 63x objective. No holding current was applied to the membrane. No blockers were added to the external solution.

Behavior

Behavior studies were carried out in the dark phase of the light cycle under red lights (open field) or white lights (rotarod and marble burying). Mice were habituated to the behavior room for at least 30 min prior to testing and covered by a black-out curtain. Mice were given at least one day in between different tests. All behavior equipment was cleaned between each trial/mouse with 70% ethanol, and additionally rinsed in diluted soap followed by water at the end of the day. If male and female mice were to be tested on the same day, male mice were run in behavior first, returned to the husbandry room, after which all equipment was thoroughly cleaned, and female mice were brought in for habituation. All animals to be tested from a given cage were run in each behavior test in the same day. Behavioral tests were performed with adult male and females (6-10 weeks old). The experimenter was blind to genotype throughout the testing and scoring procedures.

Open field

Exploratory behavior in a novel environment and general locomotor activity were assessed by a 60 min session in an open field chamber (40cm L x 40cm W x 34cm H) made of transparent plexiglass. Horizontal photobeams to measure rearing were positioned at 9cm of height. The mouse was placed in the bottom right hand corner of the arena and behavior was recorded using an overhead camera and analyzed using the ANY-maze (Stoelting Co.) behavior tracking software. An observer manually scored grooming behavior during the first 20 minutes of the test.

Marble burying

Cages were filled 5 cm deep with corn-cob bedding, and 20 marbles were evenly spaced on top of the bedding in a 4x5 grid. Mice were placed in the test cage (1 mouse per cage) for 20 min, with white noise playing. After the test, mice were removed and returned to the home cage, and the number of unburied marbles was counted. A marble was considered unburied if half or more of it was left uncovered by bedding. A photo of the cage was taken pre-test and post-test as a record.

Rotarod

The accelerating rotarod test was used to examine motor learning. Mice were run on a rotarod apparatus (Ugo Basile: 47650) for 4 consecutive days. Three trials were completed per day with a 5 min break between trials. The rotarod was accelerated from 5-40 revolutions per minute (rpm) over 300s for trials 1-6 (days 1 and 2), and from 10-80rpm over 300s for trials 7-12 (days 3 and 4). On the first testing day, mice were acclimated to the apparatus by being placed on the rotarod rotating at a constant 5 rpm for 60 s and returned to their home cage for 5 minutes prior to starting trial 1. Latency to fall, or to rotate off the top of the rotarod barrel, was measured by the rotarod stop-trigger timer.

Statistical analyses for physiology and behavioral data

Two-tailed unpaired t-tests were used for comparisons between two groups, and F-test was used to confirm that variances were not significantly different. For data that did not pass D'Agostino & Pearson normality test, Mann Whitney test was used. A one-way ANOVA with Sidak's post-doc test was used to compare the means of three or more groups. A two-way ANOVA with Sidak's post-hoc test was used to compare mean differences between groups for experiments with two independent variables. P-values were corrected for multiple comparisons. For data that did not pass the D'Agostino and Pearson normality test, the Kruskal-Wallis with Dunn's post-hoc test was used. Values for all statistical comparisons are provided in Supplemental Tables S5-7.

References

1. Benthall, K.N., S.L. Ong, and H.S. Bateup, *Corticostriatal Transmission Is Selectively Enhanced in Striatonigral Neurons with Postnatal Loss of Tsc1.* Cell Rep, 2018. **23**(11): p. 3197-3208.
2. Saxton, R.A. and D.M. Sabatini, *mTOR Signaling in Growth, Metabolism, and Disease.* Cell, 2017. **168**(6): p. 960-976.
3. Bateup, H.S., et al., *Loss of Tsc1 in vivo impairs hippocampal mGluR-LTD and increases excitatory synaptic function.* J Neurosci, 2011. **31**(24): p. 8862-9.
4. Bateup, H.S., et al., *Excitatory/inhibitory synaptic imbalance leads to hippocampal hyperexcitability in mouse models of tuberous sclerosis.* Neuron, 2013. **78**(3): p. 510-22.
5. Tavazoie, S.F., et al., *Regulation of neuronal morphology and function by the tumor suppressors Tsc1 and Tsc2.* Nat Neurosci, 2005. **8**(12): p. 1727-34.
6. Tsai, P.T., et al., *Autistic-like behaviour and cerebellar dysfunction in Purkinje cell Tsc1 mutant mice.* Nature, 2012. **488**(7413): p. 647-51.
7. Normand, E.A., et al., *Temporal and mosaic Tsc1 deletion in the developing thalamus disrupts thalamocortical circuitry, neural function, and behavior.* Neuron, 2013. **78**(5): p. 895-909.
8. Zhao, J.P. and A. Yoshii, *Hyperexcitability of the local cortical circuit in mouse models of tuberous sclerosis complex.* Mol Brain, 2019. **12**(1): p. 6.
9. Heiman, M., et al., *A translational profiling approach for the molecular characterization of CNS cell types.* Cell, 2008. **135**(4): p. 738-48.
10. Xing, X., et al., *Suppression of Akt-mTOR pathway rescued the social behavior in Cntnap2-deficient mice.* Sci Rep, 2019. **9**(1): p. 3041.
11. Ade, K.K., et al., *An Improved BAC Transgenic Fluorescent Reporter Line for Sensitive and Specific Identification of Striatonigral Medium Spiny Neurons.* Front Syst Neurosci, 2011. **5**: p. 32.
12. Arenkiel, B.R., et al., *In vivo light-induced activation of neural circuitry in transgenic mice expressing channelrhodopsin-2.* Neuron, 2007. **54**(2): p. 205-18.
13. Peixoto, R.T., et al., *Early hyperactivity and precocious maturation of corticostriatal circuits in Shank3B(-/-) mice.* Nat Neurosci, 2016. **19**(5): p. 716-24.
14. Fuccillo, M.V., *Striatal Circuits as a Common Node for Autism Pathophysiology.* Front Neurosci, 2016. **10**: p. 27.
15. Penagarikano, O., et al., *Absence of CNTNAP2 leads to epilepsy, neuronal migration abnormalities, and core autism-related deficits.* Cell, 2011. **147**(1): p. 235-46.
16. Scott, R., et al., *Loss of Cntnap2 Causes Axonal Excitability Deficits, Developmental Delay in Cortical Myelination, and Abnormal Stereotyped Motor Behavior.* Cereb Cortex, 2019. **29**(2): p. 586-597.
17. Brunner, D., et al., *Comprehensive Analysis of the 16p11.2 Deletion and Null Cntnap2 Mouse Models of Autism Spectrum Disorder.* PLoS One, 2015. **10**(8): p. e0134572.
18. Selimbeyoglu, A., Christina K. Kim, Masatoshi Inoue, Soo Yeun Lee, Alice S. O. Hong,, C.R. Isaac Kauvar, Lief E. Fenno, Thomas J. Davidson,, and K.D. Matthew Wright, *Modulation of prefrontal cortex excitation/inhibition balance*

rescues social behavior in CNTNAP2-deficient mice. Science translational medicine, 2017. **9**.
19. Antoine, M.W., et al., *Increased Excitation-Inhibition Ratio Stabilizes Synapse and Circuit Excitability in Four Autism Mouse Models.* Neuron, 2019. **101**(4): p. 648-661 e4.
20. Fernandes, D., et al., *Disrupted AMPA Receptor Function upon Genetic- or Antibody-Mediated Loss of Autism-Associated CASPR2.* Cereb Cortex, 2019.
21. Jurgensen, S. and P.E. Castillo, *Selective Dysregulation of Hippocampal Inhibition in the Mouse Lacking Autism Candidate Gene CNTNAP2.* J Neurosci, 2015. **35**(43): p. 14681-7.
22. Vogt, D., et al., *Mouse Cntnap2 and Human CNTNAP2 ASD Alleles Cell Autonomously Regulate PV+ Cortical Interneurons.* Cereb Cortex, 2018. **28**(11): p. 3868-3879.
23. Kwiatkowski, D.J., *A mouse model of TSC1 reveals sex-dependent lethality from liver hemangiomas, and up-regulation of p70S6 kinase activity in Tsc1 null cells.* Human Molecular Genetics, 2002. **11**(5): p. 525-534.
24. Gong, S., et al., *Targeting Cre recombinase to specific neuron populations with bacterial artificial chromosome constructs.* J Neurosci, 2007. **27**(37): p. 9817-23.
25. Liu, J., et al., *Cell-specific translational profiling in acute kidney injury.* J Clin Invest, 2014. **124**(3): p. 1242-54.
26. Madisen, L., et al., *A robust and high-throughput Cre reporting and characterization system for the whole mouse brain.* Nat Neurosci, 2010. **13**(1): p. 133-40.
27. Poliak, S., et al., *Juxtaparanodal clustering of Shaker-like K+ channels in myelinated axons depends on Caspr2 and TAG-1.* J Cell Biol, 2003. **162**(6): p. 1149-60.
28. Love, M.I., W. Huber, and S. Anders, *Moderated estimation of fold change and dispersion for RNA-seq data with DESeq2.* Genome Biol, 2014. **15**(12): p. 550.
29. Bray, N.L., et al., *Near-optimal probabilistic RNA-seq quantification.* Nat Biotechnol, 2016. **34**(5): p. 525-7.

Supplementary Tables

Table S1. List of genes significantly different between Tsc1-WT and Tsc1-KO dSPNs.

Gene	Base Mean	Log_2(Fold Change)	Adjusted p-value	Wikigene Description
Doc2g	109.3086	4.068152	9.29E-69	double C2, gamma
Pnmt	51.0956	2.682229	3.91E-24	phenylethanolamine-N-methyltransferase
Cplx1	19524.78	0.841535	1.45E-21	complexin 1
Rit1	915.7919	1.395069	1.42E-19	Ras-like without CAAX 1
Gpr137c	405.3666	0.984503	2.80E-15	G protein-coupled receptor 137C
Gpx3	384.277	1.715456	4.32E-12	glutathione peroxidase 3
Pik3ip1	391.6633	1.100094	2.92E-11	phosphoinositide-3-kinase interacting protein 1
Trnp1	3957.707	1.062614	2.92E-11	TMF1-regulated nuclear protein 1
Slc30a10	240.5537	1.123473	1.86E-10	solute carrier family 30, member 10
Gpsm1	982.0577	-1.02521	2.75E-10	G-protein signalling modulator 1 (AGS3-like, C. elegans)
Them6	662.4872	1.104664	4.41E-10	thioesterase superfamily member 6
Yap1	121.9581	1.198452	8.44E-10	yes-associated protein 1
Rab3b	1259.801	1.467083	2.58E-09	RAB3B, member RAS oncogene family
Marcks	2877.419	-0.68409	2.58E-09	myristoylated alanine rich protein kinase C substrate
Lmo2	1659.484	1.266894	2.76E-09	LIM domain only 2
St6galnac5	836.4327	-0.55471	2.76E-09	ST6 (alpha-N-acetyl-neuraminyl-2,3-beta-galactosyl-1,3)-N-acetylgalactosaminide alpha-2,6-sialyltransferase 5
Anxa4	67.39368	1.180264	3.25E-09	annexin A4
Pdcd11	66.40699	1.282454	3.42E-09	programmed cell death 11
Vim	246.4875	2.0177	5.97E-09	vimentin
Sesn2	124.1902	1.076318	6.32E-09	sestrin 2
Pitpnm3	528.5404	-0.93105	6.38E-09	PITPNM family member 3
Vstm5	250.5057	0.673444	6.47E-09	V-set and transmembrane domain containing 5
Mgst1	121.3694	1.761886	1.35E-08	microsomal glutathione S-transferase 1
Ctsa	1018.056	0.665958	1.46E-08	cathepsin A
Pgam2	173.8693	2.200365	2.23E-08	phosphoglycerate mutase 2
Tsc1	365.8989	-1.1528	2.89E-08	tuberous sclerosis 1
Trub2	566.7626	1.084544	2.90E-08	TruB pseudouridine (psi) synthase family member 2
Pou3f1	2188.17	-1.0031	2.93E-08	POU domain, class 3, transcription factor 1
Plppr3	517.6601	-0.66968	3.45E-08	phospholipid phosphatase related 3
N4bp3	341.937	-1.04808	3.80E-08	NEDD4 binding protein 3
Sox4	392.0073	0.884868	4.32E-08	SRY (sex determining region Y)-box 4
Hrh3	1087.511	0.738554	4.35E-08	histamine receptor H3
Nrep	1803.32	-0.76862	4.64E-08	neuronal regeneration related protein
Spred3	119.0986	-1.26349	4.83E-08	sprouty-related, EVH1 domain containing 3
Peli2	121.7728	-1.27549	7.40E-08	pellino 2

Mafa	74.02134	-1.5789	8.76E-08	v-maf musculoaponeurotic fibrosarcoma oncogene family, protein A (avian)
Lrrtm2	512.1652	-0.67704	1.05E-07	leucine rich repeat transmembrane neuronal 2
Nppa	10.03942	2.554643	2.74E-07	natriuretic peptide type A
Mpi	716.7208	0.652224	3.15E-07	mannose phosphate isomerase
Stmn4	4069.137	0.574219	3.69E-07	stathmin-like 4
Mycn	128.3818	-1.03778	4.35E-07	v-myc avian myelocytomatosis viral related oncogene, neuroblastoma derived
Atf7ip	323.3218	-0.95717	4.37E-07	activating transcription factor 7 interacting protein
Degs1	1326.918	0.594241	4.89E-07	delta(4)-desaturase, sphingolipid 1
Jcad	1937.243	0.774978	5.08E-07	junctional cadherin 5 associated
Armcx6	85.74318	1.058884	5.15E-07	armadillo repeat containing, X-linked 6
Bcl6b	17.31862	2.341094	8.69E-07	B cell CLL/lymphoma 6, member B
Mrap2	86.96957	1.096539	1.14E-06	melanocortin 2 receptor accessory protein 2
Fgf16	28.66762	-2.14391	1.32E-06	fibroblast growth factor 16
Acat2	1005.666	0.431235	2.95E-06	acetyl-Coenzyme A acetyltransferase 2
Blnk	94.16006	1.674416	2.95E-06	B cell linker
Tmem41a	525.4102	0.718282	3.41E-06	transmembrane protein 41a
Ccdc3	179.824	0.882359	3.77E-06	coiled-coil domain containing 3
Klc3	138.0089	0.899635	3.95E-06	kinesin light chain 3
Jun	773.3752	0.698796	3.95E-06	jun proto-oncogene
Col6a2	64.64721	-1.29868	4.37E-06	collagen, type VI, alpha 2
Snx10	3176.379	0.441506	4.65E-06	sorting nexin 10
Ctnna1	521.2068	-0.686	5.46E-06	catenin (cadherin associated protein), alpha 1
Tmem114	45.0425	-1.46437	6.14E-06	transmembrane protein 114
Fam189b	527.11	0.702741	7.70E-06	family with sequence similarity 189, member B
Tspyl2	724.3796	-0.59108	7.70E-06	TSPY-like 2
1700007K13Rik	52.95619	1.561374	9.36E-06	RIKEN cDNA 1700007K13 gene
Bid	184.5553	0.988011	9.61E-06	BH3 interacting domain death agonist
Timp2	4295.172	0.544575	9.61E-06	tissue inhibitor of metalloproteinase 2
Hmox1	66.0096	2.004941	1.00E-05	heme oxygenase 1
Efnb3	1265.194	-0.9332	1.04E-05	ephrin B3
Rpl10-ps3	13.17774	-20.1151	1.07E-05	
Mcoln1	625.8003	0.470434	1.15E-05	mucolipin 1
Atp2b4	338.1078	-2.22182	1.23E-05	ATPase, Ca++ transporting, plasma membrane 4
Gabbr1	4355.486	-0.4881	1.36E-05	gamma-aminobutyric acid (GABA) B receptor, 1
Scn1b	5533.702	0.612683	1.48E-05	sodium channel, voltage-gated, type I, beta
Prokr2	33.9233	1.577495	1.50E-05	prokineticin receptor 2
Tmem132e	97.00206	-1.19993	1.51E-05	transmembrane protein 132E
Rab26	742.6614	0.753243	1.51E-05	RAB26, member RAS oncogene family
Ptprr	177.7375	0.860827	1.77E-05	protein tyrosine phosphatase, receptor type, R
Zfp882	98.81038	-0.95825	2.02E-05	zinc finger protein 882
Emb	375.2467	0.586452	2.21E-05	embigin

Zbtb46	81.48516	-1.12192	2.21E-05	zinc finger and BTB domain containing 46
Pcp4l1	10906.01	0.856234	2.21E-05	Purkinje cell protein 4-like 1
Otud3	122.0893	0.831115	2.21E-05	OTU domain containing 3
Cntnap2	443.7739	0.873364	2.30E-05	contactin associated protein-like 2
Cyb5r3	1246.183	0.540653	2.34E-05	cytochrome b5 reductase 3
Nefm	4063.312	0.769326	5.10E-05	neurofilament, medium polypeptide
Pld6	21.88276	-1.91017	5.73E-05	phospholipase D family, member 6
Hs3st5	164.8502	-0.77127	7.11E-05	heparan sulfate (glucosamine) 3-O-sulfotransferase 5
Capg	31.83883	1.685352	8.23E-05	capping protein (actin filament), gelsolin-like
Car7	272.3588	0.670471	8.30E-05	carbonic anhydrase 7
Slc6a6	975.3306	0.816557	8.31E-05	solute carrier family 6 (neurotransmitter transporter, taurine), member 6
Phlpp1	332.6165	-0.64736	8.31E-05	PH domain and leucine rich repeat protein phosphatase 1
Neu1	858.6208	0.543984	8.81E-05	neuraminidase 1
Egr2	73.55932	-1.80874	8.81E-05	early growth response 2
Scpep1	187.0314	0.637396	9.06E-05	serine carboxypeptidase 1
Msmo1	1276.505	0.615605	0.000104	methylsterol monoxygenase 1
Plekha8	186.6994	0.695544	0.000106	pleckstrin homology domain containing, family A (phosphoinositide binding specific) member 8
Fabp4	7.086433	3.222865	0.000121	fatty acid binding protein 4, adipocyte
Rasgef1c	713.7098	-0.75052	0.000122	RasGEF domain family, member 1C
Rad9a	137.5748	0.664103	0.000127	RAD9 checkpoint clamp component A
Rad9a	137.5748	0.664103	0.000127	RAD9 checkpoint clamp component A
Cyp11a1	73.43704	0.980109	0.000135	cytochrome P450, family 11, subfamily a, polypeptide 1
Ctsl	951.1895	0.742214	0.000146	cathepsin L
Gba	170.1154	0.572953	0.000149	glucosidase, beta, acid
Laptm4b	764.1049	0.546529	0.000169	lysosomal-associated protein transmembrane 4B
Phf24	2974.197	-0.57606	0.000169	PHD finger protein 24
Ranbp9	528.0956	0.456343	0.000169	RAN binding protein 9
Cd200	901.2252	0.461902	0.000171	CD200 antigen
Slc25a29	286.0955	0.699607	0.000179	solute carrier family 25 (mitochondrial carrier, palmitoylcarnitine transporter), member 29
Mark3	764.1106	0.497409	0.000195	MAP/microtubule affinity regulating kinase 3
Fmnl1	807.8638	-1.00637	0.000211	formin-like 1
Sord	359.0296	1.038772	0.000212	sorbitol dehydrogenase
Tagln	123.0334	-1.64222	0.000217	transgelin
Pno1	960.2498	0.694574	0.000232	partner of NOB1 homolog
Ralyl	852.3983	0.610467	0.000233	RALY RNA binding protein-like
Cep41	58.42366	-1.3592	0.000233	centrosomal protein 41
Jsrp1	109.6785	0.937028	0.000244	junctional sarcoplasmic reticulum protein 1
Adam23	1173.465	0.73909	0.000244	a disintegrin and metallopeptidase domain 23
Nanos1	851.9306	-0.50334	0.000245	nanos C2HC-type zinc finger 1

Avpi1	1067.524	0.95893	0.000256	arginine vasopressin-induced 1
Zfp512	587.8143	-0.53527	0.000276	zinc finger protein 512
Ly6a	75.9808	1.725666	0.000276	lymphocyte antigen 6 complex, locus A
Cgref1	490.6782	-0.63046	0.000295	cell growth regulator with EF hand domain 1
Gnpda1	458.4317	0.578845	0.000319	glucosamine-6-phosphate deaminase 1
Lmnb1	23.52709	-1.96862	0.000327	lamin B1
Rab30	319.5221	0.618905	0.000327	RAB30, member RAS oncogene family
Grik2	198.9316	-1.00826	0.000338	glutamate receptor, ionotropic, kainate 2 (beta 2)
Sfn	18.49212	-2.1325	0.000339	stratifin
Npy1r	156.3575	0.773902	0.000347	neuropeptide Y receptor Y1
Pcdhgb7	48.42589	-1.3917	0.000347	protocadherin gamma subfamily B, 7
Fam98c	865.7856	-0.59201	0.000347	family with sequence similarity 98, member C
Lrrtm1	1263.38	-0.54875	0.000347	leucine rich repeat transmembrane neuronal 1
Gadd45g	546.149	0.856761	0.000349	growth arrest and DNA-damage-inducible 45 gamma
Clec14a	20.632	1.982682	0.000354	C-type lectin domain family 14, member a
Crabp1	106.5506	-1.4909	0.000358	cellular retinoic acid binding protein I
Tle3	69.17761	-1.57282	0.0004	transducin-like enhancer of split 3
Asna1	1297.049	0.464072	0.000405	arsA arsenite transporter, ATP-binding, homolog 1 (bacterial)
Tmco5	22.11926	1.590584	0.00043	transmembrane and coiled-coil domains 5
Lamp1	2825.096	0.325552	0.00043	lysosomal-associated membrane protein 1
Atp2b1	2914.721	-0.51938	0.000479	ATPase, Ca++ transporting, plasma membrane 1
Ninj1	325.9244	0.721258	0.000479	ninjurin 1
Pcf11	342.5599	-0.69909	0.000479	PCF11 cleavage and polyadenylation factor subunit
Rgs14	1093.645	-0.64412	0.000479	regulator of G-protein signaling 14
6430573F11Rik	117.4823	0.749115	0.000485	RIKEN cDNA 6430573F11 gene
Plcxd1	360.8252	-0.72895	0.0005	phosphatidylinositol-specific phospholipase C, X domain containing 1
Igsf8	2511.1	-0.60545	0.00051	immunoglobulin superfamily, member 8
Gpd2	687.5395	-0.66839	0.000523	glycerol phosphate dehydrogenase 2, mitochondrial
Cdkl2	453.5254	0.39269	0.000523	cyclin-dependent kinase-like 2 (CDC2-related kinase)
Plekhh2	29.25182	1.323772	0.000523	pleckstrin homology domain containing, family H (with MyTH4 domain) member 2
Pcdhgb6	70.31641	-1.19479	0.000523	protocadherin gamma subfamily B, 6
Clic1	104.921	0.908834	0.000535	chloride intracellular channel 1
H2-Q7	10.51107	2.804909	0.000548	histocompatibility 2, Q region locus 7
H2-Q7	10.51107	2.804909	0.000548	histocompatibility 2, Q region locus 9
Pcdhga12	126.7359	-0.8369	0.000548	protocadherin gamma subfamily A, 12
Nceh1	1188.418	0.410371	0.00055	neutral cholesterol ester hydrolase 1
Ttpa	44.7713	1.555019	0.000591	tocopherol (alpha) transfer protein
Coro2a	258.0796	-0.84353	0.000598	coronin, actin binding protein 2A
Spp1	124.4546	1.008926	0.000639	secreted phosphoprotein 1

Mro	153.9814	0.953884	0.000649	maestro
Gdap1l1	986.691	0.534243	0.000662	ganglioside-induced differentiation-associated protein 1-like 1
Cryz	274.076	0.931147	0.000691	crystallin, zeta
Tbc1d10c	24.26172	1.378996	0.000691	TBC1 domain family, member 10c
Tbc1d10c	24.26172	1.378996	0.000691	TBC1 domain family, member 10c
Papd4	229.9199	-0.54502	0.00077	PAP associated domain containing 4
AI413582	322.7429	1.320466	0.000832	expressed sequence AI413582
H2-DMa	326.5008	-0.71914	0.000832	histocompatibility 2, class II, locus DMa
Ubald2	366.4903	-0.64946	0.000832	UBA-like domain containing 2
Slc6a8	445.2209	0.648214	0.000948	solute carrier family 6 (neurotransmitter transporter, creatine), member 8
Phf1	529.5935	-0.59701	0.000948	PHD finger protein 1
4930579G24Rik	72.59647	0.711212	0.000956	RIKEN cDNA 4930579G24 gene
Rere	674.4407	0.68374	0.00096	arginine glutamic acid dipeptide (RE) repeats
Rragd	3379.843	0.775351	0.000975	Ras-related GTP binding D
Qprt	12.83372	1.999236	0.000975	quinolinate phosphoribosyltransferase
Usp11	915.2016	-0.73782	0.000995	ubiquitin specific peptidase 11
Racgap1	176.3488	0.717843	0.000997	Rac GTPase-activating protein 1
Plk5	441.728	-0.82766	0.000997	polo like kinase 5
Pmfbp1	6.978404	2.7985	0.001051	polyamine modulated factor 1 binding protein 1
B2m	551.1211	1.153703	0.001051	beta-2 microglobulin
Impa1	1842.824	0.536759	0.00111	inositol (myo)-1(or 4)-monophosphatase 1
Gria2	3790.09	-0.46637	0.001132	glutamate receptor, ionotropic, AMPA2 (alpha 2)
Nrip1	413.9848	-0.61262	0.001151	nuclear receptor interacting protein 1
Crbn	847.2107	-0.39988	0.001187	cereblon
Ppp1r2	6071.922	0.516916	0.001187	protein phosphatase 1, regulatory (inhibitor) subunit 2
Echdc1	530.7125	0.446647	0.001241	enoyl Coenzyme A hydratase domain containing 1
Ago4	154.9942	-0.89326	0.001265	argonaute RISC catalytic subunit 4
Sgk3	279.0818	0.729942	0.001276	serum/glucocorticoid regulated kinase 3
Dpp7	148.3743	0.980833	0.00131	dipeptidylpeptidase 7
Aen	562.1161	0.422736	0.00138	apoptosis enhancing nuclease
Sema5a	191.9868	-0.98356	0.001389	sema domain, seven thrombospondin repeats (type 1 and type 1-like), transmembrane domain (TM) and short cytoplasmic domain, (semaphorin) 5A
Slc35b1	404.1368	0.571816	0.00139	solute carrier family 35, member B1
Tle6	49.95226	-1.16989	0.00139	transducin-like enhancer of split 6
Cdh23	8.495378	-4.24138	0.001479	cadherin 23 (otocadherin)
Ntng2	72.826	1.255356	0.001493	netrin G2
Slc2a6	210.5269	0.622365	0.00152	solute carrier family 2 (facilitated glucose transporter), member 6
Btrc	903.367	-0.45174	0.001527	beta-transducin repeat containing protein
Frat2	214.106	-0.59495	0.001528	frequently rearranged in advanced T cell lymphomas 2

Pcdhga11	78.82137	-1.06542	0.001551	protocadherin gamma subfamily A, 11
Icam1	12.56965	1.817951	0.001569	intercellular adhesion molecule 1
Anp32e	1361.941	-0.45847	0.001603	acidic (leucine-rich) nuclear phosphoprotein 32 family, member E
Paxx	641.0477	0.601055	0.001603	non-homologous end joining factor
Smpdl3b	40.14277	1.164553	0.001616	sphingomyelin phosphodiesterase, acid-like 3B
Ddit4l	665.103	1.023662	0.001693	DNA-damage-inducible transcript 4-like
Cspg5	359.3865	-0.55499	0.001697	chondroitin sulfate proteoglycan 5
Pou3f3	585.5064	-0.66139	0.001708	POU domain, class 3, transcription factor 3
Pik3r3	291.3327	0.627019	0.001896	phosphoinositide-3-kinase regulatory subunit 3
Cyth2	142.8211	0.893188	0.001902	cytohesin 2
Gsto1	643.6991	0.621054	0.001909	glutathione S-transferase omega 1
Naga	172.6652	0.556498	0.001909	N-acetyl galactosaminidase, alpha
Tpx2	25.10117	1.252317	0.001943	TPX2, microtubule-associated
Pias1	460.5194	-0.51505	0.001974	protein inhibitor of activated STAT 1
Phgdh	488.193	-0.70808	0.001974	3-phosphoglycerate dehydrogenase
Wnt7a	92.22038	-0.78985	0.002036	wingless-type MMTV integration site family, member 7A
Dhcr7	228.8591	0.658454	0.002036	7-dehydrocholesterol reductase
Fbxo44	2197.637	0.439239	0.002273	F-box protein 44
Kcnk13	124.4142	0.833463	0.002289	potassium channel, subfamily K, member 13
Kcnq1	8.242029	3.198787	0.002291	potassium voltage-gated channel, subfamily Q, member 1
Net1	302.0992	0.8969	0.002291	neuroepithelial cell transforming gene 1
Zik1	239.0682	-0.50165	0.002305	zinc finger protein interacting with K protein 1
Arl8b	3298.381	0.299407	0.00234	ADP-ribosylation factor-like 8B
Prkcz	5225.587	0.35656	0.002371	protein kinase C, zeta
Fcho1	1057.492	-0.51818	0.002371	FCH domain only 1
Awat2	9.346797	1.70083	0.002412	acyl-CoA wax alcohol acyltransferase 2
Lpin2	576.2382	-0.4939	0.002673	lipin 2
Pdk3	535.6744	0.453821	0.002727	pyruvate dehydrogenase kinase, isoenzyme 3
Chkb	260.1301	0.49882	0.002735	choline kinase beta
Zfand5	4313.271	0.348227	0.002735	zinc finger, AN1-type domain 5
Rcor2	118.1815	0.713899	0.002802	REST corepressor 2
Zbed3	266.082	0.476333	0.002802	zinc finger, BED type containing 3
Fbxl12	110.6753	-0.62652	0.002824	F-box and leucine-rich repeat protein 12
Pcdh17	507.1211	-0.49409	0.002921	protocadherin 17
Ypel2	685.7717	0.475513	0.002927	yippee like 2
Fam131b	376.153	-0.39917	0.002968	family with sequence similarity 131, member B
Ccdc85a	660.386	-0.52441	0.002968	coiled-coil domain containing 85A
Prlr	68.31354	-1.76913	0.003014	prolactin receptor
Fnip1	292.8366	0.509775	0.003014	folliculin interacting protein 1
Rab32	42.34246	0.934919	0.003076	RAB32, member RAS oncogene family
Kif9	52.59687	0.836515	0.003076	kinesin family member 9

Clspn	60.10676	-1.3578	0.003133	claspin
Usp2	1154.68	0.528629	0.003138	ubiquitin specific peptidase 2
Tigar	229.0613	0.622093	0.003149	Trp53 induced glycolysis repulatory phosphatase
Gad2	2292.667	0.766921	0.003215	glutamic acid decarboxylase 2
Ftl1	5382.249	0.690318	0.003225	ferritin light polypeptide 1
Bicral	298.2779	-0.60958	0.003307	BRD4 interacting chromatin remodeling complex associated protein like
Rab11fip5	366.5916	0.456355	0.003327	RAB11 family interacting protein 5 (class I)
Anks1b	5972.97	-0.453	0.003364	ankyrin repeat and sterile alpha motif domain containing 1B
Nova2	352.6616	-0.44613	0.003364	neuro-oncological ventral antigen 2
Krt1	102.3941	0.712401	0.003364	keratin 1
Gli3	90.26062	-1.36412	0.003393	GLI-Kruppel family member GLI3
Tpm2	225.8791	0.573676	0.003412	tropomyosin 2, beta
Nrtn	177.1264	-0.783	0.00343	neurturin
Ing5	203.7882	-0.57394	0.003446	inhibitor of growth family, member 5
Fgd5	26.46575	1.404473	0.003523	FYVE, RhoGEF and PH domain containing 5
Smc5	128.0928	-0.61624	0.003614	structural maintenance of chromosomes 5
Mpc1	5567.862	0.728837	0.003639	mitochondrial pyruvate carrier 1
Patl2	4.812965	2.06363	0.003639	protein associated with topoisomerase II homolog 2 (yeast)
Rhebl1	37.25048	-1.14585	0.003735	Ras homolog enriched in brain like 1
Fam117a	75.45703	0.840655	0.003809	family with sequence similarity 117, member A
Kctd6	653.73	0.452115	0.003925	potassium channel tetramerisation domain containing 6
Gatsl2	926.1146	0.54597	0.00406	GATS protein-like 2
Sat1	671.0499	0.873746	0.00414	spermidine/spermine N1-acetyl transferase 1
Pyurf	421.9864	0.575541	0.00414	Pigy upstream reading frame
Rpl7a-ps11	5.603055	-20.6277	0.004239	
Ostf1	252.0963	0.660985	0.004248	osteoclast stimulating factor 1
Egr1	4598.027	-1.02677	0.004248	early growth response 1
Kcnf1	694.9228	-0.5746	0.004248	potassium voltage-gated channel, subfamily F, member 1
Insm1	83.77453	-1.08059	0.004356	insulinoma-associated 1
Hmgb3	668.9184	-0.72499	0.004361	high mobility group box 3
Zbtb10	59.52953	-0.74192	0.004515	zinc finger and BTB domain containing 10
Ing4	527.9769	-0.49087	0.004597	inhibitor of growth family, member 4
Rpp25	364.5791	0.747051	0.004597	ribonuclease P/MRP 25 subunit
Rell2	1909.336	0.420692	0.004738	RELT-like 2
Arhgap20	803.3861	-0.54017	0.004738	Rho GTPase activating protein 20
Pik3r4	296.4872	1.093516	0.004768	phosphoinositide-3-kinase regulatory subunit 4
Bcor	87.38386	-0.74846	0.004768	BCL6 interacting corepressor
Thrsp	290.2929	1.083707	0.004783	thyroid hormone responsive
Prkx	185.2551	0.572052	0.005129	protein kinase, X-linked
Krt10	370.0656	0.724107	0.005179	keratin 10

Brd8	268.2048	-0.56033	0.005238	bromodomain containing 8
Mthfd2	147.2791	0.860178	0.005238	methylenetetrahydrofolate dehydrogenase (NAD+ dependent), methenyltetrahydrofolate cyclohydrolase
Gramd2	138.2186	0.849339	0.005238	GRAM domain containing 2
Tpgs2	1245.282	0.284357	0.00545	tubulin polyglutamylase complex subunit 2
Acox1	1099.331	0.639609	0.005491	acyl-Coenzyme A oxidase 1, palmitoyl
Pgam1	12498.45	0.360014	0.005624	phosphoglycerate mutase 1
Dusp22	520.4158	0.373206	0.005624	dual specificity phosphatase 22
Ctsz	580.3296	0.514018	0.005744	cathepsin Z
Tmem192	439.1597	0.585359	0.00588	transmembrane protein 192
Atp6v1b2	8360.641	0.358174	0.005906	ATPase, H+ transporting, lysosomal V1 subunit B2
Npy5r	70.97384	0.765716	0.006212	neuropeptide Y receptor Y5
Pcdhga10	36.91551	-1.37153	0.006286	protocadherin gamma subfamily A, 10
Nfatc2	443.3795	0.610759	0.006299	nuclear factor of activated T cells, cytoplasmic, calcineurin dependent 2
Ak3	1174.106	-0.43604	0.006447	adenylate kinase 3
Gm28437	34.65206	-6.41043	0.006447	
Lztr1	1223.229	0.461502	0.006562	leucine-zipper-like transcriptional regulator, 1
Ugt2b35	22.14779	-6.84208	0.006576	UDP glucuronosyltransferase 2 family, polypeptide B35
Wdr31	160.6778	-0.72937	0.006601	WD repeat domain 31
Rexo2	1092.057	0.742645	0.006657	RNA exonuclease 2
Memo1	291.4547	0.44127	0.006657	mediator of cell motility 1
N4bp2l1	246.443	-0.65669	0.006902	NEDD4 binding protein 2-like 1
Rxrg	2275.144	-0.67684	0.006923	retinoid X receptor gamma
Syt16	1111.602	-0.46714	0.006956	synaptotagmin XVI
Ubtf	1638.334	-0.44117	0.007097	upstream binding transcription factor, RNA polymerase I
Efcab6	47.74484	1.152946	0.007097	EF-hand calcium binding domain 6
Tnfaip8l1	143.6763	-0.57725	0.007097	tumor necrosis factor, alpha-induced protein 8-like 1
Nap1l3	504.9286	-0.34918	0.007097	nucleosome assembly protein 1-like 3
Mxra8	52.46759	1.568283	0.007215	matrix-remodelling associated 8
Fgl2	11.20176	1.740868	0.007221	fibrinogen-like protein 2
Tbc1d16	309.6843	0.523121	0.007235	TBC1 domain family, member 16
Vcpkmt	58.3543	0.999557	0.007235	valosin containing protein lysine (K) methyltransferase
Mospd1	359.3539	0.417746	0.007465	motile sperm domain containing 1
Oat	924.8187	-0.42971	0.007711	ornithine aminotransferase
Wdr63	7.859384	2.002907	0.007712	WD repeat domain 63
Surf4	1071.932	0.367102	0.007824	surfeit gene 4
Zswim4	226.4788	-0.72132	0.007909	zinc finger SWIM-type containing 4
Gpr149	45.20244	1.217551	0.007909	G protein-coupled receptor 149
Slc25a44	1645.832	0.358066	0.008144	solute carrier family 25, member 44
Rflnb	211.5398	0.796434	0.008182	refilin B

Kcnip4	1396.967	-0.36153	0.008183	Kv channel interacting protein 4
Top2b	416.4109	-0.69714	0.00841	topoisomerase (DNA) II beta
Slc22a3	98.69241	-1.10659	0.008609	solute carrier family 22 (organic cation transporter), member 3
Mgarp	11.23778	2.080194	0.00869	mitochondria localized glutamic acid rich protein
Mfsd1	292.1136	0.4967	0.008789	major facilitator superfamily domain containing 1
Sart3	456.221	-0.4727	0.008899	squamous cell carcinoma antigen recognized by T cells 3
Bcat1	927.3789	0.601482	0.009191	branched chain aminotransferase 1, cytosolic
Ncf4	6.224485	-4.09711	0.009413	neutrophil cytosolic factor 4
Dexi	1016.554	0.500274	0.009433	dexamethasone-induced transcript
Slc39a11	322.4898	0.623369	0.009433	solute carrier family 39 (metal ion transporter), member 11
Dnase2a	56.60423	1.13037	0.009475	deoxyribonuclease II alpha
Slc38a8	14.60491	1.74297	0.009604	solute carrier family 38, member 8
Hexim2	181.0305	-0.77344	0.009694	hexamethylene bis-acetamide inducible 2
Pdss2	159.4665	0.421439	0.009777	prenyl (solanesyl) diphosphate synthase, subunit 2
Nos3	72.66974	0.847644	0.009892	nitric oxide synthase 3, endothelial cell
Srpx2	13.49674	1.506032	0.010113	sushi-repeat-containing protein, X-linked 2
Lamc2	57.63104	1.120099	0.0102	laminin, gamma 2
Acat3	41.04453	-1.14265	0.010348	acetyl-Coenzyme A acetyltransferase 3
Ppp1cc	4866.914	0.433964	0.010443	protein phosphatase 1, catalytic subunit, gamma isoform
Ppp1cc	4866.914	0.433964	0.010443	predicted pseudogene 5601
Sec24b	243.984	-0.69814	0.010708	Sec24 related gene family, member B (S. cerevisiae)
Atp1a2	1079.801	-0.72697	0.010708	ATPase, Na+/K+ transporting, alpha 2 polypeptide
Uhrf1bp1l	695.9329	0.291723	0.010708	UHRF1 (ICBP90) binding protein 1-like
Npc2	650.4835	0.397269	0.010708	NPC intracellular cholesterol transporter 2
Htra4	18.03275	1.341616	0.010708	HtrA serine peptidase 4
Agpat4	476.7034	-0.48616	0.010772	1-acylglycerol-3-phosphate O-acyltransferase 4 (lysophosphatidic acid acyltransferase, delta)
Prss23	18.08143	-1.65693	0.010772	protease, serine 23
Gm8730	22.61041	6.686355	0.010772	
Ism1	146.4598	-0.55773	0.010772	isthmin 1, angiogenesis inhibitor
Mob1b	205.512	0.577142	0.01084	MOB kinase activator 1B
Mme	235.3304	0.853566	0.011166	membrane metallo endopeptidase
Senp2	821.7184	0.325481	0.011226	SUMO/sentrin specific peptidase 2
Atp6v0c	21810.45	0.657271	0.011226	ATPase, H+ transporting, lysosomal V0 subunit C
Onecut2	80.64697	-0.79592	0.011272	one cut domain, family member 2
Ly6h	2341.819	-0.53889	0.011441	lymphocyte antigen 6 complex, locus H
Sirt7	454.9113	0.401297	0.011441	sirtuin 7
Arl6ip1	4829.724	0.433222	0.011574	ADP-ribosylation factor-like 6 interacting protein 1
Atp6ap2	3735.05	0.384572	0.011631	ATPase, H+ transporting, lysosomal accessory protein 2
Trp53bp1	328.7622	-0.72693	0.011631	transformation related protein 53 binding protein 1

Rell1	190.0605	0.534014	0.011631	RELT-like 1
Taok3	789.6196	0.345435	0.011631	TAO kinase 3
Btbd2	1331.49	-0.43211	0.01168	BTB (POZ) domain containing 2
Smarcc1	444.3803	-0.3548	0.011826	SWI/SNF related, matrix associated, actin dependent regulator of chromatin, subfamily c, member 1
Yipf1	453.728	0.505489	0.011861	Yip1 domain family, member 1
Slc18b1	193.6355	0.710169	0.011895	solute carrier family 18, subfamily B, member 1
Cd47	1615.172	-0.38813	0.011902	CD47 antigen (Rh-related antigen, integrin-associated signal transducer)
Ino80b	157.841	-0.60058	0.01207	INO80 complex subunit B
Hlcs	102.9314	0.846737	0.012265	holocarboxylase synthetase (biotin- [propriony-Coenzyme A-carboxylase (ATP-hydrolysing)] ligase)
Ppp2r5b	1256.824	0.540232	0.012456	protein phosphatase 2, regulatory subunit B', beta
Ahi1	715.1963	-0.56037	0.01255	Abelson helper integration site 1
Fst	18.88423	1.664337	0.01255	follistatin
Uap1l1	400.1392	0.761691	0.01255	UDP-N-acteylglucosamine pyrophosphorylase 1-like 1
Adam15	664.1442	0.521725	0.012857	a disintegrin and metallopeptidase domain 15 (metargidin)
Crym	1099.976	-0.5667	0.012857	crystallin, mu
Sox6	33.91158	-2.42653	0.012857	SRY (sex determining region Y)-box 6
Rad21	481.7316	-0.46369	0.012868	RAD21 cohesin complex component
Sp4	162.5163	-0.45839	0.012868	trans-acting transcription factor 4
Fibcd1	248.8652	-0.56554	0.012868	fibrinogen C domain containing 1
Ccdc155	40.17868	0.771061	0.012868	coiled-coil domain containing 155
Kcnq3	652.8517	-0.34317	0.012868	potassium voltage-gated channel, subfamily Q, member 3
Ddn	2932.372	0.519515	0.012868	dendrin
Cda	30.61556	1.184097	0.012886	cytidine deaminase
Gm16286	3152.085	0.230265	0.012915	thioredoxin-like 4A
Hrasls	592.8975	-0.4298	0.012964	HRAS-like suppressor
Gjc1	73.30395	-1.05613	0.01305	gap junction protein, gamma 1
Inpp5f	1181.199	-0.31229	0.013053	inositol polyphosphate-5-phosphatase F
Las1l	358.781	-0.41311	0.013053	LAS1-like (S. cerevisiae)
Tomm34	2067.354	0.4558	0.013158	translocase of outer mitochondrial membrane 34
Srsf12	531.7855	-0.33242	0.013322	serine/arginine-rich splicing factor 12
Krt77	127.4722	0.582034	0.013475	keratin 77
Plvap	433.7194	-0.95358	0.013497	plasmalemma vesicle associated protein
Tdrd7	446.0428	0.580346	0.013539	tudor domain containing 7
Pgrmc2	1196.32	-0.37454	0.013894	progesterone receptor membrane component 2
Kcnt2	106.8414	-0.87346	0.014191	potassium channel, subfamily T, member 2
Slc35e4	456.5839	0.39536	0.014296	solute carrier family 35, member E4
Atp6ap1l	243.847	0.786378	0.014296	ATPase, H+ transporting, lysosomal accessory protein 1-like
Cd93	6.724184	1.969741	0.01438	CD93 antigen

Tom1	497.1468	0.406479	0.014455	target of myb1 trafficking protein
Atrnl1	490.8347	-0.55666	0.014455	attractin like 1
Scamp3	823.2195	0.375154	0.014507	secretory carrier membrane protein 3
Sox17	42.78723	1.142668	0.014626	SRY (sex determining region Y)-box 17
Atcay	1177.432	-0.3609	0.014856	ataxia, cerebellar, Cayman type
Aard	37.38835	0.922781	0.015019	alanine and arginine rich domain containing protein
Cpn1	14.26072	1.142506	0.015037	carboxypeptidase N, polypeptide 1
2410131K14Rik	476.7094	0.400562	0.015037	RIKEN cDNA 2410131K14 gene
Spink8	10.10114	2.388354	0.015037	serine peptidase inhibitor, Kazal type 8
Shox2	187.3846	-1.05778	0.015253	short stature homeobox 2
Zpbp	46.56978	0.699418	0.015262	zona pellucida binding protein
Ttll1	760.6602	0.348181	0.015339	tubulin tyrosine ligase-like 1
Scrt2	458.3961	0.497937	0.015382	scratch family zinc finger 2
Hexa	526.7515	0.361963	0.015424	hexosaminidase A
Pcdhb6	34.87363	-1.42615	0.015561	protocadherin beta 6
Rph3a	1373.863	-0.45238	0.015602	rabphilin 3A
Fos	686.6726	-0.87732	0.015657	FBJ osteosarcoma oncogene
Rnf144a	342.5163	-0.55438	0.015693	ring finger protein 144A
Rps6ka5	9.09222	-6.6457	0.015693	ribosomal protein S6 kinase, polypeptide 5
Rnf115	1210.212	0.32043	0.015693	ring finger protein 115
Clcn1	7.294643	3.902689	0.015693	chloride channel, voltage-sensitive 1
Tspo	60.09415	1.351581	0.015718	translocator protein
Ostm1	837.821	0.384123	0.015725	osteopetrosis associated transmembrane protein 1
Bag1	2217.527	0.572105	0.015771	BCL2-associated athanogene 1
Erfe	6.756973	-3.6898	0.015771	erythroferrone
Rpl18a	126.3432	-1.01473	0.01584	ribosomal protein L18A
Tcf15	22.81824	0.929924	0.015957	transcription factor 15
Sh3d21	13.23217	-1.28016	0.015957	SH3 domain containing 21
Lamp2	439.3885	0.45824	0.016257	lysosomal-associated membrane protein 2
Rps6kb2	92.25847	0.539624	0.016257	ribosomal protein S6 kinase, polypeptide 2
Rbm43	412.7406	0.403862	0.016257	RNA binding motif protein 43
Rps6kb2	92.25847	0.539624	0.016257	ribosomal protein S6 kinase, polypeptide 2
Grina	4841.855	0.381925	0.016307	glutamate receptor, ionotropic, N-methyl D-aspartate-associated protein 1 (glutamate binding)
Astn1	589.0728	-0.45511	0.016374	astrotactin 1
Hrk	658.8085	-0.42664	0.016492	harakiri, BCL2 interacting protein (contains only BH3 domain)
Rras	124.269	0.607287	0.016511	related RAS viral (r-ras) oncogene
Cyp4f15	45.39466	-1.13861	0.01666	cytochrome P450, family 4, subfamily f, polypeptide 15
Cav1	98.4084	0.871909	0.016666	caveolin 1, caveolae protein
Mgst3	1724.896	0.920047	0.016666	microsomal glutathione S-transferase 3
Mpzl2	17.31899	-2.12904	0.016666	myelin protein zero-like 2
Tiparp	329.4562	-0.88127	0.016666	TCDD-inducible poly(ADP-ribose) polymerase

Flot2	1224.216	-0.4503	0.016666	flotillin 2
Hist1h1c	516.8302	0.692581	0.016707	histone cluster 1, H1c
Cdh13	1214.222	0.598506	0.017018	cadherin 13
Neto2	497.7548	-0.51438	0.017057	neuropilin (NRP) and tolloid (TLL)-like 2
Hibadh	1145.836	0.282877	0.017103	3-hydroxyisobutyrate dehydrogenase
Zkscan2	63.46615	-0.95461	0.017103	zinc finger with KRAB and SCAN domains 2
Crb2	34.7968	-1.20733	0.017103	crumbs family member 2
Rnf24	225.1657	-0.50906	0.017104	ring finger protein 24
Tcta	580.9695	0.537039	0.017196	T cell leukemia translocation altered gene
Inafm1	467.6301	-0.44488	0.017232	InaF motif containing 1
Wsb2	7287.741	0.324071	0.017362	WD repeat and SOCS box-containing 2
Rab40b	1368.649	0.346234	0.017409	Rab40B, member RAS oncogene family
Hnrnph1	1183.421	-0.34998	0.017442	heterogeneous nuclear ribonucleoprotein H1
Grm2	209.0651	-0.77501	0.017442	glutamate receptor, metabotropic 2
Agtrap	85.41985	1.106943	0.017442	angiotensin II, type I receptor-associated protein
Fem1b	673.7981	-0.35141	0.017442	feminization 1 homolog b (C. elegans)
Ccdc71	435.5662	-0.48763	0.017442	coiled-coil domain containing 71
Sprr1a	7.085765	1.675884	0.017442	small proline-rich protein 1A
Ntm	2101.329	-0.37363	0.017442	neurotrimin
B230307C23Rik	21.67792	1.719366	0.017442	
Limk2	1297.999	0.310053	0.017578	LIM motif-containing protein kinase 2
Vstm2a	872.8326	0.286996	0.017689	V-set and transmembrane domain containing 2A
Cfap44	16.04676	2.145588	0.017763	cilia and flagella associated protein 44
Prmt7	665.8876	-0.28319	0.018333	protein arginine N-methyltransferase 7
Tagln2	150.4442	0.861806	0.01841	transgelin 2
6820408C15Rik	44.29574	0.73441	0.018455	RIKEN cDNA 6820408C15 gene
Mvd	345.1973	0.346234	0.01865	mevalonate (diphospho) decarboxylase
Sf3b1	1836.624	-0.31684	0.018839	splicing factor 3b, subunit 1
Rab8b	449.007	-0.49998	0.01889	RAB8B, member RAS oncogene family
Smarcal1	244.3433	-0.45386	0.019038	SWI/SNF related matrix associated, actin dependent regulator of chromatin, subfamily a-like 1
Vat1l	388.3911	-0.86471	0.019052	vesicle amine transport protein 1 like
Entpd3	218.0077	0.647131	0.01908	ectonucleoside triphosphate diphosphohydrolase 3
Mon1a	402.4619	0.362724	0.019252	MON1 homolog A, secretory traffciking associated
Ffar3	12.67958	-1.67673	0.019561	free fatty acid receptor 3
Acot11	111.0474	-0.92181	0.019561	acyl-CoA thioesterase 11
Slc5a5	262.2519	0.856547	0.020076	solute carrier family 5 (sodium iodide symporter), member 5
Glce	351.8807	0.529317	0.020076	glucuronyl C5-epimerase
Ywhah	26189.9	0.371027	0.020136	tyrosine 3-monooxygenase/tryptophan 5-monooxygenase activation protein, eta polypeptide
Tmem29	240.0905	-0.45885	0.020542	transmembrane protein 29
Vps36	307.0814	0.393062	0.020725	vacuolar protein sorting 36

Chadl	244.0649	-0.58897	0.020772	chondroadherin-like
Fign	55.15329	-1.28422	0.020833	fidgetin
Zhx2	102.1976	-1.75197	0.020897	zinc fingers and homeoboxes 2
Atp2b2	6793.705	-0.38194	0.021209	ATPase, Ca++ transporting, plasma membrane 2
Ptger4	26.47113	1.187978	0.021209	prostaglandin E receptor 4 (subtype EP4)
Smarca1	210.6627	-0.62314	0.021319	SWI/SNF related, matrix associated, actin dependent regulator of chromatin, subfamily a, member 1
Musk	34.66043	1.184709	0.02176	muscle, skeletal, receptor tyrosine kinase
Naaa	214.6113	-0.48166	0.021871	N-acylethanolamine acid amidase
Pusl1	285.703	0.471915	0.022795	pseudouridylate synthase-like 1
Chrm1	1673.398	-0.48814	0.022908	cholinergic receptor, muscarinic 1, CNS
Mpnd	2542.378	0.358729	0.022945	MPN domain containing
Srprb	571.6414	0.313495	0.023032	signal recognition particle receptor, B subunit
Rasa2	211.2272	-0.60436	0.02304	RAS p21 protein activator 2
Bckdha	510.8273	-0.35624	0.02304	branched chain ketoacid dehydrogenase E1, alpha polypeptide
Hdac9	158.4912	-0.7083	0.023285	histone deacetylase 9
Cygb	1290.203	0.402119	0.023332	cytoglobin
Orai1	101.7042	0.53483	0.023651	ORAI calcium release-activated calcium modulator 1
Naf1	78.89512	0.654525	0.023785	nuclear assembly factor 1 ribonucleoprotein
Abi2	2548.943	-0.39838	0.023809	abl-interactor 2
Sipa1	173.5841	-0.63873	0.023893	signal-induced proliferation associated gene 1
Tec	20.21537	1.085817	0.023913	tec protein tyrosine kinase
Atp6v0b	4595.394	0.488033	0.024018	ATPase, H+ transporting, lysosomal V0 subunit B
Farp2	65.20345	0.643127	0.024018	FERM, RhoGEF and pleckstrin domain protein 2
Rdh11	270.4403	0.361691	0.024018	retinol dehydrogenase 11
Rbm15	33.39505	0.759047	0.02419	RNA binding motif protein 15
Cenpa	36.76574	1.192725	0.024373	centromere protein A
Ighm	410.1765	0.932354	0.024373	
Setd2	123.7837	-0.79446	0.024618	SET domain containing 2
Ier3	168.4689	0.891503	0.024944	immediate early response 3
Cnnm1	706.9718	0.341907	0.025551	cyclin M1
Arl16	578.8388	0.461454	0.025551	ADP-ribosylation factor-like 16
Cdc42ep4	352.6394	-0.5337	0.025788	CDC42 effector protein (Rho GTPase binding) 4
Polr3k	1025.307	0.445663	0.026013	polymerase (RNA) III (DNA directed) polypeptide K
Tsen54	138.607	0.489697	0.026047	tRNA splicing endonuclease subunit 54
Adhfe1	120.6297	-0.80933	0.026113	alcohol dehydrogenase, iron containing, 1
Pou3f2	182.3284	-0.55135	0.026113	POU domain, class 3, transcription factor 2
Dpy19l3	274.9465	-0.93197	0.026463	dpy-19-like 3 (C. elegans)
Spsb2	48.3393	0.78483	0.026891	splA/ryanodine receptor domain and SOCS box containing 2
Gm14569	6.322394	-2.94375	0.026891	predicted gene 14569
Cdh11	374.319	-0.34337	0.027099	cadherin 11

Negr1	966.9209	-0.25454	0.027951	neuronal growth regulator 1
Zfp944	178.5426	0.516372	0.028041	zinc finger protein 944
Lor	307.8793	0.525824	0.028068	loricrin
Pcdhb5	18.60926	-1.28841	0.028742	protocadherin beta 5
Me2	502.719	0.590558	0.028871	malic enzyme 2, NAD(+)-dependent, mitochondrial
Nsg1	6860.255	0.341908	0.028875	neuron specific gene family member 1
Cdc34	856.4513	0.442988	0.029017	cell division cycle 34
Polb	910.5413	0.435038	0.029064	polymerase (DNA directed), beta
Rbmx	643.6828	-0.44301	0.029238	RNA binding motif protein, X chromosome
Ppp2r2a	187.3229	-0.72803	0.029499	protein phosphatase 2, regulatory subunit B, alpha
Prpf8	420.8977	-0.4289	0.029706	pre-mRNA processing factor 8
Itfg1	2521.209	-0.32202	0.029752	integrin alpha FG-GAP repeat containing 1
Eno2	13725.45	0.4127	0.029777	enolase 2, gamma neuronal
Tbc1d23	192.5185	-0.69814	0.029965	TBC1 domain family, member 23
Gemin7	474.1688	0.519055	0.030057	gem nuclear organelle associated protein 7
Sirt3	1154.375	0.343751	0.030215	sirtuin 3
Ackr3	61.8929	-0.81136	0.030215	atypical chemokine receptor 3
Ints12	152.3715	-0.52539	0.030951	integrator complex subunit 12
Ggps1	1083.295	-0.33658	0.031062	geranylgeranyl diphosphate synthase 1
Abcd4	91.27058	0.591792	0.031271	ATP-binding cassette, sub-family D (ALD), member 4
Osgepl1	299.1116	0.451448	0.031271	O-sialoglycoprotein endopeptidase-like 1
Gdpgp1	198.5058	0.436438	0.031473	GDP-D-glucose phosphorylase 1
Tm4sf1	52.69809	1.276236	0.031584	transmembrane 4 superfamily member 1
Klf16	603.509	-0.66537	0.032333	Kruppel-like factor 16
Smurf1	537.6131	-0.30062	0.032333	SMAD specific E3 ubiquitin protein ligase 1
Ddx5	3515.805	-0.25322	0.032635	DEAD (Asp-Glu-Ala-Asp) box polypeptide 5
Efna1	33.42316	0.912144	0.032954	ephrin A1
Gabrb1	569.928	-0.46348	0.032966	gamma-aminobutyric acid (GABA) A receptor, subunit beta 1
Pkd2	289.9587	-0.48666	0.033127	polycystic kidney disease 2
Dmd	242.0429	-0.51496	0.033501	dystrophin, muscular dystrophy
Cyb561a3	93.78553	0.480201	0.033886	cytochrome b561 family, member A3
Atp6v1h	2268.603	0.346342	0.034402	ATPase, H+ transporting, lysosomal V1 subunit H
1700047I17Rik2	120.4342	-7.74441	0.03467	RIKEN cDNA 1700047I17 gene 2
Flcn	622.3019	0.426322	0.034983	folliculin
Mkln1	469.4698	0.564631	0.035074	muskelin 1, intracellular mediator containing kelch motifs
Aldoc	5019.997	-0.48181	0.035331	aldolase C, fructose-bisphosphate
Dmwd	2425.133	-0.31967	0.035331	dystrophia myotonica-containing WD repeat motif
Il11ra1	309.5119	-0.50596	0.035619	interleukin 11 receptor, alpha chain 1
Scnn1a	27.55718	0.81737	0.035706	sodium channel, nonvoltage-gated 1 alpha
Gad1	3178.464	0.553234	0.035725	glutamate decarboxylase 1
Atp6v1e1	8931.457	0.517558	0.035878	ATPase, H+ transporting, lysosomal V1 subunit E1

Ufm1	1185.545	0.752027	0.035878	ubiquitin-fold modifier 1
Rapgef2	757.8762	-0.38149	0.036309	Rap guanine nucleotide exchange factor (GEF) 2
Rhoc	114.5025	0.988308	0.036464	ras homolog family member C
Pqlc2	101.0526	0.645383	0.03661	PQ loop repeat containing 2
Plbd2	591.2241	0.496289	0.036719	phospholipase B domain containing 2
Bbs2	138.2359	-0.65169	0.036922	Bardet-Biedl syndrome 2 (human)
Elovl4	947.7369	0.327904	0.0371	elongation of very long chain fatty acids (FEN1/Elo2, SUR4/Elo3, yeast)-like 4
Slc7a11	55.54479	-1.0253	0.037175	solute carrier family 7 (cationic amino acid transporter, y+ system), member 11
Pcdhgb4	20.46618	-1.48103	0.037744	protocadherin gamma subfamily B, 4
Ushbp1	15.60775	1.569696	0.037756	USH1 protein network component harmonin binding protein 1
Arhgap33	1247.629	-0.67619	0.037756	Rho GTPase activating protein 33
Irf8	71.30628	-1.02502	0.037756	interferon regulatory factor 8
Senp8	76.90291	-0.71965	0.037756	SUMO/sentrin specific peptidase 8
Coch	1403.202	0.851398	0.038233	cochlin
Dmkn	87.87134	-1.40857	0.039261	dermokine
8430408G 22Rik	16.8889	1.453643	0.039453	RIKEN cDNA 8430408G22 gene
Tfrc	307.071	-0.86464	0.039454	transferrin receptor
Dgkg	871.6703	0.269286	0.039454	diacylglycerol kinase, gamma
Asb4	23.46221	1.40057	0.040357	ankyrin repeat and SOCS box-containing 4
Thy1	1124.237	0.586022	0.040476	thymus cell antigen 1, theta
Usp43	31.44357	-1.21802	0.04056	ubiquitin specific peptidase 43
Inip	594.1218	0.327337	0.04056	INTS3 and NABP interacting protein
Cyp2d22	64.71556	-0.90812	0.04056	cytochrome P450, family 2, subfamily d, polypeptide 22
She	22.115	1.232382	0.040574	src homology 2 domain-containing transforming protein E
6-Mar	958.938	-0.27774	0.040712	membrane-associated ring finger (C3HC4) 6
Usp47	374.3343	-0.3807	0.040755	ubiquitin specific peptidase 47
Chmp2b	1462.355	0.398632	0.040825	charged multivesicular body protein 2B
Nudt7	70.46013	0.737504	0.041067	nudix (nucleoside diphosphate linked moiety X)-type motif 7
A930017K 11Rik	16.45576	-1.47792	0.041821	RIKEN cDNA A930017K11 gene
Osbpl9	455.4694	0.368526	0.041821	oxysterol binding protein-like 9
Usp9x	519.0652	-0.52328	0.041821	ubiquitin specific peptidase 9, X chromosome
Pcdhga8	61.25308	-1.16587	0.041821	protocadherin gamma subfamily A, 8
Gcat	132.4681	0.430887	0.042063	glycine C-acetyltransferase (2-amino-3-ketobutyrate-coenzyme A ligase)
Zmym6	235.2883	-0.9441	0.042071	zinc finger, MYM-type 6
Ctsd	2285.299	0.263104	0.042388	cathepsin D
Rcc1	214.6627	0.387274	0.042388	regulator of chromosome condensation 1
Epb41	240.1723	0.645283	0.042388	erythrocyte membrane protein band 4.1
Mb21d1	7.388673	1.900396	0.042388	Mab-21 domain containing 1

Grn	411.5598	0.385312	0.042388	granulin
Tomm20	4770.912	0.305213	0.042388	translocase of outer mitochondrial membrane 20 homolog (yeast)
Msh2	267.305	-0.41362	0.042514	mutS homolog 2
Unc5d	100.2267	-0.77952	0.042662	unc-5 netrin receptor D
Fam118b	333.5253	0.406905	0.042663	family with sequence similarity 118, member B
Pnma1	81.33354	-0.6425	0.042663	paraneoplastic antigen MA1
Piga	101.8148	-0.6892	0.042793	phosphatidylinositol glycan anchor biosynthesis, class A
Dock4	480.1653	-0.55042	0.042793	dedicator of cytokinesis 4
Txlng	259.7736	0.414119	0.042793	taxilin gamma
Zbtb44	182.4539	-0.8736	0.042793	zinc finger and BTB domain containing 44
2-Mar	1514.475	0.315164	0.042793	membrane-associated ring finger (C3HC4) 2
Atp1b1	18899.81	0.242744	0.043068	ATPase, Na+/K+ transporting, beta 1 polypeptide
Dmac2	872.4996	-0.33843	0.043118	distal membrane arm assembly complex 2
Snf8	1027.702	0.35466	0.043132	SNF8, ESCRT-II complex subunit, homolog (S. cerevisiae)
Zfp768	86.25274	-0.63891	0.043282	zinc finger protein 768
Bmx	16.90652	1.428602	0.043379	BMX non-receptor tyrosine kinase
Ptpn3	134.9516	-1.11709	0.043472	protein tyrosine phosphatase, non-receptor type 3
Vps26a	977.1379	0.334199	0.043579	VPS26 retromer complex component A
Cadm1	1526.716	-0.39925	0.043579	cell adhesion molecule 1
Ube2g2	1460.55	0.335301	0.043913	ubiquitin-conjugating enzyme E2G 2
Gpx8	40.98642	-0.96927	0.043926	glutathione peroxidase 8 (putative)
Nalcn	441.7619	-0.36256	0.043983	sodium leak channel, non-selective
Prmt8	846.1205	0.238511	0.043983	protein arginine N-methyltransferase 8
Mapk1ip1	322.5523	0.405276	0.043983	mitogen-activated protein kinase 1 interacting protein 1
Kcne1l	38.80688	-1.00394	0.043983	potassium voltage-gated channel, Isk-related family, member 1-like, pseudogene
Tcap	74.91781	0.888374	0.044042	titin-cap
Pcdhga9	39.02339	-1.14083	0.044742	protocadherin gamma subfamily A, 9
Elfn1	63.66815	-0.87784	0.045443	leucine rich repeat and fibronectin type III, extracellular 1
Tcf4	1092.669	-0.70072	0.045463	transcription factor 4
Arl5b	150.899	-0.72217	0.045535	ADP-ribosylation factor-like 5B
Suv39h2	125.0526	0.483746	0.045649	suppressor of variegation 3-9 2
H2-Q2	17.24574	-1.22933	0.04583	histocompatibility 2, Q region locus 2
Rnf214	542.042	-0.47323	0.046145	ring finger protein 214
9930012K11Rik	18.77557	-1.44378	0.046145	RIKEN cDNA 9930012K11 gene
Grm5	1026.575	-0.37758	0.046145	glutamate receptor, metabotropic 5
Pcdhga7	143.8924	-0.80324	0.046204	protocadherin gamma subfamily A, 7
Nr4a1	1355.686	-1.30281	0.047521	nuclear receptor subfamily 4, group A, member 1
Mkl1	359.7824	-0.34989	0.047898	MKL (megakaryoblastic leukemia)/myocardin-like 1
Hes5	271.5832	-0.55161	0.047985	hes family bHLH transcription factor 5

Nagpa	157.4203	0.565524	0.048337	N-acetylglucosamine-1-phosphodiester alpha-N-acetylglucosaminidase
Lhx6	214.8019	-0.73308	0.048337	LIM homeobox protein 6
Set	2888.37	-0.45772	0.048395	SET nuclear oncogene
Glrx	790.6684	0.524131	0.04846	glutaredoxin
Gpm6b	8947.831	-0.39422	0.04846	glycoprotein m6b
Acadsb	604.976	-0.41678	0.048686	acyl-Coenzyme A dehydrogenase, short/branched chain
Cntnap3	58.95835	-0.76858	0.04894	contactin associated protein-like 3
Dcbld1	161.9664	0.405135	0.049146	discoidin, CUB and LCCL domain containing 1
Rsph1	153.8364	0.517627	0.049146	radial spoke head 1 homolog (Chlamydomonas)
Ube2t	26.91288	0.97438	0.049146	ubiquitin-conjugating enzyme E2T
Plekha2	324.971	0.620962	0.049146	pleckstrin homology domain-containing, family A (phosphoinositide binding specific) member 2
Prr3	374.4146	-0.34218	0.049146	proline-rich polypeptide 3
Fxyd2	31.2414	-1.78619	0.04951	FXYD domain-containing ion transport regulator 2
Chd8	31.12017	1.400941	0.049592	chromodomain helicase DNA binding protein 8
Ccdc92	2876.283	0.300936	0.049658	coiled-coil domain containing 92

Table S2. List of genes significantly different between Tsc1-WT and Tsc1-Het dSPNs.

Gene	Base Mean	Log2(Fold Change)	Adjusted p-value
Frzb	155.2506	-1.08626	8.37E-05
Upf1	109.5201	1.574983	0.002241
Ccdc65	84.16586	-0.63798	0.00763
Pdzrn3	215.1652	-0.78025	0.00763
Ntng2	72.826	-1.30504	0.00763
Acap2	18.31188	16.4774	0.00763
Pde1a	1384.083	-0.84671	0.00763
Col20a1	7.430206	-2.67137	0.020113
Laptm4b	764.1049	-0.46673	0.020113
Tradd	116.7908	-0.81695	0.020285
Serpini1	2027.109	-0.59701	0.022302

Table S3. List of genes significantly different between Tsc1-WT and Tsc1-KO iSPNs.

Gene	Base Mean	Log_2(Fold Change)	Adjusted p-value	Wikigene Description
Necab3	1122.304	1.782907	1.08E-29	N-terminal EF-hand calcium binding protein 3
Pgam2	276.2461	2.849402	2.36E-25	phosphoglycerate mutase 2
Doc2g	192.0642	5.409903	2.36E-25	double C2, gamma
Hmox1	122.9107	2.83062	3.56E-24	heme oxygenase 1
Th	309.759	3.658383	9.06E-24	tyrosine hydroxylase
Cplx1	17871.92	1.135458	2.80E-23	complexin 1

Mro	264.0795	1.457981	3.18E-21	maestro
Bid	149.8615	1.770451	5.44E-21	BH3 interacting domain death agonist
Sesn2	167.9794	1.898412	1.53E-19	sestrin 2
Sord	362.1303	1.20354	9.39E-19	sorbitol dehydrogenase
Sox4	507.6538	1.118669	1.59E-17	SRY (sex determining region Y)-box 4
Hmgb3	554.4211	-1.23645	3.46E-16	high mobility group box 3
Rpp25	435.3675	1.489302	9.23E-16	ribonuclease P/MRP 25 subunit
Nefm	3579.924	1.641708	1.03E-15	neurofilament, medium polypeptide
Gm20425	11.22653	-36.3037	1.03E-15	
Kcng2	299.8563	2.163473	3.14E-15	potassium voltage-gated channel, subfamily G, member 2
Pnmt	60.22828	2.935893	3.63E-15	phenylethanolamine-N-methyltransferase
Rec8	44.05254	3.16686	2.72E-14	REC8 meiotic recombination protein
Rasgef1c	588.922	-1.03329	6.31E-14	RasGEF domain family, member 1C
Cd248	65.80496	-1.75497	1.23E-13	CD248 antigen, endosialin
Ntng2	105.0564	1.629922	4.57E-13	netrin G2
Tagln	176.3247	-1.78349	1.74E-12	transgelin
Rgs5	1201.999	-1.19521	1.79E-12	regulator of G-protein signaling 5
Gpx3	355.4137	1.771209	1.83E-12	glutathione peroxidase 3
Gsto1	539.1698	0.736474	3.26E-12	glutathione S-transferase omega 1
Ajuba	80.95315	-1.89896	4.62E-12	ajuba LIM protein
Jcad	2159.144	0.717042	6.68E-12	junctional cadherin 5 associated
Rit1	843.9529	1.065904	7.26E-12	Ras-like without CAAX 1
Gpr137c	414.7728	1.007378	7.26E-12	G protein-coupled receptor 137C
Atp6ap1l	211.5039	1.480307	1.09E-11	ATPase, H+ transporting, lysosomal accessory protein 1-like
Fmnl1	898.1768	-1.08406	1.34E-11	formin-like 1
Plk5	301.295	-1.38809	2.56E-11	polo like kinase 5
Bcat1	1133.919	1.186163	4.25E-11	branched chain aminotransferase 1, cytosolic
Phf24	2193.987	-0.8222	4.25E-11	PHD finger protein 24
Rab3b	932.9128	1.418979	4.63E-11	RAB3B, member RAS oncogene family
Cpne9	611.6149	1.365175	5.82E-11	copine family member IX
Nanos1	711.1938	-0.70227	6.84E-11	nanos C2HC-type zinc finger 1
Pgam1	12553.18	0.504058	9.47E-11	phosphoglycerate mutase 1
Dgkb	1607.11	-0.77005	9.72E-11	diacylglycerol kinase, beta
Ctsl	763.1061	0.676712	1.03E-10	cathepsin L
Pou3f1	2497.546	-1.26845	1.71E-10	POU domain, class 3, transcription factor 1
Calcoco1	936.4629	-0.95744	1.80E-10	calcium binding and coiled coil domain 1
Cnn2	304.2092	-1.24656	1.83E-10	calponin 2
Trub2	637.9646	0.97572	2.31E-10	TruB pseudouridine (psi) synthase family member 2
Pik3r4	253.051	1.661843	2.62E-10	phosphoinositide-3-kinase regulatory subunit 4
Cgref1	325.7055	-1.07353	2.86E-10	cell growth regulator with EF hand domain 1
N4bp3	265.2371	-1.01958	3.89E-10	NEDD4 binding protein 3
Gpr149	60.37669	1.781138	5.74E-10	G protein-coupled receptor 149

Gatsl2	964.942	0.778803	6.46E-10	GATS protein-like 2
Peli2	186.5799	-1.09146	6.75E-10	pellino 2
Rgs10	462.5443	-1.00765	7.08E-10	regulator of G-protein signalling 10
Slc25a29	313.4452	0.871615	7.29E-10	solute carrier family 25 (mitochondrial carrier, palmitoylcarnitine transporter), member 29
Tbc1d10c	33.29931	1.837785	7.40E-10	TBC1 domain family, member 10c
Tbc1d10c	33.29931	1.837785	7.40E-10	TBC1 domain family, member 10c
Pdia6	1007.26	-0.64266	8.41E-10	protein disulfide isomerase associated 6
Igsf8	2172.207	-1.05271	1.05E-09	immunoglobulin superfamily, member 8
Pou3f3	398.9745	-0.74714	1.05E-09	POU domain, class 3, transcription factor 3
Fam189b	542.8823	0.952841	1.16E-09	family with sequence similarity 189, member B
N4bp2l1	263.2052	-0.8875	1.43E-09	NEDD4 binding protein 2-like 1
Lmo2	1270.917	1.053119	1.45E-09	LIM domain only 2
Ccdc3	166.1393	0.868781	2.14E-09	coiled-coil domain containing 3
Fam84b	180.9547	-1.35298	2.75E-09	family with sequence similarity 84, member B
Mark3	636.4543	0.537978	3.05E-09	MAP/microtubule affinity regulating kinase 3
Ctnna1	316.5771	-1.02519	3.58E-09	catenin (cadherin associated protein), alpha 1
Npy1r	111.331	1.25136	3.72E-09	neuropeptide Y receptor Y1
Ubald2	560.4934	-0.82473	4.29E-09	UBA-like domain containing 2
Foxg1	1518.42	-0.68451	5.48E-09	forkhead box G1
Man1a	228.609	-0.89622	5.74E-09	mannosidase 1, alpha
Lypd1	2122.538	1.013724	6.10E-09	Ly6/Plaur domain containing 1
Vat1l	779.834	-1.06295	6.69E-09	vesicle amine transport protein 1 like
Myl9	1106.53	-1.24579	6.91E-09	myosin, light polypeptide 9, regulatory
H2-DMa	305.8698	-1.09267	7.55E-09	histocompatibility 2, class II, locus DMa
Mt1	1554.346	1.580726	8.51E-09	metallothionein 1
Calb1	3710.885	-0.89519	1.01E-08	calbindin 1
Them6	969.8657	1.287995	1.08E-08	thioesterase superfamily member 6
Fabp3	1103.318	1.117502	1.12E-08	fatty acid binding protein 3, muscle and heart
Asb2	86.1011	1.733744	1.15E-08	ankyrin repeat and SOCS box-containing 2
Hs3st5	117.2552	-1.25039	1.23E-08	heparan sulfate (glucosamine) 3-O-sulfotransferase 5
Hhipl1	102.6553	1.821523	1.27E-08	hedgehog interacting protein-like 1
Fndc9	53.92401	-1.50366	1.27E-08	fibronectin type III domain containing 9
Tigar	227.033	0.739877	1.35E-08	Trp53 induced glycolysis repulatory phosphatase
Adssl1	372.7226	0.783184	1.48E-08	adenylosuccinate synthetase like 1
Scn1b	6935.225	0.952144	1.79E-08	sodium channel, voltage-gated, type I, beta
Aard	58.3624	2.691866	1.79E-08	alanine and arginine rich domain containing protein
Ubtf	1424.988	-0.61661	1.80E-08	upstream binding transcription factor, RNA polymerase I
Laptm4b	648.4036	0.75576	1.80E-08	lysosomal-associated protein transmembrane 4B
Zbtb8a	158.1698	-0.91276	2.05E-08	zinc finger and BTB domain containing 8a
Slc38a8	22.53743	2.322164	2.70E-08	solute carrier family 38, member 8
Drp2	271.5699	0.789437	2.89E-08	dystrophin related protein 2

Bcam	233.2626	-1.09492	3.41E-08	basal cell adhesion molecule
Rgs14	1135.259	-0.90785	3.41E-08	regulator of G-protein signaling 14
Zfp385c	25.99802	3.457338	3.57E-08	zinc finger protein 385C
Wsb2	7595.956	0.661195	3.81E-08	WD repeat and SOCS box-containing 2
Ctsa	887.5898	0.669208	3.92E-08	cathepsin A
Ing4	430.4327	-0.73028	4.28E-08	inhibitor of growth family, member 4
Serpine2	1178.122	-0.68972	7.59E-08	serine (or cysteine) peptidase inhibitor, clade E, member 2
Anks1b	6127.539	-0.59494	7.59E-08	ankyrin repeat and sterile alpha motif domain containing 1B
Ackr3	84.62362	-1.06887	8.04E-08	atypical chemokine receptor 3
Rab26	645.1823	0.813503	8.04E-08	RAB26, member RAS oncogene family
Acbd4	507.7012	0.760522	8.13E-08	acyl-Coenzyme A binding domain containing 4
Gba	173.8201	0.772672	8.34E-08	glucosidase, beta, acid
Scn9a	63.98129	1.331902	8.73E-08	sodium channel, voltage-gated, type IX, alpha
Cep41	50.55677	-1.88174	9.05E-08	centrosomal protein 41
Cyp11a1	77.09854	1.218818	9.42E-08	cytochrome P450, family 11, subfamily a, polypeptide 1
Pik3ip1	344.6606	0.667855	1.05E-07	phosphoinositide-3-kinase interacting protein 1
Marcks	3044.091	-0.76474	1.08E-07	myristoylated alanine rich protein kinase C substrate
Mfsd1	279.7646	1.054472	1.19E-07	major facilitator superfamily domain containing 1
Desi1	2209.579	0.59408	1.25E-07	desumoylating isopeptidase 1
Asb18	51.97419	1.03762	1.28E-07	ankyrin repeat and SOCS box-containing 18
D630023F18Rik	71.89705	1.293622	1.46E-07	RIKEN cDNA D630023F18 gene
Rcor2	145.9929	1.15166	1.58E-07	REST corepressor 2
Adarb1	1109.363	0.620382	2.51E-07	adenosine deaminase, RNA-specific, B1
Shisa8	64.13221	-1.7773	2.56E-07	shisa family member 8
Gpsm1	851.7943	-0.8343	2.87E-07	G-protein signalling modulator 1 (AGS3-like, C. elegans)
Wnk4	79.81482	2.029242	2.96E-07	WNK lysine deficient protein kinase 4
Bace2	40.55487	1.442996	2.97E-07	beta-site APP-cleaving enzyme 2
Acox1	1048.147	0.871194	3.11E-07	acyl-Coenzyme A oxidase 1, palmitoyl
Nts	536.8109	1.330977	3.20E-07	neurotensin
Fam213a	822.254	0.772275	3.20E-07	family with sequence similarity 213, member A
Lamp1	2456.811	0.421123	3.36E-07	lysosomal-associated membrane protein 1
Otud3	113.346	1.154788	3.38E-07	OTU domain containing 3
Egr2	59.84425	-2.11869	3.68E-07	early growth response 2
Foxo1	1054.426	-0.90772	3.85E-07	forkhead box O1
Trmt2b	135.2243	0.91804	4.18E-07	TRM2 tRNA methyltransferase 2B
Crabp1	114.8054	-1.38286	4.24E-07	cellular retinoic acid binding protein I
Sh3d21	22.18687	-1.87622	4.24E-07	SH3 domain containing 21
Cdkl2	433.0981	0.632926	4.45E-07	cyclin-dependent kinase-like 2 (CDC2-related kinase)
Neu1	751.892	0.600414	4.70E-07	neuraminidase 1

Scrt1	291.0592	0.823924	4.98E-07	scratch family zinc finger 1
Uhrf1bp1l	704.0319	0.728596	5.11E-07	UHRF1 (ICBP90) binding protein 1-like
Clmp	326.9315	1.12569	5.35E-07	CXADR-like membrane protein
AI413582	282.1439	1.314187	5.52E-07	expressed sequence AI413582
Srsf4	914.4433	-0.45521	5.70E-07	serine/arginine-rich splicing factor 4
Upk1b	17.82579	2.277751	6.13E-07	uroplakin 1B
Wdr45	467.2317	-0.51967	6.20E-07	WD repeat domain 45
Lrrtm2	420.5963	-0.94639	8.11E-07	leucine rich repeat transmembrane neuronal 2
Vcpkmt	72.51626	1.242291	8.76E-07	valosin containing protein lysine (K) methyltransferase
Scnn1b	6.157548	5.584918	8.82E-07	sodium channel, nonvoltage-gated 1 beta
1700007K 13Rik	40.93072	1.333507	9.86E-07	RIKEN cDNA 1700007K13 gene
Atg7	697.2116	-1.47437	9.94E-07	autophagy related 7
Racgap1	161.9093	0.931965	1.05E-06	Rac GTPase-activating protein 1
Notch3	74.49729	-1.07899	1.05E-06	notch 3
Ces1d	5.299943	7.079921	1.05E-06	carboxylesterase 1D
Inpp5f	1503.516	-0.68006	1.11E-06	inositol polyphosphate-5-phosphatase F
Rprml	1888.805	-0.98982	1.13E-06	reprimo-like
Rxfp1	47.87861	1.720117	1.28E-06	relaxin/insulin-like family peptide receptor 1
Ftl1	5364.642	0.854369	1.28E-06	ferritin light polypeptide 1
Anp32b	798.5038	-0.60919	1.34E-06	acidic (leucine-rich) nuclear phosphoprotein 32 family, member B
Ralyl	565.8782	1.001186	1.34E-06	RALY RNA binding protein-like
Habp4	5221.096	0.739692	1.52E-06	hyaluronic acid binding protein 4
Kcnmb1	15.75032	-2.06146	1.56E-06	potassium large conductance calcium-activated channel, subfamily M, beta member 1
Slc9a2	50.1199	-1.2831	1.62E-06	solute carrier family 9 (sodium/hydrogen exchanger), member 2
Renbp	47.02957	1.252854	1.68E-06	renin binding protein
Npl	187.5904	1.119505	1.79E-06	N-acetylneuraminate pyruvate lyase
Rnf144a	216.7498	-0.86982	1.83E-06	ring finger protein 144A
Mpi	629.0595	0.56697	1.83E-06	mannose phosphate isomerase
Slc7a6	58.7977	1.276129	1.88E-06	solute carrier family 7 (cationic amino acid transporter, y+ system), member 6
Bmp6	134.0006	-1.10433	1.88E-06	bone morphogenetic protein 6
Ano2	71.8552	-1.96275	2.01E-06	anoctamin 2
Tmem192	436.1875	0.81426	2.07E-06	transmembrane protein 192
Camk4	2115.052	-0.62595	2.08E-06	calcium/calmodulin-dependent protein kinase IV
Bsdc1	644.9979	-0.52739	2.17E-06	BSD domain containing 1
Mthfd2	138.754	0.816642	2.23E-06	methylenetetrahydrofolate dehydrogenase (NAD+ dependent), methenyltetrahydrofolate cyclohydrolase
4-Mar	194.9636	-0.9639	2.23E-06	membrane-associated ring finger (C3HC4) 4
Runx1t1	479.2474	-0.66749	2.25E-06	runt-related transcription factor 1; translocated to, 1 (cyclin D-related)
Etv5	849.3429	-0.6819	2.28E-06	ets variant 5

Rab23	221.239	0.890073	2.40E-06	RAB23, member RAS oncogene family
Pdia4	319.1599	-0.81074	2.54E-06	protein disulfide isomerase associated 4
Fam102a	1932.817	0.805381	2.74E-06	family with sequence similarity 102, member A
Mcoln1	617.9653	0.626419	2.74E-06	mucolipin 1
Fmod	66.11877	-1.81489	2.81E-06	fibromodulin
Mgarp	7.573216	2.885832	2.83E-06	mitochondria localized glutamic acid rich protein
Pcdhga12	103.3649	-1.41656	2.83E-06	protocadherin gamma subfamily A, 12
Dclk3	902.4122	-0.89563	3.13E-06	doublecortin-like kinase 3
Irf8	92.37394	-1.34284	3.22E-06	interferon regulatory factor 8
Stac2	248.9787	1.088787	3.49E-06	SH3 and cysteine rich domain 2
Impa1	1633.09	0.631481	3.52E-06	inositol (myo)-1(or 4)-monophosphatase 1
Rell2	1744.363	0.728267	3.54E-06	RELT-like 2
Pald1	89.85294	-1.11282	3.61E-06	phosphatase domain containing, paladin 1
Klhl4	108.7711	1.433812	3.61E-06	kelch-like 4
Selenop	1569.004	0.957319	3.68E-06	selenoprotein P
Pcnt	13.11786	27.66842	4.27E-06	pericentrin (kendrin)
Hnrnph3	488.5517	-0.66616	4.37E-06	heterogeneous nuclear ribonucleoprotein H3
Tnfaip8l1	125.3165	-0.77789	4.41E-06	tumor necrosis factor, alpha-induced protein 8-like 1
Prmt8	1177.475	0.529846	4.47E-06	protein arginine N-methyltransferase 8
Pqbp1	935.4485	-0.38299	4.47E-06	polyglutamine binding protein 1
S100a10	314.5994	-1.45936	4.85E-06	S100 calcium binding protein A10 (calpactin)
Tbc1d16	333.5312	0.768604	5.05E-06	TBC1 domain family, member 16
Ppp2r5b	1319.26	0.603603	5.08E-06	protein phosphatase 2, regulatory subunit B', beta
Flot2	1100.051	-0.50628	5.08E-06	flotillin 2
Tcta	609.0383	0.657169	5.27E-06	T cell leukemia translocation altered gene
Ddn	3064.995	0.79213	5.55E-06	dendrin
Ephx2	113.2565	0.896386	5.63E-06	epoxide hydrolase 2, cytoplasmic
Zfp512	354.5821	-0.70377	5.91E-06	zinc finger protein 512
Gnaz	1513.841	-0.55311	6.13E-06	guanine nucleotide binding protein, alpha z subunit
Ino80b	146.4127	-0.82207	6.13E-06	INO80 complex subunit B
Avpi1	1366.949	1.166749	6.17E-06	arginine vasopressin-induced 1
Ccdc177	317.9128	0.524513	6.26E-06	coiled-coil domain containing 177
Ppp3ca	17344.57	-0.5755	6.58E-06	protein phosphatase 3, catalytic subunit, alpha isoform
Rgs8	1447.037	-0.80535	6.58E-06	regulator of G-protein signaling 8
Tor1aip2	615.0501	0.544472	6.70E-06	torsin A interacting protein 2
Acvr1	171.8425	-0.71024	6.73E-06	activin A receptor, type 1
Pnmal1	1839.619	-0.47354	7.08E-06	PNMA-like 1
Ccdc102a	44.50607	-1.14348	7.25E-06	coiled-coil domain containing 102A
Dnase2a	74.45532	1.383269	7.36E-06	deoxyribonuclease II alpha
Slc6a8	460.7643	0.817417	7.83E-06	solute carrier family 6 (neurotransmitter transporter, creatine), member 8
Ptgs1	84.70283	1.489616	7.83E-06	prostaglandin-endoperoxide synthase 1

Rbms1	318.6203	-0.85472	8.81E-06	RNA binding motif, single stranded interacting protein 1
Asna1	1473.704	0.672576	8.81E-06	arsA arsenite transporter, ATP-binding, homolog 1 (bacterial)
Snw1	1103.279	-0.52589	9.32E-06	SNW domain containing 1
Fgf11	108.3356	-0.75588	9.32E-06	fibroblast growth factor 11
Mafa	50.6932	-1.57215	9.48E-06	v-maf musculoaponeurotic fibrosarcoma oncogene family, protein A (avian)
Efnb3	1473.089	-0.70569	9.63E-06	ephrin B3
Nfatc2	541.9172	0.976311	9.98E-06	nuclear factor of activated T cells, cytoplasmic, calcineurin dependent 2
Nos1ap	1387.344	0.612896	1.03E-05	nitric oxide synthase 1 (neuronal) adaptor protein
Brd3	748.2644	-0.52566	1.04E-05	bromodomain containing 3
Smpdl3b	52.69216	1.023481	1.09E-05	sphingomyelin phosphodiesterase, acid-like 3B
Pdk3	491.3204	0.631947	1.13E-05	pyruvate dehydrogenase kinase, isoenzyme 3
Fbln1	75.92044	1.28398	1.17E-05	fibulin 1
Inhba	108.6441	-1.09978	1.24E-05	inhibin beta-A
Slc35d3	69.94711	1.50876	1.29E-05	solute carrier family 35, member D3
Kcnd2	1188.77	-0.51639	1.39E-05	potassium voltage-gated channel, Shal-related family, member 2
Tac1	978.8547	1.011553	1.39E-05	tachykinin 1
Ackr1	133.5034	1.220152	1.41E-05	atypical chemokine receptor 1 (Duffy blood group)
Aqp6	2.723667	5.739646	1.44E-05	aquaporin 6
Me2	624.919	0.805477	1.51E-05	malic enzyme 2, NAD(+)-dependent, mitochondrial
Adam23	1163.699	0.6958	1.67E-05	a disintegrin and metallopeptidase domain 23
Ccdc112	132.2956	-0.98843	1.67E-05	coiled-coil domain containing 112
Hrk	601.1022	-0.66745	1.72E-05	harakiri, BCL2 interacting protein (contains only BH3 domain)
Scnn1a	31.61887	1.347093	1.73E-05	sodium channel, nonvoltage-gated 1 alpha
Fcho1	1011.344	-0.62028	1.73E-05	FCH domain only 1
Atp6v0d1	3210.409	0.516589	1.74E-05	ATPase, H+ transporting, lysosomal V0 subunit D1
Gli3	99.17216	-1.42067	1.75E-05	GLI-Kruppel family member GLI3
Rab30	334.2933	0.836207	1.76E-05	RAB30, member RAS oncogene family
Nrep	1196.834	-0.79285	1.77E-05	neuronal regeneration related protein
Pitpnm3	478.0847	-0.90364	1.79E-05	PITPNM family member 3
Kremen2	50.06059	-1.3691	1.80E-05	kringle containing transmembrane protein 2
Galk2	310.214	0.550761	1.81E-05	galactokinase 2
Kdf1	5.631977	3.421125	1.81E-05	keratinocyte differentiation factor 1
Glrx	797.6899	0.57626	1.92E-05	glutaredoxin
Tmem41a	623.2578	0.755813	1.94E-05	transmembrane protein 41a
Gabbr1	4551.945	-0.4742	2.06E-05	gamma-aminobutyric acid (GABA) B receptor, 1
Cited2	1105.517	0.481152	2.13E-05	Cbp/p300-interacting transactivator, with Glu/Asp-rich carboxy-terminal domain, 2
Igfbp2	487.6266	-1.0431	2.21E-05	insulin-like growth factor binding protein 2
Pno1	711.561	0.780595	2.29E-05	partner of NOB1 homolog

Plekha2	318.4242	0.766904	2.42E-05	pleckstrin homology domain-containing, family A (phosphoinositide binding specific) member 2
Nefl	6284.749	0.899038	2.42E-05	neurofilament, light polypeptide
Pax6	69.52042	1.2303	2.42E-05	paired box 6
Zfp830	197.937	-0.59594	2.42E-05	zinc finger protein 830
Epor	175.1958	-0.86711	2.45E-05	erythropoietin receptor
Cobl	459.7338	-0.52472	2.47E-05	cordon-bleu WH2 repeat
Syt16	783.6767	-0.44658	2.48E-05	synaptotagmin XVI
Fnbp1l	347.2423	-0.62742	2.75E-05	formin binding protein 1-like
Elmod1	3134.762	-0.6022	2.75E-05	ELMO/CED-12 domain containing 1
Fnip1	295.5852	0.939514	3.03E-05	folliculin interacting protein 1
Slc2a6	213.2852	0.74297	3.10E-05	solute carrier family 2 (facilitated glucose transporter), member 6
Smyd2	946.5307	0.550691	3.11E-05	SET and MYND domain containing 2
Nup93	215.4406	0.674084	3.11E-05	nucleoporin 93
Cpeb1	312.7859	0.936462	3.35E-05	cytoplasmic polyadenylation element binding protein 1
Gnpda1	377.1658	0.622441	3.45E-05	glucosamine-6-phosphate deaminase 1
Plcxd1	342.2605	-0.76735	3.45E-05	phosphatidylinositol-specific phospholipase C, X domain containing 1
Bnip3l	2562.638	-0.53009	3.58E-05	BCL2/adenovirus E1B interacting protein 3-like
Tuba8	138.1796	1.325779	3.83E-05	tubulin, alpha 8
Gcat	126.9953	0.992192	4.17E-05	glycine C-acetyltransferase (2-amino-3-ketobutyrate-coenzyme A ligase)
Slc38a5	22.4287	-2.06985	4.56E-05	solute carrier family 38, member 5
Kyat3	55.79559	1.074721	4.66E-05	kynurenine aminotransferase 3
Dtnb	1058.309	-0.52063	4.68E-05	dystrobrevin, beta
Pou3f4	161.7038	-0.77535	4.76E-05	POU domain, class 3, transcription factor 4
Lmo3	2349.842	-0.58011	4.77E-05	LIM domain only 3
Pld6	24.42295	-1.51654	4.95E-05	phospholipase D family, member 6
Ago4	137.3727	-0.93881	5.17E-05	argonaute RISC catalytic subunit 4
Fbxo44	2077.214	0.615519	5.99E-05	F-box protein 44
E2f1	231.9322	0.802264	6.16E-05	E2F transcription factor 1
Frat2	198.1565	-0.7417	6.47E-05	frequently rearranged in advanced T cell lymphomas 2
Wdr75	173.1432	0.854958	6.49E-05	WD repeat domain 75
6030408B16Rik	11.145	2.328853	6.91E-05	
Sebox	46.08841	-1.16408	7.08E-05	SEBOX homeobox
Aen	504.8093	0.515347	7.08E-05	apoptosis enhancing nuclease
Xbp1	1873.895	-0.53916	7.08E-05	X-box binding protein 1
Nell1	400.0141	-0.98406	7.26E-05	NEL-like 1
Sprn	1708.222	0.47975	7.72E-05	shadow of prion protein
Hscb	79.41937	0.956116	7.75E-05	HscB iron-sulfur cluster co-chaperone
Gpm6b	6145.471	-0.49968	7.84E-05	glycoprotein m6b
Arhgap6	168.9645	-0.59792	7.84E-05	Rho GTPase activating protein 6

Asb11	94.91078	0.795792	8.05E-05	ankyrin repeat and SOCS box-containing 11
Pyurf	388.1683	0.726879	8.09E-05	Pigy upstream reading frame
Plpp1	301.6052	0.494721	9.00E-05	phospholipid phosphatase 1
Rgs13	9.500097	2.199807	9.19E-05	regulator of G-protein signaling 13
Fam98c	787.8676	-0.68692	9.30E-05	family with sequence similarity 98, member C
Trnp1	6394.881	0.96338	9.30E-05	TMF1-regulated nuclear protein 1
Efna5	202.0466	0.672709	9.41E-05	ephrin A5
Cnnm1	809.3373	0.573731	9.44E-05	cyclin M1
Tdgf1	7.405551	3.402156	9.47E-05	teratocarcinoma-derived growth factor 1
Rbm24	435.2394	-0.55002	9.49E-05	RNA binding motif protein 24
Frat1	107.7094	-0.99808	9.49E-05	frequently rearranged in advanced T cell lymphomas
Naga	176.9452	0.681048	9.53E-05	N-acetyl galactosaminidase, alpha
F8a	566.182	-0.47639	9.59E-05	factor 8-associated gene A
Sowaha	2412.689	-0.53742	9.80E-05	sosondowah ankyrin repeat domain family member A
Hes6	244.0074	0.715188	9.97E-05	hairy and enhancer of split 6
Thsd7a	390.6409	-0.81674	9.97E-05	thrombospondin, type I, domain containing 7A
8430408G22Rik	71.06319	1.592556	0.000101	RIKEN cDNA 8430408G22 gene
Zfp467	386.4343	-0.89711	0.000101	zinc finger protein 467
Tmem132e	110.422	-1.12304	0.000105	transmembrane protein 132E
Plekha8	181.3636	0.907258	0.000106	pleckstrin homology domain containing, family A (phosphoinositide binding specific) member 8
Cpne2	341.5845	0.672832	0.000107	copine II
Gpr27	975.4058	-0.50528	0.000113	G protein-coupled receptor 27
Psip1	2892.123	-0.52756	0.000116	PC4 and SFRS1 interacting protein 1
Aldh1a2	166.1312	-1.26389	0.000117	aldehyde dehydrogenase family 1, subfamily A2
Gadd45g	590.9505	0.769566	0.00012	growth arrest and DNA-damage-inducible 45 gamma
Htr1b	244.9675	-0.93694	0.00012	5-hydroxytryptamine (serotonin) receptor 1B
Brinp3	176.4046	-0.80056	0.000121	bone morphogenetic protein/retinoic acid inducible neural specific 3
Acot13	808.5389	0.809818	0.000121	acyl-CoA thioesterase 13
Gm34302	7.988706	2.316972	0.000126	
Coro6	103.1481	0.996971	0.000127	coronin 6
Tbx2	177.6438	-0.84157	0.000128	T-box 2
Abhd12	4089.861	0.440237	0.000128	abhydrolase domain containing 12
Ina	4270.174	0.423899	0.000134	internexin neuronal intermediate filament protein, alpha
Mgst3	1500.952	0.914937	0.000135	microsomal glutathione S-transferase 3
Senp2	771.6843	0.534625	0.000142	SUMO/sentrin specific peptidase 2
Mei4	39.99031	-1.53238	0.000145	meiotic double-stranded break formation protein 4
Egr1	3889.163	-0.91302	0.000146	early growth response 1
Gnpda2	381.7016	-0.58428	0.00015	glucosamine-6-phosphate deaminase 2

Dmd	200.9682	-1.0919	0.00015	dystrophin, muscular dystrophy
Syf2	590.9062	-0.5369	0.000152	SYF2 homolog, RNA splicing factor (S. cerevisiae)
Wnt7a	97.56047	-0.94237	0.000152	wingless-type MMTV integration site family, member 7A
Hsp90b1	1820.293	-0.56216	0.000154	heat shock protein 90, beta (Grp94), member 1
Cdk16	4240.141	0.48947	0.000157	cyclin-dependent kinase 16
Gm20498	277.9916	0.772081	0.000157	predicted gene 20498
Zcchc14	666.2353	-0.44087	0.000157	zinc finger, CCHC domain containing 14
Camk1g	375.5868	-0.97566	0.000161	calcium/calmodulin-dependent protein kinase I gamma
Flcn	561.5563	0.588026	0.000166	folliculin
Nr4a1	1243.55	-1.71428	0.000169	nuclear receptor subfamily 4, group A, member 1
Spry4	126.6986	-0.92239	0.000171	sprouty RTK signaling antagonist 4
Dffa	762.0903	0.785938	0.000171	DNA fragmentation factor, alpha subunit
Cdo1	497.9671	-0.40068	0.000173	cysteine dioxygenase 1, cytosolic
Rhob	3240.234	0.384126	0.000173	ras homolog family member B
Slitrk1	200.7166	0.82397	0.000173	SLIT and NTRK-like family, member 1
Atp6v1b2	7047.872	0.493908	0.000173	ATPase, H+ transporting, lysosomal V1 subunit B2
Strip2	471.9255	0.709902	0.000173	striatin interacting protein 2
Memo1	226.9475	0.558251	0.000173	mediator of cell motility 1
Gm14322	50.07995	1.007855	0.000173	predicted gene 14322
Dpp7	117.3928	0.931405	0.000181	dipeptidylpeptidase 7
Scrt2	707.0277	0.72475	0.000189	scratch family zinc finger 2
Ctcf	785.6097	-0.58403	0.000191	CCCTC-binding factor
Inmt	62.79182	-1.76244	0.000192	indolethylamine N-methyltransferase
Kptn	489.9	-0.49531	0.000192	kaptin
Cd74	269.1042	-1.58837	0.000192	CD74 antigen (invariant polypeptide of major histocompatibility complex, class II antigen-associated)
Set	2546.626	-0.36339	0.000192	SET nuclear oncogene
Sgms1	305.4367	-0.66619	0.000192	sphingomyelin synthase 1
Stpg1	44.04066	1.408276	0.000195	sperm tail PG rich repeat containing 1
Stc1	86.91838	1.093453	0.0002	stanniocalcin 1
Rps6ka2	637.9068	0.558667	0.0002	ribosomal protein S6 kinase, polypeptide 2
Foxd1	173.078	-0.88071	0.0002	forkhead box D1
Atpif1	2627.517	1.074802	0.000202	ATPase inhibitory factor 1
Ksr1	141.3773	1.02209	0.000203	kinase suppressor of ras 1
Pdcd11	54.25889	1.147694	0.000203	programmed cell death 11
Kalrn	3038.364	-0.94535	0.000209	kalirin, RhoGEF kinase
Srgap1	356.0664	-0.60131	0.000216	SLIT-ROBO Rho GTPase activating protein 1
Man1c1	370.5785	0.682744	0.000218	mannosidase, alpha, class 1C, member 1
Mfap1b	649.9858	-0.61418	0.000227	microfibrillar-associated protein 1B
Gad2	2591.913	0.699818	0.00023	glutamic acid decarboxylase 2
Oma1	81.50659	0.8693	0.000231	OMA1 zinc metallopeptidase

Lamp2	340.2076	0.793746	0.000234	lysosomal-associated membrane protein 2
Bnip3	3012.342	0.58183	0.000238	BCL2/adenovirus E1B interacting protein 3
Mtch2	795.5016	0.444183	0.000243	mitochondrial carrier 2
Csdc2	1743.143	0.561753	0.000246	cold shock domain containing C2, RNA binding
Ccbe1	22.22496	1.739621	0.000246	collagen and calcium binding EGF domains 1
Sppl2a	228.5142	-0.75355	0.000246	signal peptide peptidase like 2A
Acp7	7.708307	3.269147	0.000253	acid phosphatase 7, tartrate resistant
Kif17	355.9511	-0.63765	0.000256	kinesin family member 17
Zeb1	312.9697	-0.77479	0.000257	zinc finger E-box binding homeobox 1
Gde1	3381.032	0.429238	0.000257	glycerophosphodiester phosphodiesterase 1
Tigd2	235.6421	0.533433	0.000257	tigger transposable element derived 2
Doc2b	200.2213	-0.72937	0.000262	double C2, beta
Kars	964.1805	-0.29062	0.00027	lysyl-tRNA synthetase
Deptor	306.1405	-0.68008	0.000275	DEP domain containing MTOR-interacting protein
Slc30a10	172.2661	0.667657	0.000281	solute carrier family 30, member 10
Col6a2	54.74498	-1.26691	0.000294	collagen, type VI, alpha 2
Zfp39	126.2396	-0.70909	0.000298	zinc finger protein 39
Zfp882	82.8571	-1.11272	0.000298	zinc finger protein 882
Wdyhv1	118.4331	-0.64844	0.000301	WDYHV motif containing 1
Galnt18	398.1015	-0.54017	0.000306	polypeptide N-acetylgalactosaminyltransferase 18
Setd6	180.6157	-0.7254	0.000319	SET domain containing 6
Syde1	63.8113	-0.88709	0.000319	synapse defective 1, Rho GTPase, homolog 1 (C. elegans)
Sfrp2	41.47406	1.474846	0.000321	secreted frizzled-related protein 2
Arg2	193.2606	0.913869	0.000326	arginase type II
Kctd6	488.6866	0.551882	0.000326	potassium channel tetramerisation domain containing 6
Galc	78.98199	0.911624	0.000341	galactosylceramidase
Slc27a4	803.1528	0.454985	0.000341	solute carrier family 27 (fatty acid transporter), member 4
Sgce	229.9692	-0.52629	0.000347	sarcoglycan, epsilon
Plscr2	27.01816	-1.78186	0.000355	phospholipid scramblase 2
Gstm7	299.0522	0.738378	0.000359	glutathione S-transferase, mu 7
Gm28437	51.44647	6.246651	0.000359	
Atp2a3	117.7852	-1.17414	0.00036	ATPase, Ca++ transporting, ubiquitous
Snai2	12.15298	-1.62415	0.000362	snail family zinc finger 2
Rnase4	64.51712	1.041514	0.000381	ribonuclease, RNase A family 4
St6galnac5	655.6737	-0.59803	0.000381	ST6 (alpha-N-acetyl-neuraminyl-2,3-beta-galactosyl-1,3)-N-acetylgalactosaminide alpha-2,6-sialyltransferase 5
Gpr22	274.7047	0.820082	0.000381	G protein-coupled receptor 22
Gdf15	3.949163	3.459519	0.000386	growth differentiation factor 15
B630019K06Rik	761.2842	0.409228	0.000387	
Vstm5	176.2761	0.491978	0.000387	V-set and transmembrane domain containing 5

Tom1	500.0384	0.600177	0.000387	target of myb1 trafficking protein
Prkcz	4741.583	0.501984	0.000392	protein kinase C, zeta
Mpc1	5267.739	0.698198	0.000405	mitochondrial pyruvate carrier 1
Id4	2862.055	-0.53184	0.00042	inhibitor of DNA binding 4
Wnt2	117.9415	-0.9038	0.000432	wingless-type MMTV integration site family, member 2
Art3	85.14047	-0.95075	0.000439	ADP-ribosyltransferase 3
Cerk	663.0131	0.563327	0.000447	ceramide kinase
Heca	300.5826	-0.66825	0.000452	hdc homolog, cell cycle regulator
Dact1	71.4644	-1.0984	0.00046	dishevelled-binding antagonist of beta-catenin 1
Rnf217	189.4493	0.500598	0.00047	ring finger protein 217
Paqr3	95.55513	0.654701	0.000476	progestin and adipoQ receptor family member III
Olfml3	88.8003	-1.04965	0.000483	olfactomedin-like 3
Elmod3	329.5455	0.458484	0.000483	ELMO/CED-12 domain containing 3
Tbl1x	649.3324	-0.37255	0.000485	transducin (beta)-like 1 X-linked
Crhr1	160.7433	0.703305	0.000492	corticotropin releasing hormone receptor 1
Mfsd11	313.4049	0.675584	0.000492	major facilitator superfamily domain containing 11
Fxn	124.0851	0.803959	0.000495	frataxin
Rbp4	440.6265	-0.69554	0.000503	retinol binding protein 4, plasma
A430033K04Rik	150.1348	-0.73886	0.000526	RIKEN cDNA A430033K04 gene
Sirt7	417.3993	0.471335	0.000527	sirtuin 7
Fabp4	7.953882	2.561149	0.00053	fatty acid binding protein 4, adipocyte
Mat2b	2691.195	-0.393	0.00053	methionine adenosyltransferase II, beta
Pex5l	1183.374	0.625024	0.00053	peroxisomal biogenesis factor 5-like
Armcx6	74.90325	0.894272	0.000536	armadillo repeat containing, X-linked 6
Epha8	101.2758	0.796725	0.000541	Eph receptor A8
Cryzl2	48.15159	0.977917	0.000555	crystallin zeta like 2
Tmem109	527.9591	-0.54569	0.000565	transmembrane protein 109
Gpr137	832.3107	0.548047	0.000569	G protein-coupled receptor 137
Stk38l	294.6031	0.465846	0.000569	serine/threonine kinase 38 like
Cap2	2328.797	-0.574	0.00057	CAP, adenylate cyclase-associated protein, 2 (yeast)
Arhgap15	174.4299	0.854993	0.000577	Rho GTPase activating protein 15
Wwc2	531.1845	-0.44421	0.00058	WW, C2 and coiled-coil domain containing 2
Cks1b	52.15928	0.849018	0.000585	CDC28 protein kinase 1b
Jade2	182.5366	-0.51886	0.000596	jade family PHD finger 2
Hspa5	1515.77	-0.63968	0.00061	heat shock protein 5
Awat2	8.326612	2.298153	0.00061	acyl-CoA wax alcohol acyltransferase 2
Asic2	694.4559	0.533112	0.000629	acid-sensing (proton-gated) ion channel 2
Dbndd1	363.2181	-0.56872	0.000645	dysbindin (dystrobrevin binding protein 1) domain containing 1
Wdr92	135.2319	-0.59815	0.000656	WD repeat domain 92
Hint3	79.46791	0.778688	0.000665	histidine triad nucleotide binding protein 3
Bgn	97.79386	-0.97261	0.000667	biglycan

Chrm1	1587.284	-0.64829	0.000668	cholinergic receptor, muscarinic 1, CNS
Vpreb3	6.232534	2.537358	0.000669	pre-B lymphocyte gene 3
Gle1	719.0754	-0.29899	0.000669	GLE1 RNA export mediator (yeast)
Pgk1	3978.453	0.381701	0.000673	phosphoglycerate kinase 1
Tspyl2	703.9607	-0.45033	0.000675	TSPY-like 2
Mme	176.7548	1.005688	0.000693	membrane metallo endopeptidase
Sh3yl1	198.0366	0.548249	0.0007	Sh3 domain YSC-like 1
Top1mt	234.3976	0.519159	0.000701	DNA topoisomerase 1, mitochondrial
Oprk1	92.45872	-0.89087	0.000701	opioid receptor, kappa 1
Tram1	382.5628	0.592432	0.000701	translocating chain-associating membrane protein 1
Gm3883	291.423	-0.67506	0.000701	
Aox3	12.01532	-2.81713	0.000703	aldehyde oxidase 3
Cryz	210.8287	0.682831	0.00072	crystallin, zeta
Slco1a4	74.66027	-1.33739	0.000727	solute carrier organic anion transporter family, member 1a4
H2-Aa	60.00985	-1.76385	0.000727	histocompatibility 2, class II antigen A, alpha
Dexi	1056.986	0.672043	0.000727	dexamethasone-induced transcript
Hs3st2	406.2175	0.69296	0.000727	heparan sulfate (glucosamine) 3-O-sulfotransferase 2
Gap43	4876.882	-0.52249	0.000727	growth associated protein 43
Oat	946.1811	-0.5852	0.000741	ornithine aminotransferase
Nceh1	1122.194	0.558662	0.000746	neutral cholesterol ester hydrolase 1
Sec14l3	19.47669	-1.7618	0.000753	SEC14-like lipid binding 3
Car7	276.2558	0.617332	0.000755	carbonic anhydrase 7
Acat2	699.3796	0.359771	0.000767	acetyl-Coenzyme A acetyltransferase 2
Fam126a	121.4488	1.141567	0.000767	family with sequence similarity 126, member A
Atp6v1e1	8542.676	0.486711	0.000788	ATPase, H+ transporting, lysosomal V1 subunit E1
Tstd3	320.8944	0.684309	0.000788	thiosulfate sulfurtransferase (rhodanese)-like domain containing 3
Pgk1-rs7	32.86203	-21.4562	0.000793	
Acad8	353.4125	0.638991	0.000818	acyl-Coenzyme A dehydrogenase family, member 8
Uap1l1	358.6966	0.900852	0.000823	UDP-N-acteylglucosamine pyrophosphorylase 1-like 1
Dusp6	658.9681	-0.68295	0.000824	dual specificity phosphatase 6
Lats2	209.6982	-0.84612	0.000827	large tumor suppressor 2
Cpn1	14.22841	1.462049	0.000827	carboxypeptidase N, polypeptide 1
Syn2	1493.939	0.718383	0.000832	synapsin II
Yars	1516.057	0.557852	0.000832	tyrosyl-tRNA synthetase
Cdr2l	426.5881	0.525489	0.000832	cerebellar degeneration-related protein 2-like
Spint1	53.25541	-1.18666	0.000833	serine protease inhibitor, Kunitz type 1
Cmc2	226.8722	0.959607	0.000834	COX assembly mitochondrial protein 2
Col1a1	33.32693	-1.24691	0.000836	collagen, type I, alpha 1
Synpr	1724.075	-0.73478	0.000845	synaptoporin
Serpina9	283.5864	-1.23224	0.000871	serine (or cysteine) peptidase inhibitor, clade A (alpha-1 antiproteinase, antitrypsin), member 9

Psph	352.9308	0.515851	0.000876	phosphoserine phosphatase
Gch1	38.13047	-0.98392	0.000876	GTP cyclohydrolase 1
Fam20c	1003.558	0.545603	0.000884	family with sequence similarity 20, member C
Degs1	1093.46	0.523959	0.000885	delta(4)-desaturase, sphingolipid 1
Pdcd1lg2	2.284882	5.444024	0.000886	programmed cell death 1 ligand 2
Bcor	73.30459	-0.84801	0.000892	BCL6 interacting corepressor
Lztr1	1134.12	0.413903	0.000928	leucine-zipper-like transcriptional regulator, 1
Cdr2	181.0144	-0.52002	0.000928	cerebellar degeneration-related 2
Arl6ip1	3939.783	0.29798	0.000957	ADP-ribosylation factor-like 6 interacting protein 1
Jsrp1	127.6877	1.178285	0.000984	junctional sarcoplasmic reticulum protein 1
Tmem186	255.8868	-0.46003	0.000984	transmembrane protein 186
Orai1	141.7537	0.59178	0.001	ORAI calcium release-activated calcium modulator 1
Xpnpep3	144.1519	-0.68986	0.001002	X-prolyl aminopeptidase 3, mitochondrial
Zfp180	535.1347	-0.49976	0.001004	zinc finger protein 180
Fblim1	92.33548	-1.08251	0.001018	filamin binding LIM protein 1
Zfp84	107.5001	-0.68255	0.001018	zinc finger protein 84
Slc36a1	128.397	0.721068	0.00102	solute carrier family 36 (proton/amino acid symporter), member 1
Pcgf6	139.7575	0.611132	0.001028	polycomb group ring finger 6
Tpi1	12907.97	0.420144	0.00103	triosephosphate isomerase 1
Gm16286	2860.302	0.482617	0.00103	thioredoxin-like 4A
Trmo	57.88119	-0.75918	0.00103	tRNA methyltransferase O
Arhgap44	1360.323	0.450343	0.00103	Rho GTPase activating protein 44
Insm1	76.81378	-0.92773	0.001039	insulinoma-associated 1
Tnfrsf4	8.999463	1.961211	0.001048	tumor necrosis factor receptor superfamily, member 4
Cd164l2	48.63352	1.220134	0.001049	CD164 sialomucin-like 2
Foxn3	588.6633	0.736295	0.001049	forkhead box N3
Bicral	275.0901	-0.6029	0.001053	BRD4 interacting chromatin remodeling complex associated protein like
Arhgef6	61.64734	1.050731	0.001057	Rac/Cdc42 guanine nucleotide exchange factor (GEF) 6
Afp	7.556599	2.214894	0.001064	alpha fetoprotein
Hrh2	13.44083	1.419402	0.001065	histamine receptor H2
Ubiad1	120.2227	-0.63367	0.00108	UbiA prenyltransferase domain containing 1
Coch	748.9811	0.773073	0.001081	cochlin
Asb10	4.61541	2.828479	0.001081	ankyrin repeat and SOCS box-containing 10
Pir	89.39489	-0.64793	0.001089	pirin
Cyth1	888.7886	0.373054	0.0011	cytohesin 1
Gins2	101.8408	0.866844	0.0011	GINS complex subunit 2 (Psf2 homolog)
Shf	502.7222	-0.54308	0.001113	Src homology 2 domain containing F
Cmbl	81.97143	-0.78051	0.001135	carboxymethylenebutenolidase-like (Pseudomonas)
Cuta	953.8362	0.851642	0.001142	cutA divalent cation tolerance homolog
Fgf17	5.285097	-3.59463	0.001162	fibroblast growth factor 17

Hmgxb4	98.06484	-1.10017	0.001162	HMG box domain containing 4
Phlda1	619.192	-0.53589	0.001176	pleckstrin homology like domain, family A, member 1
Ypel2	786.7753	0.549304	0.001188	yippee like 2
Sesn1	661.0078	0.570116	0.001196	sestrin 1
Nkd1	222.2403	-0.54868	0.001225	naked cuticle 1
Cdkl4	162.0136	-0.65076	0.00123	cyclin-dependent kinase-like 4
Rsph9	127.3304	-0.71474	0.001249	radial spoke head 9 homolog (Chlamydomonas)
Zwint	14564.71	-0.32095	0.001265	ZW10 interactor
Nagk	732.0459	0.595342	0.001283	N-acetylglucosamine kinase
Tbrg4	143.2793	0.770584	0.001301	transforming growth factor beta regulated gene 4
Pkn1	282.8121	-0.75863	0.001306	protein kinase N1
Gm15645	22.68332	1.023374	0.001314	
Rit1	3354.654	-0.55005	0.001333	B cell leukemia/lymphoma 11B
Atg14	242.9316	-0.58101	0.001348	autophagy related 14
Rexo2	1100.837	0.603833	0.001348	RNA exonuclease 2
Tspan7	13493.45	-0.36366	0.001362	tetraspanin 7
Smarcc2	1251.063	-0.58108	0.001417	SWI/SNF related, matrix associated, actin dependent regulator of chromatin, subfamily c, member 2
Rfx1	124.4263	-0.56571	0.001418	regulatory factor X, 1 (influences HLA class II expression)
Hspb1	183.163	-1.14357	0.001418	heat shock protein 1
Vegfa	336.1141	0.675369	0.001433	vascular endothelial growth factor A
Rbm22	289.665	-0.44664	0.001445	RNA binding motif protein 22
Phf1	583.1131	-0.67709	0.001449	PHD finger protein 1
6430571L13Rik	123.3303	0.674061	0.001458	RIKEN cDNA 6430571L13 gene
Myh7b	147.2412	-0.92686	0.001458	myosin, heavy chain 7B, cardiac muscle, beta
Ppp1r13l	31.94016	1.543651	0.001466	protein phosphatase 1, regulatory (inhibitor) subunit 13 like
Tpm3	2956.328	-0.2676	0.001483	tropomyosin 3, gamma
Slc25a33	1256.603	0.510285	0.001541	solute carrier family 25, member 33
Myo3b	36.07071	-1.12923	0.001544	myosin IIIB
Myl12a	940.5391	-0.62246	0.001557	myosin, light chain 12A, regulatory, non-sarcomeric
Ralgapa2	67.86422	1.166155	0.001557	Ral GTPase activating protein, alpha subunit 2 (catalytic)
Rgl2	207.5356	0.674032	0.001557	ral guanine nucleotide dissociation stimulator-like 2
Gm5619	33.91927	-7.77906	0.001557	
Dnaic1	24.79464	1.399914	0.001579	dynein, axonemal, intermediate chain 1
Zfp277	300.0362	-0.55202	0.001583	zinc finger protein 277
Alox12	8.449666	-1.62883	0.001585	arachidonate 12-lipoxygenase
Mvd	337.4736	0.498456	0.001585	mevalonate (diphospho) decarboxylase
Anp32e	943.3629	-0.5405	0.001585	acidic (leucine-rich) nuclear phosphoprotein 32 family, member E
Limd1	188.556	-0.57504	0.001585	LIM domains containing 1

Kctd8	255.0256	-0.52797	0.001585	potassium channel tetramerisation domain containing 8
Sp4	132.1883	-0.86008	0.001586	trans-acting transcription factor 4
Dhrs11	50.59726	0.92477	0.001608	dehydrogenase/reductase (SDR family) member 11
Tcf7l1	82.75608	-0.84261	0.001608	transcription factor 7 like 1 (T cell specific, HMG box)
Mcam	104.5653	-0.9427	0.001615	melanoma cell adhesion molecule
Ccno	60.83028	-1.04271	0.001615	cyclin O
Wdr12	529.7504	0.430517	0.001691	WD repeat domain 12
Klhdc8a	465.701	0.604623	0.001716	kelch domain containing 8A
Pcp4l1	15614.21	0.709303	0.001725	Purkinje cell protein 4-like 1
Foxc1	243.3965	-0.93421	0.001726	forkhead box C1
Rps6kb2	86.44651	0.704081	0.001739	ribosomal protein S6 kinase, polypeptide 2
Rps6kb2	86.44651	0.704081	0.001739	ribosomal protein S6 kinase, polypeptide 2
Nova2	426.8271	-0.48611	0.001745	neuro-oncological ventral antigen 2
Clec2l	1216.666	0.525	0.001745	C-type lectin domain family 2, member L
Rtn4rl2	320.1731	0.794035	0.001779	reticulon 4 receptor-like 2
Rbm20	25.90095	1.569331	0.001786	RNA binding motif protein 20
Cks2	35.35777	0.985645	0.001799	CDC28 protein kinase regulatory subunit 2
Rnf24	210.5014	-0.61036	0.00181	ring finger protein 24
Cdc27	286.8543	0.652452	0.001814	cell division cycle 27
Zfp689	141.7215	-0.59311	0.001814	zinc finger protein 689
Inafm1	370.0238	-0.52223	0.001814	InaF motif containing 1
Mep1a	5.592436	5.815581	0.001822	meprin 1 alpha
Rhbdl1	673.096	-0.48552	0.001828	rhomboid like 1
Cygb	1175.523	0.464706	0.001856	cytoglobin
Rad9a	128.33	0.532538	0.001856	RAD9 checkpoint clamp component A
Rad9a	128.33	0.532538	0.001856	RAD9 checkpoint clamp component A
Zik1	177.9746	-0.56172	0.001856	zinc finger protein interacting with K protein 1
Spred3	149.7073	-0.59343	0.001857	sprouty-related, EVH1 domain containing 3
Cbx4	1195.108	-0.67977	0.001895	chromobox 4
Thsd7b	35.97211	1.632971	0.001895	thrombospondin, type I, domain containing 7B
Ier5	1189.354	-0.55977	0.001917	immediate early response 5
Thrb	341.2039	-0.55571	0.001956	thyroid hormone receptor beta
Clk2	228.8366	-0.45176	0.001987	CDC-like kinase 2
Rasl10a	503.2432	-0.57879	0.00209	RAS-like, family 10, member A
Rrad	55.9287	-1.05526	0.00209	Ras-related associated with diabetes
Nit2	148.6314	-0.56289	0.002143	nitrilase family, member 2
Smad3	408.4607	-0.52396	0.00215	SMAD family member 3
Pla2g2f	4.860104	3.986491	0.002247	phospholipase A2, group IIF
Col23a1	57.523	1.176796	0.002248	collagen, type XXIII, alpha 1
Ddit4	569.7667	0.926139	0.002279	DNA-damage-inducible transcript 4
Prok2	11.74563	1.418669	0.002279	prokineticin 2
Chkb	214.7332	0.497699	0.002287	choline kinase beta

Idnk	292.7367	0.700213	0.002297	idnK gluconokinase homolog (E. coli)
Ffar3	7.918962	-2.19855	0.00233	free fatty acid receptor 3
R3hdm2	1093.354	-0.39322	0.002368	R3H domain containing 2
Rassf1	343.1494	-0.41706	0.002401	Ras association (RalGDS/AF-6) domain family member 1
Relt	187.9914	0.643071	0.002415	RELT tumor necrosis factor receptor
Pik3r3	215.5459	0.699394	0.002418	phosphoinositide-3-kinase regulatory subunit 3
Polg	457.1175	0.328849	0.002448	polymerase (DNA directed), gamma
Mafb	236.9657	0.628692	0.002469	v-maf musculoaponeurotic fibrosarcoma oncogene family, protein B (avian)
Wdr48	506.2401	-0.40719	0.002499	WD repeat domain 48
Csgalnact 1	174.3391	0.59981	0.002499	chondroitin sulfate N-acetylgalactosaminyltransferase 1
1500009L 16Rik	283.7952	-0.53221	0.002499	RIKEN cDNA 1500009L16 gene
Abcc9	27.95451	-1.06932	0.002511	ATP-binding cassette, sub-family C (CFTR/MRP), member 9
Prdx1	2694.301	-0.4069	0.00252	peroxiredoxin 1
6820408C 15Rik	40.99341	1.034132	0.00252	RIKEN cDNA 6820408C15 gene
Zcchc3	225.0448	-0.46112	0.00252	zinc finger, CCHC domain containing 3
F930015N 05Rik	13.57625	1.425923	0.00252	
Plbd2	649.2409	0.515515	0.002531	phospholipase B domain containing 2
Perp	86.11488	-0.82897	0.002549	PERP, TP53 apoptosis effector
Tmem144	62.81829	0.92683	0.002562	transmembrane protein 144
Zfp1	151.0693	-0.79639	0.002585	zinc finger protein 1
Ifi27l2b	4.235719	-2.7897	0.002588	interferon, alpha-inducible protein 27 like 2B
Pex6	956.5079	-0.51298	0.00259	peroxisomal biogenesis factor 6
Hnrnpl	2123.131	-0.36134	0.002602	heterogeneous nuclear ribonucleoprotein L
Asic4	242.9371	-0.7295	0.00262	acid-sensing (proton-gated) ion channel family member 4
1500009C 09Rik	688.5803	0.76573	0.002621	
Proser2	70.01987	-0.96391	0.002633	proline and serine rich 2
Prkag2	1015.212	0.510971	0.002647	protein kinase, AMP-activated, gamma 2 non-catalytic subunit
Gtpbp6	516.2328	0.641961	0.002653	GTP binding protein 6 (putative)
Lrrc55	115.272	0.789932	0.002653	leucine rich repeat containing 55
Efnb2	362.9854	-0.46704	0.002692	ephrin B2
Ncs1	3911.569	0.384042	0.002697	neuronal calcium sensor 1
Klhl3	222.3956	0.419342	0.002712	kelch-like 3
Pik3r5	21.30038	-1.26708	0.002712	phosphoinositide-3-kinase regulatory subunit 5
Cdkn2c	46.55685	-0.90259	0.002712	cyclin-dependent kinase inhibitor 2C (p18, inhibits CDK4)
Bod1l	11.35508	19.66848	0.002712	biorientation of chromosomes in cell division 1-like
Grm5	922.4286	-0.54784	0.002726	glutamate receptor, metabotropic 5

Mif	4262.843	0.883406	0.00274	macrophage migration inhibitory factor (glycosylation-inhibiting factor)
Hnrnpr	930.1281	-0.42933	0.002755	heterogeneous nuclear ribonucleoprotein R
Gucy2g	53.2833	0.93882	0.002768	guanylate cyclase 2g
Lypd6	149.1624	0.985016	0.002778	LY6/PLAUR domain containing 6
Hdac3	938.5603	0.328296	0.002814	histone deacetylase 3
Pcnx4	276.3974	0.468052	0.002831	pecanex homolog 4
Cdk19	360.9547	-0.94355	0.002831	cyclin-dependent kinase 19
Nudt5	322.581	0.519965	0.002854	nudix (nucleoside diphosphate linked moiety X)-type motif 5
Pusl1	287.7143	0.56524	0.002854	pseudouridylate synthase-like 1
Spred2	643.9386	-0.58372	0.002858	sprouty-related, EVH1 domain containing 2
Slc16a6	130.1012	0.726089	0.002901	solute carrier family 16 (monocarboxylic acid transporters), member 6
Amotl2	170.711	-0.95641	0.002937	angiomotin-like 2
Zar1l	11.58727	1.614429	0.002945	zygote arrest 1-like
Hes1	169.2349	-0.60437	0.002983	hes family bHLH transcription factor 1
Pip4k2c	924.4908	0.347188	0.002983	phosphatidylinositol-5-phosphate 4-kinase, type II, gamma
Fuca1	379.2382	0.583813	0.002983	fucosidase, alpha-L- 1, tissue
Hnrnph1	951.3458	-0.59427	0.002998	heterogeneous nuclear ribonucleoprotein H1
Pou2f2	59.11242	-1.10351	0.003005	POU domain, class 2, transcription factor 2
Igfbp4	515.6123	-0.70288	0.003005	insulin-like growth factor binding protein 4
Slc25a39	1830.11	0.560393	0.003022	solute carrier family 25, member 39
Klf5	212.1182	-0.6195	0.003043	Kruppel-like factor 5
Gm10925	202.3766	3.770042	0.003054	
Rfx5	172.5286	0.625179	0.003073	regulatory factor X, 5 (influences HLA class II expression)
Panx2	386.6542	0.635256	0.003073	pannexin 2
Hmcn2	14.13038	-1.8895	0.003083	hemicentin 2
Mtap	198.7555	-0.51091	0.003083	methylthioadenosine phosphorylase
Twf2	625.7442	-0.39239	0.003111	twinfilin actin binding protein 2
Itgb4	96.70283	1.357923	0.003116	integrin beta 4
Ptpro	112.0232	0.940378	0.003116	protein tyrosine phosphatase, receptor type, O
Tnip2	131.5799	-0.54807	0.003128	TNFAIP3 interacting protein 2
Cyp2a5	13.3858	-1.68647	0.003167	cytochrome P450, family 2, subfamily a, polypeptide 5
Ing5	176.9882	-0.57515	0.003212	inhibitor of growth family, member 5
Sult5a1	9.565368	2.134325	0.003218	sulfotransferase family 5A, member 1
Zdhhc8	429.4611	0.461843	0.003247	zinc finger, DHHC domain containing 8
Dact3	1913.612	0.451731	0.003262	dishevelled-binding antagonist of beta-catenin 3
Tlcd2	90.05044	0.625313	0.003263	TLC domain containing 2
Pbx1	901.6483	-0.38707	0.003281	pre B cell leukemia homeobox 1
Ppp1r17	9.312219	2.040398	0.00329	protein phosphatase 1, regulatory subunit 17
Atp6v0a2	428.6884	0.408496	0.00329	ATPase, H+ transporting, lysosomal V0 subunit A2

Rybp	499.5878	-0.48749	0.003301	RING1 and YY1 binding protein
Mgst1	96.73606	0.819094	0.003323	microsomal glutathione S-transferase 1
Tagln3	3598.052	-0.49864	0.003339	transgelin 3
Surf2	503.5453	0.50751	0.003369	surfeit gene 2
Kcnk1	1222.695	-0.2577	0.003369	potassium channel, subfamily K, member 1
Cavin2	99.68924	-0.94052	0.003369	caveolae associated 2
Tspyl1	2985.311	-0.37624	0.003376	testis-specific protein, Y-encoded-like 1
Commd3	1031.455	0.519231	0.003399	COMM domain containing 3
Lrrn1	274.5488	0.857981	0.003462	leucine rich repeat protein 1, neuronal
Itpk1	714.4677	0.484276	0.003466	inositol 1,3,4-triphosphate 5/6 kinase
Fam214b	385.0078	0.460026	0.00353	family with sequence similarity 214, member B
Eif4a3	852.684	-0.33707	0.003619	eukaryotic translation initiation factor 4A3
Garnl3	603.7887	0.508229	0.003636	GTPase activating RANGAP domain-like 3
Fam107b	145.053	-0.6609	0.003654	family with sequence similarity 107, member B
Tsr2	1146.723	-0.34307	0.003665	TSR2 20S rRNA accumulation
Atp2b1	2608.725	-0.4733	0.003715	ATPase, Ca++ transporting, plasma membrane 1
Rbm38	19.42743	1.069701	0.003727	RNA binding motif protein 38
H2-Ab1	65.26675	-1.49037	0.00373	histocompatibility 2, class II antigen A, beta 1
Mier2	403.4987	-0.44838	0.003735	MIER family member 2
Ubqln4	889.4459	-0.37416	0.003768	ubiquilin 4
Ldha	4929.758	0.364803	0.003802	lactate dehydrogenase A
Phtf2	118.1834	0.686994	0.003821	putative homeodomain transcription factor 2
Crbn	605.6924	-0.46394	0.003828	cereblon
Gdpd1	518.4743	0.399851	0.003832	glycerophosphodiester phosphodiesterase domain containing 1
Ech1	488.0915	-0.46964	0.003841	enoyl coenzyme A hydratase 1, peroxisomal
Flt1	62.64098	-1.36911	0.003846	FMS-like tyrosine kinase 1
Plagl1	151.2896	1.125254	0.003846	pleiomorphic adenoma gene-like 1
Smtnl2	47.00365	1.12597	0.003883	smoothelin-like 2
Sfxn1	849.7303	0.425031	0.003918	sideroflexin 1
C1ql1	183.4807	-0.90032	0.003928	complement component 1, q subcomponent-like 1
Cd200	684.9174	0.546215	0.003965	CD200 antigen
Gpd1	1364.522	-0.53791	0.003965	glycerol-3-phosphate dehydrogenase 1 (soluble)
Rere	771.6184	0.619978	0.00398	arginine glutamic acid dipeptide (RE) repeats
Cald1	387.2936	-0.83385	0.003996	caldesmon 1
Bud13	136.7721	-0.55202	0.003996	BUD13 homolog
Cnr1	1154.359	-0.4976	0.003996	cannabinoid receptor 1 (brain)
Pdzd4	277.8235	0.90669	0.004003	PDZ domain containing 4
1700013F07Rik	19.89387	-1.02903	0.004003	RIKEN cDNA 1700013F07 gene
11-Mar	93.70118	0.673225	0.004006	membrane-associated ring finger (C3HC4) 11
Smyd1	14.64211	2.344007	0.004007	SET and MYND domain containing 1
Ptbp1	253.8666	-0.64965	0.004016	polypyrimidine tract binding protein 1
Mkrn1	3005.795	0.282163	0.004069	makorin, ring finger protein, 1

Thumpd1	618.848	-0.32286	0.004069	THUMP domain containing 1
Ptk2	281.3056	-0.79547	0.004071	PTK2 protein tyrosine kinase 2
Xpo6	749.675	0.554764	0.004083	exportin 6
Akt1	3114.991	-0.36224	0.004124	thymoma viral proto-oncogene 1
Marveld1	108.3677	-0.70222	0.004158	MARVEL (membrane-associating) domain containing 1
Bcl6b	19.74745	1.45928	0.004171	B cell CLL/lymphoma 6, member B
Rcan1	983.8554	-0.37657	0.004214	regulator of calcineurin 1
Fam117a	107.0755	0.839173	0.004246	family with sequence similarity 117, member A
Htr1d	208.4543	-1.01558	0.004254	5-hydroxytryptamine (serotonin) receptor 1D
Nudt8	141.5957	0.696288	0.004258	
Pcdh17	519.0977	-0.46989	0.004258	protocadherin 17
Bdh2	23.23029	1.169253	0.004259	3-hydroxybutyrate dehydrogenase, type 2
Alpl	33.11391	-1.14188	0.004259	alkaline phosphatase, liver/bone/kidney
Cog7	519.4869	0.42692	0.004295	component of oligomeric golgi complex 7
P2rx4	145.3666	0.6546	0.004349	purinergic receptor P2X, ligand-gated ion channel 4
Npc1	161.7505	0.86901	0.004355	NPC intracellular cholesterol transporter 1
Dus1l	441.3461	0.442696	0.004355	dihydrouridine synthase 1-like (S. cerevisiae)
Umad1	1085.708	-0.50421	0.00439	UMAP1-MVP12 associated (UMA) domain containing 1
Dhcr7	239.2027	0.714881	0.004484	7-dehydrocholesterol reductase
Pstk	236.6247	0.68987	0.00449	phosphoseryl-tRNA kinase
E430018J23Rik	68.48941	-0.73208	0.004578	RIKEN cDNA E430018J23 gene
Nppa	6.34951	1.933782	0.004595	natriuretic peptide type A
Spp1	188.8505	1.21471	0.004603	secreted phosphoprotein 1
Fam163a	138.3308	0.615435	0.004636	family with sequence similarity 163, member A
Edc3	403.3316	-0.39761	0.004679	enhancer of mRNA decapping 3
Card9	17.70608	1.616858	0.004744	caspase recruitment domain family, member 9
Rfc5	273.211	-0.47876	0.004754	replication factor C (activator 1) 5
Cnst	552.0712	-0.43284	0.004754	consortin, connexin sorting protein
Slc9a3r2	1128.095	-0.54555	0.004772	solute carrier family 9 (sodium/hydrogen exchanger), member 3 regulator 2
Tsg101	1067.837	-0.31805	0.004772	tumor susceptibility gene 101
Usp11	903.059	-0.72528	0.004833	ubiquitin specific peptidase 11
Tmem189	704.8458	0.379937	0.004833	transmembrane protein 189
Pdgfrb	105.3616	-0.80766	0.004902	platelet derived growth factor receptor, beta polypeptide
Nudt19	1878.2	0.39267	0.004904	nudix (nucleoside diphosphate linked moiety X)-type motif 19
Ifngr2	619.0647	0.487182	0.004924	interferon gamma receptor 2
Rpl7a-ps10	9.901068	-6.54411	0.004954	
Ccm2	1895.562	0.556684	0.004967	cerebral cavernous malformation 2
Slc35f1	460.2217	-0.52616	0.004985	solute carrier family 35, member F1
Tymp	83.31529	0.672818	0.005105	thymidine phosphorylase

Nr1d1	1263.819	-0.56784	0.005144	nuclear receptor subfamily 1, group D, member 1
Tmem200c	15.76589	1.522483	0.005174	transmembrane protein 200C
Mospd1	307.7506	0.619289	0.005259	motile sperm domain containing 1
Aggf1	1264.509	0.384717	0.005265	angiogenic factor with G patch and FHA domains 1
Arl4d	864.4364	-0.64673	0.005282	ADP-ribosylation factor-like 4D
Zswim4	208.3108	-0.65961	0.005282	zinc finger SWIM-type containing 4
Lrrtm1	1144.06	-0.34252	0.005302	leucine rich repeat transmembrane neuronal 1
Taf7	124.467	-0.68222	0.005326	TATA-box binding protein associated factor 7
3-Sep	4394.821	0.244399	0.005362	septin 3
Tpst1	618.4082	-0.38648	0.005362	protein-tyrosine sulfotransferase 1
Klf16	839.0168	-0.64863	0.005388	Kruppel-like factor 16
Gpbp1l1	259.8229	-0.3929	0.005399	GC-rich promoter binding protein 1-like 1
Junb	2056.024	-0.72485	0.005433	jun B proto-oncogene
Cdc42ep4	525.4245	-0.61721	0.005435	CDC42 effector protein (Rho GTPase binding) 4
Hmgcs2	46.61553	-1.00449	0.00546	3-hydroxy-3-methylglutaryl-Coenzyme A synthase 2
Pqlc1	332.5495	0.493757	0.005465	PQ loop repeat containing 1
Fam171a1	657.9898	-0.42989	0.005477	family with sequence similarity 171, member A1
Ptpn5	3520.542	-0.52065	0.005501	protein tyrosine phosphatase, non-receptor type 5
Epn2	1222.029	-0.43119	0.005508	epsin 2
Pank1	280.0242	0.335382	0.005508	pantothenate kinase 1
Slc13a4	68.38047	-1.04972	0.005512	solute carrier family 13 (sodium/sulfate symporters), member 4
Cdca3	10.36166	1.75567	0.005527	cell division cycle associated 3
Acvrl1	207.8068	-0.8243	0.005558	activin A receptor, type II-like 1
Ace2	13.10104	-1.57054	0.005558	angiotensin I converting enzyme (peptidyl-dipeptidase A) 2
Cbx2	28.36435	-1.15461	0.005558	chromobox 2
Mon1a	351.8943	0.453779	0.005558	MON1 homolog A, secretory traffciking associated
Pdcd7	585.3441	-0.36414	0.005558	programmed cell death 7
Pcdhgb5	30.63467	-1.26864	0.005558	protocadherin gamma subfamily B, 5
Vrk1	262.9283	-0.48774	0.005586	vaccinia related kinase 1
Podxl	64.59776	-0.84108	0.005587	podocalyxin-like
Chac2	307.4635	0.551159	0.005604	ChaC, cation transport regulator 2
Tsc1	273.0087	-0.86755	0.00561	tuberous sclerosis 1
H2-T22	222.8351	0.729668	0.005691	histocompatibility 2, T region locus 22
H2-T22	222.8351	0.729668	0.005691	histocompatibility 2, T region locus 9
Samd1	100.4654	-0.79885	0.005692	sterile alpha motif domain containing 1
Gadd45a	209.7129	0.709629	0.005712	growth arrest and DNA-damage-inducible 45 alpha
Mmp14	73.31053	0.826125	0.005725	matrix metallopeptidase 14 (membrane-inserted)
Prelid3b	1174.057	0.493903	0.005725	PRELI domain containing 3B
Fgf16	20.50044	-1.32219	0.005725	fibroblast growth factor 16
Btbd2	1594.124	-0.38965	0.005731	BTB (POZ) domain containing 2
Prkci	557.0291	-0.60814	0.005732	protein kinase C, iota

Ell2	325.875	0.603876	0.005747	elongation factor RNA polymerase II 2
Ints11	346.6654	0.388238	0.005857	integrator complex subunit 11
Man2b1	192.7103	0.626126	0.00586	mannosidase 2, alpha B1
Bag2	115.2704	0.571593	0.005912	BCL2-associated athanogene 2
Cyc1	2017.51	0.423187	0.005931	cytochrome c-1
Dek	629.5486	-0.53964	0.005955	DEK oncogene (DNA binding)
Zfp523	972.9901	0.424646	0.005955	zinc finger protein 523
Pink1	3962.241	-0.32676	0.005955	PTEN induced putative kinase 1
Aifm3	252.8714	0.582864	0.005986	apoptosis-inducing factor, mitochondrion-associated 3
Hp1bp3	2129.515	-0.45956	0.005986	heterochromatin protein 1, binding protein 3
Rbp1	183.1745	-0.78939	0.005986	retinol binding protein 1, cellular
Fndc5	1134.073	0.39369	0.006	fibronectin type III domain containing 5
Nosip	708.9187	-0.38837	0.006	nitric oxide synthase interacting protein
Irf2bp1	1109.595	-0.51566	0.006	interferon regulatory factor 2 binding protein 1
Cystm1	1736.721	0.629839	0.006	cysteine-rich transmembrane module containing 1
Nat8l	2511.452	0.361632	0.006	N-acetyltransferase 8-like
Msx1	138.963	-0.48062	0.006	msh homeobox 1
Wdfy1	499.3142	1.070461	0.006	WD repeat and FYVE domain containing 1
Acta2	176.4324	-1.053	0.006087	actin, alpha 2, smooth muscle, aorta
Yap1	132.3428	0.560442	0.006099	yes-associated protein 1
Lysmd1	374.99	0.336248	0.006103	LysM, putative peptidoglycan-binding, domain containing 1
Fam196b	22.28685	-1.15014	0.006113	family with sequence similarity 196, member B
Acsl6	774.5488	0.505083	0.006157	acyl-CoA synthetase long-chain family member 6
Zfp30	204.9075	0.574571	0.006209	zinc finger protein 30
Jade1	770.8095	-0.35101	0.006219	jade family PHD finger 1
Stoml1	658.6245	0.354797	0.006219	stomatin-like 1
Ptafr	3.38334	-3.70913	0.006306	platelet-activating factor receptor
Slc25a22	3711.211	0.508434	0.006533	solute carrier family 25 (mitochondrial carrier, glutamate), member 22
Gdpgp1	188.3234	0.433053	0.006558	GDP-D-glucose phosphorylase 1
Zfp869	132.3639	-0.56022	0.00659	zinc finger protein 869
Tagln2	468.9846	-0.62989	0.006594	transgelin 2
Pcdhga7	129.8675	-0.9468	0.006615	protocadherin gamma subfamily A, 7
Diaph2	226.2655	-0.60982	0.006635	diaphanous related formin 2
Taf8	208.0806	-0.42553	0.006682	TATA-box binding protein associated factor 8
Slc25a44	1469.268	0.453674	0.006682	solute carrier family 25, member 44
Cacnb3	1011.949	-0.57762	0.006829	calcium channel, voltage-dependent, beta 3 subunit
Kcnh2	161.016	0.833179	0.006829	potassium voltage-gated channel, subfamily H (eag-related), member 2
9230110C19Rik	85.27022	-0.6749	0.006829	RIKEN cDNA 9230110C19 gene
Cdkn1c	172.7386	-0.6809	0.006838	cyclin-dependent kinase inhibitor 1C (P57)
Nup35	242.7149	-0.47864	0.006866	nucleoporin 35

Ccdc88b	36.14281	-1.04088	0.006873	coiled-coil domain containing 88B
Patj	235.9937	0.796262	0.006873	PATJ, crumbs cell polarity complex component
Timp2	3675.131	0.332198	0.006881	tissue inhibitor of metalloproteinase 2
Sgpl1	136.5124	0.709183	0.006881	sphingosine phosphate lyase 1
Nuak2	21.30961	-1.0726	0.006963	NUAK family, SNF1-like kinase, 2
Kcnf1	522.899	-0.75478	0.006963	potassium voltage-gated channel, subfamily F, member 1
Telo2	124.3652	0.920868	0.007007	telomere maintenance 2
Prmt2	1427.8	-0.32808	0.007033	protein arginine N-methyltransferase 2
Dach1	276.0007	-0.67761	0.007057	dachshund family transcription factor 1
Itga1	21.98815	-1.06861	0.007095	integrin alpha 1
Oaz2-ps	4.65964	5.68757	0.007187	
Med20	235.692	-0.3721	0.007206	mediator complex subunit 20
Matn2	46.01167	1.57839	0.007217	matrilin 2
Dmgdh	21.73789	1.256526	0.007268	dimethylglycine dehydrogenase precursor
Epas1	380.854	-0.55461	0.007283	endothelial PAS domain protein 1
Myd88	74.04978	-0.61191	0.007283	myeloid differentiation primary response gene 88
Yipf1	442.1359	0.529073	0.007283	Yip1 domain family, member 1
Gfra1	145.434	0.967365	0.007298	glial cell line derived neurotrophic factor family receptor alpha 1
Crym	1007.954	-0.56125	0.007398	crystallin, mu
Sf3a3	376.888	-0.3871	0.007398	splicing factor 3a, subunit 3
Tgfb1i1	253.4651	-0.55588	0.007468	transforming growth factor beta 1 induced transcript 1
Cspg4	76.91553	-0.95024	0.007523	chondroitin sulfate proteoglycan 4
Osr1	28.43778	-1.20707	0.007572	odd-skipped related transcription factor 1
Sema4c	66.09136	-0.84069	0.007865	sema domain, immunoglobulin domain (Ig), transmembrane domain (TM) and short cytoplasmic domain, (semaphorin) 4C
Nyap1	484.3957	-0.51515	0.007873	neuronal tyrosine-phosphorylated phosphoinositide 3-kinase adaptor 1
Rab11fip4	1898.985	0.352044	0.007891	RAB11 family interacting protein 4 (class II)
Bckdhb	473.5514	0.491181	0.007895	branched chain ketoacid dehydrogenase E1, beta polypeptide
Npy5r	48.91406	0.891208	0.007939	neuropeptide Y receptor Y5
Dazap2	2145.921	-0.34564	0.007963	DAZ associated protein 2
Cacng5	163.7803	0.735861	0.007973	calcium channel, voltage-dependent, gamma subunit 5
Tcea3	8.295829	-1.68118	0.007989	transcription elongation factor A (SII), 3
Uhmk1	1105.699	0.479069	0.007992	U2AF homology motif (UHM) kinase 1
Egr4	1630.254	-0.71241	0.008	early growth response 4
Cyth2	203.4478	0.761666	0.008031	cytohesin 2
Plppr5	574.5586	-0.41461	0.008082	phospholipid phosphatase related 5
Klhl14	20.00844	1.335334	0.008119	kelch-like 14
Kcnd1	77.13969	0.772732	0.008124	potassium voltage-gated channel, Shal-related family, member 1

Txndc12	180.9764	-0.46369	0.008134	thioredoxin domain containing 12 (endoplasmic reticulum)
1700003F12Rik	7.582614	1.865803	0.00836	RIKEN cDNA 1700003F12 gene
Zfp438	52.6411	-0.8331	0.008375	zinc finger protein 438
Plek2	9.173736	1.995806	0.008385	pleckstrin 2
Mrps30	405.7906	0.357626	0.008385	mitochondrial ribosomal protein S30
Kat8	232.0175	-0.39836	0.008394	K(lysine) acetyltransferase 8
Pcdhga2	67.04918	-0.97527	0.0084	protocadherin gamma subfamily A, 2
Stmn3	9374.065	0.479899	0.008425	stathmin-like 3
Map2k2	2394.682	0.481783	0.008464	mitogen-activated protein kinase kinase 2
Stard5	182.8599	0.592457	0.008511	StAR-related lipid transfer (START) domain containing 5
Gpr139	38.30476	-1.02671	0.008511	G protein-coupled receptor 139
Agpat5	488.6176	0.522813	0.008524	1-acylglycerol-3-phosphate O-acyltransferase 5 (lysophosphatidic acid acyltransferase, epsilon)
Mlx	706.1318	0.544674	0.008537	MAX-like protein X
Lct	27.28442	1.835769	0.008537	lactase
Gpr150	61.76956	1.000703	0.008537	G protein-coupled receptor 150
Nub1	1116.434	-0.26737	0.008651	negative regulator of ubiquitin-like proteins 1
Gkn3	30.58961	-1.32993	0.008714	gastrokine 3
Gm10053	3242.131	0.462852	0.008763	
Gm14403	24.89329	0.95375	0.008791	
Ptger4	21.00837	1.170549	0.008926	prostaglandin E receptor 4 (subtype EP4)
Cfap61	27.30023	1.42602	0.008937	cilia and flagella associated protein 61
Ly6h	3046.312	-0.56732	0.008957	lymphocyte antigen 6 complex, locus H
Csrnp1	109.1308	-0.63257	0.009016	cysteine-serine-rich nuclear protein 1
Lsamp	722.5663	0.471659	0.009016	limbic system-associated membrane protein
Gm10642	28.7127	0.946014	0.009173	
Dmrtc1a	171.5568	-0.43482	0.009203	DMRT-like family C1a
Gale	190.3749	0.509862	0.009204	galactose-4-epimerase, UDP
Ano4	108.8088	0.769692	0.00933	anoctamin 4
Tmem47	937.4771	-0.59426	0.009356	transmembrane protein 47
Fkbp9	239.0991	-0.55917	0.00943	FK506 binding protein 9
Higd1a	1490.329	0.39264	0.009485	HIG1 domain family, member 1A
Tmem33	455.7472	0.619632	0.00951	transmembrane protein 33
Pawr	33.78687	0.992682	0.009531	PRKC, apoptosis, WT1, regulator
Mttp	115.7981	-0.51076	0.009535	microsomal triglyceride transfer protein
Rab3d	146.022	-0.53376	0.009583	RAB3D, member RAS oncogene family
Sf3b2	2174.608	-0.35387	0.00962	splicing factor 3b, subunit 2
Ldhb	10135.89	0.349466	0.00962	lactate dehydrogenase B
2900055J20Rik	133.376	0.570431	0.00962	
Puf60	2153.123	-0.27691	0.009639	poly-U binding splicing factor 60

Serping1	43.76581	-1.06191	0.00964	serine (or cysteine) peptidase inhibitor, clade G, member 1
Pnma1	62.00318	-0.73421	0.009648	paraneoplastic antigen MA1
Ccsap	1147.892	-0.38148	0.009672	centriole, cilia and spindle associated protein
Gys1	126.1063	0.54876	0.009674	glycogen synthase 1, muscle
Melk	13.34541	-1.34201	0.009716	maternal embryonic leucine zipper kinase
Caprin2	24.0048	-1.26634	0.009743	caprin family member 2
Hmces	266.213	-0.40264	0.00976	5-hydroxymethylcytosine (hmC) binding, ES cell specific
Fmnl3	72.89323	-0.73355	0.009863	formin-like 3
Tcp11l1	114.3382	0.69031	0.009863	t-complex 11 like 1
Prrx2	20.00364	-0.91227	0.009889	paired related homeobox 2
Phf13	165.0113	-0.57693	0.009889	PHD finger protein 13
Rraga	1411.311	0.38935	0.009889	Ras-related GTP binding A
Tirap	49.4831	-1.00616	0.009976	toll-interleukin 1 receptor (TIR) domain-containing adaptor protein
Sms	880.4214	-0.43357	0.010001	spermine synthase
Sms	880.4214	-0.43357	0.010001	spermine synthase, pseudogene
Creld2	260.8373	-0.53141	0.010005	cysteine-rich with EGF-like domains 2
Cep126	240.3941	-0.53653	0.010041	centrosomal protein 126
Nr2c2ap	122.3229	0.839148	0.01005	nuclear receptor 2C2-associated protein
Klf11	73.32576	-0.82342	0.010058	Kruppel-like factor 11
Kcnab3	528.3528	0.609486	0.01012	potassium voltage-gated channel, shaker-related subfamily, beta member 3
Lims2	229.3775	-0.52904	0.01012	LIM and senescent cell antigen like domains 2
Cdk8	246.8912	0.417616	0.01012	cyclin-dependent kinase 8
Heatr3	380.6532	0.673147	0.01012	HEAT repeat containing 3
Pias1	415.991	-0.62166	0.01012	protein inhibitor of activated STAT 1
Agpat3	1544.518	0.36003	0.010143	1-acylglycerol-3-phosphate O-acyltransferase 3
Psmc4	1555.949	0.274764	0.010143	proteasome (prosome, macropain) 26S subunit, ATPase, 4
Eral1	255.4969	-0.37175	0.010257	Era (G-protein)-like 1 (E. coli)
Gjb2	68.85242	-1.15479	0.010257	gap junction protein, beta 2
Krt222	479.0345	0.571487	0.0103	keratin 222
Cyb5rl	102.9116	0.724792	0.010371	cytochrome b5 reductase-like
Sgsm2	525.7524	-0.45231	0.010373	small G protein signaling modulator 2
Ikzf3	49.32045	1.061404	0.010483	IKAROS family zinc finger 3
Mthfsd	408.5951	0.513256	0.010509	methenyltetrahydrofolate synthetase domain containing
Spsb4	68.09428	0.974128	0.01057	splA/ryanodine receptor domain and SOCS box containing 4
Tmem25	388.9396	0.676476	0.01062	transmembrane protein 25
Tsen34	1397.461	-0.3544	0.010694	tRNA splicing endonuclease subunit 34
Pigq	577.6771	0.744681	0.010914	phosphatidylinositol glycan anchor biosynthesis, class Q
Vasn	52.52269	-0.82949	0.010914	vasorin

Oscp1	373.8508	-0.36217	0.010914	organic solute carrier partner 1
Kcnip1	433.874	0.484759	0.010918	Kv channel-interacting protein 1
Gnptg	926.567	0.35461	0.010932	N-acetylglucosamine-1-phosphotransferase, gamma subunit
Fam98a	225.7021	0.493997	0.011038	family with sequence similarity 98, member A
Degs2	27.4897	-1.37655	0.01105	delta(4)-desaturase, sphingolipid 2
Phf2	210.6197	-0.45088	0.011063	PHD finger protein 2
Foxk1	136.4	-0.49205	0.011063	forkhead box K1
C1qtnf9	2.349863	3.438944	0.011063	C1q and tumor necrosis factor related protein 9
Zkscan16	44.19763	-1.09773	0.011067	zinc finger with KRAB and SCAN domains 16
Msi2	381.0538	0.62059	0.011114	musashi RNA-binding protein 2
Abhd17a	4603.187	0.51207	0.01116	abhydrolase domain containing 17A
Timm8a1	413.6552	0.494442	0.01116	translocase of inner mitochondrial membrane 8A1
Syt7	1091.995	0.468695	0.011212	synaptotagmin VII
Ak3	1118.783	-0.37382	0.01129	adenylate kinase 3
Tmem114	30.16589	-0.81089	0.011314	transmembrane protein 114
Tfap4	12.81184	-1.29436	0.011323	transcription factor AP4
U2af2	538.0243	-0.47818	0.01133	U2 small nuclear ribonucleoprotein auxiliary factor (U2AF) 2
L3mbtl4	10.57744	1.500777	0.011334	L3MBTL4 histone methyl-lysine binding protein
Smyd4	167.112	0.545128	0.011523	SET and MYND domain containing 4
Ptprg	189.2924	0.903558	0.011523	protein tyrosine phosphatase, receptor type, G
Sphkap	382.9684	1.383418	0.011571	SPHK1 interactor, AKAP domain containing
Ctsk	38.25049	0.870127	0.011595	cathepsin K
Plaa	360.2102	0.50032	0.011612	phospholipase A2, activating protein
Gm8226	42.23079	-5.91156	0.011616	
Tiam1	437.8298	0.595528	0.011799	T cell lymphoma invasion and metastasis 1
Grik2	101.0286	-0.82599	0.011799	glutamate receptor, ionotropic, kainate 2 (beta 2)
Smad6	77.12635	-0.83163	0.011868	SMAD family member 6
H2afv	933.6925	-0.65971	0.011868	H2A histone family, member V
Zfp879	22.23275	-1.00685	0.011868	zinc finger protein 879
Pcdhgb6	54.09675	-1.07026	0.011868	protocadherin gamma subfamily B, 6
Acsf2	62.51303	-0.83503	0.011893	acyl-CoA synthetase family member 2
Bex4	301.0656	-0.8188	0.011921	brain expressed X-linked 4
Tnfrsf17	1.777262	4.099901	0.012061	tumor necrosis factor receptor superfamily, member 17
Tomm34	1890.654	0.330323	0.012078	translocase of outer mitochondrial membrane 34
Zyx	253.179	-0.5305	0.012078	zyxin
Afmid	38.09362	1.390102	0.012083	arylformamidase
Phka2	72.40896	1.018983	0.012083	phosphorylase kinase alpha 2
H2afy2	449.5125	-0.36155	0.012149	H2A histone family, member Y2
Rarb	1189.653	-0.59587	0.01219	retinoic acid receptor, beta
Entpd3	150.5258	0.582172	0.01219	ectonucleoside triphosphate diphosphohydrolase 3
Fos	574.8772	-1.07569	0.0122	FBJ osteosarcoma oncogene

Taco1	65.86034	0.709528	0.012267	translational activator of mitochondrially encoded cytochrome c oxidase I
Hmgn2	1966.017	-0.74705	0.01238	high mobility group nucleosomal binding domain 2
4930452B06Rik	139.9553	0.911961	0.01238	RIKEN cDNA 4930452B06 gene
Abhd3	342.6235	0.59628	0.012456	abhydrolase domain containing 3
Sav1	129.082	0.485137	0.01247	salvador family WW domain containing 1
Edn3	93.46962	-0.85824	0.012479	endothelin 3
Wdr4	313.0448	0.474196	0.012529	WD repeat domain 4
P4ha2	98.41847	0.575054	0.012539	procollagen-proline, 2-oxoglutarate 4-dioxygenase (proline 4-hydroxylase), alpha II polypeptide
Pex13	355.9628	0.554846	0.012563	peroxisomal biogenesis factor 13
Gabra3	255.8161	0.760255	0.0126	gamma-aminobutyric acid (GABA) A receptor, subunit alpha 3
Cacng3	1626.598	-0.41877	0.012664	calcium channel, voltage-dependent, gamma subunit 3
2300009A05Rik	192.619	0.659691	0.012673	RIKEN cDNA 2300009A05 gene
Zfp455	15.98005	1.094788	0.012714	zinc finger protein 455
Lyz2	137.1572	-1.10863	0.012739	lysozyme 2
Ush1c	6.261019	1.976035	0.012749	USH1 protein network component harmonin
Foxp1	3523.225	-0.50087	0.012751	forkhead box P1
Pcdhga9	30.99054	-1.56248	0.012772	protocadherin gamma subfamily A, 9
Miip	88.83481	0.706912	0.012875	migration and invasion inhibitory protein
Rbmx	534.632	-0.39603	0.012875	RNA binding motif protein, X chromosome
Mfsd5	677.4221	0.348444	0.012875	major facilitator superfamily domain containing 5
Cetn4	140.5801	-0.83343	0.012893	centrin 4
Pole	4.33913	3.386217	0.012973	polymerase (DNA directed), epsilon
Psmc3ip	84.50366	-0.53773	0.012999	proteasome (prosome, macropain) 26S subunit, ATPase 3, interacting protein
Tspan4	175.518	-0.51218	0.013007	tetraspanin 4
Prmt3	326.9874	0.355408	0.013007	protein arginine N-methyltransferase 3
Atp6ap2	3155.06	0.459187	0.013007	ATPase, H+ transporting, lysosomal accessory protein 2
Zfp319	226.8355	-0.54138	0.013007	zinc finger protein 319
Irf2bp2	1104.3	-0.36425	0.013007	interferon regulatory factor 2 binding protein 2
Actn3	10.95895	1.647796	0.013028	actinin alpha 3
H2-Eb1	67.57496	-1.34339	0.01303	histocompatibility 2, class II antigen E beta
Creb3	531.9798	0.404678	0.013094	cAMP responsive element binding protein 3
Cbfa2t3	278.1026	-0.48734	0.013096	core-binding factor, runt domain, alpha subunit 2, translocated to, 3 (human)
Ubr3	1006.263	-0.76869	0.013129	ubiquitin protein ligase E3 component n-recognin 3
Hrasls	321.6835	-0.44361	0.013137	HRAS-like suppressor
Prkacb	4470.648	-0.41661	0.013155	protein kinase, cAMP dependent, catalytic, beta
Il6st	206.1757	-0.64987	0.013173	interleukin 6 signal transducer
Suv39h2	98.53757	0.689391	0.013214	suppressor of variegation 3-9 2
Shisa7	431.64	-0.42294	0.013214	shisa family member 7

Spdl1	7.348441	2.012231	0.013214	spindle apparatus coiled-coil protein 1
1700019D03Rik	239.3849	0.589753	0.01323	RIKEN cDNA 1700019D03 gene
D030056L22Rik	648.368	-0.34402	0.01323	RIKEN cDNA D030056L22 gene
Otof	63.15706	0.72577	0.01323	otoferlin
Cdkl3	135.0968	-0.70919	0.013263	cyclin-dependent kinase-like 3
Cox19	342.6123	0.506052	0.013324	cytochrome c oxidase assembly protein 19
Isoc1	3209.599	-0.48364	0.013377	isochorismatase domain containing 1
Atp6v1c1	2040.151	0.346193	0.013398	ATPase, H+ transporting, lysosomal V1 subunit C1
Uchl3	452.959	0.481048	0.013417	ubiquitin carboxyl-terminal esterase L3 (ubiquitin thiolesterase)
Pdlim5	151.9114	0.553908	0.013417	PDZ and LIM domain 5
Slc28a1	4.093889	2.393497	0.013471	solute carrier family 28 (sodium-coupled nucleoside transporter), member 1
Bcas3	511.0145	0.500733	0.013476	breast carcinoma amplified sequence 3
Scpep1	183.4592	0.414304	0.013663	serine carboxypeptidase 1
Tspyl5	677.2738	-0.3798	0.013663	testis-specific protein, Y-encoded-like 5
Apol8	49.97785	0.686463	0.013663	apolipoprotein L 8
Tmem179	2403.876	0.351251	0.013718	transmembrane protein 179
Kcna1	472.2149	0.427578	0.013731	potassium voltage-gated channel, shaker-related subfamily, member 1
Atp5k	332.2803	0.819466	0.013731	ATP synthase, H+ transporting, mitochondrial F1F0 complex, subunit E
Adra2b	18.51298	-1.24709	0.013731	adrenergic receptor, alpha 2b
Parp6	2281.543	0.333664	0.013742	poly (ADP-ribose) polymerase family, member 6
E2f3	21.26908	2.17586	0.013757	E2F transcription factor 3
Celf5	1436.752	-0.45211	0.013769	CUGBP, Elav-like family member 5
9430038I01Rik	36.21278	1.020256	0.013773	RIKEN cDNA 9430038I01 gene
Msmo1	946.9857	0.376146	0.013829	methylsterol monoxygenase 1
C1qc	115.6289	-0.81863	0.013829	complement component 1, q subcomponent, C chain
Abl1	298.5041	-0.47599	0.013924	c-abl oncogene 1, non-receptor tyrosine kinase
Calr	1544.55	-0.48332	0.013926	calreticulin
Atg13	959.5389	-0.41908	0.01397	autophagy related 13
Zcwpw1	68.97258	-0.61012	0.014036	zinc finger, CW type with PWWP domain 1
Ccdc85c	173.5944	0.537628	0.014049	coiled-coil domain containing 85C
Ddx39b	1095.674	-0.26926	0.014167	DEAD (Asp-Glu-Ala-Asp) box polypeptide 39B
Khdrbs2	239.2681	-0.52627	0.014167	KH domain containing, RNA binding, signal transduction associated 2
Greb1l	24.50587	1.93469	0.014167	growth regulation by estrogen in breast cancer-like
Tmem248	511.086	0.304654	0.014167	transmembrane protein 248
Gm8707	15.62858	-1.25023	0.014167	
Ssbp2	861.5716	-0.2819	0.014212	single-stranded DNA binding protein 2
Nr3c1	820.1612	-0.36824	0.014214	nuclear receptor subfamily 3, group C, member 1
Kcnip4	941.2653	-0.53898	0.014214	Kv channel interacting protein 4

Rcn1	733.413	-0.46093	0.01437	reticulocalbin 1
Pkdcc	44.31402	-0.97871	0.014382	protein kinase domain containing, cytoplasmic
Itm2c	11667.56	-0.42734	0.01441	integral membrane protein 2C
Fbxl21	65.03735	-0.74555	0.014472	F-box and leucine-rich repeat protein 21
Pnpla2	252.4591	-0.52965	0.014511	patatin-like phospholipase domain containing 2
Pgrmc2	1016.97	-0.38224	0.014519	progesterone receptor membrane component 2
Ttbk1	232.0955	0.512707	0.014604	tau tubulin kinase 1
Ecel1	210.618	0.619372	0.014734	endothelin converting enzyme-like 1
Armc6	462.7628	0.489502	0.014758	armadillo repeat containing 6
Llph	648.9248	0.64094	0.014758	LLP homolog, long-term synaptic facilitation (Aplysia)
Fas	7.107956	-1.85004	0.014767	Fas (TNF receptor superfamily member 6)
AI314180	382.3459	0.801598	0.014974	expressed sequence AI314180
Bmp4	39.73752	-0.99065	0.015029	bone morphogenetic protein 4
Nubp1	288.4982	0.420209	0.015074	nucleotide binding protein 1
Nup188	66.9515	-0.79691	0.015107	nucleoporin 188
Crlf1	48.18472	1.158326	0.015152	cytokine receptor-like factor 1
Wdr34	533.8522	-0.40368	0.015157	WD repeat domain 34
Fibcd1	273.2774	-0.6468	0.015176	fibrinogen C domain containing 1
Arc	2411.108	-0.84077	0.015364	activity regulated cytoskeletal-associated protein
Zfp64	328.9327	-0.4256	0.015364	zinc finger protein 64
Igfbp7	793.2943	-0.62337	0.015364	insulin-like growth factor binding protein 7
Ndufa10	2806.312	0.254078	0.015413	NADH dehydrogenase (ubiquinone) 1 alpha subcomplex 10
Relb	106.9197	0.5828	0.015462	avian reticuloendotheliosis viral (v-rel) oncogene related B
Zfp128	79.56744	-0.53167	0.015575	zinc finger protein 128
Txnl4b	193.9209	-0.39439	0.015601	thioredoxin-like 4B
Nes	22.29621	-1.27829	0.015702	nestin
Slc18b1	165.8437	0.598014	0.015712	solute carrier family 18, subfamily B, member 1
Mpl	6.032863	1.987147	0.015741	myeloproliferative leukemia virus oncogene
Atp6v0b	4214.568	0.571265	0.015781	ATPase, H+ transporting, lysosomal V0 subunit B
Ostm1	455.3251	0.502913	0.015781	osteopetrosis associated transmembrane protein 1
Rnf10	3286.077	0.357349	0.01581	ring finger protein 10
Psen1	404.2043	-0.44003	0.015822	presenilin 1
Pkm	14155.09	0.416484	0.015975	pyruvate kinase, muscle
Afap1l2	86.75182	-0.78967	0.015978	actin filament associated protein 1-like 2
Mcm7	120.918	-0.45256	0.016017	minichromosome maintenance complex component 7
Apip	224.2569	0.526778	0.016088	APAF1 interacting protein
Mgll	1783.363	0.420314	0.01609	monoglyceride lipase
Btrc	811.7261	-0.31801	0.016097	beta-transducin repeat containing protein
Ggt1	31.96058	0.847174	0.016137	gamma-glutamyltransferase 1
Ndrg3	4318.559	0.306428	0.016143	N-myc downstream regulated gene 3
Ssx2ip	1256.007	0.3036	0.0162	synovial sarcoma, X 2 interacting protein

Cops7b	332.5428	0.361357	0.016242	COP9 signalosome subunit 7B
Larp7	169.6759	-0.49079	0.016249	La ribonucleoprotein domain family, member 7
Fut11	154.35	0.515616	0.016249	fucosyltransferase 11
Snx10	2457.951	0.317247	0.016264	sorting nexin 10
Xrcc4	144.632	-0.51357	0.016298	X-ray repair complementing defective repair in Chinese hamster cells 4
Trp53i11	931.0377	-0.40703	0.016337	transformation related protein 53 inducible protein 11
Vcl	68.6736	-0.77108	0.016388	vinculin
Usp2	1322.226	0.445062	0.016541	ubiquitin specific peptidase 2
Dock4	307.4499	-0.75655	0.016541	dedicator of cytokinesis 4
Zswim5	181.5886	-0.40962	0.016584	zinc finger SWIM-type containing 5
Oser1	386.2255	-0.29053	0.016584	oxidative stress responsive serine rich 1
Atg12	1031.864	-0.2883	0.016828	autophagy related 12
Hdgfl3	1361.216	-0.40776	0.016843	HDGF like 3
Ido1	198.3437	0.678258	0.016865	indoleamine 2,3-dioxygenase 1
Nlrp10	3.959877	1.839207	0.016926	NLR family, pyrin domain containing 10
Enpep	12.49627	-1.29011	0.016927	glutamyl aminopeptidase
Lama1	14.01329	1.198714	0.016929	laminin, alpha 1
Kcnh4	272.0663	0.608659	0.017048	potassium voltage-gated channel, subfamily H (eag-related), member 4
Uqcc1	653.5949	-0.37439	0.017076	ubiquinol-cytochrome c reductase complex assembly factor 1
Hapln4	830.0911	0.864834	0.017076	hyaluronan and proteoglycan link protein 4
Ctgf	250.025	-0.67161	0.017076	connective tissue growth factor
Xpo7	471.6672	-0.50001	0.017076	exportin 7
F3	242.4882	-0.59649	0.017076	coagulation factor III
Inppl1	165.8268	-0.59047	0.017076	inositol polyphosphate phosphatase-like 1
Rxrb	1769.971	-0.41278	0.017076	retinoid X receptor beta
Fam155a	490.3363	0.364223	0.017105	family with sequence similarity 155, member A
Mkl1	422.6527	-0.57735	0.017111	MKL (megakaryoblastic leukemia)/myocardin-like 1
Ptpn11	955.2234	0.326324	0.017116	protein tyrosine phosphatase, non-receptor type 11
Car12	209.8603	-0.63155	0.017119	carbonic anhydrase 12
Zranb3	68.77035	1.011061	0.017119	zinc finger, RAN-binding domain containing 3
Car5b	22.62062	1.021618	0.017131	carbonic anhydrase 5b, mitochondrial
Kcns1	225.8496	-0.60183	0.017148	K+ voltage-gated channel, subfamily S, 1
Nfe2l1	1800.503	0.296019	0.017159	nuclear factor, erythroid derived 2,-like 1
Cyp39a1	40.80742	0.929955	0.01717	cytochrome P450, family 39, subfamily a, polypeptide 1
Pcdhb8	21.01059	-1.32125	0.01717	protocadherin beta 8
Cd63	626.746	0.525097	0.017241	CD63 antigen
Slc25a35	76.9476	0.616321	0.017285	solute carrier family 25, member 35
Prnd	3.344667	2.960734	0.017319	prion like protein doppel
Ppip5k2	238.5321	0.525436	0.017319	diphosphoinositol pentakisphosphate kinase 2
Sp2	242.6338	-0.51327	0.017329	Sp2 transcription factor

Scly	147.6136	0.50525	0.017383	selenocysteine lyase
Sf1	781.8809	-0.46173	0.01745	splicing factor 1
Ptprm	160.8998	-0.46783	0.01745	protein tyrosine phosphatase, receptor type, M
Osbp2	869.4856	0.368404	0.01748	oxysterol binding protein 2
Fam222b	428.2155	0.475535	0.01748	family with sequence similarity 222, member B
Lamc2	51.07758	1.108834	0.017527	laminin, gamma 2
Wnt4	213.4904	-0.57229	0.017527	wingless-type MMTV integration site family, member 4
Brwd3	37.87477	0.984195	0.017527	bromodomain and WD repeat domain containing 3
Efhd2	4463.601	-0.38432	0.017641	EF hand domain containing 2
Lta4h	359.4972	0.356375	0.017699	leukotriene A4 hydrolase
Pstpip1	20.17447	1.289993	0.017699	proline-serine-threonine phosphatase-interacting protein 1
Ttc7b	1281.713	0.48066	0.017699	tetratricopeptide repeat domain 7B
Tpp1	368.0826	0.423747	0.017737	tripeptidyl peptidase I
Cacna1a	272.1564	0.99265	0.017737	calcium channel, voltage-dependent, P/Q type, alpha 1A subunit
Cdc34	968.6598	0.513838	0.017835	cell division cycle 34
Rapsn	24.67147	1.02007	0.017849	receptor-associated protein of the synapse
Srxn1	1267.475	0.428535	0.018032	sulfiredoxin 1 homolog (S. cerevisiae)
Mvk	283.6407	0.424317	0.018042	mevalonate kinase
Dazap1	498.3491	-0.33382	0.018053	DAZ associated protein 1
Fam43b	657.6056	-0.4061	0.018063	family with sequence similarity 43, member B
Trim54	4.30202	3.92903	0.018232	tripartite motif-containing 54
Stim1	386.4221	-0.35708	0.018267	stromal interaction molecule 1
Elavl1	718.9621	-0.32662	0.018267	ELAV (embryonic lethal, abnormal vision)-like 1 (Hu antigen R)
Rab9b	344.4517	-0.55532	0.018327	RAB9B, member RAS oncogene family
Npc2	561.7115	0.465006	0.018397	NPC intracellular cholesterol transporter 2
Slc22a7	3.412091	2.68747	0.01851	solute carrier family 22 (organic anion transporter), member 7
Usp50	49.5675	0.863502	0.018768	ubiquitin specific peptidase 50
Dusp22	491.3243	0.334279	0.018836	dual specificity phosphatase 22
Phkg2	578.6484	0.281013	0.01885	phosphorylase kinase, gamma 2 (testis)
Adamtsl2	84.24863	-0.85838	0.018891	ADAMTS-like 2
Arpp19	12954.24	-0.45844	0.019101	cAMP-regulated phosphoprotein 19
Chmp5	1286.746	-0.44391	0.019229	charged multivesicular body protein 5
Lrp12	358.8091	0.40701	0.019246	low density lipoprotein-related protein 12
Tmc8	7.23406	-2.17505	0.019246	transmembrane channel-like gene family 8
Cnn1	3.002233	-3.45113	0.019333	calponin 1
Cactin	713.845	-0.31409	0.01942	cactin, spliceosome C complex subunit
Trim9	1318.824	-0.34362	0.019458	tripartite motif-containing 9
Mphosph9	125.7493	0.841767	0.019643	M-phase phosphoprotein 9
Cxcl14	778.9609	0.45305	0.019665	chemokine (C-X-C motif) ligand 14
Tmem59	3089.714	-0.35144	0.019665	transmembrane protein 59

Adgrg6	8.55345	1.931499	0.019692	adhesion G protein-coupled receptor G6
Gmeb2	111.786	-0.58777	0.019785	glucocorticoid modulatory element binding protein 2
Timm23	1744.271	0.436638	0.019831	translocase of inner mitochondrial membrane 23
Ttc19	1027.961	0.294864	0.019865	tetratricopeptide repeat domain 19
Rpf1	152.7508	-0.43037	0.019869	ribosome production factor 1 homolog
Pef1	1615.546	-0.41299	0.019916	penta-EF hand domain containing 1
Tfe3	495.3452	0.483339	0.020164	transcription factor E3
Vps13c	40.6721	1.423518	0.020221	vacuolar protein sorting 13C
Rad54l2	65.74702	-0.86433	0.020471	RAD54 like 2 (S. cerevisiae)
Bcar3	145.0023	-0.41256	0.020594	breast cancer anti-estrogen resistance 3
Fastk	1361.263	0.326465	0.02069	Fas-activated serine/threonine kinase
Gng12	534.463	0.440091	0.02069	guanine nucleotide binding protein (G protein), gamma 12
Gm10330	2.647188	-3.30211	0.020697	
Ccdc155	39.22131	0.918358	0.020729	coiled-coil domain containing 155
Pex16	371.6104	0.472905	0.020828	peroxisomal biogenesis factor 16
Nf1	95.7674	0.753692	0.02083	neurofibromin 1
Tpst2	476.7159	0.406533	0.020843	protein-tyrosine sulfotransferase 2
Tango2	535.3322	0.352195	0.020944	transport and golgi organization 2
	535.3322	0.352195	0.020944	transport and golgi organization 2
Svop	3221.915	0.304258	0.021103	SV2 related protein
Agl	89.05177	1.012953	0.021224	amylo-1,6-glucosidase, 4-alpha-glucanotransferase
Ctns	100.5678	0.448796	0.021248	cystinosis, nephropathic
Dusp15	189.4451	0.593355	0.021297	dual specificity phosphatase-like 15
Ski	1594.85	-0.3321	0.021325	ski sarcoma viral oncogene homolog (avian)
Gm12182	2.661493	2.451864	0.021325	
Nrip3	1462.537	0.582892	0.021519	nuclear receptor interacting protein 3
Rxrg	1707.714	-0.60709	0.021526	retinoid X receptor gamma
Ccdc181	299.7176	-0.37097	0.021574	coiled-coil domain containing 181
Tmem123	102.0098	-0.6579	0.021574	transmembrane protein 123
Grk6	583.0208	-0.33975	0.021574	G protein-coupled receptor kinase 6
Vwa1	261.9466	-0.54673	0.021612	von Willebrand factor A domain containing 1
Snca	6901.294	-0.34592	0.021682	synuclein, alpha
Grik3	328.0847	0.339465	0.021714	glutamate receptor, ionotropic, kainate 3
Rasl11a	95.57416	-0.60563	0.021841	RAS-like, family 11, member A
Hhatl	85.00483	0.866634	0.021841	hedgehog acyltransferase-like
Pcdhga4	44.21555	-1.34749	0.021884	protocadherin gamma subfamily A, 4
Mrs2	378.4897	0.336326	0.021965	MRS2 magnesium transporter
Ttc5	573.1983	-0.32483	0.022023	tetratricopeptide repeat domain 5
Atf4	1077.8	0.422054	0.02211	activating transcription factor 4
Cubn	5.456638	2.20353	0.022131	cubilin (intrinsic factor-cobalamin receptor)
Atf7ip	279.7102	-0.69713	0.022143	activating transcription factor 7 interacting protein
Zdhhc3	1061.011	0.284599	0.022196	zinc finger, DHHC domain containing 3

Ebna1bp2	742.0507	-0.35493	0.022283	EBNA1 binding protein 2
Mpp6	912.1434	0.442546	0.022283	membrane protein, palmitoylated 6 (MAGUK p55 subfamily member 6)
Cend1	6827.569	0.336774	0.022704	cell cycle exit and neuronal differentiation 1
Rnf130	388.8736	0.389768	0.022737	ring finger protein 130
Rint1	115.3088	0.611324	0.022737	RAD50 interactor 1
Map3k10	1348.49	0.3913	0.022737	mitogen-activated protein kinase kinase kinase 10
Pwwp2a	411.4631	-0.43017	0.022737	PWWP domain containing 2A
4933434E20Rik	840.1155	0.443923	0.022795	RIKEN cDNA 1700094D03 gene
4933434E20Rik	840.1155	0.443923	0.022795	RIKEN cDNA 4933434E20 gene
Ranbp10	211.6511	0.398687	0.022824	RAN binding protein 10
Pcmtd2	727.3212	-0.499	0.022888	protein-L-isoaspartate (D-aspartate) O-methyltransferase domain containing 2
Pcp4	20247.49	0.76103	0.022888	Purkinje cell protein 4
Rassf3	348.5231	-0.44744	0.022972	Ras association (RalGDS/AF-6) domain family member 3
Cox7c	1605.537	0.861967	0.023	cytochrome c oxidase subunit VIIc
Hook2	96.93847	0.627106	0.023135	hook microtubule tethering protein 2
Smpd1	1193.793	0.26979	0.023186	sphingomyelin phosphodiesterase 1, acid lysosomal
Tmem204	288.3642	-0.64467	0.023286	transmembrane protein 204
Paxx	697.5637	0.572918	0.0234	non-homologous end joining factor
Fgf3	103.6594	-0.96327	0.023531	fibroblast growth factor 3
Lgi1	693.1778	0.328679	0.023753	leucine-rich repeat LGI family, member 1
Gramd1c	4.787229	2.961529	0.023761	GRAM domain containing 1C
Fgf9	381.6836	0.433003	0.023769	fibroblast growth factor 9
Patl2	4.236206	2.482688	0.023781	protein associated with topoisomerase II homolog 2 (yeast)
Ptrhd1	193.1965	0.512764	0.023808	peptidyl-tRNA hydrolase domain containing 1
Cyb5r4	556.7997	0.616602	0.023876	cytochrome b5 reductase 4
Aplp1	27119.23	-0.40102	0.023887	amyloid beta (A4) precursor-like protein 1
Oxct1	3062.575	0.399816	0.023887	3-oxoacid CoA transferase 1
Cdh7	125.2651	-0.72949	0.023887	cadherin 7, type 2
Tspan9	387.1202	0.345191	0.023887	tetraspanin 9
Kcnk3	254.316	0.505722	0.023887	potassium channel, subfamily K, member 3
Nkd2	72.54563	-0.63662	0.023898	naked cuticle 2
Ctsh	55.88456	-0.77662	0.024037	cathepsin H
Nabp1	122.4033	0.633697	0.024049	nucleic acid binding protein 1
Serbp1	521.7923	-0.54736	0.024072	serpine1 mRNA binding protein 1
Prss56	7.09901	2.152355	0.024124	protease, serine 56
Oprl1	337.016	0.468598	0.024142	opioid receptor-like 1
Ube2e2	1375.14	-0.26912	0.024264	ubiquitin-conjugating enzyme E2E 2
Ccdc117	166.5926	-0.59391	0.02444	coiled-coil domain containing 117
Rgs20	725.8123	-0.52673	0.0245	regulator of G-protein signaling 20

Kif4	5.105011	2.571788	0.0245	kinesin family member 4
Phldb2	43.31418	-1.02473	0.024649	pleckstrin homology like domain, family B, member 2
Lgals1	175.7236	0.833874	0.024868	lectin, galactose binding, soluble 1
Lingo1	1923.826	0.37637	0.024935	leucine rich repeat and Ig domain containing 1
Mtss1l	639.3714	0.670205	0.024949	metastasis suppressor 1-like
Nkain2	139.3449	-0.70945	0.024997	Na+/K+ transporting ATPase interacting 2
Tnfrsf11b	10.79146	1.462105	0.025163	tumor necrosis factor receptor superfamily, member 11b (osteoprotegerin)
Isy1	224.6655	-0.41239	0.02525	ISY1 splicing factor homolog
Agtrap	81.83028	0.85372	0.025253	angiotensin II, type I receptor-associated protein
Arhgap33	1190.451	-0.7837	0.025253	Rho GTPase activating protein 33
Sirt3	909.3649	0.358249	0.025269	sirtuin 3
Mum1	364.6139	-0.35581	0.025351	melanoma associated antigen (mutated) 1
Zfp740	594.4651	-0.33696	0.025351	zinc finger protein 740
Cdyl2	193.5011	-0.55623	0.02536	chromodomain protein, Y chromosome-like 2
9930104L06Rik	158.4823	-0.53315	0.02536	RIKEN cDNA 9930104L06 gene
Blvrb	284.8245	-0.64326	0.025362	biliverdin reductase B (flavin reductase (NADPH))
Tmco6	62.44645	-0.57818	0.025551	transmembrane and coiled-coil domains 6
Dennd2d	4.477386	-2.85935	0.025551	DENN/MADD domain containing 2D
Nmral1	157.3881	-0.47521	0.025564	NmrA-like family domain containing 1
Exoc3l2	5.663819	-1.80503	0.025858	exocyst complex component 3-like 2
Bok	1082.228	0.609468	0.025858	BCL2-related ovarian killer
Hlcs	105.7022	0.554483	0.025858	holocarboxylase synthetase (biotin- [propriony-Coenzyme A-carboxylase (ATP-hydrolysing)] ligase)
Ndufv3	751.5164	0.765451	0.025933	NADH dehydrogenase (ubiquinone) flavoprotein 3
Cox4i2	113.2796	-0.77127	0.02599	cytochrome c oxidase subunit 4I2
Eml1	1044.603	-0.23458	0.026	echinoderm microtubule associated protein like 1
Micu2	263.2487	-0.35352	0.026078	mitochondrial calcium uptake 2
Exoc5	694.2885	0.482129	0.026139	exocyst complex component 5
Zbtb42	7.200841	-1.77611	0.026164	zinc finger and BTB domain containing 42
Plekhh2	29.39075	0.836754	0.026368	pleckstrin homology domain containing, family H (with MyTH4 domain) member 2
Ckb	38892.4	0.378832	0.026394	creatine kinase, brain
Riox2	145.7967	-0.45296	0.02642	ribosomal oxygenase 2
Rpsa	864.862	0.668743	0.026494	ribosomal protein SA
Snrnp25	338.4058	0.618147	0.0265	small nuclear ribonucleoprotein 25 (U11/U12)
Olfm1	11722.59	0.487572	0.026668	olfactomedin 1
Nptn	5525.22	-0.44879	0.026668	neuroplastin
Alk	16.37302	1.070747	0.02672	anaplastic lymphoma kinase
Prune1	203.2195	-0.35363	0.026744	prune exopolyphosphatase
Ankk1	9.167871	1.327975	0.02682	ankyrin repeat and kinase domain containing 1
Zfp971	108.9434	0.544749	0.02682	zinc finger protein 971
Mtfr1l	1401.524	0.329561	0.027028	mitochondrial fission regulator 1-like

Rab40b	1441.784	0.368505	0.02713	Rab40B, member RAS oncogene family
Etf1	742.3732	0.363374	0.027156	eukaryotic translation termination factor 1
Kbtbd4	202.8325	0.358418	0.027157	kelch repeat and BTB (POZ) domain containing 4
Echdc1	334.3921	0.516225	0.027233	enoyl Coenzyme A hydratase domain containing 1
Crtc1	2079.47	-0.44754	0.027287	CREB regulated transcription coactivator 1
Elmo3	7.316932	-3.40318	0.027287	engulfment and cell motility 3
3-Mar	38.60217	0.664533	0.027326	membrane-associated ring finger (C3HC4) 3
Rabggta	500.6054	-0.32246	0.027358	Rab geranylgeranyl transferase, a subunit
Prrt1	1455.737	-0.48146	0.027421	proline-rich transmembrane protein 1
Foxq1	147.0988	-0.58047	0.027421	forkhead box Q1
Mfsd13a	424.5617	0.413899	0.027446	major facilitator superfamily domain containing 13a
Acot5	40.40024	0.816409	0.027501	acyl-CoA thioesterase 5
Tcf19	106.278	0.6444	0.027522	transcription factor 19
Tbc1d23	141.5496	-0.62516	0.027967	TBC1 domain family, member 23
Iqcb1	320.8399	-0.41009	0.027974	IQ calmodulin-binding motif containing 1
Lmf1	195.7209	0.441677	0.027982	lipase maturation factor 1
Necap1	3358.796	-0.24463	0.028075	NECAP endocytosis associated 1
Mlxip	249.0731	0.38021	0.028075	MLX interacting protein
Zcchc12	858.7894	-0.50545	0.028079	zinc finger, CCHC domain containing 12
Fam180a	21.53623	-0.92986	0.028079	family with sequence similarity 180, member A
Psrc1	43.45283	0.797739	0.028079	proline/serine-rich coiled-coil 1
Negr1	803.5301	-0.3185	0.028107	neuronal growth regulator 1
Faap100	136.3086	0.70308	0.02822	Fanconi anemia core complex associated protein 100
Sat1	519.6093	0.506039	0.02827	spermidine/spermine N1-acetyl transferase 1
Cmss1	162.3125	-0.34145	0.028278	cms small ribosomal subunit 1
Slc9a9	58.48103	0.996076	0.028278	solute carrier family 9 (sodium/hydrogen exchanger), member 9
2-Mar	1335.536	0.440287	0.028278	membrane-associated ring finger (C3HC4) 2
Plcg2	30.16795	0.684987	0.028312	phospholipase C, gamma 2
Ufsp2	498.2699	0.344889	0.028359	UFM1-specific peptidase 2
Gas2l2	17.01827	0.943183	0.028371	growth arrest-specific 2 like 2
Gemin6	174.6516	-0.45474	0.02847	gem nuclear organelle associated protein 6
Tm4sf1	97.04797	-0.8805	0.028732	transmembrane 4 superfamily member 1
Fer1l5	32.7391	0.810851	0.028732	fer-1-like 5 (C. elegans)
Spred1	1327.88	-0.53141	0.028867	sprouty protein with EVH-1 domain 1, related sequence
Fam103a 1	2012.653	-0.4629	0.029087	family with sequence similarity 103, member A1
Gm5127	2.747973	-2.57225	0.029139	predicted gene 5127
Rbm15b	716.7089	-0.25722	0.029371	RNA binding motif protein 15B
Piwil1	2.312067	3.689204	0.029415	piwi-like RNA-mediated gene silencing 1
Bckdha	536.1488	-0.3968	0.029521	branched chain ketoacid dehydrogenase E1, alpha polypeptide
Musk	30.91942	0.965479	0.02966	muscle, skeletal, receptor tyrosine kinase

Smim1	131.6996	0.776883	0.029726	small integral membrane protein 1
Otud1	362.9322	-0.52717	0.029771	OTU domain containing 1
Slco1c1	150.9373	-0.70324	0.029988	solute carrier organic anion transporter family, member 1c1
Lyrm7	261.6673	-0.58757	0.029995	LYR motif containing 7
Arrb1	769.4707	0.358841	0.030018	arrestin, beta 1
Sgo1	3.421536	2.90809	0.030065	shugoshin 1
Ctsz	793.464	0.546687	0.030124	cathepsin Z
Trhde	116.3486	0.644975	0.030148	TRH-degrading enzyme
Wdr5b	77.06747	-0.5357	0.030216	WD repeat domain 5B
Cavin1	174.5966	-0.70431	0.030309	caveolae associated 1
Mrpl1	272.0664	0.444267	0.030309	mitochondrial ribosomal protein L1
Rtca	1029.603	0.349973	0.030331	RNA 3'-terminal phosphate cyclase
Vps53	541.9454	0.269222	0.030331	VPS53 GARP complex subunit
1110008P14Rik	1580.996	0.786205	0.030378	RIKEN cDNA 1110008P14 gene
Kif7	45.31434	0.56128	0.030468	kinesin family member 7
Syngr2	89.08829	-0.7096	0.030523	synaptogyrin 2
Ahnak2	4.584698	4.005404	0.030544	AHNAK nucleoprotein 2
Fndc10	757.9523	0.379556	0.03058	fibronectin type III domain containing 10
Teddm2	39.50406	0.673343	0.030692	transmembrane epididymal family member 2
Ift57	893.4531	-0.361	0.030796	intraflagellar transport 57
Slc27a2	62.08868	-0.75634	0.031005	solute carrier family 27 (fatty acid transporter), member 2
Ptprh	22.66746	0.987285	0.031005	protein tyrosine phosphatase, receptor type, H
Mto1	253.7299	-0.35691	0.031027	mitochondrial tRNA translation optimization 1
Ccnl1	387.432	-0.32836	0.03112	cyclin L1
Ier2	285.2351	-0.57673	0.03112	immediate early response 2
Aloxe3	51.3628	-0.98934	0.0312	arachidonate lipoxygenase 3
Prps1	977.381	-0.25744	0.031224	phosphoribosyl pyrophosphate synthetase 1
Zfp324	87.3777	-0.44131	0.031446	zinc finger protein 324
Pcdh18	42.53899	-0.79511	0.031587	protocadherin 18
9330159F19Rik	191.9604	-0.69303	0.031656	RIKEN cDNA 9330159F19 gene
Qrsl1	195.3141	0.325145	0.031857	glutaminyl-tRNA synthase (glutamine-hydrolyzing)-like 1
Psg16	106.5656	0.506158	0.031897	pregnancy specific glycoprotein 16
Rtkn	708.196	-0.33281	0.031914	rhotekin
Rmnd5b	1232.139	-0.33065	0.032026	required for meiotic nuclear division 5 homolog B
Cntln	114.482	-0.55267	0.03212	centlein, centrosomal protein
Fn3k	392.5352	0.439505	0.032153	fructosamine 3 kinase
Timm8b	1296.273	0.832124	0.032295	translocase of inner mitochondrial membrane 8B
Rpl31	818.9109	0.795518	0.0323	ribosomal protein L31
Gm9903	8.192223	1.334034	0.0323	
Tgds	56.63279	-0.5193	0.032508	TDP-glucose 4,6-dehydratase

Dusp19	221.6151	-0.40044	0.032513	dual specificity phosphatase 19
Mfap4	31.80009	-1.02749	0.032567	microfibrillar-associated protein 4
Ccdc116	17.34197	1.063731	0.032674	coiled-coil domain containing 116
Lgi2	34.80801	1.411245	0.032736	leucine-rich repeat LGI family, member 2
Col11a2	32.01901	1.607505	0.0328	collagen, type XI, alpha 2
Tmbim6	1418.198	-0.24981	0.03282	transmembrane BAX inhibitor motif containing 6
Msh2	211.9217	-0.58855	0.032828	mutS homolog 2
Ets1	99.6604	-0.77208	0.032828	E26 avian leukemia oncogene 1, 5' domain
Grp	50.01547	0.857884	0.032846	gastrin releasing peptide
Tmem37	18.55363	0.994463	0.033013	transmembrane protein 37
Mfsd4a	471.9717	0.527861	0.033077	major facilitator superfamily domain containing 4A
Ulk1	717.6783	0.403649	0.03309	unc-51 like kinase 1
Ttc1	616.8899	0.330865	0.03309	tetratricopeptide repeat domain 1
Dmwd	2522.703	-0.32212	0.033263	dystrophia myotonica-containing WD repeat motif
Fam117b	584.6353	-0.46488	0.033326	family with sequence similarity 117, member B
Azin2	747.1911	0.24172	0.03337	antizyme inhibitor 2
Cotl1	594.1445	0.526398	0.033394	coactosin-like 1 (Dictyostelium)
Tmem175	409.9028	0.344884	0.033434	transmembrane protein 175
Nsd2	459.5938	-0.56057	0.033434	nuclear receptor binding SET domain protein 2
Slc35b1	423.0344	0.332776	0.033438	solute carrier family 35, member B1
Tapbp	224.1426	-0.47547	0.033462	TAP binding protein
Grn	430.0638	0.459022	0.033462	granulin
Acaca	149.5765	0.79234	0.033685	acetyl-Coenzyme A carboxylase alpha
Cnih3	828.9603	0.406969	0.033769	cornichon family AMPA receptor auxiliary protein 3
Angptl2	78.92997	0.642424	0.033773	angiopoietin-like 2
Cttnbp2nl	207.0904	-0.49322	0.03383	CTTNBP2 N-terminal like
Psmb5	2050.839	0.548549	0.033911	proteasome (prosome, macropain) subunit, beta type 5
Gm11225	183.513	0.576034	0.03398	
Paqr5	43.35505	-0.90553	0.033986	progestin and adipoQ receptor family member V
Kdelc2	55.6128	-0.63647	0.033986	KDEL (Lys-Asp-Glu-Leu) containing 2
Ehmt1	233.4201	-0.50245	0.034034	euchromatic histone methyltransferase 1
Pkib	127.741	0.739615	0.034079	protein kinase inhibitor beta, cAMP dependent, testis specific
Xpnpep1	621.8672	0.314974	0.034266	X-prolyl aminopeptidase (aminopeptidase P) 1, soluble
Dcaf17	138.7649	-0.53452	0.034266	DDB1 and CUL4 associated factor 17
Gm12183	2.289484	2.422633	0.034266	
Rpusd3	172.8004	0.379063	0.034365	RNA pseudouridylate synthase domain containing 3
Uqcr11	1847.294	0.843438	0.034442	ubiquinol-cytochrome c reductase, complex III subunit XI
Prtg	24.2213	1.059649	0.034477	protogenin
Zfp839	87.54203	-0.45907	0.034585	zinc finger protein 839
Epha2	5.557804	-2.05299	0.0348	Eph receptor A2

Kcna4	272.1206	-0.5529	0.0348	potassium voltage-gated channel, shaker-related subfamily, member 4
Entpd2	77.87015	0.733587	0.034899	ectonucleoside triphosphate diphosphohydrolase 2
Atg3	539.6398	0.346492	0.034905	autophagy related 3
Tbx6	4.192822	-1.87662	0.034905	T-box 6
Diras2	3375.438	-0.28481	0.034905	DIRAS family, GTP-binding RAS-like 2
Cwc22	112.9876	-0.57449	0.035097	CWC22 spliceosome-associated protein
Gramd4	288.1971	-0.39606	0.035097	GRAM domain containing 4
Prss41	38.19054	1.144859	0.035313	protease, serine 41
Ssu2	3.661052	1.751861	0.035313	ssu-2 homolog (C. elegans)
Steap4	3.957694	-2.12941	0.035591	STEAP family member 4
Fam57b	135.0913	0.666151	0.035591	family with sequence similarity 57, member B
Inpp5a	1471.016	0.301429	0.035612	inositol polyphosphate-5-phosphatase A
Klc4	246.933	-0.37397	0.035628	kinesin light chain 4
Snai3	33.15195	0.899731	0.035628	snail family zinc finger 3
Oaf	140.2645	0.51354	0.035628	out at first homolog
Rsrp1	2892.065	-0.48752	0.035628	arginine/serine rich protein 1
Selenow	12629.82	0.695061	0.035628	selenoprotein W
Uevld	77.0676	-0.76901	0.035628	UEV and lactate/malate dehyrogenase domains
Sytl5	24.39227	-0.81363	0.035628	synaptotagmin-like 5
Cytl1	8.032287	-3.08698	0.035628	cytokine-like 1
Rps28	157.3679	0.813668	0.035628	ribosomal protein S28
Carhsp1	1308.275	-0.35338	0.035845	calcium regulated heat stable protein 1
Trpc3	207.352	0.830241	0.035919	transient receptor potential cation channel, subfamily C, member 3
Lum	30.10933	-1.22203	0.03618	lumican
Gm28845	8.714777	1.315689	0.036259	
Entpd4b	654.7231	0.474012	0.036381	ectonucleoside triphosphate diphosphohydrolase 4B
Deaf1	720.869	0.249464	0.036381	DEAF1, transcription factor
Ceacam9	2.296136	-3.10018	0.036435	carcinoembryonic antigen-related cell adhesion molecule 9
Fntb	262.4934	-0.48321	0.036435	farnesyltransferase, CAAX box, beta
Abat	1706.718	0.456549	0.036435	4-aminobutyrate aminotransferase
Rnf207	52.38616	0.867707	0.036449	ring finger protein 207
Armcx3	952.5729	0.397921	0.036547	armadillo repeat containing, X-linked 3
Sertad2	368.8962	-0.41167	0.036547	SERTA domain containing 2
Tprgl	4358.868	-0.28329	0.036694	transformation related protein 63 regulated like
Atp6v1h	2049.759	0.39092	0.036694	ATPase, H+ transporting, lysosomal V1 subunit H
Slc16a4	14.69923	-1.06148	0.0367	solute carrier family 16 (monocarboxylic acid transporters), member 4
Fchsd2	260.2645	-0.45305	0.036781	FCH and double SH3 domains 2
Eif5	1656.478	0.339296	0.036789	eukaryotic translation initiation factor 5
Hnrnpdl	1309.116	-0.35566	0.036789	heterogeneous nuclear ribonucleoprotein D-like
Aldh1l1	178.554	0.943759	0.036789	aldehyde dehydrogenase 1 family, member L1
Pcdhga8	36.24526	-1.3649	0.036821	protocadherin gamma subfamily A, 8

Basp1	10345.78	-0.36395	0.03697	brain abundant, membrane attached signal protein 1
Ndufa12	1451.582	0.600288	0.037008	NADH dehydrogenase (ubiquinone) 1 alpha subcomplex, 12
Vps36	297.6935	0.291998	0.037028	vacuolar protein sorting 36
Tnfrsf18	14.14684	1.225735	0.037028	tumor necrosis factor receptor superfamily, member 18
Snu13	1600.597	-0.33677	0.037028	SNU13 homolog, small nuclear ribonucleoprotein (U4/U6.U5)
Snu13	1600.597	-0.33677	0.037028	NHP2-like protein 1
Zbtb48	159.8377	-0.51154	0.037073	zinc finger and BTB domain containing 48
Rnf157	3178.126	0.306207	0.037073	ring finger protein 157
Tmem208	338.2635	0.608995	0.037183	transmembrane protein 208
Cldnd1	725.9669	-0.36669	0.037279	claudin domain containing 1
Sdccag3	920.4564	0.287227	0.037279	serologically defined colon cancer antigen 3
Slc22a3	73.07036	-0.70632	0.037313	solute carrier family 22 (organic cation transporter), member 3
Uqcrfs1	2623.169	0.274337	0.037371	ubiquinol-cytochrome c reductase, Rieske iron-sulfur polypeptide 1
Bag1	2604.213	0.516213	0.037384	BCL2-associated athanogene 1
Atp6v0c	19602.31	0.367939	0.037391	ATPase, H+ transporting, lysosomal V0 subunit C
Kcnip2	4206.528	0.362414	0.037425	Kv channel-interacting protein 2
Zfp804a	320.882	0.483936	0.037437	zinc finger protein 804A
Psma3	1665.656	0.421878	0.037691	proteasome (prosome, macropain) subunit, alpha type 3
Igsf1	38.84929	1.04195	0.037924	immunoglobulin superfamily, member 1
Fam76b	104.8599	-0.75608	0.038014	family with sequence similarity 76, member B
Asb8	870.0155	0.244826	0.038133	ankyrin repeat and SOCS box-containing 8
B3gat2	66.72415	0.523139	0.038252	beta-1,3-glucuronyltransferase 2 (glucuronosyltransferase S)
Mtcl1	479.5587	-0.41956	0.038252	microtubule crosslinking factor 1
Shpk	43.56592	-0.65633	0.038275	sedoheptulokinase
Fnip2	90.83978	0.602594	0.038458	folliculin interacting protein 2
Lactb2	167.0348	0.585378	0.038554	lactamase, beta 2
9530053A07Rik	3.988231	2.131203	0.038554	RIKEN cDNA 9530053A07 gene
Nrip2	334.8949	0.485301	0.038656	nuclear receptor interacting protein 2
Bub1b	14.85853	1.449	0.038698	BUB1B, mitotic checkpoint serine/threonine kinase
Rwdd4a	372.8503	0.430335	0.038893	RWD domain containing 4A
Mxra7	178.9665	-0.55679	0.038923	matrix-remodelling associated 7
Tes	24.03178	0.85675	0.039023	testis derived transcript
Max	439.9627	0.849336	0.039124	Max protein
Ubtd1	328.031	0.514863	0.039689	ubiquitin domain containing 1
Ears2	110.864	-0.42018	0.039689	glutamyl-tRNA synthetase 2, mitochondrial
Tbrg1	588.7892	-0.27653	0.039736	transforming growth factor beta regulated gene 1
Terf2ip	723.4229	-0.33183	0.039799	telomeric repeat binding factor 2, interacting protein
Pgm2l1	1374.01	0.611443	0.039933	phosphoglucomutase 2-like 1

Gm3696	62.31456	1.234033	0.039933	predicted gene 3696
Pxdc1	95.83541	-0.6609	0.039963	PX domain containing 1
Tle4	754.6847	-0.38707	0.039964	transducin-like enhancer of split 4
Plscr1	37.19732	-0.75644	0.039964	phospholipid scramblase 1
4930579G24Rik	55.55883	0.668212	0.040118	RIKEN cDNA 4930579G24 gene
Ncoa5	505.8439	-0.30285	0.040162	nuclear receptor coactivator 5
Efcab2	151.9018	0.593846	0.04038	EF-hand calcium binding domain 2
Ppp1r3c	132.3492	0.599334	0.040637	protein phosphatase 1, regulatory (inhibitor) subunit 3C
Wbp4	1000.133	0.380514	0.040685	WW domain binding protein 4
Plxna2	485.086	0.419698	0.040744	plexin A2
Mettl7a1	189.3276	0.501563	0.040744	methyltransferase like 7A1
Naf1	91.24822	0.451638	0.040777	nuclear assembly factor 1 ribonucleoprotein
Scamp5	3588.39	0.328953	0.040825	secretory carrier membrane protein 5
Vps72	953.102	-0.35193	0.040915	vacuolar protein sorting 72
Angel2	900.0008	0.327084	0.04116	angel homolog 2
Efcc1	242.5003	-0.41489	0.04116	EF hand and coiled-coil domain containing 1
Anxa11	290.6762	0.451184	0.041209	annexin A11
Rps6ka4	1106.231	-0.38636	0.041321	ribosomal protein S6 kinase, polypeptide 4
Phyh	856.0981	0.364234	0.041321	phytanoyl-CoA hydroxylase
Rasgrp4	4.385675	-2.50056	0.041321	RAS guanyl releasing protein 4
Dmac2	904.9158	-0.3527	0.041374	distal membrane arm assembly complex 2
Sel1l3	192.7449	0.594638	0.041445	sel-1 suppressor of lin-12-like 3 (C. elegans)
Maf	140.5226	0.458492	0.041503	avian musculoaponeurotic fibrosarcoma oncogene homolog
Rpl27	610.4982	0.736534	0.041503	ribosomal protein L27
Rpl27	610.4982	0.736534	0.041503	60S ribosomal protein L27
Cul1	789.8731	-0.34805	0.041507	cullin 1
Dtx1	930.8233	-0.29285	0.041698	deltex 1, E3 ubiquitin ligase
Msrb1	197.3509	0.622001	0.041698	methionine sulfoxide reductase B1
Hmg20a	565.7858	-0.35206	0.041704	high mobility group 20A
Rfx2	27.75627	-0.90002	0.041733	regulatory factor X, 2 (influences HLA class II expression)
Cdkn2aipnl	924.2468	-0.26601	0.041968	CDKN2A interacting protein N-terminal like
Uox	7.430339	1.728968	0.042149	urate oxidase
Nfil3	122.194	-0.37807	0.042149	nuclear factor, interleukin 3, regulated
Kcnk2	1037.629	-0.40983	0.042295	potassium channel, subfamily K, member 2
Tmem35b	24.25299	-0.82493	0.042295	transmembrane protein 35B
Pcdhga6	44.10251	-1.11328	0.04231	protocadherin gamma subfamily A, 6
Ywhaq	7742.76	-0.22785	0.042446	tyrosine 3-monooxygenase/tryptophan 5-monooxygenase activation protein theta
Usp31	834.0576	0.340779	0.042627	ubiquitin specific peptidase 31
Caly	1065	-0.47787	0.042907	calcyon neuron-specific vesicular protein

Cxcl16	20.8947	-1.09458	0.042949	chemokine (C-X-C motif) ligand 16
Rbpms	148.5844	-0.58387	0.043054	RNA binding protein gene with multiple splicing
Thap1	166.7886	-0.52267	0.043289	THAP domain containing, apoptosis associated protein 1
Hnrnpm	894.3608	-0.37571	0.043289	heterogeneous nuclear ribonucleoprotein M
Ctbs	55.76521	-0.77479	0.043358	chitobiase, di-N-acetyl-
Hlf	1884.138	-0.35265	0.043516	hepatic leukemia factor
Sncaip	83.21885	-0.72615	0.043551	synuclein, alpha interacting protein (synphilin)
Dok2	8.91141	-1.61475	0.043741	docking protein 2
Ttll1	674.157	0.194956	0.043741	tubulin tyrosine ligase-like 1
Nagpa	138.1461	0.526365	0.043741	N-acetylglucosamine-1-phosphodiester alpha-N-acetylglucosaminidase
Rab3ip	295.6462	-0.36775	0.043741	RAB3A interacting protein
Ccdc113	46.65093	-0.60846	0.043958	coiled-coil domain containing 113
Togaram2	30.7943	1.206286	0.043958	TOG array regulator of axonemal microtubules 2
Siglec5	2.54554	3.798354	0.043981	sialic acid binding Ig-like lectin F
Abca12	3.11767	2.965126	0.043981	ATP-binding cassette, sub-family A (ABC1), member 12
Abtb2	92.37451	0.839152	0.044013	ankyrin repeat and BTB (POZ) domain containing 2
Cstb	466.1646	0.589834	0.044047	cystatin B
Foxo6	699.5636	-0.49435	0.044081	forkhead box O6
Katnal2	46.57305	-0.53416	0.04416	katanin p60 subunit A-like 2
Apln	144.7062	0.696611	0.044229	apelin
Bcl2	201.529	-0.37667	0.044309	B cell leukemia/lymphoma 2
Lrpap1	1997.836	0.290285	0.044321	low density lipoprotein receptor-related protein associated protein 1
Ccne1	155.8542	0.518548	0.044619	cyclin E1
Ddt	437.3005	0.656403	0.044669	D-dopachrome tautomerase
Icam5	2119.555	-0.38737	0.044927	intercellular adhesion molecule 5, telencephalin
B4gat1	1542.551	-0.22776	0.044927	beta-1,4-glucuronyltransferase 1
Selplg	108.4917	-0.69596	0.044927	selectin, platelet (p-selectin) ligand
Arpc5	2616.988	0.260373	0.044964	actin related protein 2/3 complex, subunit 5
Nhej1	67.29902	1.269372	0.045147	nonhomologous end-joining factor 1
Stk16	849.5754	0.396892	0.045147	serine/threonine kinase 16
Pid1	540.9022	-0.29942	0.045147	phosphotyrosine interaction domain containing 1
Rfx8	3.007316	3.163456	0.045147	regulatory factor X 8
C2cd5	179.6895	-0.47372	0.045246	C2 calcium-dependent domain containing 5
Asb13	875.2328	0.290892	0.045258	ankyrin repeat and SOCS box-containing 13
Kank3	330.6289	0.596933	0.045368	KN motif and ankyrin repeat domains 3
H2-Bl	19.4643	2.150829	0.045368	histocompatibility 2, blastocyst
St8sia2	34.52971	-0.86133	0.045434	ST8 alpha-N-acetyl-neuraminide alpha-2,8-sialyltransferase 2
Slc29a1	177.8904	0.410015	0.045651	solute carrier family 29 (nucleoside transporters), member 1
Abi2	2388.116	-0.37561	0.045656	abl-interactor 2

Nsmce1	306.0095	-0.40448	0.045656	NSE1 homolog, SMC5-SMC6 complex component
Gramd1b	396.6744	0.31059	0.045656	GRAM domain containing 1B
Cenph	17.64621	0.891239	0.045656	centromere protein H
Aldh1a1	360.5207	-0.50458	0.045656	aldehyde dehydrogenase family 1, subfamily A1
Gm4951	3.303625	-3.21406	0.045656	predicted gene 4951
Reck	47.18105	-0.67934	0.045804	reversion-inducing-cysteine-rich protein with kazal motifs
Mroh1	340.962	0.875703	0.046099	maestro heat-like repeat family member 1
Tmem44	326.2769	0.597866	0.046101	transmembrane protein 44
Arf2	841.1949	-0.217	0.046101	ADP-ribosylation factor 2
Gdf11	51.71049	0.703665	0.046107	growth differentiation factor 11
Sptlc2	170.7158	-0.5756	0.046278	serine palmitoyltransferase, long chain base subunit 2
2610002M06Rik	539.5506	-0.38484	0.046332	RIKEN cDNA 2610002M06 gene
AU021092	16.66527	-1.00834	0.046332	expressed sequence AU021092
Dmap1	451.2489	-0.31556	0.046962	DNA methyltransferase 1-associated protein 1
Dapk1	751.9379	-0.32255	0.046962	death associated protein kinase 1
Cirbp	1934.894	-0.4332	0.046962	cold inducible RNA binding protein
Sars2	182.8813	0.452516	0.046962	seryl-aminoacyl-tRNA synthetase 2
Ppm1h	463.7644	0.412536	0.047116	protein phosphatase 1H (PP2C domain containing)
Fbln7	14.78742	-0.98795	0.047118	fibulin 7
Gcsh	869.0724	0.373003	0.047118	glycine cleavage system protein H (aminomethyl carrier)
Nxpe3	114.9837	0.536866	0.047118	neurexophilin and PC-esterase domain family, member 3
Atp5g1	3460.425	0.675168	0.047157	ATP synthase, H+ transporting, mitochondrial F0 complex, subunit C1 (subunit 9)
Slc35f4	153.2802	-0.33779	0.047157	solute carrier family 35, member F4
Dcbld1	136.7412	0.394495	0.047197	discoidin, CUB and LCCL domain containing 1
Chst11	215.8681	-0.41653	0.047197	carbohydrate sulfotransferase 11
Cdkal1	120.6409	-0.46019	0.047369	CDK5 regulatory subunit associated protein 1-like 1
Rilpl1	636.5403	-0.23665	0.047369	Rab interacting lysosomal protein-like 1
Lrfn2	45.13058	0.756098	0.047369	leucine rich repeat and fibronectin type III domain containing 2
Zfp938	332.1842	0.405347	0.047369	zinc finger protein 938
Sp5	5.272175	-1.44419	0.047595	trans-acting transcription factor 5
Ifitm7	2.273578	2.921735	0.047785	interferon induced transmembrane protein 7
Fam134b	255.959	-0.5013	0.04781	reticulophagy regulator 1
Ulk4	43.18035	0.824802	0.04781	unc-51-like kinase 4
Slc52a3	26.5899	-1.20464	0.048018	solute carrier protein family 52, member 3
Krt1	82.54474	0.556814	0.048093	keratin 1
Mpnd	2241.484	0.380093	0.048207	MPN domain containing
Bin3	135.141	0.372123	0.048207	bridging integrator 3
Vwa5b2	106.9487	0.74188	0.048321	von Willebrand factor A domain containing 5B2
Terf2	369.5304	-0.23533	0.048333	telomeric repeat binding factor 2

Dap3	1089.898	0.241611	0.048464	death associated protein 3
Adamts2	61.16365	-0.84052	0.048536	a disintegrin-like and metallopeptidase (reprolysin type) with thrombospondin type 1 motif, 2
Hrct1	28.75551	-0.69351	0.048536	histidine rich carboxyl terminus 1
Tnni3k	2.220124	3.076062	0.048632	TNNI3 interacting kinase
Ubl3	4226.39	-0.39871	0.048662	ubiquitin-like 3
Tmem160	773.5033	0.721523	0.048695	transmembrane protein 160
9530077C05Rik	78.77416	0.524406	0.048695	RIKEN cDNA 9530077C05 gene
Saxo2	44.59262	0.827374	0.048695	stabilizer of axonemal microtubules 2
Rhbdd2	886.923	-0.28944	0.048695	rhomboid domain containing 2
Maob	161.2828	0.625769	0.048695	monoamine oxidase B
Insl6	12.39181	1.072699	0.048695	insulin-like 6
Arid3c	2.731761	-3.34256	0.048894	AT rich interactive domain 3C (BRIGHT-like)
Zfp454	64.40684	0.507272	0.049034	zinc finger protein 454
Tmem256	422.6511	0.799231	0.049049	transmembrane protein 256
Nop56	716.7717	0.256105	0.049073	NOP56 ribonucleoprotein
Sh2d4a	1.696498	3.954181	0.049231	SH2 domain containing 4A
Cdh8	335.5799	-0.46574	0.049388	cadherin 8
Slc35g2	154.9772	0.534809	0.049388	solute carrier family 35, member G2
Tmem57	567.1915	-0.25397	0.049402	transmembrane protein 57
Acaa1b	25.16102	-0.88003	0.049434	acetyl-Coenzyme A acyltransferase 1B
Plscr3	160.2824	-0.4052	0.049434	phospholipid scramblase 3
Scn3b	699.6487	-0.34943	0.049583	sodium channel, voltage-gated, type III, beta
Tpm2	387.6219	0.530246	0.049711	tropomyosin 2, beta
Kcnj2	104.2684	-0.52866	0.049822	potassium inwardly-rectifying channel, subfamily J, member 2
Frg2f1	67.47599	0.550961	0.049822	FSHD region gene 2 family member 1
Utp6	299.2209	-0.49192	0.049863	UTP6 small subunit processome component
Chst10	943.6158	0.26234	0.049937	carbohydrate sulfotransferase 10
1110008F13Rik	1302.632	0.396916	0.049937	RIKEN cDNA 1110008F13 gene
Plxnd1	228.8713	0.505641	0.049937	plexin D1
Gtpbp10	86.98073	-0.71904	0.049937	GTP-binding protein 10 (putative)
Tigd3	30.97281	-0.72741	0.049937	tigger transposable element derived 3

Table S4. List of genes significantly different between Tsc1-WT and Tsc1-Het iSPNs.

Gene	Base Mean	log_2(Fold Change)	Adjusted p-value
Tsc2	29.16033	20.48096	9.62E-16
Pcnt	13.11786	-29.4822	5.55E-05
Ntng2	105.0564	-1.14975	0.000124
Acaca	149.5765	-1.23695	0.013487
Slit2	112.23	-1.41908	0.013487

Gm20425	11.22653	18.82381	0.014213
Bod1l	11.35508	-22.7927	0.018325
Serac1	63.57049	-0.89641	0.018376

Table S5. Two-way ANOVA values.

Figure panel	Test	Source of variation	F value	Comparison	DF	P value
3B	ANOVA	Interaction	1.385		10	0.1894
		Light intensity	45.68		10	< 0.0001
		Genotype	25.44		1	< 0.0001
	Sidak post-hoc			1%	198	> 0.9999
				2%		> 0.9999
				3%		> 0.9999
				5%		> 0.9999
				8%		0.2780
				10%		0.0658
				12%		0.0951
				15%		0.0951
				20%		0.1202
				50%		0.5306
				100%		0.6494
3C	ANOVA	Interaction	1.106		10	0.3600
		Light intensity	72.33		10	< 0.0001
		Genotype	6.461		1	0.0119
	Sidak post-hoc			1%	176	> 0.9999
				2%		> 0.9999
				3%		0.9983
				5%		0.9996
				8%		0.1203
				10%		0.2667
				12%		0.4995
				15%		0.9855
				20%		0.9996
				50%		> 0.9999
				100%		> 0.9999

3D	ANOVA	Interaction	2.859		11	0.0011
		Trial	56.53		11	< 0.0001
		Genotype	91.86		1	< 0.0001
	Sidak post-hoc			Trial 1	683	0.9532
				Trial 2		0.9347
				Trial 3		0.9258
				Trial 4		0.8154
				Trial 5		0.9999
				Trial 6		0.6413
				Trial 7		0.0011
				Trial 8		0.0005
				Trial 9		0.0020
				Trial 10		0.0016
				Trial 11		0.0024
				Trial 12		< 0.0001

Table S6. Student's t-test values.

Figure panel	Test	t and p values
3E	Two-tailed Student's paired t-test	t_{57}=4.037, p=0.0002
3G	Two-tailed Student's paired t-test	t_{73}=1.325, p=0.1892
3I	Two-tailed Student's paired t-test	t_{64}=2.101, p=0.0396

Table S7. Mann Whitney test.

Figure panel	Mann-Whitney U	p-value
3F	609	p=0.3527
3H	425	p=0.0034